Title
Development of Novel Adeno-Associated Virus-Mediated Gene Therapies for the Treatment of Inherited Retinal Degeneration

Author
Fortuny, Cecile

Publication Date
2019

Peer reviewed|Thesis/dissertation

Development of Novel Adeno-Associated Virus-Mediated Gene Therapies for the Treatment of Inherited Retinal Degeneration

By

Cecile Fortuny

A dissertation submitted in partial satisfaction of the

requirements for the degree of

Doctor of Philosophy

in

Vision Science

in the

Graduate Division

of the

University of California, Berkeley

Committee in charge:

Professor John G. Flannery, Chair
Professor Karsten Gronert
Professor Christine Wildsoet
Professor Laurent Coscoy

Summer 2019

Abstract

Development of Novel Adeno-Associated Virus-Mediated Gene Therapies for the Treatment of Inherited Retinal Degeneration

By

Cecile Fortuny

Doctor of Philosophy in Vision Science

University of California Berkeley

Professor John G. Flannery, Chair

The retina contributes to the first steps in processing visual information. Rods and cone photoreceptors are the two main retina cells contributing to the initial steps in sensing light and translating it to an electrical signal to the downstream neuronal cells finally to be processed in the primary visual cortex. Many cells and hundreds of genes are involved in the light response and keeping retinal cells metabolically active. This high degree of activity makes the retina more vulnerable to mutations and degeneration. The majority of mutations identified in patients affect genes involved in either the photoreceptor structural integrity or in the phototransduction cascade. Many inherited retinal degenerative (IRDs) diseases, such as retinitis pigmentosa, lead to blindness as a result of initial rod photoreceptor cell death followed by cones and a remodeling of the retina.

Gene therapy has been a growing field in the past decade and has proven to be an efficient and safe way of treating single-gene mutations leading to blindness by providing therapeutic DNA to targeted cells in the retina. The clinical trials for Leber congenital amaurosis type 2 (LCA) were the first to validate the proof-of-concept for gene therapy in retina, after the successful use of adeno-associated viruses (AAVs) to deliver a healthy copy of the RPE65 gene to the affected cells. AAV, a small and nonpathogenic virus, has been used widely in many clinical trials, due to its safety profile and efficiency at targeting a wide range of tissues and cell types.

However, many obstacles remain from the optimization of delivery and design of viral vectors to elucidating molecular mechanisms behind the heterogenous genetic complexity in retinal diseases. While over 250 gene-causing diseases have been identified, more than 30-40% of genes involved remain unknown or outside of canonical coding sequences. For these patients, a gene replacement is not yet possible or applicable and therefore requires novel approaches.

My dissertation focuses on the use and optimization of engineered AAV vectors to achieve cell-selective targeting of retinal cells and organelles, to design novel mutation-independent gene therapies adapted for progressive degenerative diseases such as retinitis pigmentosa. It also aims at elucidating and characterizing molecular mechanisms underlying non-coding region mutations, with the use of genome editing tools to engineer mouse models of untranslated region mutations found in LCA patients. My thesis provides new knowledge and AAV toolkit to better tackle patients' unmet need for novel gene therapy strategies addressing undiagnosed and noncanonical mutations in inherited retinal diseases.

Table of Contents

Acknowledgements

« Dans la vie, rien n'est à craindre, tout est à comprendre. »
- Marie Curie

This scientific journey would not have been possible without the support and love of friends and family. I also have been lucky for great mentoring figures during my undergraduate studies who believed in me and always pushed me to give the best of my abilities in anything I undertook.

My mom, who always has been positive and kept her head up through hardships, has been my biggest inspiration to keep going no matter what happens, just as she did when she raised me and my brothers. To my closest friends from the hexagon, Élodie, Florian, Julie, Stéphanie, Michael, Claire and Pauline, thank you for your unconditional friendship through the years.

I would like to first thank Dr. Christine Wildsoet, Dr. Karsten Gronert, and Dr. Laurent Coscoy for their constant support and time through my time at Berkeley, beginning with my qualification exam to our thesis committee meetings. Thank you to Dr. Michael Silver for our annual advisory meetings that always turned into therapy sessions.

I can't find words to express my gratitude to Dr. John Flannery for allowing me to join his lab. John has always given equal opportunities to students from diverse backgrounds. He taught me the value of collaboration and kindness. John gave me full freedom to grow as a scientist. I will always be grateful for all the opportunities he has given me.

I would also like to thank Dr.Georgeann Sack, and Dr. Marla Feller for their mentorship during my rotation in the Feller Lab.

This adventure would not have been the same without the wonderful AAVengers Flannery team. Dr. Leah Byrne and Dr. Deniz Dalkara-Mourot were both critical in my admission to the Vision Science Graduate Group at UC Berkeley. They advised and trusted me with their research. They are among the best female scientist role models I could have asked for as a student. I definitely tried to raise myself to their level through the years of my PhD. I will always look forward to reading about the next innovative and challenging research endeavors from their labs.

Dr. Angela Bowman was another wonderful postdoc I had the chance to work with closely. She expanded my research skills and gave me a lot of scientific insights. Her mentoring greatly contributed to my thesis research. Meike Visel's help through the years has been tremendous. She always takes care of everyone and is always there to help. Things would have been so much more painful without her expertise, spirit and kindness. Thank you to my fellow graduate students and labmates for the help and fun. Cameron, specifically, you definitely taught me how to curse and many American slang vocabulary. It was quite awesome to be the HBIC with you. Little Jon, your kindness and help was invaluable. I benefited so much from our long conversations. Trevor Lee taught me all the animal skills (and reddit awareness) I needed when I joined the lab. Yvonne, wherever you go, you are always a little sunshine. I am so glad we were able to pursue our friendship outside of the lab. Special thanks to Benji Gaub, Mervi Kuronen, and the Schaffer crew David, Thom, Sabrina Christina, and Benjamin for their support and help.

I have deep gratitude for all the undergraduate students that I mentored and worked with through the URAP, NIH T35 and B2B research programs: Alice Levett, Mahnoor Baker Allawala,

Janette Shepard, Niki Sabetfakhri, Rachel Choi and Jamie Ngo. I would like to specifically acknowledge the hard work of Carolyn Dunlap and Jamie Xie, who both worked with me for two full academic years. I feel blessed for their support during the busiest times in graduate school. Always motivated, hard-working and joyful students, I know they will be successful with whatever comes next.

Next, I would like to thank the Vision Science graduate community. This PhD has been an incredible human experience because of you all. There are too many people to acknowledge them all correctly. To my 2013 cohort: Kaleb, Dylan, Brian, Mayur, Taras, Patrick, Ally, Jessica and Kelly. You are nothing short of amazing. I look forward to following the next chapters of your life. Brian, Ally and Kaleb, you guys carried me through my first year while I was adjusting from my move across the ocean. Thank you for your patience, and help. Jessica, thank you for being my teaching buddy during our first two years. Your resilience and hard work are unbelievable. Our friendship is one of the best things that came out of this PhD. Hope we will have many other hipster trips around the globe.

Kelly, there are no words I could possibly write to describe how thankful I am for our friendship and how great of a person you are. You've been by my side through the hardest times and many happy celebrations, constantly cheering me up. I look forward to the next chapters of our life, as I know we will be writing them alongside each other.

Lastly, I would like to thank and dedicate my thesis to Dr. Timothy Day, my labmate, best friend, partner in crime and most significant finding of my PhD years at Berkeley. I would have given up many times without your support and love. Your constant kindness, your scientific excitement was inspiring at all times and encouraged me to always try my best. You showed me that I hold all the resources for my own success. Thank you for believing in me like no one else.

Chapter 1: Introduction

The retina and the visual circuit

Vision is the ability to perceive our surrounding environment and is considered one of the most important senses we use in our everyday life. The first steps happen in furthest back tissue of the eye, the retina[1,2]. The retina is a neuro-sensory tissue that shares similar cellular architecture and function with the brain. The retina and optic nerve are embryonically derived from the diencephalon, and therefore classified as part of the central nervous system (CNS). The retina is a laminated structure with three major layers of cell bodies; the outer nuclear layer (ONL), inner nuclear layer (INL), and ganglion cell layer (GCL); separated by two synaptic layers referred to as the inner and outer plexiform layers. Those connected layers allow visual information to be processed vertically by photoreceptors, bipolar, and ganglion cells, as well as horizontally by horizontal and amacrine cells. Adjacent to the ONL, the retinal pigment epithelium (RPE) constitutes part of the blood-retina barrier and is involved in metabolic functions (support, nutrients, etc.) as well as the phototransduction cascade (recycling of the photopigment).

When light enters the eye through the transparent cornea, it passes through the pupil, is refracted by the lens and converges on the retina. Counterintuitively, photons have to travel through the cell layers of the retina, to be sensed by the photoreceptors (PRs) and converted to an electrical signal (phototransduction) that is sent back to the inner retina and conveyed to the brain via the optic nerve (**Fig1.A-B**)

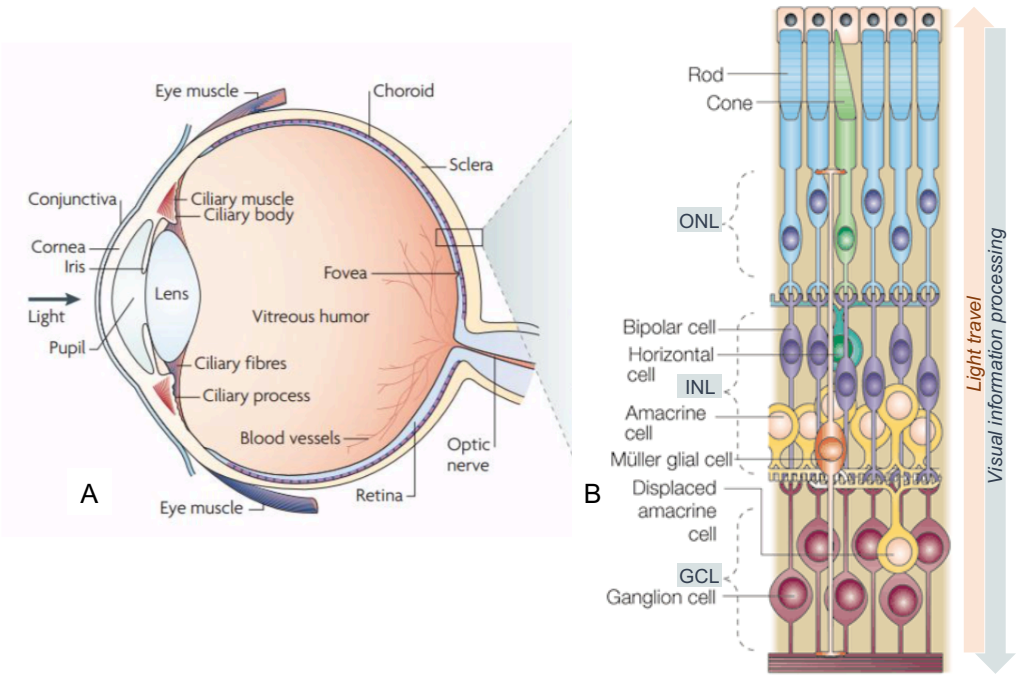

Figure 1: Structure of the mammalian eye (**A**) and neurosensory tissue, the retina (**B**) showing the opposite direction that light travels to the back of the retina and the direction of visual information processing to the brain. Adapted from Wright et al. 2010[3]

There are two types of photoreceptors, rods and cones, that contribute to different components of vision. Rods detect dim levels of light (scotopic vision) as they contain more photosensitive pigment than cones. They are incredibly sensitive: a single photon, instead of ten or hundred for the cones, needs to be absorbed by the rod to evoke an identical response [4]. Cones mediate day-time (photopic) and color vision through three types of cones which express distinct pigments, sensitive to varying wavelengths in the visible light spectrum[5].

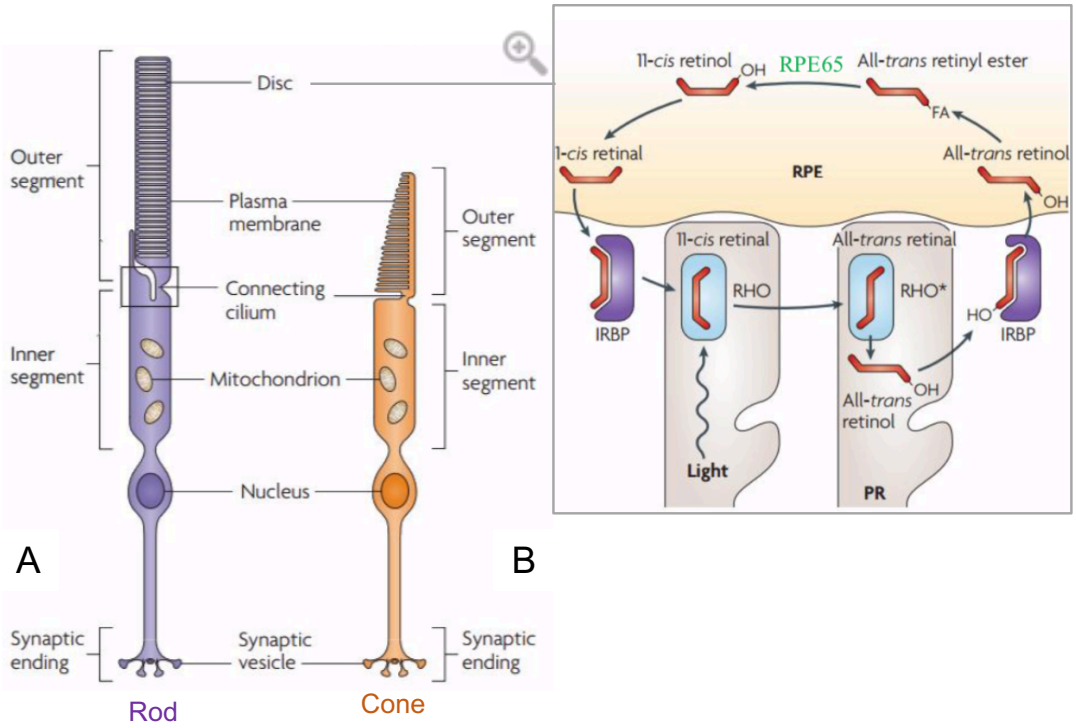

Figure 2: Cone and rod photoreceptor structure. Synaptic ending connects to bipolar cells and horizontal cells (**A**) Phototransduction takes place in the outer segment of PR, with the assistance of the RPE layer in recycling the light sensitive opsin (**B**). Adapted from Wright et al (2010).

Their sensitive photopigment resides both within the membrane of the discs and in the surrounding plasma membrane (**Fig 2.A**). Although a different component of the photopigment contributes to phototransduction in rods and cones, the general mechanism remains similar. Rhodopsin, the rod G-coupled transmembrane protein, is composed of an apoprotein, opsin bound to a light-sensitive chromophore, retinal 11-cis retinaldehyde, in its "dark" state[6].When not light-stimulated, photoreceptors are in a constant depolarized state: cyclic GMP (cGMP) ion channels present in the outer disc membrane are open, triggering the release of glutamate in the synaptic space. When light hits the photoreceptors, absorption of photons triggers the isomerization of retinal from its 11-cis form to an all-trans retinal structure. This conformational change activates the G-protein, resulting in transducin activating the phosphodiesterase 6 and the hydrolysis of cGMP into GMP[4,7,8]. The concentration in cGMP decreases, and related channels close, altering glutamate release and depolarizing bipolar cells. The all-trans retinal is later recycled back to its 11-cis confirmation by the RPE[9] and trafficked back to allow PRs to be sensitive again to light (**Fig 2.B**).

Downstream, different types of bipolar cells respond to the photoreceptor's level of glutamate released onto the synaptic cleft. ON-bipolar cells expressed a metabotropic glutamate receptor, mostly mGluR6 (G-protein coupled receptor): when glutamate is released from the cone synapse, it binds to the receptor, leading to the downstream closure (sign inverting) of the cation channel. This means that ON-BCs depolarized (cationic channels open) in response to the decrease in glutamate signaled by hyperpolarized PRs in response to light. OFF-bipolar cells differ by expressing AMPA and kainite[10] type of glutamate receptors (ionotropic cation channel). Oppositely, OFF-BCs cells are depolarized by increased level glutamate (cation channel opens) from depolarized PRs, in their "dark current" stage. ON- and OFF-BCs are further differentiated into distinct subclasses for more intricate signal segregation for transient versus sustained signals. While many rod PRs are in synaptic contact with the same bipolar cell, cones may have a one-one ratio synapsing on BCs. BCs also release glutamate based on their membrane potential state to amacrine cells and retinal ganglion cells (RGCs).

Ganglion cells are the only retinal neurons that project to the brain. The majority of their axons, forming the optic nerve, carry the output information from the retina to the lateral geniculate nucleus (LGN), which then projects to the visual cortex and results in conscious vision as an end result of visual processing from the brain. Many subclasses of RGCs can be found in the mammalian retina, they are grouped in two main categories relative to their ON or OFF center-surround receptive fields and the layer in the LGN they project to: parvocellular P (midget) and magnocellular M (parasol) cells. Midget cells have smaller receptive fields, sense changes in color and have a slow conduction velocity. They account for ~80% of RGCs in contrast to (10%) parasol cells. Those have bigger receptive fields, quick conduction velocity but are insensitive to changes in color. Other types of ganglion cells[11] have been since discovered and characterized. K-type RGCs projects to the koniocellular layers of the LGN and have moderate spatial resolution as well as medium conduction velocity, responding to moderate-contrast stimuli. Photosensitive ganglion cells[12], which express a photopigment called melanopsin, project to the suprachiasmatic nucleus (involved in circadian rhythm maintenance) as well as the LGN (controls pupillary light reflex).

Inter-neurons, such as horizontal cells (HCs) and amacrine cells (ACs) also play critical roles as well in the visual circuitry. HCs receive glutamatergic inputs from the PRs and provide inhibitory feedback and feedforward to PRs and BCs, respectively. It has been recently found that HCs are also involved in light adaptation at the retina output levels, spatial frequency tuning, and firing rate of RGCs[13–15]. Amacrine cells (ACs) receive inputs from both bipolar and amacrine cells and pass on the information to ganglion and other amacrine cells. Different types of amacrine cells have been characterized (dopaminergic, starburst,…), showcasing the myriad of functions they are involved with in the retinal circuit, such as responsiveness of the retina in response to a diverse range of light intensities and ganglion cell direction selectivity[16].

While the human retina is quite a thin tissue (~200 μm), the network complexity and metabolic demand behind the visual system is quite astonishing. Large supplies of ATP from the oxidative metabolism in the mitochondria is needed for the maintenance of the neural circuitry. Phototransduction, neurotransmitter release, and protein transport are energy-dependent, with the bulk majority spent on the repolarization of the membrane potential after depolarization.

Inherited retinal degenerations

The medical and genomic revolution that started a few decades ago led us to better knowledge and understanding of structural and functional defects in genes involved in ocular diseases[17,18]. The human genome project drove genetic mapping and genomic breakthroughs such as the identification of novel genes and variants as well as improvement of genetic testing with next-generation sequencing (NGS)[19]. There are about 4000 diseases/syndromes known to affect humans, with one third associated with just the eye. Retinopathies with complex inheritance (autosomal recessive, dominant or X-linked) are responsible for most forms of blindness. To date, over 270 genes/loci have been mapped to a specific chromosomal site, with 250 of these identified at a sequence level, leaving still 25-30% of the cases not elucidated yet[20] (**Fig 3A**). Due to the high degree of metabolic activity in the retina, genetic mutations occur, affecting the protein it encodes. Whether incorrectly synthesized or not expressed at all, it leads to degeneration of those cells and progressive loss of vision. The majority of the mutations identified affect genes involved in either the photoreceptor structural integrity or in the phototransduction cascade happening in the photoreceptor and RPE layers.

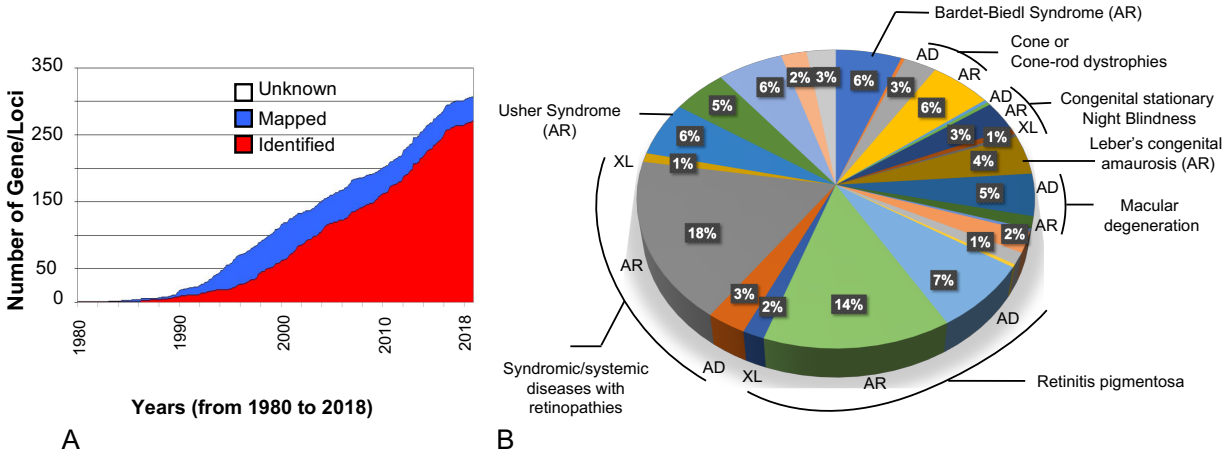

Figure 3: Graph showing progression of the mapping and identification of gene/loci with mutations in patients with inherited retinal degenerations (IRD) from 1980 to 2018 (**A**) About 250 genes have now been identified in 2018, with retinitis pigmentosa accounting for the majority of the cases (~25%), as well as syndromic diseases with retinopathy manifestation (**B**). Pie chart also show different modes of inheritance transmission in IRDs, with majority of them being recessive. AD: Autosomal dominant, AR: autosomal recessive; XL: X- Linked. Adapted from http://www.sph.uth.tmc.edu/retnet (2018).

Retinitis pigmentosa (RP) is the most common form of inherited blindness (**Fig 3.B**) in the world, affecting 1:3000-4000 people from ages 20-64 years[21–23]. Over 800,000 people in the United States suffer some level of visual impairment from RP. Of those, 30,000 are totally blind. RP is characterized by pigment deposits[24] predominant in the peripheral retina and by a relative sparing of the central retina.

Patients suffer from progressive night blindness, a reduction or loss of visual acuity, starting in the mid-periphery and advancing toward the macula and fovea, leading to tunnel vision (**Fig 4).**

Figure 4: Retinitis pigmentosa leads to progressive loss of peripheral vision, leading to residual tunnel vision in more advanced stages of the disease.

More severe cases will result in complete blindness. RP is generally described as a rod-cone dystrophy: at the cellular level, rod photoreceptors are first affected, and their loss leads to the secondary death of cones, followed by retinal remodeling. The progression and severity of RP is largely dictated by the underlying gene inheritance and transmission. With over 60 known causative genes, autosomal recessive RP (ARRP) accounts for 5-45% of the cases, autosomal dominant (ADRP) 15-35% and X-Linked 5-17% (XLRP). Most common RP genes for each inheritance are Usherin (USH2A, ~15% of ARRP), rhodopsin (RHO, over 30% of ADDRP), and retinitis pigmentosa GTPase regulator (RPGR, ~70-90% of XLRP).

RP also associates with other symptoms. The most frequent forms of syndromic RP is Usher Syndrome (~14% of all RP), which is characterized by a congenital hearing impairment followed by later visual loss. Bardet-Biedl is a rod-cone dystrophy associated with obesity (72%), mental retardation and psychomotor impairment, as well as renal abnormality (major cause of morbidity). Many other syndromes, rarer, associate with RP (e.g., Refsum disease*)* typically starting in the mid-periphery and advancing toward the macula and fovea. Typical symptoms include night blindness followed by decreasing visual fields, leading to tunnel vision and eventually legal blindness or, complete blindness.

Leber Congenital Amaurosis (LCA), is one of the earliest and most severe forms of congenital IRD[25]. Predominantly recessive, it affects 2-3 newborns out of 100,000, often diagnosed during infancy as a result of more severe onset of degeneration. To date, 19 genes (70% of all patient cases) have been identified and studied, with a particular focus on the most frequently occurring mutations/genes: CEP290 accounts for 20%, GUCY2D ~15% and RPE65, CRB1, RDH12 ~10% each, respectively. LCA is distinguished from other forms of IRD by three features: severe/early visual impairment, no or very limited pupillary responses, and severely subnormal or non-detectable electroretinogram (ERG) traces. Phenotypic variability is observed within patients, but common features are macular coloboma, bone-spicule pigment migration as well as pale optic nerve (vasculature attenuation).

Due to the complexity of its genetics, age-related macular degeneration (AMD) is not traditionally classified as an inherited retinal degeneration although half of the cases have been linked to a genetic component [26]. It is a leading cause of visual loss in the elderly (>40 years old) in Western populations. This progressive neurodegenerative disease affects a specific part of the retina, called the macula, which is essential for high acuity and daylight vision. Two forms of AMD can be distinguished: atrophic (referred to as dry AMD) or neovascular (wet AMD). A common hallmark of the disease is the progressive accumulation of drusen, lipid aggregates of extracellular material, in the RPE layer over time. The most common form, dry AMD, is characterized by excessive drusen accumulation between the RPE and the choroid layer, impacting

the transport of nutrients and oxygen from the choriocapillaris to the RPE/retina, leading to progressive cell death of RPE, followed by photoreceptors. Some advanced geographic atrophy (dry) forms progress towards the wet form of AMD, characterized by choroidal neovascularization. This form is more aggressive, as abnormal angiogenesis leads to disruption of the inner blood retinal barrier and bleeding and disruption of RPE and photoreceptor cells, as well as severe vision loss.

There is no known treatment for dry AMD. Intravitreal injection of Lucentis, an antibody binding to the vascular endothelial growth factor A (VEGF), is FDA-approved for the treatment of patients with wet AMD and is the current gold standard for inhibiting choroid neovascularization.

Rarely, inherited retinal diseases are caused not only by mutations in a single gene but rather multiple[18], showcasing the vast genetic and clinical heterogeneity of these groups of diseases. Mutations in different genes can lead to the same disease phenotype and different mutations in a single gene can result in different clinical phenotypes, as well as intra- or inter-familial variability: different severity of visual loss, onset and rate of progression for a same gene/mutations can be found in different members of the same family.

Gene therapy for the retina

There is currently no cure for the treatment of IRDs. Before recent progress in gene-based therapeutics, surgery and vitaminotherapy were the most common treatments employed to treat these diseases. Nowadays, gene therapy is one of the fastest growing fields of therapeutic research for treating ocular diseases and has already achieved multiple proof-of-concepts and recent commercialization for inherited diseases [27,28].

The concept behind gene therapy is the delivery of nucleic acids (DNA or RNA) directly to the affected cell to rescue or attenuate its degeneration by altering its diseased gene expression pattern. It can be applied differently based on the genetic disease and inheritance transmission. In the cases of recessive diseases, both alleles are mutated for a specific gene and triggers the complete loss of the protein; or haploinsufficiency, not enough is made to support its biological function. Supplying a copy of the unmutated gene to restore protein level close to wild-type (WT) level has enabled recovery of biological function and effective treatment of the related disease. It is referred to as “gene replacement”. On the other hand, only one allele is mutated in autosomal dominant cases, meaning that either the WT allele doesn’t make enough of the protein (haploinsuffiency) to compensate for the mutated allele, or that the resulting mutant protein is toxic or affects negatively the cells (e.g. interfering with the WT protein, creating oxidative damage for the cell...). Disruption of the expression of the mutant gene can be achieved by knockdown using either nucleases[29–31] to create DNA deletion and frameshift or using RNA interference[32–34] systems to prevent the translation and downstream translation of the mutated gene into the nonfunctional protein. This gene silencing approach can be complemented by gene replacement or augmentation.

Gene therapy is particularly well suited for the retina due to its accessibility, the ease with which the treatment can be administrated to one eye, and the outcome measured noninvasively and compared to the control eye by imaging the eye/retina using optical coherence tomography[35] (OCT) or recording electroretinogram (ERG) traces in response to a flash of light. The eye is also a pseudo-immune privileged organ, separated from the general vasculature by the blood-retina

barrier formed by RPE tight junctions, which makes it possible to deliver drugs without risk of organ off-target effects through systemic circulation.

A critical aspect of the gene therapy is the delivery vector. Although non-viral approaches have been growing (nanoparticles, lipids), the current gold standard has been using viruses as delivery vectors and most particularly adeno-associated viruses (AAV) due to their safety profile, ease of use and ability of infecting a wide-range of mammalian tissues[36] and cell types[37,38].

AAV is a small (25nm) icosahedral, nonenveloped viruses that belongs to the Parvovirus family and was initially discovered as a contaminant of adenovirus isolate. Nonpathogenic, it is able to transduce both diving and non-diving cells. It contains a single-stranded linear DNA genome with positive and negative strands packaged equally. It is composed of a *Rep* and *Cap* gene (**Fig. 5.A-B**) that encode for all the replication proteins and the capsid subunits (VP1, VP2, VP3 and AAP) respectively.

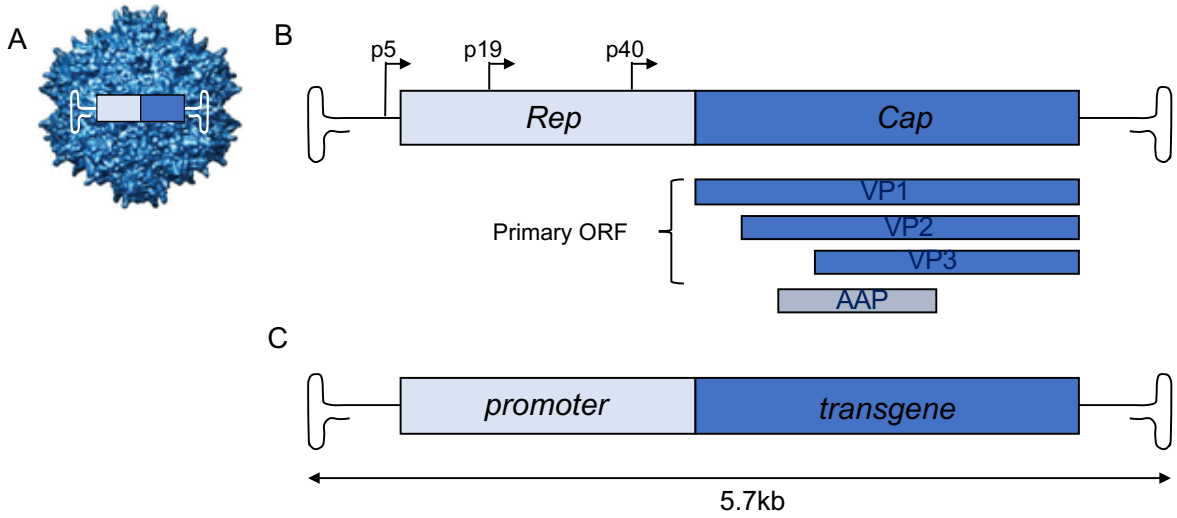

Figure 5: AAV viral genome is internalized in the capsid (**A**). It is composed of 2 main genes, *Rep* and *Cap*, which through the combination of 3 transcription start sites (black arrows showing p5, p9 and p40 viral promoters) encode for all the replication (Rep78, Rep68, Rep52 and Rep40) and the capsid (VP1, VP2, VP3 and AAP) proteins. (B) The viral genome is replaced by a transgene construct, expressing the DNA of choice under the control of a promoter (C) when engineering recombinant AAV for gene therapies.

Its p40 promoter drives expression of the VP1, VP2 and VP3 proteins that form the 60 viral subunits of the mature capsid, in a stoichiometric ratio 1:1:10, respectively. The assembly activating protein (AAP) is important for the VP subunit stability and assembly during packaging [39–41]. Interestingly, not only is VP2 the only subunit to have different translation initiation site (ACG site), but it is non-essential during packaging unlike the VP1 and VP3 subunits. Its N-terminal being exposed on the external surface of the capsid had led to many research groups taking advantages of those properties to tag peptides/ligands on the surface of AAV to twist its biological uses from more selective receptor binding or viral particle tracking[42,43].

The *rep/cap* coding region is flanked by 145bp palindromic sequences at the 3' and 5' ends with inverted terminal repeats (ITRs). These cis-active sequences fold back on themselves and form "hairpin" structures. They are critical for viral replication and DNA packaging as well as AAV's integration on the human chromosome 19 (AAV1S location), mediated by the ternary complex formation with the *rep* proteins. To generate recombinant AAVs suitable and safe for

gene therapy, the wild-type AAV structure has been modified. The *rep* and *cap* sequences, substituted with a gene of choice driven by a promoter (**Fig 5.C**), are supplied separately *in trans* along with a helper plasmid containing all necessary replication genes from adenovirus.

The ITRs[44] are the only cis-element conserved, allowing the proper packaging/internalization of the transgene into the rAAV capsid, losing the ability to integrate into the host genome[45]. Instead, the transgenes concatemerized and form extrachromosal episomes, achieving long and stable expression in non-dividing cells.

To date, thirteen serotypes and hundreds of variants have been isolated and described. Although structurally and functionally distinguishable, they share common infectivity mechanisms: the capsid first interacts with the target cell via cell surface receptor binding sites[46–49] and is then internalized through endocytosis from the cell membrane (formation of an early endosome) and trafficking to the Golgi. The virus senses a pH change and escapes from the late endosome, to travel to the nucleus where it will release its single-stranded DNA which will go under second-strand synthesis and later episomal expression.

Different serotypes differ from their ability to infect and efficiently transduce diverse tissue types, from the capsid sequence to the route of AAV administration. To target photoreceptors in the retina, the virus can be delivered either intravitreally, in the center of the vitreous cavity, or subretinally, in the RPE and the retina interspace. The latter has been the most used procedure in the clinic. AAV2, 4, and 5 can efficiently transduce RPE cells. AAV5 has a strong tropism for photoreceptors as well as AAV8 and AAV9. AAV8 and 9 can also infect Müller glia, and RPE when administered subretinally[50]. To date, over 200 gene therapy trials are in progress[51]. The positive outcome of clinical trials for RPE65-mediated gene replacement clinical trials[52,53] led to the first US regulatory approval[54] of an AAV-mediated gene therapy, Luxterna (Spark Therapeutics), giving hope for other gene therapies for inherited retinal degeneration in the clinical pipeline such as Choroideremia, achromatopsia and X-linked Retinoschisis [55].

Despite the tremendous potential for curing genetic diseases, challenges both from the gene therapy approach and the genetic heterogeneity in between IRDs aspect emerged. Wild-type AAVs' 1) limited tropism depending on the route of delivery, 2) slow gene expression onset, 3) immune recognition from the host cell due to pre-existing humoral immunity to the capsid as well as a 4) limited cargo (~5kb) challenge its use for a large portion of disease indications[56]. In response, novel AAV variants were engineered and therapeutic transgenes optimized to tackle those issues. Growing knowledge of the viral genome, more particularly capsid structure-function, allowed the rational modification of specific amino acid residues. For example, mutations of specific tyrosine residues[57–59] were shown to help escape capsid ubiquitination during cell infection and expanded the tropisms and efficiency of AAV2, AAV8 in the retina and AAV9 in the CNS when injected intravenously. Furthermore, development of novel AAV capsids by random mutagenesis (error prone, peptide insertion at different capsid loop position, different serotype capsid sequence shuffling)[60,61] and *in vivo* high-throughput screening enable the isolation and characterization of efficient capsid variants for a desirable cell type such as 7m8[62], an AAV2-based 7mer variant with increased tropisms from the vitreous for all retinal cell type, or ShH10[63,64], an AAV6 error prone variant with increased capsid tropism for muller glia from the vitreous. These novel AAVs could possibly one day substitute naturally occurring serotypes in the future and are currently evaluated in several preclinical and clinical studies.

Self-complementary AAV (scAAV) vectors[65–67] were also engineered by mutating one of the ITRs flanking the transgene, circumventing the use of single-stranded vectors, to speedup

transgene expression. While achieving faster and higher level of transgene expression in many animal models, its use is restricted to a limited number of applications based on size, as only ~2.4 to 3.3 kilobase pairs can be packaged. The small carrying capacity of AAV excludes its application for large genes. Packaging oversized AAVs (>5kb) has led to both a decrease in yield and truncation of transgene. A dual vector strategy emerged, where the transgene cassette is split in two separate halves with different recombination mechanisms to reconstitute the full-length transgene upon the dual-AAVs[68,69] coinfecting the same cells. While promising, the efficiency and safety profile of these systems still remains lower in comparison to single AAV delivery.

Preexisting and adaptive immune responses to the AAV capsid and transgene has been learned the hard way, specifically with liver diseases such as Hemophilia and organs exposed to the blood circulation. With early child-hood exposure, over 70% of people are seropositive for one or more serotype and possess pre-existing neutralizing and circulating antibodies[70] that will trigger the clearance of the AAV vectors and/the infected cells. Moreover, it has been shown that cis-AAV regulatory and transgene sequences can elicit toxicity[64,] or an immune response [72]in many animal models and clinical trials. It highlights that the choice of AAV serotype as well as vector (ubiquitous or specific promoter) are critical when designing a successful gene therapy for inherited retinal degenerations.

My dissertation explores the use and optimization of engineering adeno-associated viral vectors to design novel gene therapy treatments targeting progressive degenerative diseases such as retinitis pigmentosa, for which the underlying causative mutations are unknown or found outside of the canonical coding sequence, such as noncoding regions or in the mitochondria DNA.

In **chapter 2**, we explored natural tropisms for Müller glia cells (MGCs) of the 7m8 and ShH10 variants, and designed vectors with strong and MGC restricted expression. We reviewed in **chapter 3** current mutation-independent strategies applied to counter progressive degeneration in RP patients. We highlighted treatment options that are relevant to early stages, such as secretion of neuroprotective factors as well as blockage of cell death pathways in mutated photoreceptors. While both stand-alone strategies have shown therapeutic effect, we uniquely designed a combination therapy that is pathway and cell-specific as well as non-invasive. We demonstrated in **chapter 4** that AAV-mediated secretion of glial-derived neurotrophic factor in MGCs in combination with an anti-apoptotic factor in photoreceptor cells, leads to a synergistic effect in rd10 mice, a developmental model of retinitis pigmentosa.

Recent studies have shed light on mitochondria involvement in inherited retinal degeneration, beyond its primary metabolic role. However, current tools do not allow for selective targeting in vivo, and has only been achieved efficiently in ganglion cells, one of the easiest layers to transduce from the vitreous. In **chapter 5**, we optimized and created an AAV-toolbox for efficient inner and outer retina mitochondria targeting to better investigate the organelle's role and potential gene candidates for novel mutation independent strategies. Lastly, we explored in **chapter 6** the effect of noncoding regions, which could explain the remaining 20-25% of undiagnosed cases of IRDs. We studied the impact of mutations in the untranslated region of the NMNAT1 gene in vitro and engineered mouse models of LCA.

Together these studies help to address the unmet need of developing treatment strategies for undiagnosed and noncanonical mutations that lead to inherited retinal degenerations.

References

1. Nickells, R. W. The First Steps in Seeing. *Arch. Ophthalmol.* (2012). doi:10.1001/archopht.117.4.550
2. Ryan, S. J., Hinton, D. R., Schachat, A. P. & Wilkinson, C. P. *Retina: Fourth Edition*. *Retina: Fourth Edition* (2005). doi:10.1016/C2009-1-59310-0
3. Wright, A. F., Chakarova, C. F., Abd El-Aziz, M. M. & Bhattacharya, S. S. Photoreceptor degeneration: Genetic and mechanistic dissection of a complex trait. *Nature Reviews Genetics* (2010). doi:10.1038/nrg2717
4. Korenbrot, J. I. Speed, sensitivity, and stability of the light response in rod and cone photoreceptors: Facts and models. *Progress in Retinal and Eye Research* (2012). doi:10.1016/j.preteyeres.2012.05.002
5. Rodieck, R. W. The First Steps in Seeing. *Arch. Ophthalmol.* (1999). doi:10.1001/archopht.117.4.550
6. Saari, J. C. Vitamin A Metabolism in Rod and Cone Visual Cycles. *Annu. Rev. Nutr.* (2012). doi:10.1146/annurev-nutr-071811-150748
7. Boughman, J. A. & Fishman, G. A. A genetic analysis of retinitis pigmentosa. *Br. J. Ophthalmol.* (1983). doi:10.1136/bjo.67.7.449
8. Koch, K.-W. & Dell'Orco, D. Protein and Signaling Networks in Vertebrate Photoreceptor Cells. *Front. Mol. Neurosci.* (2015). doi:10.3389/fnmol.2015.00067
9. Moiseyev, G., Chen, Y., Takahashi, Y., Wu, B. X. & Ma, J. -x. RPE65 is the isomerohydrolase in the retinoid visual cycle. *Proc. Natl. Acad. Sci.* (2005). doi:10.1073/pnas.0503460102
10. DeVries, S. H., Li, W. & Saszik, S. Parallel Processing in Two Transmitter Microenvironments at the Cone Photoreceptor Synapse. *Neuron* **50**, 735–748 (2006).
11. Sanes, J. R. & Masland, R. H. The Types of Retinal Ganglion Cells: Current Status and Implications for Neuronal Classification. *Annu. Rev. Neurosci.* **38**, 221–246 (2015).
12. Graham, D. M. & Wong, K. Y. *Melanopsin-expressing, Intrinsically Photosensitive Retinal Ganglion Cells (ipRGCs)*. *Webvision: The Organization of the Retina and Visual System* (1995).
13. Thoreson, W. B. & Mangel, S. C. Lateral interactions in the outer retina. *Progress in Retinal and Eye Research* (2012). doi:10.1016/j.preteyeres.2012.04.003
14. Chaya, T. *et al.* Versatile functional roles of horizontal cells in the retinal circuit. *Sci. Rep.* **7**, 1–15 (2017).
15. Poche, R. A. & Reese, B. E. Retinal horizontal cells: challenging paradigms of neural development and cancer biology. *Development* (2009). doi:10.1242/dev.033175
16. Masland, R. H. The tasks of amacrine cells. *Visual Neuroscience* (2012). doi:10.1017/S0952523811000344
17. Lev, S. Molecular aspects of retinal degenerative diseases. *Cellular and Molecular Neurobiology* (2001). doi:10.1023/A:1015183500719
18. Bravo-Gil, N. *et al.* Unravelling the genetic basis of simplex Retinitis Pigmentosa cases. *Sci. Rep.* **7**, 41937 (2017).
19. Goodwin, S., McPherson, J. D. & McCombie, W. R. Coming of age: Ten years of next-generation sequencing technologies. *Nature Reviews Genetics* (2016). doi:10.1038/nrg.2016.49

20. Daiger, S. P., Sullivan, L. S. & Bowne, S. J. RetNet. *Retinal Information Network* (2017).
21. Ferrari, S. *et al.* Retinitis Pigmentosa: Genes and Disease Mechanisms. *Curr. Genomics* **12**, 238–249 (2011).
22. Hartong, D. T., Berson, E. L. & Dryja, T. P. Retinitis pigmentosa Prevalence and inheritance patterns. *Lancet* (2006).
23. Hamel, C. Retinitis pigmentosa Disease name. *Orphanet J. Rare Dis.* (2006).
24. Li, Z. Y., Possin, D. E. & Milam, A. H. Histopathology of Bone Spicule Pigmentation in Retinitis Pigmentosa. *Ophthalmology* (1995). doi:10.1016/S0161-6420(95)30953-0
25. Tsang, S. H. & Sharma, T. Leber congenital amaurosis. in *Advances in Experimental Medicine and Biology* (2018). doi:10.1007/978-3-319-95046-4_26
26. Deangelis, M. M., Silveira, A. C., Carr, E. A. & Kim, I. K. Genetics of age-related macular degeneration: current concepts, future directions. *Semin. Ophthalmol.* **26**, 77–93 (2011).
27. Rodrigues, G. A. *et al.* Pharmaceutical Development of AAV-Based Gene Therapy Products for the Eye. *Pharm. Res.* **36**, (2019).
28. FDA. FDA approves novel gene therapy to treat patients with a rare form of inherited vision loss.
29. Yu, W. & Wu, Z. In Vivo Applications of CRISPR-Based Genome Editing in the Retina. *Front. Cell Dev. Biol.* (2018). doi:10.3389/fcell.2018.00053
30. Meissner, T. B., Mandal, P. K., Ferreira, L. M. R., Rossi, D. J. & Cowan, C. A. Genome editing for human gene therapy. in *Methods in Enzymology* (2014). doi:10.1016/B978-0-12-801185-0.00013-1
31. Gammage, P. A., Moraes, C. T. & Minczuk, M. Mitochondrial Genome Engineering: The Revolution May Not Be CRISPR-Ized. *Trends in Genetics* (2018). doi:10.1016/j.tig.2017.11.001
32. Bagasra, O. & Prilliman, K. R. RNA interference: The molecular immune system. in *Journal of Molecular Histology* (2004). doi:10.1007/s10735-004-2192-8
33. Zetsche, B. *et al.* Cpf1 Is a Single RNA-Guided Endonuclease of a Class 2 CRISPR-Cas System. *Cell* (2015). doi:10.1016/j.cell.2015.09.038
34. Qi, L. S. *et al.* Repurposing CRISPR as an RNA-γuided platform for sequence-specific control of gene expression. *Cell* (2013). doi:10.1016/j.cell.2013.02.022
35. Zeng, Y. *et al.* Retinal structure and gene therapy outcome in retinoschisin-deficient mice assessed by spectral-domain optical coherence tomography. *Investig. Ophthalmol. Vis. Sci.* (2016). doi:10.1167/iovs.15-18920
36. Carter, B. J. Adeno-Associated Virus Vectors in Clinical Trials. *Hum. Gene Ther.* (2005). doi:10.1089/hum.2005.16.541
37. Watanabe, S. *et al.* Tropisms of AAV for Subretinal Delivery to the Neonatal Mouse Retina and Its Application for In Vivo Rescue of Developmental Photoreceptor Disorders. *PLoS One* (2013). doi:10.1371/journal.pone.0054146
38. Muzyczka, N. Use of Adeno-Associated Virus as a General Transduction Vector for Mammalian Cells. in (1992). doi:10.1007/978-3-642-75608-5_5
39. Maurer, A. C. *et al.* The Assembly-Activating Protein Promotes Stability and Interactions between AAV's Viral Proteins to Nucleate Capsid Assembly Specific capsid residues at trimer interface influence dependence on AAP. *Cell Rep.* **23**, (2018).
40. Sonntag, F. *et al.* The Assembly-Activating Protein Promotes Capsid Assembly of Different Adeno-Associated Virus Serotypes. *J. Virol.* (2011). doi:10.1128/JVI.05359-11

41. Naumer, M. *et al.* Properties of the Adeno-Associated Virus Assembly-Activating Protein. *J. Virol.* (2012). doi:10.1128/jvi.01675-12
42. Lux, K. *et al.* Green fluorescent protein-tagged adeno-associated virus particles allow the study of cytosolic and nuclear trafficking. *J. Virol.* **79**, 11776–87 (2005).
43. Warrington, K. H. *et al.* Adeno-Associated Virus Type 2 VP2 Capsid Protein Is Nonessential and Can Tolerate Large Peptide Insertions at Its N Terminus †. *J. Virol.* **78**, 6595–6609 (2004).
44. Yan, Z., Zak, R., Zhang, Y. & Engelhardt, J. F. Inverted Terminal Repeat Sequences Are Important for Intermolecular Recombination and Circularization of Adeno-Associated Virus Genomes. *J. Virol.* (2005). doi:10.1128/jvi.79.1.364-379.2005
45. Johnson, J. S. & Samulski, R. J. Enhancement of Adeno-Associated Virus Infection by Mobilizing Capsids into and Out of the Nucleolus. *J. Virol.* (2009). doi:10.1128/jvi.02309-08
46. Wu, Z., Miller, E., Agbandje-McKenna, M. & Samulski, R. J. 2,3 and 2,6 N-Linked Sialic Acids Facilitate Efficient Binding and Transduction by Adeno-Associated Virus Types 1 and 6. *J. Virol.* (2006). doi:10.1128/jvi.00895-06
47. Xiao, P.-J. & Samulski, R. J. Cytoplasmic trafficking, endosomal escape, and perinuclear accumulation of adeno-associated virus type 2 particles are facilitated by microtubule network. *J. Virol.* **86**, 10462–73 (2012).
48. Grimm, D. & Büning, H. Small But Increasingly Mighty: Latest Advances in AAV Vector Research, Design, and Evolution. *Hum. Gene Ther.* **28**, 1075–1086 (2017).
49. Summerford, C. & Samulski, R. J. AAVR: A multi-serotype receptor for AAV. *Molecular Therapy* (2016). doi:10.1038/mt.2016.49
50. Martin, K. R. G., Klein, R. L. & Quigley, H. A. Gene delivery to the eye using adeno-associated viral vectors. *Methods* (2002). doi:10.1016/S1046-2023(02)00232-3
51. Https://clinicaltrials.gov. Https://ClinicalTrials.gov. *U.S. National Institutes of Health* (2016).
52. Pierce, E. A. & Bennett, J. The status of RPE65 gene therapy trials: Safety and efficacy. *Cold Spring Harb. Perspect. Med.* (2015). doi:10.1101/cshperspect.a017285
53. Cideciyan, A. V. *et al.* Human retinal gene therapy for Leber congenital amaurosis shows advancing retinal degeneration despite enduring visual improvement. *Proc. Natl. Acad. Sci.* (2013). doi:10.1073/pnas.1218933110
54. Ameri, H. Prospect of retinal gene therapy following commercialization of voretigene neparvovec-rzyl for retinal dystrophy mediated by RPE65 mutation. *Journal of Current Ophthalmology* (2018). doi:10.1016/j.joco.2018.01.006
55. Fu, X. *et al.* Clinical applications of retinal gene therapies. *Precis. Clin. Med.* **1**, 5–20 (2018).
56. Colella, P., Ronzitti, G. & Mingozzi, F. Emerging Issues in AAV-Mediated In Vivo Gene Therapy. *Mol. Ther. Methods Clin. Dev.* **8**, 87–104 (2018).
57. Dalkara, D. *et al.* Enhanced gene delivery to the neonatal retina through systemic administration of tyrosine-mutated AAV9. *Gene Ther.* (2012). doi:10.1038/gt.2011.163
58. Zhong, L. *et al.* Next generation of adeno-associated virus 2 vectors: Point mutations in tyrosines lead to high-efficiency transduction at lower doses. *Proc. Natl. Acad. Sci.* (2008). doi:10.1073/pnas.0802866105
59. Petrs-Silva, H. *et al.* High-efficiency transduction of the mouse retina by tyrosine-mutant AAV serotype vectors. *Mol. Ther.* (2009). doi:10.1038/mt.2008.269

60. Bartel, M. A., Weinstein, J. R. & Schaffer, D. V. Directed evolution of novel adeno-associated viruses for therapeutic gene delivery. *Gene Therapy* (2012). doi:10.1038/gt.2012.20
61. Koerber, J. T., Jang, J. H. & Schaffer, D. V. DNA shuffling of adeno-associated virus yields functionally diverse viral progeny. *Mol. Ther.* (2008). doi:10.1038/mt.2008.167
62. Dalkara, D. *et al.* In vivo-directed evolution of a new adeno-associated virus for therapeutic outer retinal gene delivery from the vitreous. *Sci. Transl. Med.* (2013). doi:10.1126/scitranslmed.3005708
63. Klimczak, R. R., Koerber, J. T., Dalkara, D., Flannery, J. G. & Schaffer, D. V. A novel adeno-associated viral variant for efficient and selective intravitreal transduction of rat Müller cells. *PLoS One* (2009). doi:10.1371/journal.pone.0007467
64. Koerber, J. T. *et al.* Molecular evolution of adeno-associated virus for enhanced glial gene delivery. *Mol. Ther.* (2009). doi:10.1038/mt.2009.184
65. McCarty, D. M., Monahan, P. E. & Samulski, R. J. Self-complementary recombinant adeno-associated virus (scAAV) vectors promote efficient transduction independently of DNA synthesis. *Gene Ther.* (2001). doi:10.1038/sj.gt.3301514
66. McCarty, D. M. Self-complementary AAV vectors; advances and applications. *Molecular Therapy* (2008). doi:10.1038/mt.2008.171
67. Wu, J. *et al.* Self-Complementary Recombinant Adeno-Associated Viral Vectors: Packaging Capacity And The Role of Rep Proteins in Vector Purity. *Hum. Gene Ther.* (2007). doi:10.1089/hum.2006.088
68. Chamberlain, K., Riyad, J. M. & Weber, T. Expressing Transgenes That Exceed the Packaging Capacity of Adeno-Associated Virus Capsids. *Hum. Gene Ther. Methods* (2016). doi:10.1089/hgtb.2015.140
69. Trapani, I. *et al.* Effective delivery of large genes to the retina by dual AAV vectors. *EMBO Mol. Med.* (2014). doi:10.1002/emmm.201302948
70. Calcedo, R. *et al.* Adeno-Associated Virus Antibody Profiles in Newborns, Children, and Adolescents. *Clin. Vaccine Immunol.* 18, 1586 (2011).
71. Xiong, W. *et al.* AAV cis -regulatory sequences are correlated with ocular toxicity . *Proc. Natl. Acad. Sci.* (2019). doi:10.1073/pnas.1821000116
72. Mingozzi, F. & A. High, K. Immune Responses to AAV in Clinical Trials. *Curr. Gene Ther.* (2011). doi:10.2174/156652311796150354

Chapter 2: AAV-mediated targeting of Müller Glia in Health and Disease Retina

Abstract

Müller glia-based gene therapies hold promise to alleviate or cure many retinal degenerative disorders including retinitis pigmentosa and macular degenerations. Adeno-associated virus (AAV) is currently the standard vector for gene delivery with strong clinical proof-of-concept for eye therapies. However, selective AAV-mediated transduction of Müller glia remained difficult until the development of novel AAV variants, 7m8 and ShH10. Both variants can transduce Müller glia from the vitreous, with different tropism profiles but specificity is still a challenge and must be overcome to prevent off-target effects depending on the therapeutic application. In this study, we show that selective glial expression requires specific promoters to restrict off-target expression. We evaluated the tropism of 7m8 and ShH10 for glia with either a ubiquitous promoter CAG, or glial-specific promoters GLAST and gfaABC1D driving eGFP expression in wildtype and *rd10* mice.

While ShH10 had preferential tropism for Müller glia compared to 7m8, it displayed patchy expression along the vasculature. 7m8 was able to reach and efficiently transduce Müller glia pan-retinally but not selectively. Evaluating promoters, we found the short GfaABC1D (688bp) promoter drove strong and restricted expression in Müller glia, as opposed to the GLAST promoter (2.2kb), which showed significant ganglion off-target expression. Transcription factor binding site analysis confirmed promoter tropism, with a higher number of conserved glia specific transcription factor binding motifs found in the Gfa_{ABC1D} promoter compared to its full-length promoter (2.2kb). Changes in Müller glia during degeneration did not affect the tropism pattern of the different vectors tested, but the efficiency of transduction was lower in the degenerated retina, showing an alteration in glial capsid-cell receptor binding.

Introduction

Müller glia cells (MGC) are the most predominant type of glia cell found in the retina, among astrocytes and microglia. Similar to glial function in the brain, they serve as a support cells for neurons but also foster communication between retinal cells due to its architectural morphology: they span the retina radially and their endfeet contribute to the inner limiting membrane (ILM), a basement membrane made of extracellular matrix proteins. Their cell bodies sit in the inner nuclear layer (INL) and the processes are in contact with other neuron cell bodies and processes in the nuclear and plexiform layers, respectively. From developmental to therapeutic approaches, MGCs have been a critical cell type to dissect its functional roles in both the developing and mature as well as healthy and diseased retina.

MGCs have a major role in the maturation of the neural circuit in murine retinas, responding to transient flux[1,2] occurring pre-light stimulation. Recent studies also shed light on the role of MGCs in the non-canonical cone visual cycle when the absorption of photons by visual pigment within the cone photoreceptor outer segment leads to photoisomerization of 11-*cis*-retinal to all-*trans*-retinal. The all-*trans*-retinal is then exported from the photoreceptor to the retinal pigment epithelium (RPE) and Müller glia through the retinaldehyde-binding protein, CRALBP, and then returned to the photoreceptors as 11-cis-retinal[3].

In the past few years, MGCs have emerged as a promising therapeutic cell target to treat inherited and age-related retinal degenerations. Many reports confirm the ability of MGCs to confer neuroprotection to the diseased retina. Most inherited retinal diseases majorly affect rod and cone photoreceptors (95% of mutations in over 300 different genes) as well as the RPE layer, with progressive cell atrophy leading to progressive blindness. While photoreceptors die in the first stage of the disease, Müller glia cells survive throughout the retinal degeneration and respond to retinal injury in a variety of ways such as secreting neurotrophic factors like CNTF[4], GDNF[5], and BDNF[6]. MGC mediated-overexpression of these factors led to promising results [7–10] in delaying photoreceptor cell death, with CNTF intraocular implants currently in clinical trials[11,12]. This therapeutic option is attractive for early degeneration stages since it can be applied to phenotypically related diseases regardless of the underlying genetic mutation. A similar approach has been applied to wet age-related macular degeneration characterized by choroidal neovascularization following the loss of RPE and photoreceptors. While the current gold standard treatment involves intraocular injection of FDA-approved anti-vascular endothelial growth factor A (VEGF-A) antibody protein, overexpression of genetically encoded anti-VEGF-A[13] and anti-angiogenic factors[14] in MGCs shows promise in preventing neovascularization.

Lastly, MGCs also hold regenerative properties. Under injury, in species such as zebrafish, MGCs possess the capacity to transdifferentiate into photoreceptors and other retinal cells[15,16]. It has been then extrapolated that similar progenitor cell-like mechanisms could be applied to the injured mammal retina, especially in patients at a later retinal degenerative stage, wherein the original photoreceptor cell layer is lost. Given these supportive and regenerative roles, MGCs represent an attractive target for novel therapies.

However, these approaches require tools able to selectively reach MGCs. The field of gene therapy for inherited retinal degeneration has emerged in the past decade with the ability to efficiently target and deliver therapeutic DNA to specific cells. Adeno-associated viral (AAV) vectors are among the most promising delivery mechanisms, with FDA approval of one AAV-based gene therapy in the retina[17] and many other clinical trials currently underway[11]. The classic route of delivery for retinal gene therapy has been a subretinal injection, with diffusion of AAV particles in an enclosed retina/RPE subspace, to achieve increased transduction efficiency. However, this method leads to frequent complications in the clinic, such as retinal detachment, recurrence of vitreous and submacular hemorrhages, and postoperative development of CNV[18]. Intravitreal injections, while on the other hand safer, encounter physical challenges such as AAV penetration through retinal barriers like the inner limiting membrane (ILM), a meshwork of extracellular matrix proteoglycans located between the ganglion cell layer and vitreous.

AAV-mediated glial targeting from the vitreous was challenging. Limitations included the natural infectivity of rAAV serotypes to cross, which is mostly dictated by AAV cell surface receptor binding site preference. AAV2/6 was shown to be the most effective at infecting rat Müller cells (22% of all cells infected)[19]. The engineering of a novel viral variant through directed evolution[20] tackles both the pan-retinal penetration limitation as well as achieving a high level of MGC transduction. The 7m8 variant, based from AAV2, has a broad tropism and can infect any retinal cell[21], while ShH10, based from AAV6, showed high specificity for MGCs, and still low transduction in other retinal cells[22]. However, while both variants can efficiently transduce MGCs, specificity remains a challenge. In this study, we evaluated the tropism of 7m8 and ShH10 for glia as well as the use of previously uncharacterized CNS glial promoters driving eGFP expression in wildtype and *rd10* retina to identify the best AAV capsid/transgene approach to high levels and selective transduction of MGCs.

Results

Intravitreal injections of 7m8 and ShH10 both effectively infect MGCs

Until the development of the 7m8 and ShH10 AAV variants, MGC transduction from the vitreous was achieved with low transduction efficiency and selectively[21,22]. In order to evaluate both vectors' natural tropism for MGCs and other retinal cells, eGFP under the under the control of the ubiquitous CAG promoter was packaged with each variant and intravitreally injected into the eyes of 2-month old adult C57Bl6J mice.

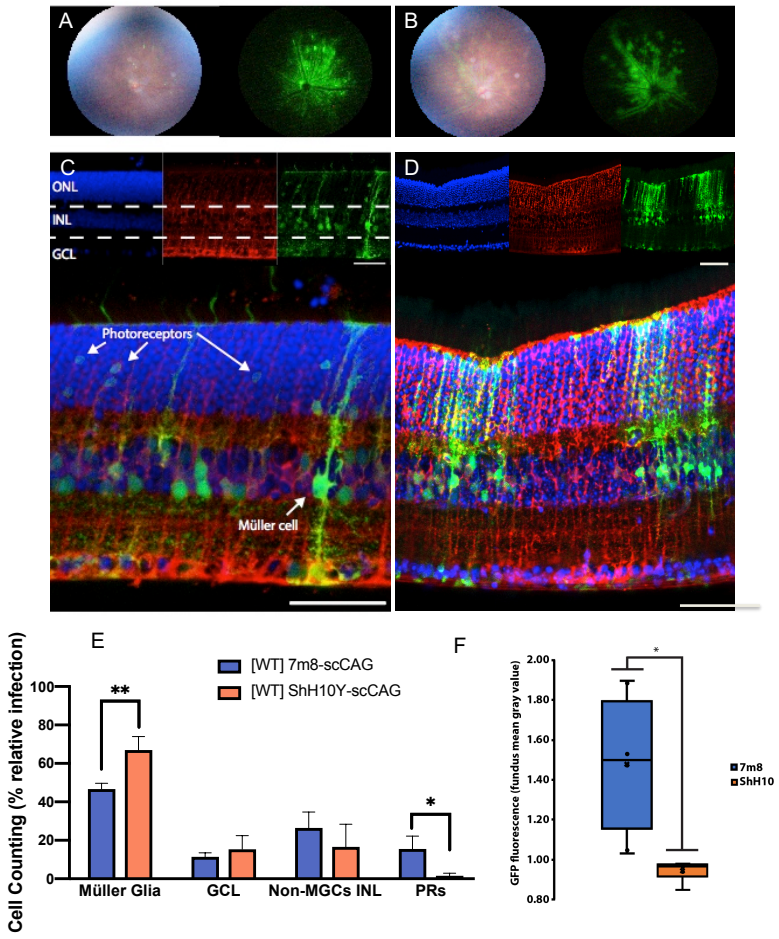

Figure 1: 7m8 and ShH10 infect Müller glia and other retinal cell types from the vitreous. Expression profiles of 7m8 and ShH10 were established by packaging eGFP under the ubiquitous CAG promoter into both virus capsids and evaluating retinal fluorescence. Eye fundus images from 7m8 (**A**) and ShH10 (**B**) intravitreally injected in adult C57Bl6J eyes showed panretinal eGFP (green) expression (left).. Sections from 7m8 (**C**) and ShH10 (**D**) injected eyes were used to identify cell types for quantification (**E**). Retinal cell layers were determined by DAPI staining (blue) and eGFP^{+} cells (green) were identified as Müller cells based on co-labeling with GS (red). Both viruses were able to infect all retinal layers. ShH10 infected significantly more Müller cells than 7m8. Data represent the mean ± SD. **=$p < 0.01$, *=$p<0.05$ by 2-way Anova, tukey's multiple comparisons test. Quantification of eGFP fluorescence (**F**) from fundus images (n=10) from 7m8 and ShH10 infected eyes imaged at identical light intensities (*=$p>0.05$) by unpaired student t-test. The scales bar represents 50 µm.

One-month post-injection, fundus imaging (**Fig1.A-B**) showed widespread eGFP expression stemming from the optic nerve head spreading out towards the periphery. Quantification of fluorescence by fundus imaging showed that 7m8 achieved significantly greater transgene expression than ShH10 (**Fig1.F**). While both serotypes show the greatest eGFP expression along the retinal vasculature, eGFP expression was more restrained to blood vessel areas with ShH10 than for 7m8. The cell bodies of the MGCs lay in the inner nuclear layer (INL) with the cell bodies of amacrine cells, bipolar cells, and horizontal cells. Both viruses primarily infected cells in the INL at the similar rates (>~70% of the cells infected). We used a glia marker, glutamine synthetase (GS), to identify MGCs. MGC bodies are radial and span the entire retina with irregularly shaped somas (**Fig1.C&D**). Counter staining with PKCα illuminates the oblong bipolar cells closer to the ONL and to a lesser extent amacrine cells whose round somas are closer to the GCL (**Supplemental S1.A-B**). ShH10 displayed a significantly greater MGC tropism than 7m8, with MGCs being 67.0 ± 7.4% of the cells infected by ShH10, while 46.7 ± 3.0% of the cells 7m8 infected were MGCs (p=0.017, **Fig1.C-E**). Of the remaining non-Müller INL, predominately amacrine cells were infected followed by bipolar cells. In our study, ShH10 had a high level of off-target in those cells (16.7 5 ± 9.2) of infected cells. 7m8 also significantly (15.7 ± 6.7,) infected higher rate of photoreceptors than ShH10 (1.5 ±1.4%, p=0.05).

Based on the fraction of cell type infected ShH10 displayed preferential capsid tropism for MGCs, however, 7m8 achieved overall greater retinal infection, with pan-retinal penetration instead of ShH10-restricted expression along the vasculature. Therefore, 7m8 might infect as many if not more MGCs, although non-selectively.

Physical and transcriptional alterations in the rd10 degenerative model affect AAV infectivity

Most viral vector and variant characterizations are primary performed in healthy retinas, but therapeutic use will be in a diseased tissue at different stages of degeneration. In addition to the loss of the photoreceptor layer observed in mid-stages, there is also profound physical and transcriptional remodeling of the remaining cells in degenerative retinas. Viral serotype infectivity as well as promoter tropism can be affected by the retinal remodeling happening in the inner retina and MGCs[23,24]. The *rd10* mouse degeneration model, is commonly used as a developmental model of degeneration to assess changes in transcription, expression and transduction in retinal disease. In this model, a mutation in exon 13 of the beta subunit of rod phosphodiesterase[25] slowly triggers the loss of rod photoreceptors; closely mimicking the human disease, retinitis pigmentosa (RP). Ninety days after degeneration plateau is achieved, only a thin layer of degenerating cone photoreceptors persists in the ONL.

Key MGC transcripts associated with homeostatic and immune activities are upregulated in the *rd10* mice compared to age-matched WT mice (**Fig 2.A**). Following progressive loss of rod photoreceptors, with already 2-fold downregulation of *RHO* by P20 in the *rd10* compared to WT to complete loss in *rd10* by P85, all MGC markers including the glutamate-aspartate transporter (*GLAST*), and glial fibrillary acidic protein (GFAP) transcripts are significantly elevated in P85 and P360 *rd10* (~2-fold and 4-fold compared to WT retina, respectively). GS is slightly upregulated in the *rd10* retinas but remains at constant transcription levels throughout degeneration.

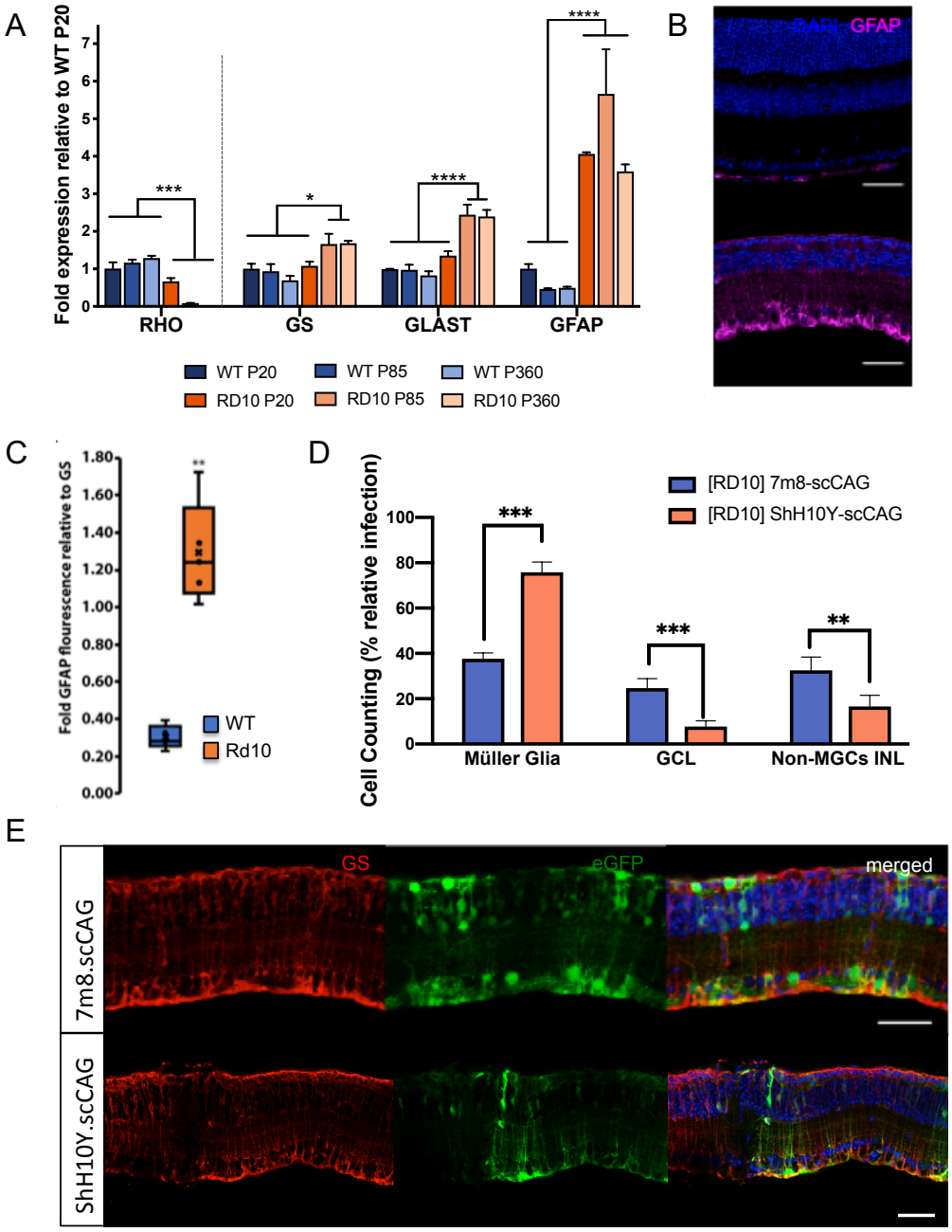

Figure 2: Physical and transcriptional alterations in the *rd10* degenerate model affect 7m8 and ShH10 retinal infectivity. The *rd10* mouse retinal degeneration model gradually degenerates after eye opening at P15. (**A**) RT-qPCR analysis from RNA extracted from wildtype and *rd10* retinas at P20, P85, and P360 (normalized to GAPDH). Data represent the mean ± SD. 2way Anova, Dunnett's multiple comparisons test was performed. (**B**) P60 retinas from wildtype (top) and *rd10* (below). The remnants of the ONL is a single layer of DAPI labeled nuclei (blue) above the INL. GFAP staining (magenta) increases upon degeneration. (**C**) Quantification of B. 2way Anova, Dunnett's multiple comparisons test was performed. (**D**) Quantification of cell counting in 7m8- and ShH10-CAG-eGFP sections. 2way Anova, Sidak's multiple comparisons statistical analysis was performed. (**E**), which were stained with GS (red) to localize MGCs and DAPI (blue) to identify retinal layers. The scale bars represent 50 µm. For all statistical test, ***=p<0.001, **=p < 0.01, *=p<0.05. . Data represent the mean ± SD.

GFAP is not expressed at high levels in the mature retina, except during developmental stages. Although astrocytes are the primary cell type to express GFAP in the retina, the intermediate filament's expression is greatly increased[26] in reactive MGCs during degeneration[26,27]. GFAP-staining in P60 *rd10* retinas was stronger, and showed protein penetration towards the outer retina, compared to WT retinas (~3-fold less GFAP protein) with the majority of staining localized within the GCL (**Fig 2.B-C**).

Loss of the photoreceptor layer during degeneration induces not only retinal architectural restructuring but also cell surface receptor and transcriptional changes that affect AAV infectivity in individual cells. Molecular changes on the MGC surface as well as state of reactivity may affect serotype infectivity through upregulation of the intermediate GFAP, which is associated with glial scar production and hardening of the ILM[28,29]. 7m8 and ShH10's ability to intravitreally infect MGCs and other retinal cells was evaluated in the *rd10* degeneration model (**Fig 2.D-F**).

Unsurprisingly, 7m8-mediated ONL transduction decreased, as a result of photoreceptors loss. Occasional lingering cone photoreceptors were infected at low rates (5.4 ± 1.4% of $eGFP^+$ cells) for 7m8. No photoreceptors were infected by ShH10. 7m8 displayed reduced MGC infection compared to WT retinas (37.5 ± 2.6% vs 46.7± 3%, respectively; **Fig 2. D-E**). Instead, high infection rates were observed for the GCL and in other INL cells (24.6 ± 4.2% and 32.44 ± 6%, respectively).

On the other hand, ShH10 maintained a similar ratio of MGCs infected (75.0 ± 5% vs 67 ± 7% in *rd10* versus WT retinas; **Fig 2.D-F**), significantly superior to 7m8 (p <0.0001). Infectivity in the INL (amacrine and bipolar cells) remained similar than in WT retinas (~16 ± 5%). Lower infectivity in ganglion cells was noticed, although not significant compared to WT (8 ± 2.5% vs 15 ± 7.0%, respectively). A decrease in overall transduction levels was observed with both vectors in injected *rd10* retinas compared to WT, with similar titer.

The GLAST and Gfa_{ABC1D} promoters improve Müller cell specificity

As previously shown, although 7m8 and ShH10 mediate high transgene levels in MGC transduction, none of the viral variants enable selective and restrictive expression. Moreover, we as well as other research groups (**Supplemental S3**) found increased ShH10 off-target in retinas where degeneration was chemically induced, with higher levels of photoreceptor and ganglion cell targeting. Although it might have a minor effect for some therapeutic applications (e.g., neurotrophic secretion), others require full-selectivity, such as the expression of transcription factors to achieve trans- or dedifferentiation after stimulating MGCs with induced-retinal injuries[30]. Not only this but studies have reported that ubiquitous promoters increase transgene-induced ocular toxicity [31,32].

Taking advantage of GFAP and GLAST up regulation of MGCs in degenerative retinas, we investigated both a previously established human promoter in the CNS, the putatively glia-selective truncated GFAP called Gfa_{ABC1D} as well as 2.1kb GLAST promoter.

GLAST is only expressed in MGCs[33,34] and astrocytes. Previously, an engineered GLAST1-Cre mouse achieved glia specific expression[35] but with an integral genomic sequence used. The 2.1kb GLAST promoter drove high levels of expression in MGCs when either delivered by 7m8 or ShH10Y in both WT and *rd10* mice. The promoter eliminated all ONL expression and significantly limited INL expression to MGCs. While MGCs were by far the most commonly infected cell by 7m8 and ShH10Y in healthy (83.0 ± 5.8% vs. 84.3 ± 3.8%) and diseased retinas

(67.1 ± 4.8% vs 79.3 ± 5.8%, respectively; **Fig 3.I**). Unexpectedly, ganglion cells were also transduced comprising 13.0 ± 3.6% of cells infected by 7m8 and 13.7 ± 2.0% for ShH10 (**Fig 3.A,C,I**) in wildtype. In the *rd10* degenerative model, ganglion cell off-targeting rose to 30.4 ± 2.6% for 7m8 and 19.2 ± 6.9% for ShH10 (**Fig 3.B,D,I**).

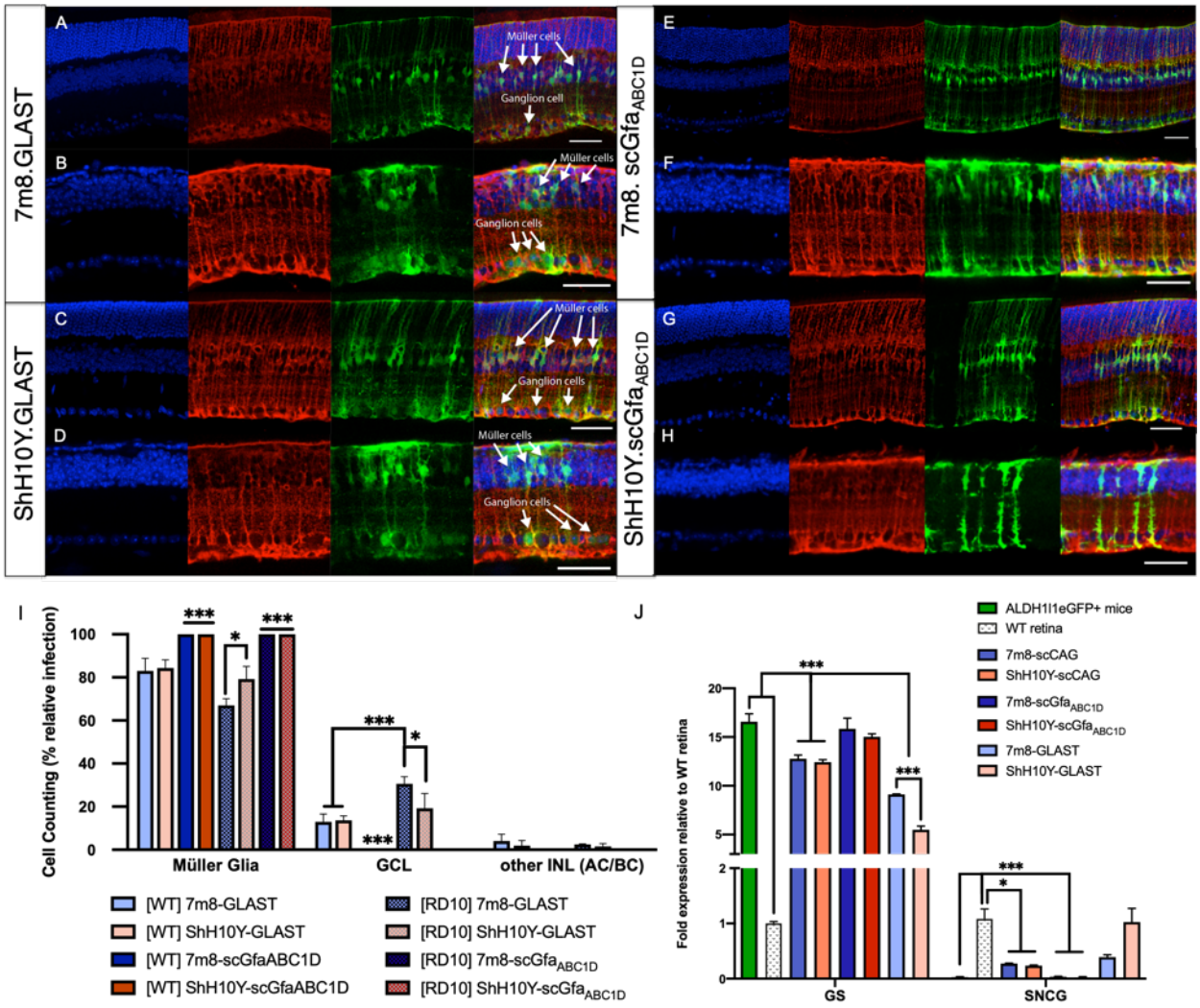

Figure 3: GLAST promoter partially restricts eGFP expression to Müller glia while Gfa$_{ABC1D}$ fully restricts **7m8 or ShH10Y-eGFP expression in WT and *rd10* mice injected intravitreally.** C57Bl6J (**A**,**C,E,G**) and *rd10* mice (**B**,**D,F,H**) were injected with 7m8-GLAST (**A**,**B**), ShH10-GLAST-eGFP (**C**,**D**), 7m8-Gfa$_{ABC1D}$ (**E,F**), ShH10-Gfa$_{ABC1D}$ (**G,H**). Müller cells were identified by eGFP (green) co-labeling with GS (red). DAPI labeled cell nuclei (blue). The scale bars represent 50 µm. (**I**) Quantification of MGCs, GCL and INL cell counting in retinal sections. 2way Anova, Tukey's multiple comparison test was performed on means. Data shown mean ± SD. Müller glia enrichment was confirmed by gene expression analysis of FAC sorted eGFP^{+} cells in WT animals injected with 7m8 and ShH10-CAG-GLAST and Gfa$_{ABC1D}$ vectors one-month post-injection (**J**). Means were compared using 2way ANOVA, Sidak's multiple comparisons test. For all statistical test, ***=p<0.05, **=p<0.01, *=p<0.05 and mean values ± SD were plotted.

Similar to GLAST-1, GFAP is a glial marker, expressed in MGCs although primarily in astrocytes. Transgenic mice using full length mouse and human GFAP regulatory elements have restricted expression in retinal astrocytes and MGCs[36]. A research group truncated the original 2.2kb human GFAP promoter down to 681 bp, creating a shorter promoter, Gfa_{ABC1D}, with conserved binding regions to maintain astrocytes[37]. Its small size makes it very amendable to use for both self-complementary and single-stranded AAV vectors, enabling expression of bigger size transgenes. When injected intravitreally, 7m8 and ShH10Y-Gfa_{ABC1D} were able to completely restrict eGFP expression to MGCs in both WT (**Fig 3.E,G**) and *rd10* (**Fig 3.F,H**). Despite low level of GFAP in the mature wild-type retina, the Gfa_{ABC1D} promoter led to strong transgene expression in C57BL6/J retinas. While still glia-specific, transduction levels were lower in the *rd10* retinas.

To confirm cell counting approaches, we analyzed levels of GS and SNCG gene expression assuming a correlation with MGC and ganglion cell enrichment in the isolated GFP^+ cell fraction. We extracted RNA from FAC sorted GFP^+ cells. A pool of five WT retinas were each injected with 7m8 or ShH10-CAG-, GLAST- and scGfa_{ABC1D}-eGFP (**Fig 3. J**). We used $eGFP^+$ cells isolated from transgenic Aldh1l1-eGFP mice, driving GFP expression in MGCs and astrocytes (**Supplemental S4**), and unsorted, dissociated cells from uninfected retinas as positive and negative controls. We compared GS levels to WT retina levels. Aldh1l1 GFP sorted cells were 16.5-fold enriched in glia. 7m8- and ShH10-Gfa_{ABC1D} vectors showed similar GS levels (15.85 ± 1.1 vs. 15.03 ± 0.3-fold increase, respectively). Interestingly, 7m8- and ShH10-CAG also expressed similar levels of GS (12.77 vs 12.52 ±0.2), but significantly lower than the Gfa_{ABC1D} vectors ($p<0.001$). The GLAST promoter led to the least MGC enriched fraction and was significantly lower in ShH10Y (5.485±0.4) than in 7m8 (9.12 ± fold increase) injected retinas. These findings correlated with the SNCG marker results. Aldh1l1-$eGFP^+$ and Gfa_{ABC1D} vectors showed no detectable levels of SNGC, while ShH10.GLAST showed similar levels than non-sorted cells compared to 7m8 (1.025±0.25 vs. 0.4±0.04). All CAG vectors led to a ~4-fold decreased in the number of ganglion cells compared to WT ($p=0.043$).

Promoter analysis correlates with promoter-driven retinal tropism of viral vectors

Transcriptional analysis of regulatory elements is a powerful tool used to identify promoter regions that can fit in AAV vectors and still retain cell-specific expression. Here, we took the reverse approach, and analyzed the predicted transcription factor binding sites (TFBS) found in the GLAST, GFAP and Gfa_{ABC1D} promoters to better understand which TFBSs drive glial selectivity. While native GLAST gene expression is specific to MGCs in the retina, the engineered 2.1kb promoter permitted ganglion cell off-target expression. On the other hand, truncation of the Gfa_{ABC1D} promoter retain glia specificity with its 2.2kb parent while reducing off-target expression.

Similar to GLAST, the GFAP promoter includes the regulatory 5' untranslated region (UTR) but also the beginning of the coding region (**Fig 4.A-B**). We both analyzed predictive TFBSs and searched for TFBSs driving pro-glia fate. Reports associated the Glia Cell Missing homolog 1 (GCM1), a transcription factor in early neural development, showed that when knocked out in *Drosophila* it led progenitors to switch from a glial to neuronal fate. Ectopic GCM1 expression was also shown to drive pro-glia cell fate in presumptive neurons[38]. Another factor, Oct-6/Tst-1[39–41], has low expression in non-dividing mature neurons and is mostly found in glial cells. We found that the GFAP promoter sequence was enriched in these two TFBSs (8 and 2 sites

for GMC1 and Oct-6, respectively) compared to the GLAST promoter (3 and 0 sites; **Fig 4.C**).

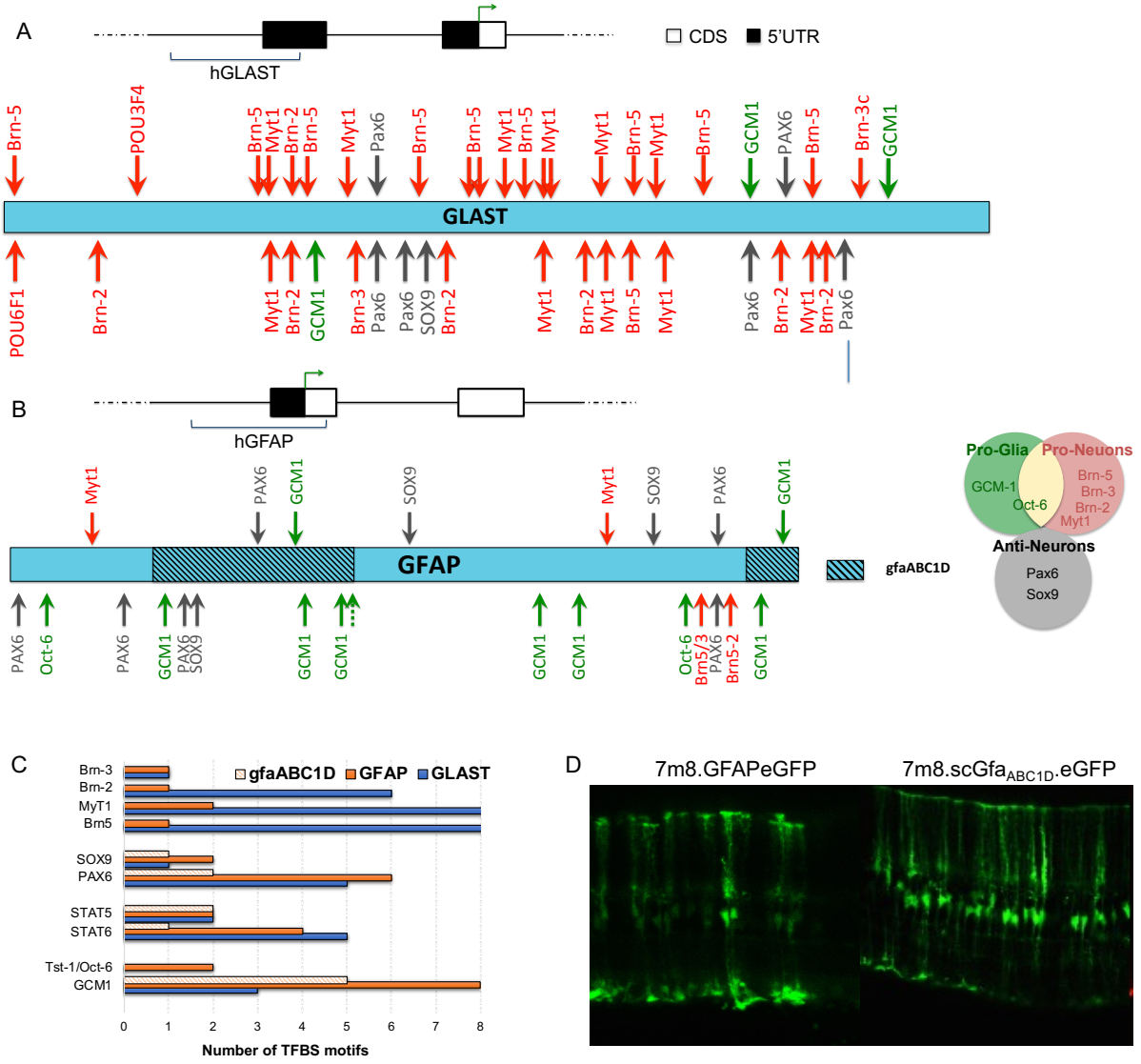

Figure 4: GFAP promoters are enriched in pro-glia transcription factors.
Diagram showing the **(A)** GLAST and **(B)** GFAP promoter sequences, as well as predictive location of neuronal and glia transcription factors binding sites. Major pro-glia transcription factors are listed in green, "anti-neuron" transcription factors in black, and pro-neuron transcription factors are listed in red, as well as quantified (**C**) in a graph. Conserved sequence regions in Gfa$_{ABC1D}$ shown in the GFAP sequence retain glia specificity. Representative confocal images (**D**) of WT retinas injected with 7m8.scGfa$_{ABC1D}$.eGFP and 7m8.GFAP.eGFP.

We also found TFBSs associated with pro-neuronal fates, particularly in the GLAST sequence which was enriched in POU domain TBFS motifs Brn-2, Brn-5 and Myt-1. The Brn family is predominately expressed in the CNS. Brn-2 and Brn-5 are specific to the establishment of early neural cell lineages. Decrease/inhibition of Brn-2 in the CNS prevented neural progenitors differentiation to neurons and astrocytes[42]. Brn-3 is known to drive differentiation of retinal ganglion cells. Related TFBSs were present in GLAST and GFAP sequences. Both promoters had

binding sites for transcription factors that were categorized as anti-neural. Of note are Pax6 and Sox9, transcription factors expressed by retinal progenitor cells and some adult MGCs[43,44]. In development, these transcription factors are turned off when the cell is terminally differentiating into a retinal neuron. Their presence can implicate an inhibition of neuronal expression for these promoters.

Interestingly, Gfa_{ABC1D} GFAP-conserved regions, which are enriched in pro-glia GCM1 and completely depleted in Brn/Pou domain TFBS family, seem to completely retain full promoter specificity for MGCs **(Fig 4.D)**.

Gfa_{ABC1D} greatly reduces GFAP-induced AAV-cis toxicity

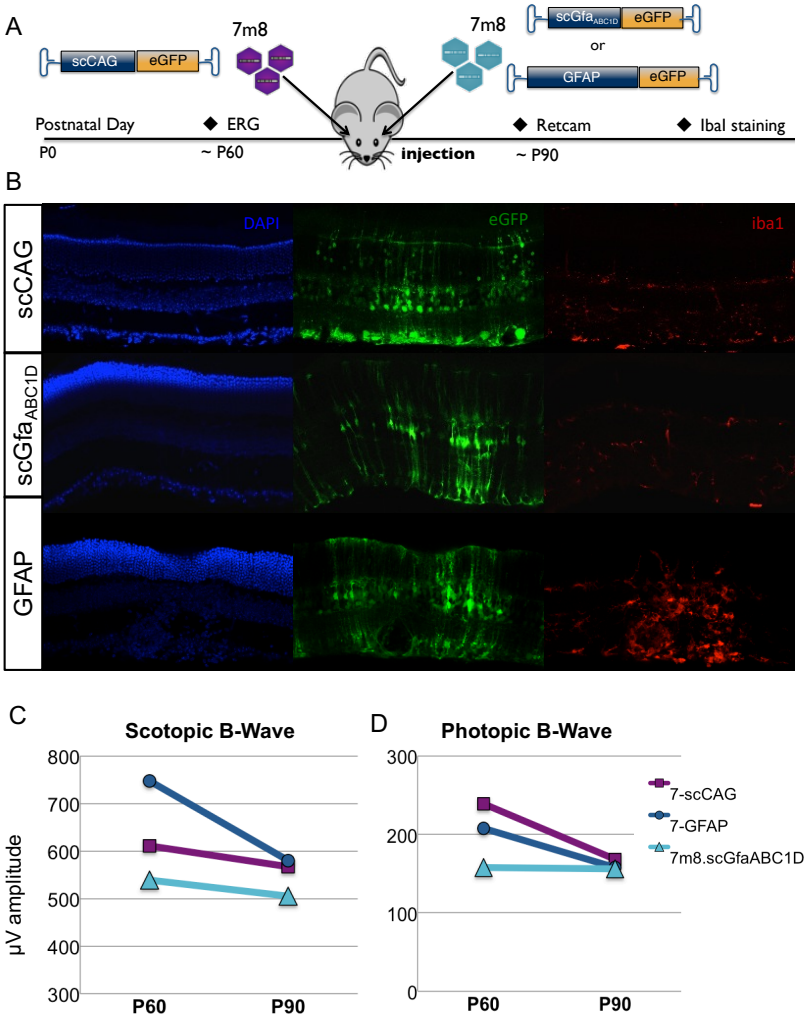

Figure 8: Bio-safety profile of MGC cell-specific versus ubiquitous promoter driving eGFP. Diagram of experimental design (**A**) to assess ocular toxicity: C57BL6/J mice were injected in each eye with a high viral dose (2.0E+11 vg) of 7m8.scCAG.eGFP and 7m8.GFAP or Gfa_{ABC1D}.eGFP. Retinal fundus was imaged with a micron retcam to observe any injection related damage before electroretinogram (ERG) measurements. Representative cross sections (**B**) were stained with Iba1 macrophages/microglia marker,

and DAPI stained nuclei to observe evidence of transgene-induced toxicity. Scotopic & photopic ERGs (**C**) were performed on WT (n=3 eyes) mice pre- and 4 weeks post-injection.

Although cell specific, the human GFAP promoter has not been consistently used for AAV-mediated gene targeting of MGCs due to AAV-cis toxicity observed with both subretinal[9] and intravitreal injections[45]. This is interesting, as other studies have shown that cell-specific transgene expression decreased the immune response observed against AAV-cis element (transgene) compared to the use of a ubiquitous promoter[31]. Here, we wanted to compare the safety profile of AAV-scGfa$_{ABC1D}$ and AAV-GFAP to AAV-scCAG. We started with injecting a high dose of AAV particles in one-month C57BL6/J mice with one eye with 7m8.scCAG.eGFP and the contralateral with either 7m8.scGfa$_{ABC1D}$ or 7m8.GFAP.eGFP (**Fig 8.A**).

We recorded photopic and scotopic ERGs pre- and 4-weeks post injection. We monitored for potential damage induced by induced by ocular injections. We found that for both light stimuli, 7m8-GFAP decreased B-waves amplitudes. Decrease was more pronounced in scotopic conditions (~750 µV down to ~580 µV) than photopic (~210 µV down to 160 µV). 7m8.scCAG expression decreased cone-mediated amplitudes, with a 60 µV drop one month after expression. 7m8.scGfa$_{ABC1D}$ led to minimal toxicity in scotopic as well as photopic conditions (**Fig 8.D**). These findings correlated with intensity of Iba1 marker in sectioned retinas. As shown in the representative retina cross-section images, 7m8.scCAG and scGfa$_{ABC1D}$.eGFP displayed similar Iba1 staining across all retinal layers. General retinal structure was also normal. Oppositely, Iba1 staining was stronger in 7m8.GFAP.eGFP injected retinas (**Fig 8.B**), with rosette formation in the ONL, a sign of inflammation. We conclude here that unlike parental GFAP, Gfa$_{ABC1D}$ mediated a high level, selective and safe transgene expression at higher vector doses.

Discussion

Müller cells are an attractive therapeutic target for treating retinal disease due to their role in homeostasis and ability to survive during degeneration. However, selective and effective MGC targeting has been a challenge with naturally occurring AAV serotypes, due to either low-transduction efficiency or being tropism-permissive to other retinal cell types until the engineering of novel AAV variants. ShH10 became the gold standard AAV vector for intravitreal MGC targeting, being the first and, to our knowledge, only capsid with high cell-preference tropism. Efficacy was proven for a wide range of therapeutic and fundamental applications[3,30,46].

However, our study and other reports highlighted ShH10 capsid tropism varies based on models (e.g., induced or inherited) of degeneration, plus route of delivery. Similar to another published study[47], we found that from the intravitreal route ~67% of the cells infected by ShH10Y in the murine retina are MGCs, with 15% of ganglion cells, and the other inner retinal neurons accounting for the remaining transduced cells. In *rd10* mice, glial specificity reached ~80%. However, in a chemically induced model of degeneration, higher levels of expression in off-target cells were observed[48] with ShH10. Drug-induced retinal toxicity led to higher levels of ganglion cell and photoreceptor expression, which we hypothesized was due to compromised inner limiting membrane integrity, affecting viral particle uptake. Subretinal delivery of ShH10Y triggered different expression patterns compared to intravitreal, with strong targeting of RPE and photoreceptor cells[41] (**Supplemental S2**). Stepping outside of the visual system, another group

showed that intraganglionic injection of ShH10 in the dorsal root ganglia resulted in a selective and efficient switch to sensory neuron expression, with few satellite glia cells infected.

Currently, use of tissue-specific promoters in the vector cassette is the most selective approach to restrict unwanted transgene expression and promote stable and persistent expression in the target cell. Before ShH10, several glia promoters had been identified to be selective at targeting glia in the brain and retina, however their large size (2 – 3kb) prohibited AAV-mediated transgene delivery, due to limited cargo carrying capacity. Bioinformatic tools revolutionized the gene targeting landscape, with the identification and engineering of shorter and efficient promoters, retaining key regulatory elements of the genomic parental promoters. AAVs with high transduction and tissue penetration profiles, such as 7m8 in the retina, can benefit over glia-prone capsid variants when combined with a strong and selective promoter. 7m8 displayed efficient and high, although non-selective, cell infectivity with MGCs accounting for 46% and 39% of infected cells in WT and *rd10* retinas, respectively. 7m8 leads to pan-retinal cell transduction, spreading away from the vasculature, therefore achieving a higher rate of infection than ShH10, whose expression is often restricted along the vasculature. Here, we characterized the selectivity and strength of two, unprecedently tested in the retina, human glia promoters: the 2.1kb GLAST and short 681bp Gfa_{ABC1D} promoters.

Despite the fact that GLAST-transgenic mice had selective expression in MGCs[34], we found that GLAST drove strong expression in both ganglion cells and MGCs with 7m8 and ShH10. Transcriptional analyses of the 2.1kb sequence revealed the presence of TFBS motifs with preferential neuronal fate, such as Brn2, Brn5 and the GC-specific Brn3. Likely, inhibitory regulatory elements to repress neuronal-fate mediated factors must be missing in a 2.1kb promoter sequence compared to the full genomic sequence used in transgenic mice. Grippingly, in glutamate-mediated excitotoxicity conditions, ganglion cells were reported to abnormally express parental glutamate-transporter transcript EEAT-2, found in cone, bipolar and amacrine cells in the healthy retina[49], highlighting potential cell transcript "leakiness" for RGCs. Overall, although not specific only to MGCs, there are a variety of therapeutic strategies in which one would want to target both glia and ganglion cells. For example, Müller and ganglion cell mediated expression of neurotrophic factors could be an efficacious treatment for glaucoma or Leber hereditary optic nerve neuropathy diseases that primarily affect GCL and astrocytes[6,10].

We found that 7m8.Gfa_{ABC1D} achieves high and selective expression in MGCs. It retains the selectivity of its parental 2.2-2.5 kb GFAP promoter, regardless of the route of administration (**Supplemental S6**). To-date, it is the shortest selective glial promoter (681bp), enabling self-complementary AAV transgene compatibility. While comparing TFBS motifs present in GFAP and GLAST promoter sequences, we found that long and short GFAP regulatory regions were enriched in glial cell missing transcription factor, which has been shown to drive glia-cell fate during development and can ectopically increase glia expression.

We also show that significant ocular toxicity induced by transgene expression under the control of the long GFAP promoter expression was abolished with Gfa_{ABC1D}. Another striking finding is that although GFAP is expressed at a low level in the mature retina, Gfa_{ABC1D} still drove strong and high levels of expression in both WT and diseased retinas. GFAP, unlike other transcript based AAV promoters (e.g. RHO), also has the advantage of being upregulated in during retinal degeneration and we found that both ShH10Y and 7m8.Gfa_{ABC1D}-mediated expression remained glia-selective in *rd10* mice.

Another consideration for in vector choice is the intended glial target. While our paper mainly focuses on Müller glia, the major glia cell type found in the retina, selective targeting of astrocytes, which make up the majority of the cells in many brain regions, had growing interest the retina as well with recent evidences of neuroprotective role in glaucoma[50–52]. ShH10, was initially isolated from an *in vitro* screen in primary human brain. We also found that it displays higher tropisms than 7m8 and parental AAV2 *in vitro (***Supplemental S5.A-C)**. Dissociating AAV-mediated astrocyte versus MGC targeting in the retina has been more challenging, due to low number of astrocytes compared to MGCs, and physical proximity. While we did not find major capsid differences with astrocyte-based promoter GLAST and Gfa_{ABC1D}, ShH10 under the control of a ubiquitous promoter seemed to have higher colocalization with GFAP staining than 7m8 (**S5-D**) in healthy retinas. GFAP is expressed in reactive glia, which MGCs have been shown to express developmental models of retinitis pigmentosa such as *rd1* and *rd10.* Further investigation with selective astrocytes (S100-beta) markers needs to be undertaken to compare capsid tropism for astrocytes *in vivo.*

General AAV infectivity is significantly reduced in the *rd10* model, consistent with other reports[53] that retinal remodeling occurring after loss of photoreceptors affecting retinal cell structure but also surface receptors, potentially due to morphological and transcriptional changes. We then concluded in our study, that since no AAV capsid-mediated tropism difference was observed with the Gfa_{ABC1D} promoter that 7m8.scGfa$_{ABC1D}$ represents to date the best viral vector for MGC expression. This capsid and promoter combination achieve pan-retinal expression from the vitreous, uses a small promoter making it compatible with self-complementary AAV approaches, has no off-target expression due to enrichment of glia-specific TFBSs, reduces toxicity, and drives high expression levels in both healthy and diseased retinas. This has great potential to benefit translational approaches to rescue inherited retinal degenerations, investigate the ability of MGCs to differentiate into photoreceptors, and other *in vivo* applications with a need for strict-cell targeting, such as genome editing.

Materials and Methods

Generation and purification of AAV Vectors

The pAAV-GLAST-eGFP vector was cloned by inserting the GLAST promoter from pGLASTp-dsRed2 (addgene.org/17706) into the backbone of a pAAV-CAG-EGFP cassette, containing inverted terminal repeats (ITRs), the simian virus 40 (SV40) polyadenylation signal and the woodchuck post-transcriptional regulatory element (WPRE). The pAAV-GFAP-eGFP and pAAV-scGfa$_{ABC1D}$.eGFP vector was purchased from Addgene (#50473). Endotoxin-free AAV plasmids were co-transfected with pHelper and 7m8 or ShH10-Y445F capsid plasmids into HEK293T cells. After 72 hours, cells were harvested and centrifuged at 1000rpm for 10 minutes. The supernatant was then collected and resuspended in PEG 8000 (2.5 M NaCl) to precipitate virus at 4 ºC for 2 hours and then pelleted (4000 rpm for 20 min at 4ºC). Cells were lysed in AAV lysis media (0.15 NaCl, 50 mM Tris HCl, 0.05% Tween, pH 8.5) by three consecutive freeze/thaws and then treated with Benzonase (250 U/µl Novagen #71205-3) for 30 minutes at 37ºC. The media pellet was resuspended with the crude lysate and incubated at 4ºC overnight. The lysate was then spun down at 4000 rpm for 20 min at 4ºC. The supernatant was loaded onto an iodixanol density gradient (Opti-prep) and centrifuged for 60 minutes in a Beckman XL-100K ultracentrifuge at 69000 rpm at 18°C. Fractions containing the viral vectors were collected and concentrated using Amicon Ultra-15 Centrifugal Filter Units. Viral titers were quantified by qPCR and all viral stocks with titers above 1×10^{12} genome copies/ml were stored at 4°C.

In vitro astrocyte infectivity

Primary normal human astrocytes (NHA) isolated from human brain (cerebral cortex) were purchased from the Sciencell Research Laboratories (Carlsbad, CA) and cultured at P1 according to the manufacturer's instructions using the Astrocyte Medium. All culture vessels were coated with poly-L-Lysine 24 hrs before passing. Cells were not passaged more than 8 times to preserve lineage.

Astrocytes were seeded either onto glass coverslips or directly into 12-well plates at a density of ~100,000 cells per coverslip/well and infected the following day with an MOI of 10^5-10^6. After 72 hrs, GFP fluorescence is either quantitatively measured by mRNA extraction to assess GFP expression levels or qualitatively by fixing the cells on a coverslip and imaging GFP$^+$ fluorescence using a confocal microscope.

Animals and intravitreal injections

All procedures concerning animals adhered to the ARVO statement for the use of animals in ophthalmic and vision research as well as in accordance with USDA Animal Welfare Act, PHS Policy on Humane Care and Use of Laboratory Animals, UC Berkeley Association for Assessment and Accreditation of Laboratory Animal Care, International, and UC Berkeley Animal Care and Use Committee. Wild-type (WT) mice, C57Bl6J and *rd10* (B6.CXB1-*Pde6b*^{rd10}*/J*) mice were purchased from Jackson Laboratories and used for all experiments. For intraocular intravitreal injections, *rd10* mice were injected at 2 months of age to ensure adequate degeneration. Mice were

anesthetized with ketamine (58 mg/kg) and xylazine (6.5 mg/kg) by intraperitoneal injection. The topical anesthetic proparacaine (0.5%) was applied and the pupils were dilated with phenylephrine (2.5%) and tropicamide (1%). An ultrafine 30 1/2-gauge disposable needle was passed through the sclera, at the equator and next to the limbus, to create a small hole into the vitreous cavity. Two µl of virus with a titer 2-5.0×10^{13} vg/ml was then injected into the vitreous with direct observation of the needle above the optic nerve.

Fundus photography

Transgene expression was assessed one to eight weeks after injections using a fundus camera (Retcam II; Clarity Medical Systems Inc., Pleasanton, CA) equipped with a wide angle 130° retinopathy of prematurity (ROP) lens to monitor eGFP expression in live, anesthetized mice. Pupils were dilated for fundus imaging with phenylephrine (2.5%) and Tropicamide (1%).

Immunohistochemical analysis, confocal microscopy, and cell counting

Mice were euthanized at 3-4 weeks after injection using CO_2 inhalation followed by cervical dislocation. Enucleated eyes were placed in 10% formalin overnight at 4ºC and then dissected and rinsed in PBS. Retinas were embedded in 5% agarose and sectioned at 125 µM. The sections were blocked for ≥2 hours at room temperature in blocking buffer (1% normal goat serum, 1% FBS, 0.5% Triton-X 100) before antibody labeling overnight. The antibodies used were: rabbit anti-GS (Sigma G-2781, 1:1000), rabbit anti-PKC alpha (Abcam ab32376, 1:500), mouse anti-GFAP (Sigma G3893, 1:500), Alexa Fluor 594 goat anti-rabbit (Invitrogen, 1:2000), and Alexa Fluor 633 goat anti-mouse (Invitrogen, 1:2000). Images were taken on a Zeiss LSM 710 laser scanning confocal microscope (NIH Grant 1S10RR026866-01). Images were analyzed on FIJI[54] from ImageJ[55]. For each virus and promoter combination, three retinas were counted with five images of each retina.

Gene expression analysis of Müller glia cell markers in the healthy and degenerate retina

Animals were euthanized and eyes were enucleated (n= 4-6 each) from P20, P85 and P365 WT and *rd10* mice. RNeasy mini kit (Qiagen) was used to extract RNA from retinas, and cDNA synthetized. qRT-PCR samples were run in triplicate. Primer sequences are listed in **Supplemental S1**.

Gene expression analysis of FACs sorted eGFP^{+} retinal cells

Fluorescence was confirmed 4 weeks after injections and mice were euthanized. Eyes were enucleated in ice-cold PBS, retinas were isolated by removing non-neuronal tissue and then dissociated for FAC sorting using a Papain dissociation system (Worthington Biochemical). Briefly, retinas were incubated for 40-60 minutes in a papain protease solution, in a shaker at 37ºC and 450 rpm. Tubes were gently flicked every 10-15 minutes to allow for proper cell dissociation. Cells were then triturated by pipetting 5-10x times up and down until tissue pieces were not visible and the lysate was homogenous. Cells were spun down, resuspended in PBS + 1% FBS and filtered through a 40 µm mesh cell Strainer Cap (Falcon). Positive GFP cells were sorted through the BD Influx and Aria Fusion (UC Berkeley, Flow Cytometry Core) sorters directly into lysis buffer for

RNA extraction using the RNeasy micro kit (Qiagen). The resulting RNA was used to synthetize cDNA. qRT-PCR samples were run in triplicate and primer sequences can be found in **Supplemental S1**.

ERG analysis

Electroretinograms were recorded (Espion E2 ERG System; Diagnosys LLC) in response to six light flash intensities ranging from −3 to 1 log cd × s/m^2 on a dark background as described previously each stimulus was presented in a series of three. For photopic ERGs, the animal was first exposed to a rod-saturating background for 5 min. Stimuli ranging from −0.9 to 1.4 log cd × s/m^2 were presented 20 times on a light background. ERG amplitude traces were analyzed with MATLAB (v7.7; MathWorks).

Transcription factor binding sites analysis

Human DNA sequences of the GLAST and GFAP promoters were analyzed for putative transcription factor binding sites using Mat Inspector software version 8.1, Matrix Library 9.1 from the Genomatix suite v3.4. Parameters for binding sites were set at matrix similarity and core similarity of 0.8.

Supplemental Materials

Primer name	Sequence
GFAP F	5’-AAG CTC CAA GAT GAA ACC AAC-3’
GFAP R	5’-GGC CAC ATC CAT CTC CA-3’
GLAST F	5’-AAA CCG GAG AAA CCC GTG-3’
GLAST R	5’-TGA GCC CAG GGA GAT GGA TA-3’
GS F	5’-GGA TAG CCC GTT TTA TCT TGC-3’
GS R	5’-GTG GTA CTG GTG CCT CTT GC-3’
mGAPDH 3’	5’-GGA TGC AGG GAT GAT GTT CT-3’
mGAPDH 5’	5’-AAC TTT GGC ATT GTG GAA GG-3’
Rhodopsin F	5’-CAA GAA TCC ACT GGG AGA TGA-3’
Rhodopsin R	5’-GTG TGT GGG GAC AGG AGA CT-3’
SNCG F	5’-GTCTCAACCTGGCACACTGAATG -3’
SNCG R	5’-AGAGGACCATAGGGTAAAAGGAGC-3’

S1: Table of RT-PCR PCR primers

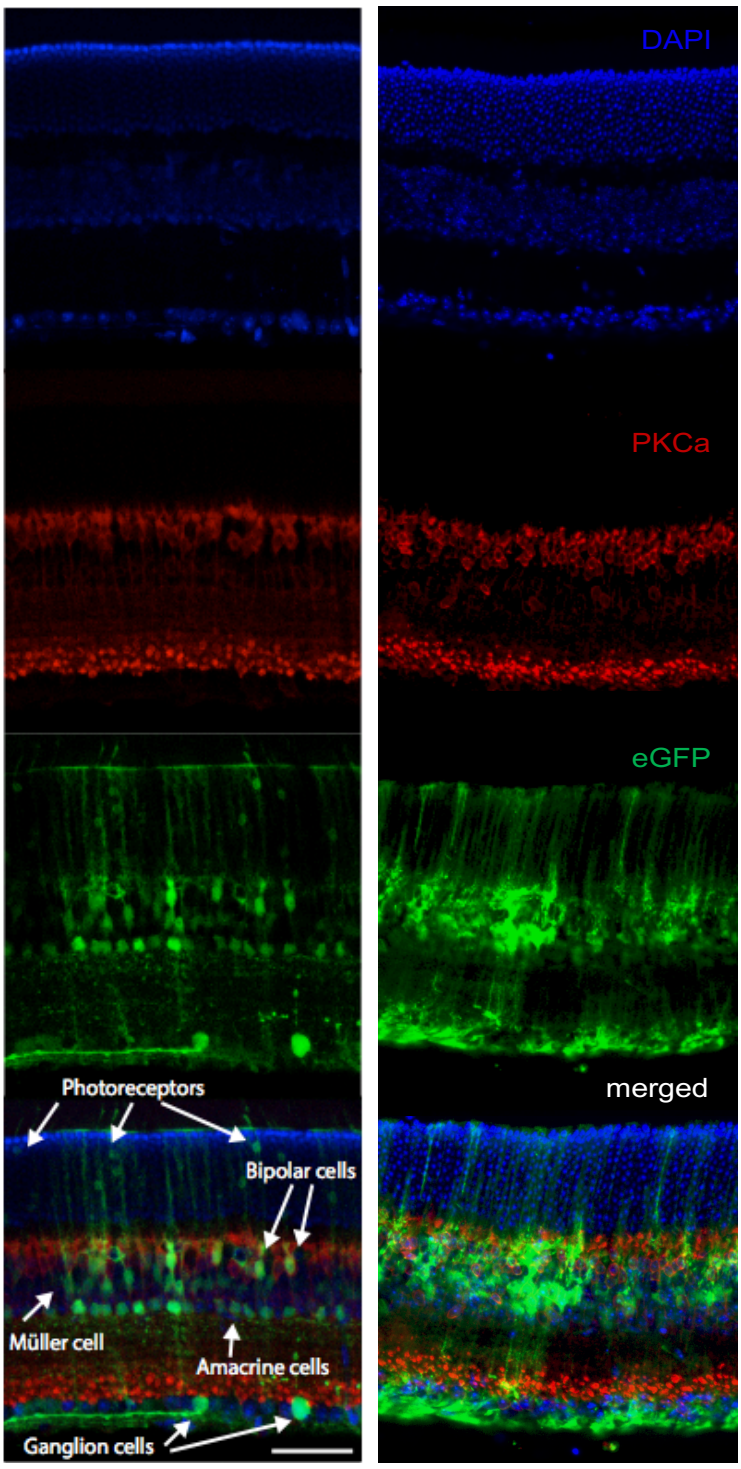

S2: Intravitreally delivered 7m8 and ShH10 eGFP expression profiles driven by the CAG promoter. eGFP expression (green) was countered stained with PKCalpha (red) to identify non-Müller INL cell somas belong to bipolar cells. Cell nuclei were stained with DAPI (blue). Scar bars represent 50 μm.

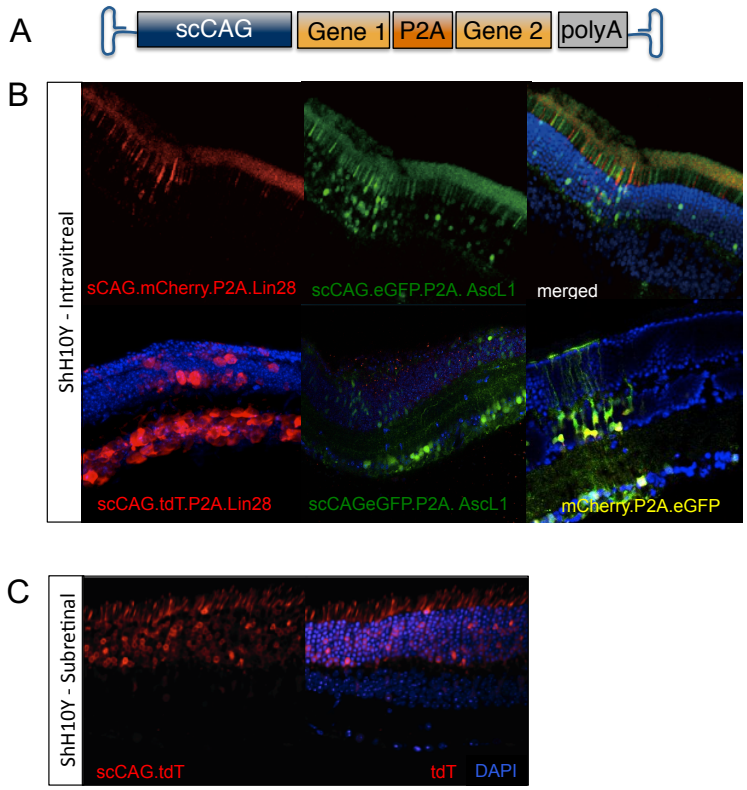

S3: Transgene, route of delivery and retinal damage affects ShH10Y capsid preferential tropism for glia. (**A**) Cross-sections of retinas injected intravitreally with diverse ShH10Y.scCAG.mCherry/eGFP – P2A-X constructs. Strong off-target expression in inner- and ganglion cells, as well as photoreceptors observed. Retinas were damaged with N-methyl-D-aspartate. (**B**) Route of infection affects tropism. Representative cross section of retina injected with ShH10Y.scCAG.tdTomato. Subretinal ShH10 injection shows strong tropism for photoreceptors.

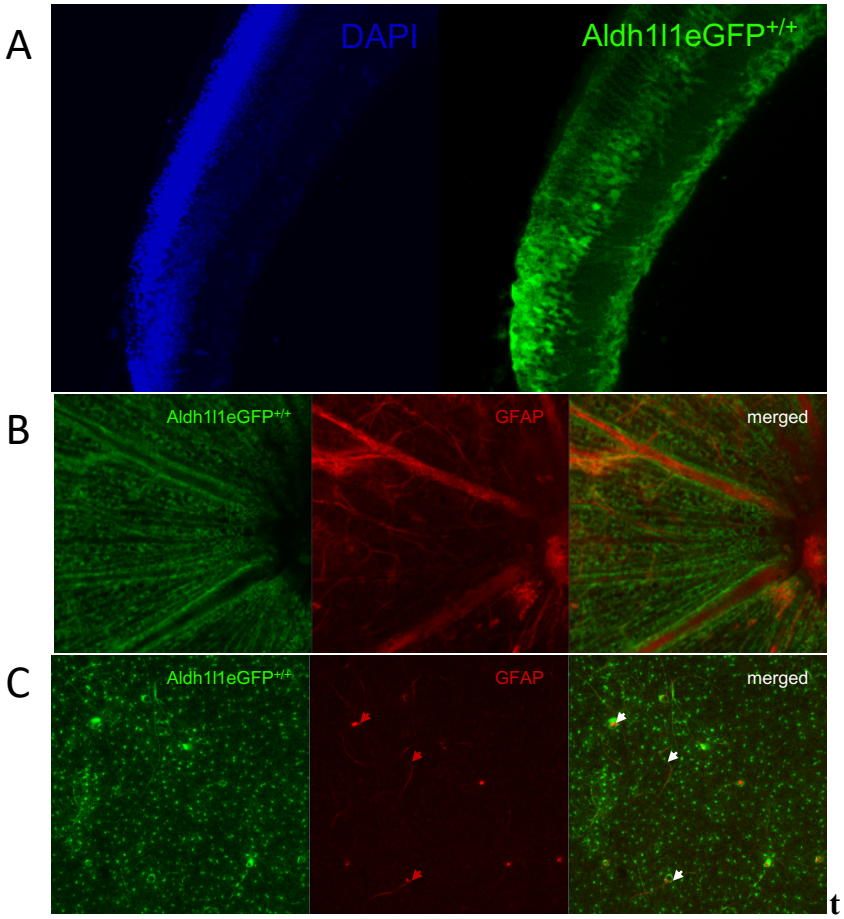

S4: Aldh1l1eGFP transgenic mouse expresses reporter selectively in Müller glia and astrocytes
Representative confocal images (**A**) of cross-section of a Aldh1l1-eGFP$^{+/+}$ retina. Retinas were flatmounted and stained with astrocytic marker GFAP (red). Representative confocal pictures of (**B**) optic nerve area and periphery (**C**). White/red arrows show colocalization with astrocytes, GFAP staining (magnification 20x).

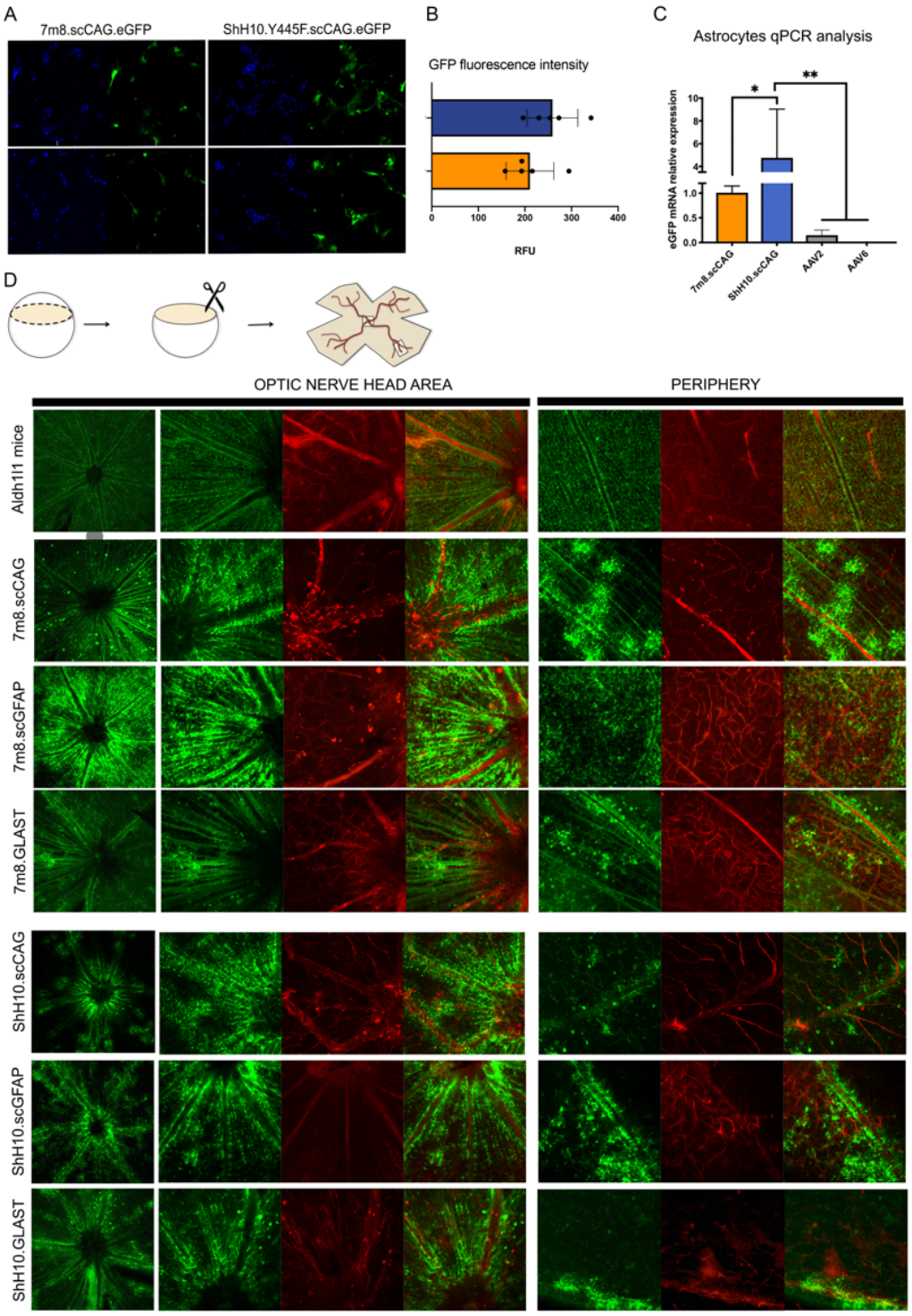

S5: ShH10Y and 7m8 astrocyte tropism

Human astrocyte cell line was infected with ShH10- or 7m8- scCAG.eGFP. Representative confocal (20x) images (**A**) and quantification of eGFP fluorescence (**B**) normalized to DAPI staining. RNA extracted to quantify eGFP expression (**C**) through RT-PCR. Flatmounts of WT retinas (**D**) injected with 7m8 and ShH10 expressing eGFP under the control of CAG, Gfa_{ABC1D} or GLAST were stained with GFAP antibody (red).

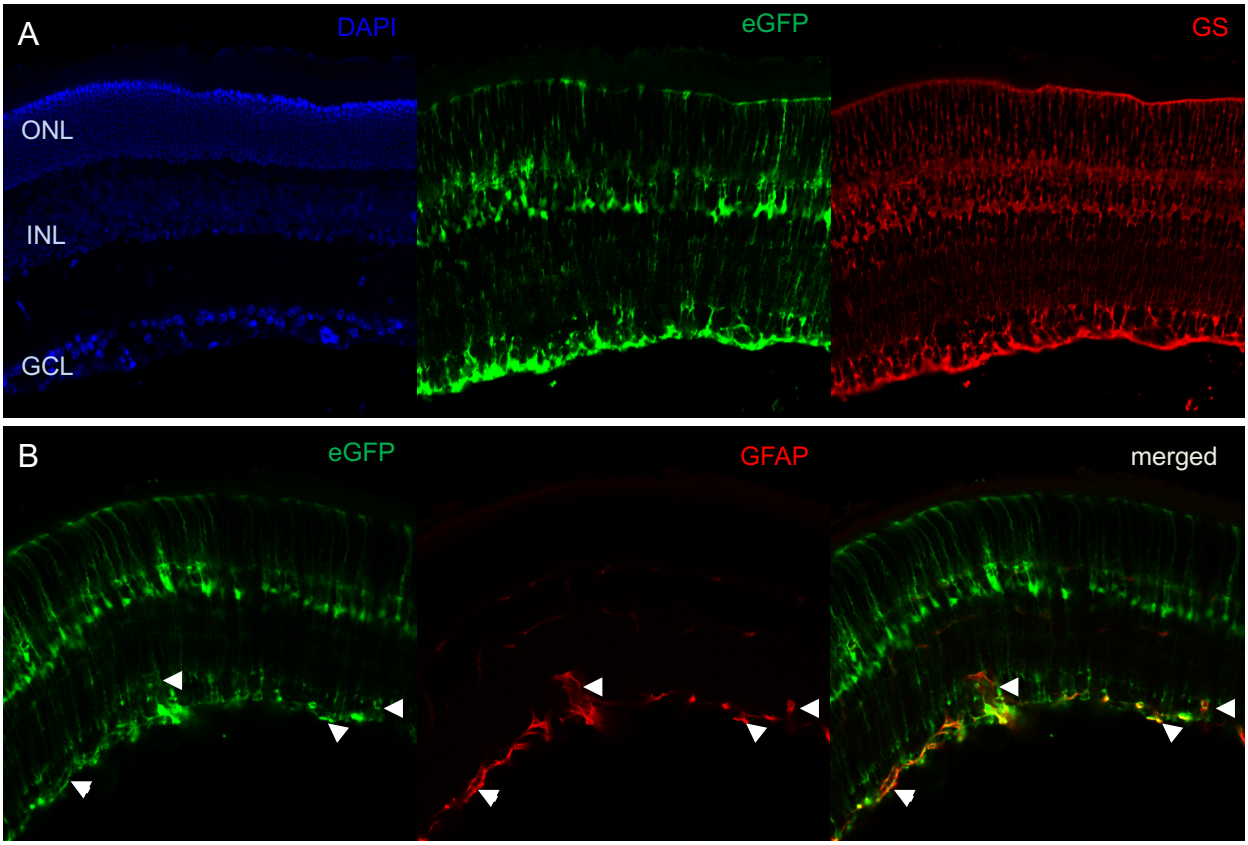

S6: AAV9.2YF Gfa$_{ABC1D}$ drove strong glia specificity in a neonatal intravenous injection with differential Müller glia and astrocytes targeting.

Confocal of representative images (40x magnification) of P15-P17 pups, tail-vein injected at P2-P3 with AAV9.2YF.scGfa$_{ABC1D}$.eGFP. Strong (**A**) transgene expression co-localized with MGC marker, GS (red). DAPI counter stained cell nuclei (blue). AAV9-scGfa$_{ACB1D}$ achieves astrocytes labeling (**B**), co-localizing with astrocytes marker GFAP (red). White triangles show astrocytes location in each channel.

References

1. Rosa, J. M. *et al.* Neuron-glia signaling in developing retina mediated by neurotransmitter spillover. *Elife* (2015). doi:10.7554/elife.09590
2. Kurth-Nelson, Z. L., Mishra, A. & Newman, E. A. Spontaneous Glial Calcium Waves in the Retina Develop over Early Adulthood. *J. Neurosci.* (2009). doi:10.1523/jneurosci.2493-09.2009
3. Xue, Y. *et al.* CRALBP supports the mammalian retinal visual cycle and cone vision. *J. Clin. Invest.* (2015). doi:10.1172/JCI79651
4. Wen, R., Tao, W., Li, Y. & Sieving, P. A. CNTF and retina. *Progress in Retinal and Eye Research* (2012). doi:10.1016/j.preteyeres.2011.11.005
5. Hauck, S. M. *et al.* GDNF Family Ligands Trigger Indirect Neuroprotective Signaling in Retinal Glial Cells. *Mol. Cell. Biol.* (2006). doi:10.1128/mcb.26.7.2746-2757.2006
6. Seki, M. *et al.* Müller cells as a source of brain-derived neurotrophic factor in the retina: Noradrenaline upregulates brain-derived neurotrophic factor levels in cultured rat Müller cells. *Neurochem. Res.* (2005). doi:10.1007/s11064-005-7936-7
7. Lipinski, D. M. *et al.* CNTF Gene Therapy Confers Lifelong Neuroprotection in a Mouse Model of Human Retinitis Pigmentosa. *Mol. Ther.* (2015). doi:10.1038/mt.2015.68
8. Kassen, S. C. *et al.* CNTF induces photoreceptor neuroprotection and Müller glial cell proliferation through two different signaling pathways in the adult zebrafish retina. *Exp. Eye Res.* (2009). doi:10.1016/j.exer.2009.01.007
9. Dalkara, D. *et al.* AAV mediated GDNF secretion from retinal glia slows down retinal degeneration in a rat model of retinitis pigmentosa. *Mol. Ther.* (2011). doi:10.1038/mt.2011.62
10. Daly, C. *et al.* Brain-derived neurotrophic factor as a treatment option for retinal degeneration. in *Advances in Experimental Medicine and Biology* (2018). doi:10.1007/978-3-319-75402-4_57
11. ClinicalTrials.gov.
12. Sieving, P. A. *et al.* Ciliary neurotrophic factor (CNTF) for human retinal degeneration: Phase I trial of CNTF delivered by encapsulated cell intraocular implants. *Proc. Natl. Acad. Sci.* (2006). doi:10.1073/pnas.0600236103
13. Becker, S. *et al.* Targeted Knockdown of Overexpressed VEGFA or VEGF164 in Müller cells maintains retinal function by triggering different signaling mechanisms. *Sci. Rep.* (2018). doi:10.1038/s41598-018-20278-4
14. Haurigot, V. *et al.* Long-term retinal PEDF overexpression prevents neovascularization in a murine adult model of retinopathy. *PLoS One* (2012). doi:10.1371/journal.pone.0041511
15. Ahmad, I., del Debbio, C. B., Das, A. V. & Parameswaran, S. Müller glia: A promising target for therapeutic regeneration. *Investig. Ophthalmol. Vis. Sci.* (2011). doi:10.1167/iovs.11-7308
16. Goldman, D. Müller glial cell reprogramming and retina regeneration. *Nature Reviews Neuroscience* (2014). doi:10.1038/nrn3723
17. FDA. FDA approves novel gene therapy to treat patients with a rare form of inherited vision loss.
18. Duncan, J. L. *et al.* Inherited Retinal Degenerations: Current Landscape and Knowledge Gaps. *Transl. Vis. Sci. Technol.* **7**, 6 (2018).

19. Hellström, M. *et al.* Cellular tropism and transduction properties of seven adeno-associated viral vector serotypes in adult retina after intravitreal injection. *Gene Ther.* (2009). doi:10.1038/gt.2008.178
20. Bartel, M. A., Weinstein, J. R. & Schaffer, D. V. Directed evolution of novel adeno-associated viruses for therapeutic gene delivery. *Gene Therapy* (2012). doi:10.1038/gt.2012.20
21. Dalkara, D. *et al.* In vivo-directed evolution of a new adeno-associated virus for therapeutic outer retinal gene delivery from the vitreous. *Sci. Transl. Med.* (2013). doi:10.1126/scitranslmed.3005708
22. Klimczak, R. R., Koerber, J. T., Dalkara, D., Flannery, J. G. & Schaffer, D. V. A novel adeno-associated viral variant for efficient and selective intravitreal transduction of rat Müller cells. *PLoS One* (2009). doi:10.1371/journal.pone.0007467
23. Jones, B. W. *et al.* Retinal remodeling. *Jpn. J. Ophthalmol.* **56**, 289–306 (2012).
24. Jones, B. W. *et al.* Retinal remodeling in human retinitis pigmentosa. *Experimental Eye Research* **150**, (2016).
25. Chang, B. *et al.* Retinal degeneration mutants in the mouse. *Vision Res.* (2002). doi:10.1016/S0042-6989(01)00146-8
26. Fernández-Sánchez, L., Lax, P., Campello, L., Pinilla, I. & Cuenca, N. Astrocytes and Müller Cell Alterations During Retinal Degeneration in a Transgenic Rat Model of Retinitis Pigmentosa. *Front. Cell. Neurosci.* (2015). doi:10.3389/fncel.2015.00484
27. Lupien, C., Brenner, M., Guérin, S. L. & Salesse, C. Expression of glial fibrillary acidic protein in primary cultures of human Müller cells. *Exp. Eye Res.* **79**, 423–429 (2004).
28. Sofroniew, M. V & Vinters, H. V. Astrocytes: biology and pathology. *Acta Neuropathol.* (2010). doi:10.1007/s00401-009-0619-8
29. Bringmann, A. *et al.* Müller cells in the healthy and diseased retina. *Prog. Retin. Eye Res.* **25**, 397–424 (2006).
30. Elsaeidi, F. *et al.* Notch Suppression Collaborates with Ascl1 and Lin28 to Unleash a Regenerative Response in Fish Retina, But Not in Mice. *J. Neurosci.* **38**, 2246–2261 (2018).
31. Xiong, W. *et al.* AAV cis -regulatory sequences are correlated with ocular toxicity . *Proc. Natl. Acad. Sci.* (2019). doi:10.1073/pnas.1821000116
32. Wang, S. *et al.* Pin1 Promotes Regulated Necrosis Induced by Glutamate in Rat Retinal Neurons via CAST/Calpain2 Pathway. *Front. Cell. Neurosci.* **11**, 425 (2017).
33. Harada, T. *et al.* Functions of the two glutamate transporters GLAST and GLT-1 in the retina. *Proc. Natl. Acad. Sci.* (2002). doi:10.1073/pnas.95.8.4663
34. Regan, M. R. *et al.* Variations in Promoter Activity Reveal a Differential Expression and Physiology of Glutamate Transporters by Glia in the Developing and Mature CNS. *J. Neurosci.* (2007). doi:10.1523/JNEUROSCI.0790-07.2007
35. Wang, J. *et al.* Anatomy and spatial organization of Müller glia in mouse retina. *J. Comp. Neurol.* **525**, 1759–1777 (2017).
36. Kuzmanovic, M., Dudley, V. J. & Sarthy, V. P. GFAP Promoter Drives Müller Cell–Specific Expression in Transgenic Mice. *Investig. Opthalmology Vis. Sci.* **44**, 3606 (2003).
37. Lee, Y., Messing, A., Su, M. & Brenner, M. GFAP promoter elements required for region-specific and astrocyte-specific expression. *Glia* (2008). doi:10.1002/glia.20622
38. Jones, B. W., Fetter, R. D., Tear, G. & Goodman, C. S. glial cells missing: a genetic switch that controls glial versus neuronal fate. *Cell* (1995). doi:10.1016/0092-

8674(95)90280-5
39. Jaegle, M. *et al.* The POU proteins Brn-2 and Oct-6 share important functions in Schwann cell development. *Genes Dev.* (2003).
40. Renner, K., Leger, H. & Wegner, M. The POU domain protein Tst-1 and papovaviral large tumor antigen function synergistically to stimulate glia-specific gene expression of JC virus. *Proc. Natl. Acad. Sci.* (2006). doi:10.1073/pnas.91.14.6433
41. Kiyota, T., Kato, A., Altmann, C. R. & Kato, Y. The POU homeobox protein Oct-1 regulates radial glia formation downstream of Notch signaling. *Dev. Biol.* (2008). doi:10.1016/j.ydbio.2007.12.013
42. Fujii, H. & Hamada, H. A CNS-specific POU transcription factor, Brn-2, is required for establishing mammalian neural cell lineages. *Neuron* **11**, 1197–206 (1993).
43. Joly, S., Pernet, V., Samardzija, M. & Grimm, C. PAX6-positive müller glia cells express cell cycle markers but do not proliferate after photoreceptor injury in the mouse retina. *Glia* (2011). doi:10.1002/glia.21174
44. Poché, R. A., Furuta, Y., Chaboissier, M. C., Schedl, A. & Behringer, R. R. Sox9 is expressed in mouse multipotent retinal progenitor cells and functions in Müller Glial cell development. *J. Comp. Neurol.* (2008). doi:10.1002/cne.21746
45. Cao, J. *et al.* A rAAV6 Mutant with Enhanced Targeting for Mouse Retinal Müller Cells. *https://doi.org/10.1080/02713683.2019.1639768* (2019). doi:10.1080/02713683.2019.1639768
46. Byrne, L. C. *et al.* AAV-Mediated, Optogenetic Ablation of Müller Glia Leads to Structural and Functional Changes in the Mouse Retina. *PLoS One* **8**, 1–13 (2013).
47. Pellissier, L. P. *et al.* Specific tools for targeting and expression in Müller glial cells. *Mol. Ther. Methods Clin. Dev.* **1**, 14009 (2014).
48. Yao, K. *et al.* Wnt Regulates Proliferation and Neurogenic Potential of Müller Glial Cells via a Lin28/let-7 miRNA-Dependent Pathway in Adult Mammalian Retinas. *Cell Rep.* **17**, 165–178 (2016).
49. Rauen, T. & Wießner, M. Fine tuning of glutamate uptake and degradation in glial cells: Common transcriptional regulation of GLAST1 and GS. *Neurochem. Int.* (2000). doi:10.1016/S0197-0186(00)00021-8
50. Livne-Bar, I. *et al.* Astrocyte-derived lipoxins A4 and B4 promote neuroprotection from acute and chronic injury. *J. Clin. Invest.* **127**, 4403–4414 (2017).
51. Takahama, S. *et al.* Retinal Astrocytes and GABAergic Wide-Field Amacrine Cells Express PDGFRα: Connection to Retinal Ganglion Cell Neuroprotection by PDGF-AA. *Invest. Ophthalmol. Vis. Sci.* **58**, 4703–4711 (2017).
52. Alqawlaq, S., Flanagan, J. G. & Sivak, J. M. All roads lead to glaucoma: Induced retinal injury cascades contribute to a common neurodegenerative outcome. *Exp. Eye Res.* **183**, 88–97 (2019).
53. van Wyk, M., Hulliger, E. C., Girod, L., Ebneter, A. & Kleinlogel, S. Present molecular limitations of ON-bipolar cell targeted gene therapy. *Front. Neurosci.* **11**, (2017).
54. Schindelin, J. *et al.* Fiji: an open-source platform for biological-image analysis. *Nat. Methods* (2012). doi:10.1038/nmeth.2019
55. Rueden, C. T. *et al.* ImageJ2: ImageJ for the next generation of scientific image data. *BMC Bioinformatics* (2017). doi:10.1186/s12859-017-1934-z

Chapter 3: Mutation-independent gene therapies for rod-cone dystrophies

Cécile Fortuny, John G. Flannery

Book chapter published in Advances in Experimental Medicine and Biology (2018)

Abstract

The clinical success of gene replacement therapies in recent years has served as a proof-of-concept for the treatment of inherited retinal degenerations using adeno-associated virus (AAV) as a vector. However, inherited retinal degenerative diseases showcase a broad genetic and mechanistic heterogeneity, challenging the development of mutation-specific therapies for each mutation. Mutation-independent approaches must be developed to slow down retinal degeneration regardless of the underlying genetic mutation and onset of the disease. New understanding of cell death mechanisms in rod-cone dystrophies have led to promising rescue of photoreceptor cell death by viral-mediated expression of anti-apoptotic factors and secretion of retinal neurotrophic factors. Optogenetic therapies are also able to restore light sensitivities in blind retinas.

Introduction

Rods and cones are the two main photoreceptor cells contributing to the first steps in sensing light in the retina and translating it to an electric signal to the other neuronal cells downstream to finally be processed in the primary visual cortex. Many hundreds of proteins are involved in the light response and keeping the cells of the retina nourished and healthy. This high degree of metabolic activity makes the retina more sensitive to mutations and degeneration: when a gene mutation occurs, the protein may be incorrectly synthetized and act abnormally or may not be expressed, triggering a loss of function and vision. The majority of inherited retinal degenerations (IRDs) are caused by mutations found in photoreceptors and to a lesser extent in the retinal pigment epithelium (RPE). Most of the mutations identified in IRDs effect genes involved in either the photoreceptor structural integrity (*CEP290, USH2A…*) or in the phototransduction cascade (*RHO, PD6EB, CNGA3*…) leading to blindness as a result of loss of photoreceptors. Among them, retinitis pigmentosa (RP) is the most common inherited cause of blindness in the world [1]. Currently, no effective treatment exists to treat these diseases, but gene therapy approaches have been developed and have begun to show success at delaying retinal degeneration. This review will focus on current mutation-independent gene therapy approaches for treating different stages of RP.

Gene therapy for the retina

Different therapies have attempted to reduce retinal degeneration in RP. Before recent progress in gene-based therapeutics, surgery and vitaminotherapy were the most common treatments employed to treat RP. Gene therapy has been a growing field in the past decade for

treating ocular disease and has proven to be an efficient and safe way of treating single-gene mutations leading to blindness by providing therapeutic DNA to targeted cells in the retina by the use of viral or non-viral vectors. A determining element in gene therapy studies is the vector used to administer the payload. *In vivo* viral vectors are the most successful in long-term expression and delivery of genetic material to cells within tissues. Different viruses have been used in clinical trials although AAV is currently the gold standard for gene delivery in the retina due to its excellent safety profile as well as its efficiency in transducing a large spectrum of cells. AAV is a small non-enveloped icosahedral parvovirus with a genome (4.9kb) that consists of three open reading frames (rep, cap, and the assembly-activating protein), flanked by two inverted terminal repeats (ITRs) that form hairpin structures and are essential for viral packaging. The rep gene encodes for proteins involved in viral replication and packaging, and the cap gene encodes for the capsid proteins (VP1, VP2, VP3) of the virus. The assembly-activating protein participates in the process of capsid assembly[2,3]. AAV-mediated gene therapy has shown many advantages over other viruses as viral vectors for the retina. As a dependovirus, AAV is unable to replicate in the absence of a helper virus with no risk of genetic integration in the genome. The virus infects quiescent and dividing cells, leading to long-term expression of the transgene in the cells without any known pathogenicity for the host. Different serotypes of AAV have been discovered and used to infect retinal cells, highlighting that the AAV capsid sequence and the route of delivery (intravitreal or subretinal) are two majors components affecting the cell tropism [4].The clinical trials for Leber's congenital amaurosis type 2[5] were the first to validate the proof-of-concept for safe AAV-mediated therapies after successfully rescuing vision in patients after delivery of a healthy copy of the affected RPE65 gene to the RPE.

Most of the successful clinical trials for retinal degeneration have been gene replacement therapies. However, it requires the disease to be monogenic and the genetic cause to be known as well as its retinal phenotype characterized. It also only holds promise if implemented early on in the disease progression of the patient. However, more than 40-50% of genes involved in degeneration remain unknown in RP. For those patients, a gene replacement strategy is not possible and requires other approaches such as mutation-independent gene therapies.

Cell death mechanisms in RP

Despite the genetic heterogeneity of RP, all degenerations included in this group of diseases recapitulate a similar phenotype in which rod photoreceptors die first, followed by cone cell death and a remodeling of the inner retina layers. One treatment approach is to delay rod photoreceptor cell death, in order to preserve cone health and function as long as possible considering these cells are responsible for central, color and day vision.

Cell death mechanisms governing retinal degenerations were poorly understood at the time. Animals of RP mimicking human diseases have been used to study these mechanisms. The classical pathway for rod photoreceptor cell death was believed to be caspase-mediated apoptosis (Fig1). A number of anti-apoptotic genes have been identified and used in therapeutic approaches including the BCL-2 family [6]and the anti-apoptotic protein family (IAP)[7] (Liston et al., 2003). X-Linked Inhibitor of Apoptosis Protein (XIAP), is one of the most potent proteins from IAP family and has been shown to efficiently delay cell death in models of retinal degeneration[8,9]. However, recent work demonstrated that caspase-independent pathways are activated as a result of secondary cell messenger increase (e.g cGMP, calcium). Research performed in rd1 and rd10 mice by Paquet-

Durant et al. showed that PDE6B deficiency leads to an increase in extracellular levels of calcium by 190% compared to a healthy retina [10,11]. Calpains, calcium-activated cysteines, are known to contribute to this secondary neurodegenerative cascade in the same pattern as caspases, by cleaving cellular substrates and are also involved in the cell's autophagy pathway [12]. Calpastatin is the only known endogenous inhibitor of calpains and has been studied as a potential gene candidate for delaying cell death in rod photoreceptors. Other caspase-independent pathways involving poly-ADP ribose-polymerase or histone deacetylase [13] are activated in dying rods in several models of RP and will lead to the development of new therapeutics to treat rod photoreceptor cell death. In contrast, cone cell death mechanisms are less well characterized. It has been shown that these cells undergo necrosis after the loss of rods.

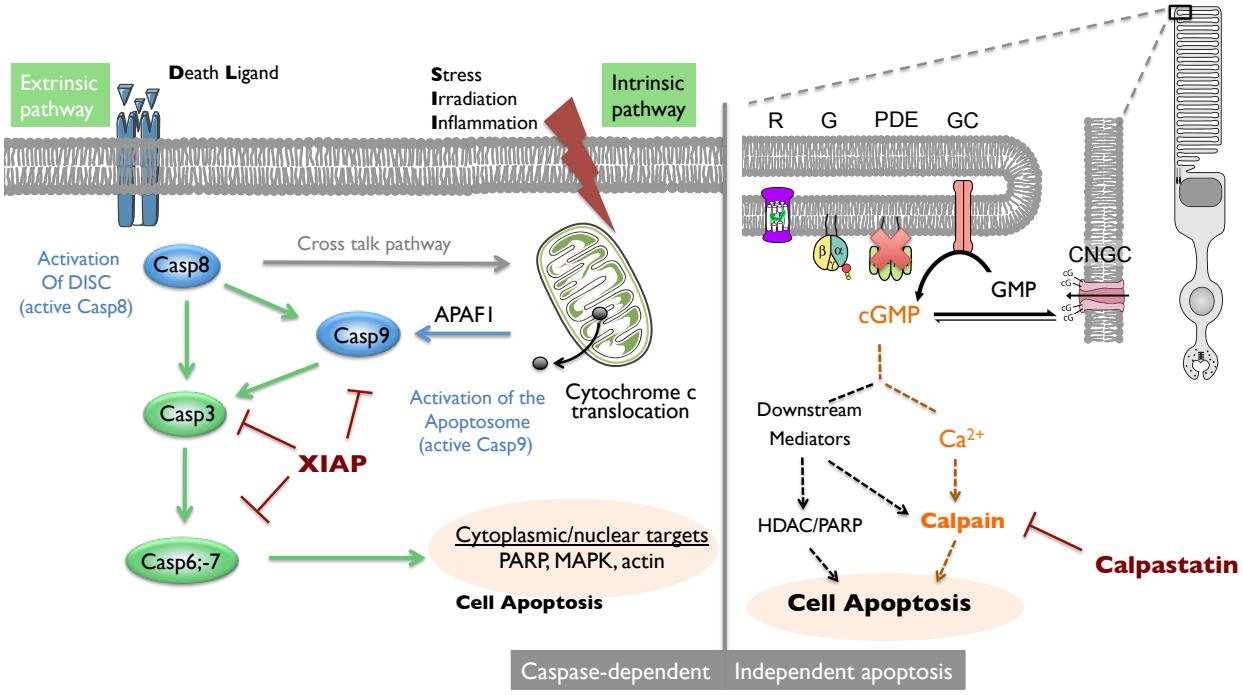

Figure 1: Sketch representing two cell death mechanisms in retinal degenerations: caspase-dependent (**left**) or -independent (**right**) apoptosis. Classical pathways for photoreceptor death have been thought to be caspase-mediated by either extrinsic (receptor signaling) or intrinsic (within cell inflammation, stress signaling…) stimulus triggering activation of caspases, a family of enzymes that when activated cleave cellular substrates, leading to cell apoptosis. XIAP was found to be the most potent inhibitor of caspases. Recently a new cell death pathway was identified in a few model of retinitis pigmentosa. Increased concentration of cGMP due to a defective phototransduction due to mutations (e.g. PDE6E in rd1 and rd10 models) correlated with an increased Ca^{2+} as a second messenger of degeneration, activating calpains, calcium-activated cysteines that contribute to apoptosis in a similar pattern as caspases by cleaving substrates.
R: Rhodopsin, **G**: G-couple transducing, **PDE**=Phosphodiesterase, **GC**= Guanine Cyclase, **CNGC**: Cyclic nucleotide-gated ion channel. **Casp**: Caspase

Previous studies[14,15] have suggested that this could be due to environmental alterations such as the release of toxins or damage-associated molecular patterns (DAMPs) from rod apoptosis,

loss of rod-cone gap junctions, microglia activation, and oxidative stress that trigger cell death signaling to neighboring cells. Indeed, the later and slower onset of cone death suggested that rod cell death is not the primary reason for cone cell death, but a long-term change of photoreceptor environment (e.g. cell density, levels of proinflammatory cytokines…).

The insulin/signaling pathway is key in sensing trophic factors, nutrients and assessing the energy status of the cell. In RP, mTOR levels in cones after rod loss are downregulated. Punzo et al . found that degenerative cones expressed higher levels of HIF-1, a transcription factor that improves glycolysis in stressed conditions, proving that cones are dying as a result of starvation and nutritional losses [16,17].

Recently, more therapies started focusing on the inflammation component of RP cell death mechanisms. Overexpression of the antioxidant transcription factor NRF2 countered inflammation and oxidative damage[18] and led to significant cone survival in different models of RP. A similar therapeutic effect[19] [20]was observed with increased levels of soluble CX3CL1, a neuronal-derived chemokine involved in microglia maintenance and its homeostasis role in the retina. However, inflammation responses in retinal degeneration involve a very delicate balance between being protective and deleterious for photoreceptors survival, which is not yet fully understood.

Neuroprotection

Studies have highlighted the importance of neurotrophic factor signaling in the healthy and diseased retina. Trophic or growth factors are endogenously secreted molecules that stimulate cellular growth, proliferation, cellular differentiation, and regeneration. In the eye, the major layers secreting these factors are the RPE and Müller cells. The Müller glial cells represent an excellent target for neurotrophin secretions. Being very numerous, they span the entire retina and are directly involved in maintaining photoreceptors. Also, their close contact with neuronal cells makes them ideal candidates for the secretion of neurotrophic factors.

Dalkara et al.[21] showed that a novel AAV vector, ShH10, was able to transduce efficiently and selectively glia cells through intravitreal injection, generating high levels of Glial cell-Derived Neurotrophic Factor (GDNF) expression, which promotes neuronal survival, and leads to rescue in S334-4ter rat model lasting up to 6 months post injection. José-Alain Sahel and Thierry Léveillard groups discovered and characterized the rod-derived cone viability factor (RdCVF), a survival factor secreted by rod photoreceptors that signal to the cone photoreceptors[22]. During degeneration, the loss of neurotrophic support due to rods cell death has been hypothesized as the main cause of secondary cone degeneration. AAV-RdCVF has been shown to delay cone cell death in models of RP [23,24].

Other trophic factors such as the ciliary neurotrophic factor (CNTF), brain-derived neurotropic factor (BDNF) and basic fibroblast growth factor (bFGF), recently mesenphelalic astrocyte-derived neurotrophic factor (MANF) have also been extensively studied as potential neuroprotective candidates[25,26]. However, contradictory results for a same molecule has been found in different studies, highlighting the complex growth factor balance between promoting survival or cell damage. For example, CNTF treatments delayed photoreceptor degeneration in multiple models of degeneration [27,28] and showed promising results in clinical trials (for Usher syndrome 2 or AMD). However, it has been also shown to have no therapeutic effect in other human clinical trials and pre-clinical studies, with a decrease in electroretinogram responses post-treatment later on found to be due to transient photoreceptor deconstruction before regeneration [29].

Optogenetics for the blind retina

At the final stages of RP, the photoreceptor layer is completely lost. Optogenetic therapies have emerged as a promising approach, focusing on converting the surviving vertical retinal interneurons into light-sensitive cells using genetically-encoded light gated proteins. Major challenges quickly arise in engineering alternative systems that would allow to respond to light as sensitively as photoreceptor do, and reach the high temporal sensitivity and frequency needed to process human visual information. The major two types of actuators currently used are ion channels and G protein coupled receptors.

Optogenetic ion channels were the first tools optimized for vision restoration. Upon photoactivation and light stimulus removal, the opening and closing of the channel happens in an order of milliseconds, conferring temporal sensitivity but at the cost of light sensitivity (threshold required $>10^{15}$ photons cm^{-2} s^{-1}), operating in high and unsafe photonic range). ChannelRhodopsin 2 (ChR2) was the first used *in vivo*. It mediates an excitatory cation current when activated with blue light. Bi et al. [30] delivered AAV-ChR2 to ganglion cells in the rd1 mouse and showed that visually evoked responses were restored in the retina and visual cortex. Since, novel ChR variants with improved kinetics have been engineered to increase the efficiency of the system: mVCHR1, ChrimsonR, ReaChR[31–33], but still failed at decreasing the level of light needed to activate them. Choride Ion pomp halorhopdsin (NpHR) mediates an inhibitory current in response to yellow light and has been used to mimic the OFF response. However, high levels of NpHR in cells led to intracellular aggregates[34] and since have been optimized as well with different variants.

Chemically engineered mammalian channels have been also engineered to be light-responsive: the light-gated ionotropic glutamate receptor (LiGluR) consists of iGluR6 with an introduced cysteine in position 439 (L439C) for the covalent attachment of a photoisomerable molecule ("photoswitch") that reversibly activates the receptor. The LiGluR photoswitch has a maleimide linked to a glutamate by a photoisomerizable azobenzene linker (maleimide-azobenzene-glutamate (MAG)). When excited at 380nm (near UV-range), MAG triggers the opening of the ion channel, which could be closed when excited at a different wavelength, enabling the channel to be turned on and off with light stimulation. This system was optimized by engineering a second generation photoswitch, MAG(460), that is activated by white light and naturally turns off in the dark[35,36].

G-protein coupled receptors (GPCRs) opsins, are found naturally in the retina. While they have great sensitivity to light compared to ion channels, they have low temporal sensitivity (order of seconds) due the involvement on a secondary cascade to open or close their ion channel. Melanopsin, the photosensitive ganglion cells opsin was the first GPCR tested, before rhodopsin emerged as a potential candidate. When expressed in inner neurons, rhodopsin was found to be as light sensitive than melanopsin ($\sim 10^{12}$ photons cm^{-2} s^{-1}) with a ten-fold temporal sensitivity than melanopsin[37,38]. An explanation for the sensitivity of rhodopsin outside of photoreceptors is that RPE and close by Muller cells might still be producing regenerated 11-cis and delivering it after photoreceptor cell death. Cone opsins play a major role in high acuity, central and color vision, are being investigated. M-cone opsin showed higher kinetics (10-fold) than rhodopsin with similar light sensitivity when expressed in ganglion cells[39]. Moving away from naturally found GPCRs in the retina, engineered GPCRs have been used to improve upon current kinetics, such as Opto-

mGlur6[40] with increased light sensitivity ($5.0x10^{11}$photons cm^{-2} s^{-1} at 473nm). Constantly new, innovative and safer optogenetic tools are being developed. This approach has high potential for vision restoration in RP patients.

Conclusion

The rare nature of most retinal dystrophies, associated with genotypic and phenotypic heterogeneity observed in patients, means that only a relatively small number might benefit from treatments targeting specific gene mutations. Alternatives such as mutation independent therapies must be developed and adapted to the patient's particular stage of degeneration.

Our increased knowledge of common cell death mechanisms led to investigating inhibitors of the main cell death effectors as well as neuroprotective agents as therapeutic candidates for early-stages of RP degenerations where most defective photoreceptors are still present. However, much is left to understand in the sensitive balance between degeneration and survival. Single-treatment therapies marked the beginning of vector gene therapy, but emerging studies show a synergistic effect by combining two treatments. AAV vector gene replacement therapy can be complemented with anti-apoptotic proteins to prolong the efficacy of the treatment or the combination of trophic factors, demonstrating that these approaches can promote photoreceptor survival through a synergistic combination and be adapted to orphan diseases. Targeting two different pathways/cell types in a combination therapy is also promising, increasing the protection of photoreceptors[41].

Optogenetics have also been an emerging field for vision restoration in later stages of degeneration when the photoreceptor layer is lost. Native photoreceptor transduction is a very fast and sensitive system due to the involvement of hundreds of proteins and neighboring cells involved in replenishing the 11-*cis* chromophores needed for the opsin to be sensitive. Mimicking it naturally in non-light sensitive cells such as ganglion cells has been rendered possible with optically light sensitive GPCR, opsins and ion channels, initially in paled in comparison in terms of speed and light sensitivity coverage, which is being improved upon. Targeting ON-bipolar cells to recreate the ON/OFF light response has been investigated in the past few years but often felt short due to the low efficiency at targeting those cells. Challenges in AAV-mediated gene delivery remain to be overcome such as the vector capacity (4.7kb cargo capacity) or to keep improving retinal transduction efficiency and specificity while remaining safe, non-invasive and cell-specific.

References

1. Hartong, D. T., Berson, E. L. & Dryja, T. P. Retinitis pigmentosa. *Lancet (London, England)* (2006). doi:10.1016/S0140-6736(06)69740-7
2. Mitchell #1, A. M., Nicolson, S. C., Warischalk, J. K. & Samulski, R. J. AAV's Anatomy: Roadmap for Optimizing Vectors for Translational Success. *Curr Gene Ther* **10**, 319–340 (2010).
3. Sonntag, F., Schmidt, K. & Kleinschmidt, J. A. A viral assembly factor promotes AAV2 capsid formation in the nucleolus. *Proc. Natl. Acad. Sci.* (2010). doi:10.1073/pnas.1001673107
4. Watanabe, S. *et al.* Tropisms of AAV for Subretinal Delivery to the Neonatal Mouse Retina and Its Application for In Vivo Rescue of Developmental Photoreceptor Disorders. *PLoS One* (2013). doi:10.1371/journal.pone.0054146
5. Pierce, E. A. & Bennett, J. The status of RPE65 gene therapy trials: Safety and efficacy. *Cold Spring Harb. Perspect. Med.* (2015). doi:10.1101/cshperspect.a017285
6. Chen, J. *et al.* bcl-2 overexpression reduces apoptotic photoreceptor cell death in three different retinal degenerations. *Proc. Natl. Acad. Sci.* (2002). doi:10.1073/pnas.93.14.7042
7. Liston, P., Fong, W. G. & Korneluk, R. G. The inhibitors of apoptosis: There is more to life than Bcl2. *Oncogene* (2003). doi:10.1038/sj.onc.1207101
8. Leonard, K. C. *et al.* XIAP protection of photoreceptors in animal models of retinitis pigmentosa. *PLoS One* (2007). doi:10.1371/journal.pone.0000314
9. Shan, H. *et al.* AAV-mediated gene transfer of human X-linked inhibitor of apoptosis protects against oxidative cell death in human RPE cells. *Investig. Ophthalmol. Vis. Sci.* (2011). doi:10.1167/iovs.10-6850
10. Zhivotovsky, B. & Orrenius, S. Calcium and cell death mechanisms: A perspective from the cell death community. *Cell Calcium* (2011). doi:10.1016/j.ceca.2011.03.003
11. Sahaboglu, A. *et al.* Retinitis pigmentosa: Rapid neurodegeneration is governed by slow cell death mechanisms. *Cell Death Dis.* (2013). doi:10.1038/cddis.2013.12
12. Nguyen, A. T. H. *et al.* Calpain and photoreceptor apoptosis. in *Advances in Experimental Medicine and Biology* (2012). doi:10.1007/978-1-4614-0631-0_69
13. Kaur, J. *et al.* Calpain and PARP activation during photoreceptor cell death in P23H and S334ter rhodopsin mutant rats. *PLoS One* (2011). doi:10.1371/journal.pone.0022181
14. Sudharsan, R., Beiting, D. P., Aguirre, G. D. & Beltran, W. A. Involvement of Innate Immune System in Late Stages of Inherited Photoreceptor Degeneration. *Sci. Rep.* **7**, 17897 (2017).
15. Syeda, S., Patel, A. K., Lee, T. & Hackam, A. S. Reduced photoreceptor death and improved retinal function during retinal degeneration in mice lacking innate immunity adaptor protein MyD88. *Exp. Neurol.* **267**, 1–12 (2015).
16. Bovolenta, P. & Cisneros, E. Retinitis pigmentosa: Cone photoreceptors starving to death. *Nature Neuroscience* (2009). doi:10.1038/nn0109-5
17. Ma, S. *et al.* Loss of mTOR signaling affects cone function, cone structure and expression of cone specific proteins without affecting cone survival. *Exp. Eye Res.* (2015). doi:10.1016/j.exer.2015.04.006
18. Xiong, W., Garfinkel, A. E. M. C., Li, Y., Benowitz, L. I. & Cepko, C. L. NRF2 promotes neuronal survival in neurodegeneration and acute nerve damage. *J. Clin. Invest.* (2015). doi:10.1172/JCI79735

19. Wang, S. *et al.* Pin1 Promotes Regulated Necrosis Induced by Glutamate in Rat Retinal Neurons via CAST/Calpain2 Pathway. *Front. Cell. Neurosci.* **11**, 425 (2017).
20. Wang, S. K., Xue, Y., Rana, P., Hong, C. M. & Cepko, C. L. Soluble CX3CL1 gene therapy improves cone survival and function in mouse models of retinitis pigmentosa. *Proc. Natl. Acad. Sci.* **116**, 201901787 (2019).
21. Dalkara, D. *et al.* AAV mediated GDNF secretion from retinal glia slows down retinal degeneration in a rat model of retinitis pigmentosa. *Mol. Ther.* (2011). doi:10.1038/mt.2011.62
22. Aït-Ali, N. *et al.* Rod-derived cone viability factor promotes cone survival by stimulating aerobic glycolysis. *Cell* (2015). doi:10.1016/j.cell.2015.03.023
23. Byrne, L. C. *et al.* AAV-mediated Delivery of Rod-derived Cone Viability Factor in a Mouse Model of Retinal Degeneration. in *ARVO* (2011). doi:10.1163/1574-9347_bnp_e827420
24. Byrne, L. C. *et al.* Viral-mediated RdCVF and RdCVFL expression protects cone and rod photoreceptors in retinal degeneration. *J. Clin. Invest.* (2015). doi:10.1172/JCI65654
25. Buch, P. K. *et al.* In Contrast to AAV-Mediated Cntf Expression, AAV-Mediated Gdnf Expression Enhances Gene Replacement Therapy in Rodent Models of Retinal Degeneration. *Mol. Ther.* (2006). doi:10.1016/j.ymthe.2006.05.019
26. Neves, J. *et al.* Immune modulation by MANF promotes tissue repair and regenerative success in the retina. *Science (80-.).* (2016). doi:10.1126/science.aaf3646
27. Liang, F. Q. *et al.* AAV-mediated delivery of ciliary neurotrophic factor prolongs photoreceptor survival in the rhodopsin knockout mouse. *Mol. Ther.* (2001). doi:10.1006/mthe.2000.0252
28. Leaver, S. G. *et al.* AAV-mediated expression of CNTF promotes long-term survival and regeneration of adult rat retinal ganglion cells. *Gene Ther.* (2006). doi:10.1038/sj.gt.3302791
29. Birch, D. G., Bennett, L. D., Duncan, J. L., Weleber, R. G. & Pennesi, M. E. Long-term follow-up of patients with retinitis pigmentosa (RP) receiving intraocular ciliary neurotrophic factor implants. *Am. J. Ophthalmol.* **170**, 10 (2016).
30. Bi, A. *et al.* Ectopic Expression of a Microbial-Type Rhodopsin Restores Visual Responses in Mice with Photoreceptor Degeneration. *Neuron* (2006). doi:10.1016/j.neuron.2006.02.026
31. Klapoetke, N. C. *et al.* Independent optical excitation of distinct neural populations. *Nat. Methods* **11**, 338–46 (2014).
32. Lin, J. Y., Knutsen, P. M., Muller, A., Kleinfeld, D. & Tsien, R. Y. ReaChR: a red-shifted variant of channelrhodopsin enables deep transcranial optogenetic excitation. *Nat. Neurosci.* **16**, 1499–1508 (2013).
33. Zhang, F. *et al.* Red-shifted optogenetic excitation: a tool for fast neural control derived from Volvox carteri. *Nat. Neurosci.* **11**, 631–633 (2008).
34. Gradinaru, V., Thompson, K. R. & Deisseroth, K. eNpHR: a Natronomonas halorhodopsin enhanced for optogenetic applications. *Brain Cell Biol.* **36**, 129–139 (2008).
35. Caporale, N. *et al.* LiGluR restores visual responses in rodent models of inherited blindness. *Mol. Ther.* (2011). doi:10.1038/mt.2011.103
36. Gaub, B. M. *et al.* Restoration of visual function by expression of a light-gated mammalian ion channel in retinal ganglion cells or ON-bipolar cells.

doi:10.1073/pnas.1414162111
37. Cehajic-Kapetanovic, J., Bishop, P. & Lucas, R. Enhancement of light sensitivity in retinal degeneration in mice by use of novel optogenetic approaches. *Lancet* (2014). doi:10.1016/s0140-6736(14)60296-8
38. Gaub, B. M., Berry, M. H., Holt, A. E., Isacoff, E. Y. & Flannery, J. G. Optogenetic Vision Restoration Using Rhodopsin for Enhanced Sensitivity. *Mol. Ther.* (2015). doi:10.1038/mt.2015.121
39. Berry, M. H. *et al.* Restoration of high-sensitivity and adapting vision with a cone opsin. *Nat. Commun.* **10**, 1–12 (2019).
40. Van Wyk, M., Pielecka-Fortuna, J., Löwel, S. & Kleinlogel, S. Restoring the ON Switch in Blind Retinas: Opto-mGluR6, a Next-Generation, Cell-Tailored Optogenetic Tool. *PLoS Biol* **13**, 1002143 (2015).
41. Fortuny, C., Byrne, L., Dalkara, D., Lee, T. & Ozturk, B. E. AAV-mediated Combination Therapy of Neurotrophic and Anti-apoptotic Factors in a Mouse Model of Inherited Retinal Degeneration. *Investigative Ophthalmology & Visual Science* **54**, ([Association for Research in Vision and Ophthalmology], 2013).

Chapter 4: AAV-mediated Combination Therapy of Neurotrophic and Anti-Apoptotic in a mouse model of Inherited Retinal Degeneration

Abstract

Many inherited retinal degenerative diseases, such as retinitis pigmentosa, result in blindness as a result of photoreceptor cell death. Since numerous different genetic mutations are involved in these disorders and more than 40-50% of these genes remain unknown, it is advantageous to develop general therapies that promote photoreceptor survival regardless of the underlying mutation. We investigated the therapeutic potential of a combination cell survival therapy using intravitreal injections of two serotypes of adeno-associated virus (AAV) to express a secreted trophic factor in Müller glia, and an inhibitor of cell death signaling in photoreceptors. Delaying rod cell death in tandem to increasing neurotrophic support to the retina led to a synergistic therapeutic effect compared to each approach alone. Our study also highlights how vector optimization, such as the use of self-complementary AAV vectors and cell-specific promoters, enhance gene therapy treatment.

Introduction

The success of the RPE65 clinical trials[1] for Leber Congenital Amaurosis led to the USA FDA's first approval and commercialization of a gene therapy, Luxturna[2] by Spark Therapeutics, which marked the beginning of a new era for gene therapy treatments for inherited retinal and other monogenic diseases. The field of gene therapy has been exponentially growing ever since with a series of on-going clinical trials for retinal diseases such as Choroideremia, X-Linked Retinoschisis and Achromatopsia.

A determining element of these studies has been the vector used to administer the therapeutic payload. Adeno-associated viruses (AAV) quickly became the gold standard for gene delivery due to its many benefits: small sized and nonpathogenic with the ability to lead to stable transgene expression in both dividing and non-diving cells without integrating into the genome. AAV has proven to be safe and efficient delivery vector in a variety of animal studies and clinical trials, leading to many proof-of-concept studies for gene replacement therapies in the retina[3].

While this approach was successfully applied to identified recessive, null mutations diseases, it is still yet to be efficient for dominant, negative gain-of-function cases that would require silencing of the mutant protein. Moreover, the complex genetic heterogeneity underlying retinal diseases leaves a majority of patients stranded with no treatments due to either cost-prohibitive options if causative mutation is not widely represented in the population, or the genetic cause is (25-30%) unknown. The development of mutation-independent treatments emerged to help mitigate the neurodegenerative disease process and is adapted to a wide group of diseases sharing similar disease phenotypes, such as retinitis pigmentosa (RP). RP represents a heterogeneous group of diseases, with to date, over 70 genes/loci involved. It is characterized by pigment deposits predominant in the peripheral retina and by a relative sparing of the central

retina[4,5]. Patients suffer from progressive night blindness, a reduction or loss of visual acuity, and the constriction and gradual loss of the mid-peripheral field of vision.

RP is generally described as a rod-cone dystrophy, as rod photoreceptors are primarily affected by the genetic mutation, triggering their loss and secondary death of cone photoreceptors. Targeting directly the downstream cell death pathway underlying the causal mutation has been one of the other promising strategies to slow down the photoreceptor degeneration. Several genes have been identified which prevent caspase-dependent apoptosis[6,7]. X-linked inhibitor of apoptosis (XIAP) is the most potent member of the gene family inhibitor of apoptosis, promoting the degradation of the caspases. Previous studies showed that XIAP exerts protective effects in various models of retinal injury and disorders[8,9]. However, in the past few years novel mechanisms independent of caspases cleavage were found[10–12]. Calcium-activated cysteines, calpains, contribute to a secondary neurodegenerative cascade in a similar pattern to caspases in a few models of degeneration and are associated with RP recessive mutations. Calpastatin (CAST), is the only known endogenous inhibitor of calpains. CAST peptides demonstrated efficacy *in vitro* but have yet to show clear *in vivo* rescue.

Another approach undertaken in delaying retinal degeneration is the supply of neurotrophic factors to the retina. The Müller glia cells, very numerous, span the entire retina and are directly involved in maintaining photoreceptors, persisting through the retina degeneration. Their close contact with neuronal cells makes them ideal candidates for the secretion of neurotrophic factors. We previously showed that AAV-mediated gene augmentation of the Glial cell line Derived Neurotrophic Factor (GDNF) leads to efficiently and selectively high levels of GDNF expression in glia cells[13] and promotes neuronal survival, leading to rescue in a S334-4ter rat model lasting up to 6 months post injection.

This study shows the potential of a combination therapy targeting two different cell pathways: cell death as well as the secretion of survival factors to increase efficiency of each single approach in delaying photoreceptor degeneration. This mutation-independent approach is cell-specific, using two AAV variants previously described, 7m8 and ShH10, to respectively target photoreceptors and Müller glia from the vitreous without any competition for cell receptor binding. Secondly, we show that each gene therapy individually slows retinal degeneration but when combined, can lead to a synergistic and consistent functional rescue in the *rd10* mouse model.

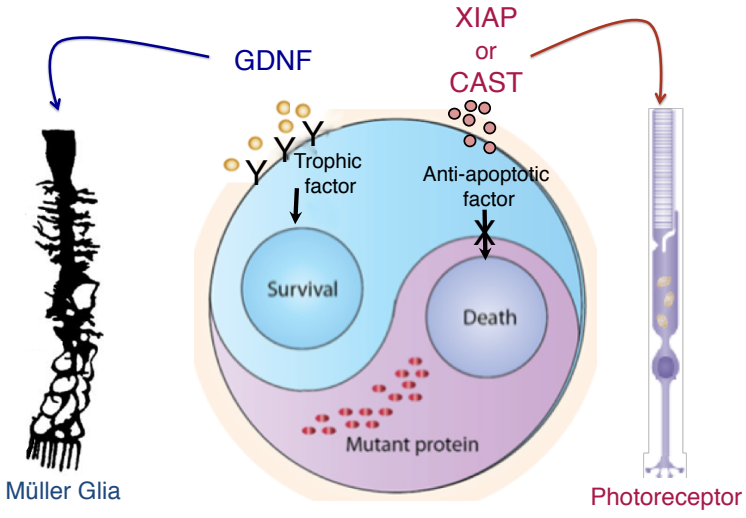

Figure 1: Schematic representation of study aims: gene therapy using **intravitreal** injections of two AAV variants to express a secreted trophic factor, Glial-derived neurotrophic factor (GDNF) in the Müller glia, and an anti-apoptotic factor, X-linked inhibitor of apoptosis protein (XIAP) or calpastatin (CAST) in photoreceptors affected by genetic mutations. This mutation-independent approach is aimed to be non-invasive, and pathway and cell-specific.

Results

7m8 and ShH10 engineered variants do not compete for cell receptor binding

We used previously engineered AAV variants, 7m8 and ShH10, to selectively express our proteins of interest in photoreceptors cells and Müller glia. 7m8 was generated from an AAV2 library pool with randomized 7mer peptide sequences inserted between residues N587 and R588 of the cap gene. Through directed evolution and in-vivo screening to bypass physical barriers, 7m8 was isolated due to its ability to transduce cells efficiently in mice from the inner to outer nuclear layers where photoreceptor cells bodies reside when injected intravitreally. Increased penetration was explained by the. Disruption of the native heparin sulfate proteoglycan (HSPG) binding site of AAV2 explained increase penetration of 7m8 compared to its wild-type parent. 7m8, in combination with a transgene expressed under the control of the human *rhodopsin* (RHO) promoter, has already been used to expression therapeutic DNA in photoreceptors and rescue degeneration in a variety of mouse models and is currently used in clinical trials.

ShH10 was also engineered through directed evolution[14]. It differs from AAV6 by only 4 residues (I319V, N451D, D532N, and H642N) that confer it HSPG dependence, bestowing better penetration through the inner limiting membrane. Glia-transduction abilities from the vitreous[15] were improved with increased binding affinity for epidermal growth factor receptor (EGFR), believed to enable Muller cell infection. To our knowledge, this is the only capsid exhibiting increased cell-specific tropism in the retina. Additional capsid mutagenesis of a tyrosine to a phenylephrine at the Y455 residue location resulted in increased AAV nuclear trafficking and subsequent cell transduction in glial cells. To date, our studies uniquely use the combination of two different viral vectors with different receptor binding properties to infect host cells.

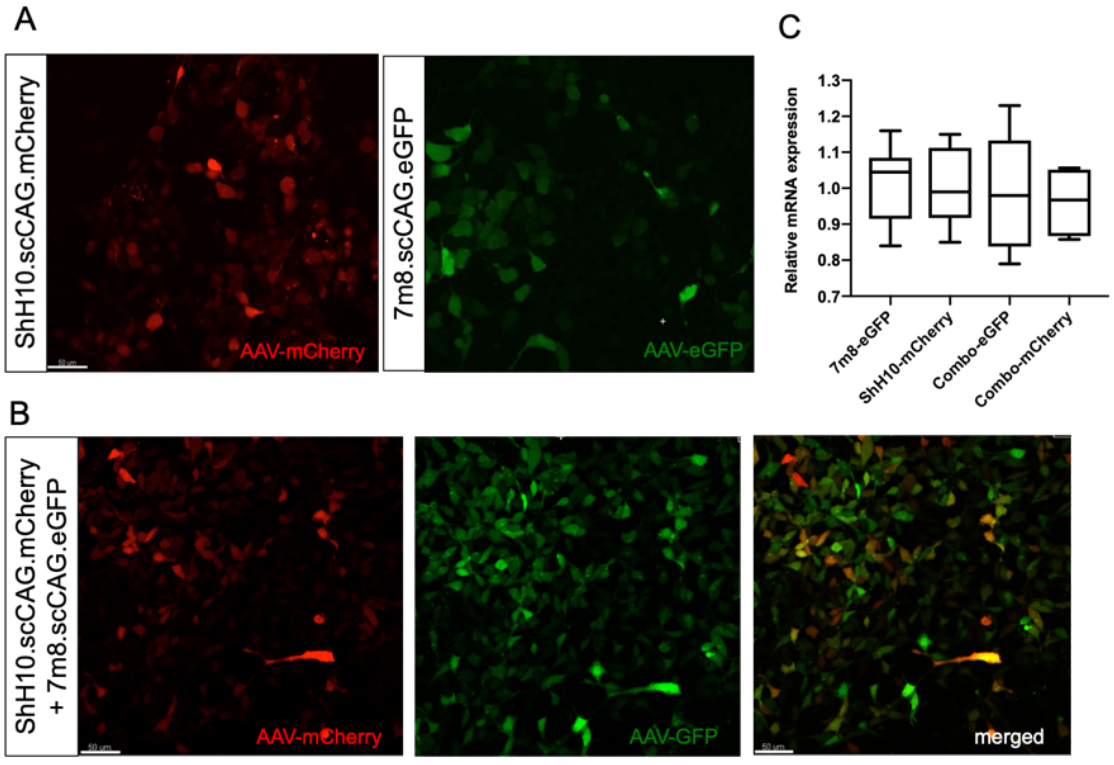

Figure 3: AAVs do not compete for host cell receptor binding *in vitro* when co-infected.
Representative images of reporter (GFP or mCherry) expression in HEK293T cells infected with 7m8.scCAG. eGFP and ShH10Y.scCAG.mCherry separately (**A**) or co-infected with 1:1 mix ratio of both (**B**), at an MOI of $2x10^5$. Cells were fixed 3 days after infection and imaged on LSM70 confocal microscope (20x magnification). Scale bar is 50uM. Relative gene expression of eGFP and mCherry in HEK293T cells infected with single dose of ShH10-mCherry and 7m8-GFP or co-infected with 1:1 mix was measured. Both eGFP and mCherry levels were normalized to levels found in the separately AAV-infected condition (**C**). Means ± SD were plotted. One-way ANOVA, Sidak's multiple comparisons test.

We used HEK293T cells since both AAV variants efficiently infect them and are standardly use for viral packaging. A ubiquitous promoter CAG was used to drive expression of reporter gene eGFP and mCherry when packaged respectively in 7m8 and ShH10, since retinal promoters such as *RHO* wouldn't express in HEK293T cells. HEK293T cells were infected with either single or equal molar ratio 1:1 of 7m8.scCAG.eGFP and ShH10.455YF.scCAG.mCherry at an MOI of 10^5. Three days post-infection, cells grown on coverslips were fixed and imaged to visualized fluorescence while RNA was extracted from a separate set of cells to quantify mRNA gene expression levels. mRNA levels were normalized to GFP and mCherry levels found in HEK293T cells only infected with ShH10Y or 7m8 vectors. 7m8 and ShH10Y led to strong GFP and mCherry expression when expressed separately (**Fig3.A**) or in combination (**Fig3.B**). Gene expression analysis (**Fig3.C**) showed equivalent levels of GFP or mCherry in co-infected cells than single infection of 7m8-GFP and ShH10Y-mCherry. No significant difference was found between each condition (1.015 vs. 0.980, and 1.003 vs. 0.9615-fold change for single compared to co-injection of eGFP vs. mCherry gene expression levels).

We then characterize its co-transduction profile in wild-type mice. Three different ratios of mixed 7m8.scRho.eGFP and SH10Y445F.scCAG.mCherry (~2.0E+13vg/mL) were tested, 1:1, 4:1 and 1:4. WT mice (n=3). Mice were injected subretinally at P15 with 2µL of 1:1 or intravitreally with 1:1, 1:4 or 4:1 mix of 7m8-GFP and ShH10Y-mCherry. Fundus GFP fluorescence was monitored 4 weeks post-injection before eyes were enucleated, fixed, and sectioned.

Injections of 7m8-GFP 1:1 ShH10-mCherry ratio in mice were subretinal (**Fig4.A-D**) whereas the two other ratios 1:4 and 4:1 were injected intravitreally (**Fig4.E-L**). Gradual levels of GFP were observed on the fundus and confocal images (**Fig4.I-E**): higher levels of GFP were expressed in retinas for the ratio of 4:1, while for the 1:4 ratio, the opposite was observable, with high mCherry expression in Müller cells. For the ratio 1:1, a subretinal injection led to a diffuse and homogenous GFP expression in the photoreceptor layer (**Fig4.B**). While ShH10Y can to transduce glia from the vitreous, its capsid tropism differs when delivered in the subretinal space between the photoreceptor and RPE layer, with restricted expression to photoreceptors and RPE cells. As expected, after subretinal injection, ShH10Y led to strong expression in photoreceptors (**Fig4.C**). Imaging showed equal colocalization (**Fig4.D**, yellow merged expression), and strong expression of GFP and mCherry. While quantitative experiments are needed (e.g., mRNA gene analysis or FACs sorting isolation of GFP+ and mCherry+ cell population to estimate the level of co-transduction, this data suggests absence of receptor competition between the two variants when co-injected *in vivo. Rd10* mice were injected with the 1:1 ratio at P15 and enucleated at a similar timepoint than WT mice. We could already see a severe outer nuclear layer thinning compared to WT (**Fig4.M-N**) retinas, also resulting in fewer cells infected by 7m8.Rho.GFP (**Fig4.P**). ShH10Y445F.scCAG.mCherry led to similar glial expression pattern than in WT (**Fig4.O**).

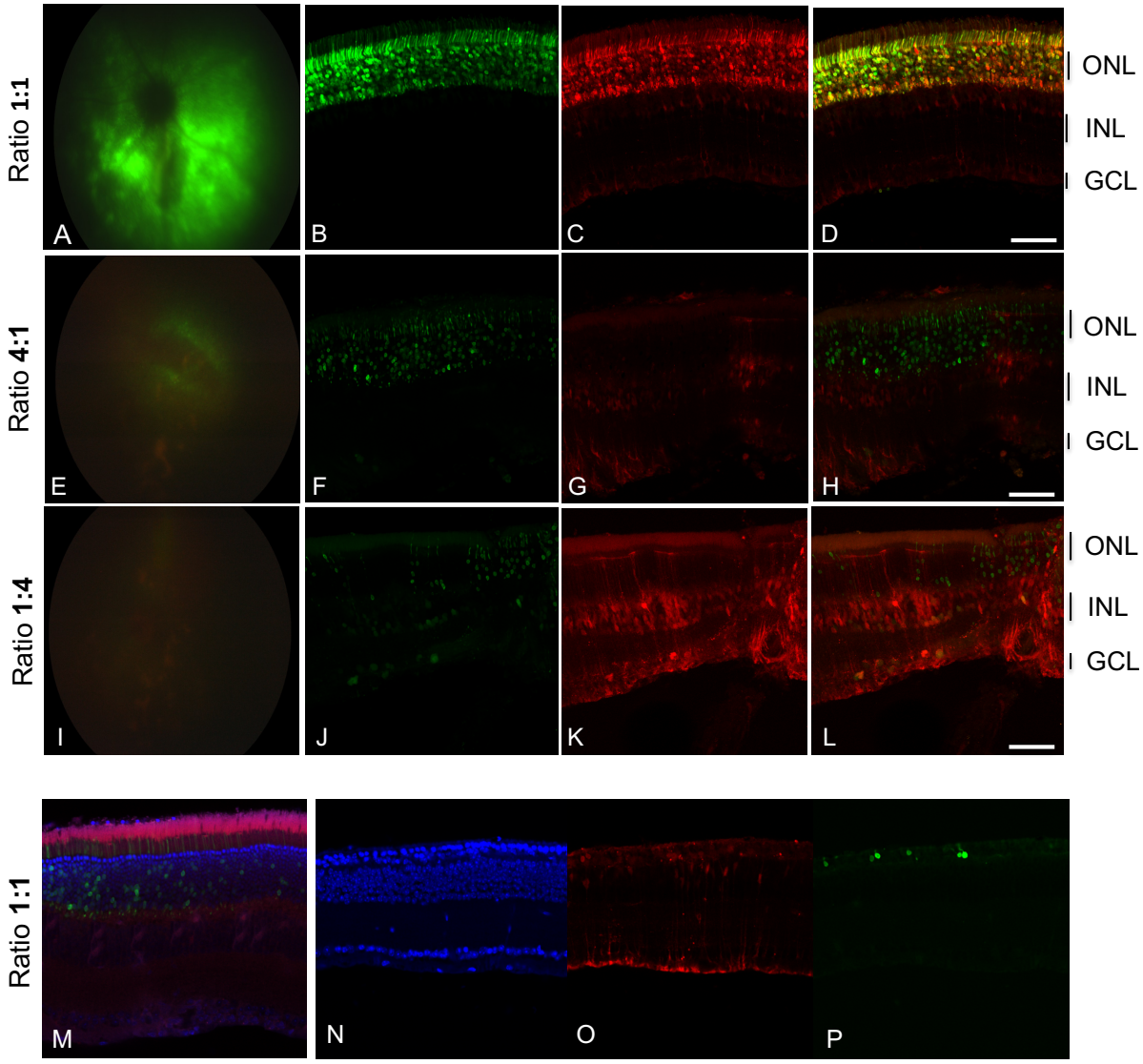

Figure 4: *In vivo* transduction profile of different ratios of 7m8.Rho.GFP and ShH10Y.scCAG.mCherry

Representative fundus images and confocal imaging (20x) of agarose-embedded retinal sections from eyes injected with 7m8.rho.GFP/ShH10Y.scCAG.mCherry mixes from WT (**A-M**) and *rd10* (**N-P**) mice. Separate and yellow-colocalization channels show overlap between GFP and mCherry expression in the outer nuclear layer when injected with 1:1 ratio subretinally **(top row, A-D)**. Images from intravitreal injections showed coherent increase of GFP expression level in photoreceptors: higher expression in 4:1 and weaker in 1:4 whereas strong mCherry expression was observable in Muller glia (**bottom row, E-L**). Structural and transduction comparisons in between WT (**M**) and *rd10* (**N,O,P**) mice injected with a 1:1 ratio show photoreceptor degeneration impact on viral infectivity efficiency in *rd10*. Retinas were imaged at 20x magnification on a laser scanning confocal microscope.

Müller glia secretion of hGDNF slows down rd10 retinal degeneration.

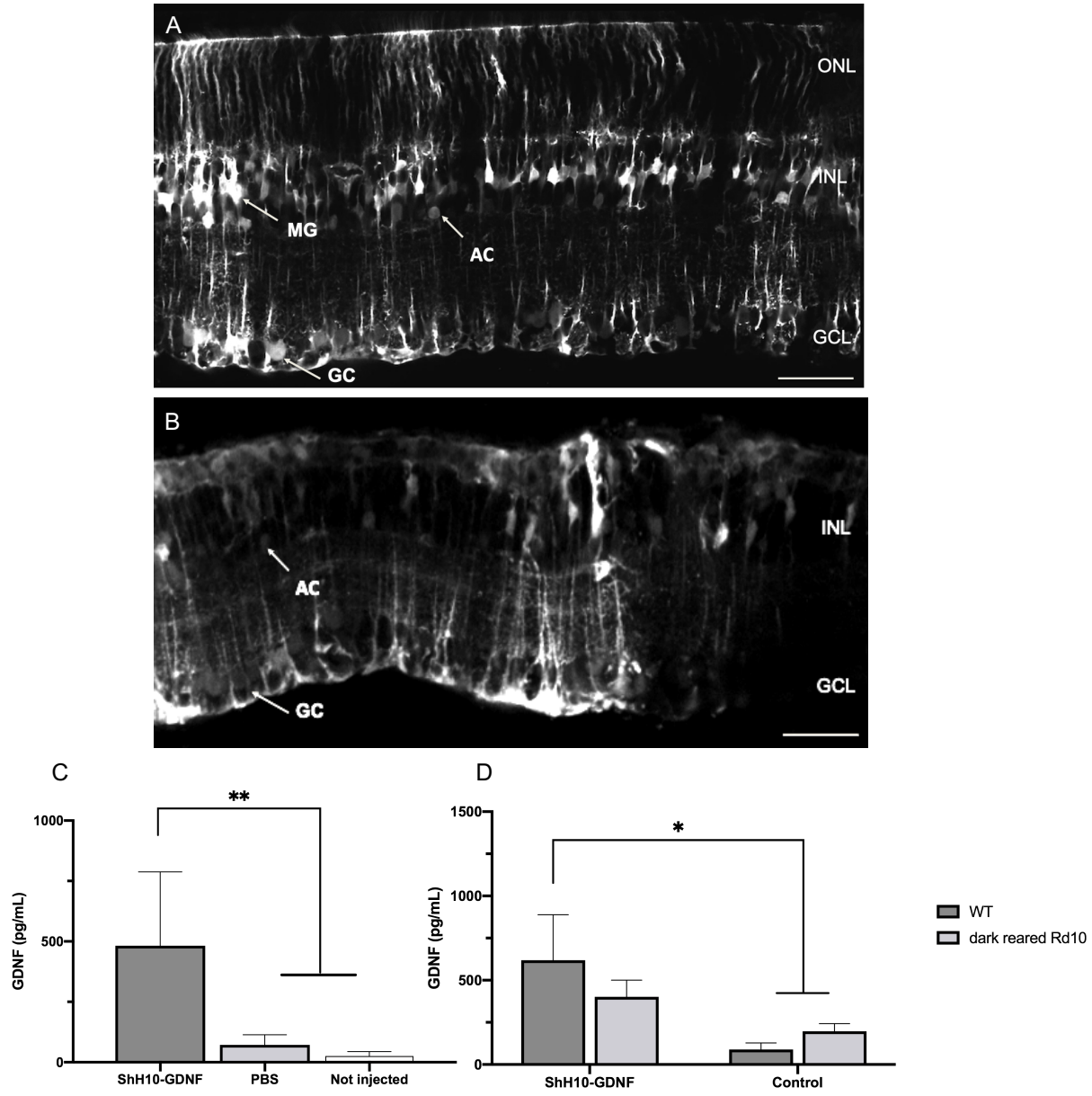

Figure 5: Validation of Müller glia secretion of hGDNF in WT and *Rd10* mice

Characterization of ShH10.Y445FscCAG.eGFP tropism in WT C57BL6 mice (**A**) and *rd10* (**B**) mice injected intravitreally at 1 month. Eyes were enucleated at 2 months, fixed, embedded in agarose and sectioned. Confocal images were acquired (20x magnification, 50μM scale bars).

Enzyme-linked immunosorbent assay (ELISA) was performed to measure human-glial-derived neurotrophic factor (hGDNF) protein in retinal homogenates 1-month post injection (n=3) following intravitreal delivery of ShH10.Y445F.scCAG.hGDNF. The contralateral eye had a sham intravitreal injection of PBS. Non-injected WT eyes were also used as control (**C**). One-way ANOVA, tuckey's test was performed on mean values. (**D**) GDNF Secretion between WT and dark-reared *rd10* mice injections was also compared using 2way ANOVA, Sidak's multiple comparisons test. All eyes/retinas were collected at 2 months, 1-month post-injection. For all statistical test, ***=$p<0.001$, **=$p < 0.01$, *=$p<0.05$. Data represent mean ± SD.

While AAV-mediated secretion of GDNF was previously shown to be neuroprotective and delay photoreceptor degeneration in a rat model of RP, S334ter rhodopsin, it had not been replicated yet in a mouse model of RP. We first confirmed that ShH10Y-mediated GDNF transgene expression leads as well to functional rescue before assessing its synergetic effect in combination with another therapeutic agent. We performed an ELISA on WT and *rd10* eyes injected with ~2.0E+13 vg/mL ShH10Y-GDNF to assess proper secretion of the neurotrophic factor to the retinal cells. We compared WT eyes virally injected with sham injection of PBS as well not injected eyes (**Fig5.C**). Robust secretion of hGDNF from Müller cells was measured (481.0 +/- 305.7 pg/mL), significant compared to PBS (71.70 +/- 42.9, p=0.0089) and noninjected eyes (25.45 +/- 18.35, p=0.0043). In our previous studies in S-334-4ter rats, quantified hGDNF secretion was close to 2.5ng/mL. However, the rat retina contains higher number of cells than in mouse due to bigger retinal surface, which can explain the ~5-fold lower concentrations we found. No significant difference (**Fig5.D**) was found in between WT and *rd10* eyes (n=3 each) injected with ShH10Y-GDNF, although mean values were slightly lower (617.877 +/- 270.288 vs 401.1 +/- 99.671 pg/mL) in *rd10*. ShH10Y transduction profile in WT and *rd10* can explain this outcome: the viral vector transduced a higher number of Müller glia in WT retinas (**Fig5.A**) compared to in *rd10* (**Fig5.B**) at 2 months old, where the expression was dimmer and patchy. Retinal remodeling happening in *rd10* has been hypothesized to affect inner retinal neurons and glial cell surface receptors, and therefore could decrease AAV cell binding infectivity.

rd10 mice were raised and maintained in constant darkness as it has been previously being shown to preserve photoreceptors from light-evoked damage[18] and delay ONL degeneration. This strategy enables longer time window for AAV vector expression. Electroretinograms (ERGs) were recorded to assess visual function in dark-reared *rd10* mice injected intravitreally at P15 with ShH10Y-GDNF. Mice were exposed to a brief flash of light only detectable by rod photoreceptors (scotopic light intensity), before being light-adapted to saturate their response to isolate cone response to brighter light intensity stimuli (photopic). At one-month post-injection, no difference was detected in the scotopic or photopic induced-amplitudes of the treated eyes relative to the control untreated eyes injected with PBS (**Fig6.A-B**). We repeated the experiment with an increased viral titer of 2.0E+14vg/mL and noted improved scotopic B-wave values of 397±79.63 µV for the treated eye versus 277 µV ±102.7 for the contralateral control (p=0.025). When results were plotted to look at individual mouse traces, close to a 2-fold increase was noticed in all, except one, animals. Increase in scotopic A-wave amplitudes (283 ±29.9µV versus 216 ±26µV) was also detected (**Fig6.C-D**). However, we did not detect a protective effect in cone-mediated photopic ERG amplitudes. Amplitudes were quite heterogeneous among treated animals (**Fig6.E-F**), highlighting inter-variation in the onset of degeneration within the same mouse litter.

Furthermore, ten days later, the protective effect of GDNF dissipated, with B-wave mean of 251 µV ±147.25 versus 241 µV (±128.48) in the treated and control eye respectively. Same finding for A-wave of treated and non-treated eyes (49 ±29µV versus 53 ±38µV). While hGDNF secretion was able to delay retinal degeneration, and more particularly rod photoreceptors cell death significantly, this effect was not sustainable at P55, neither was observed in cones at any time point.

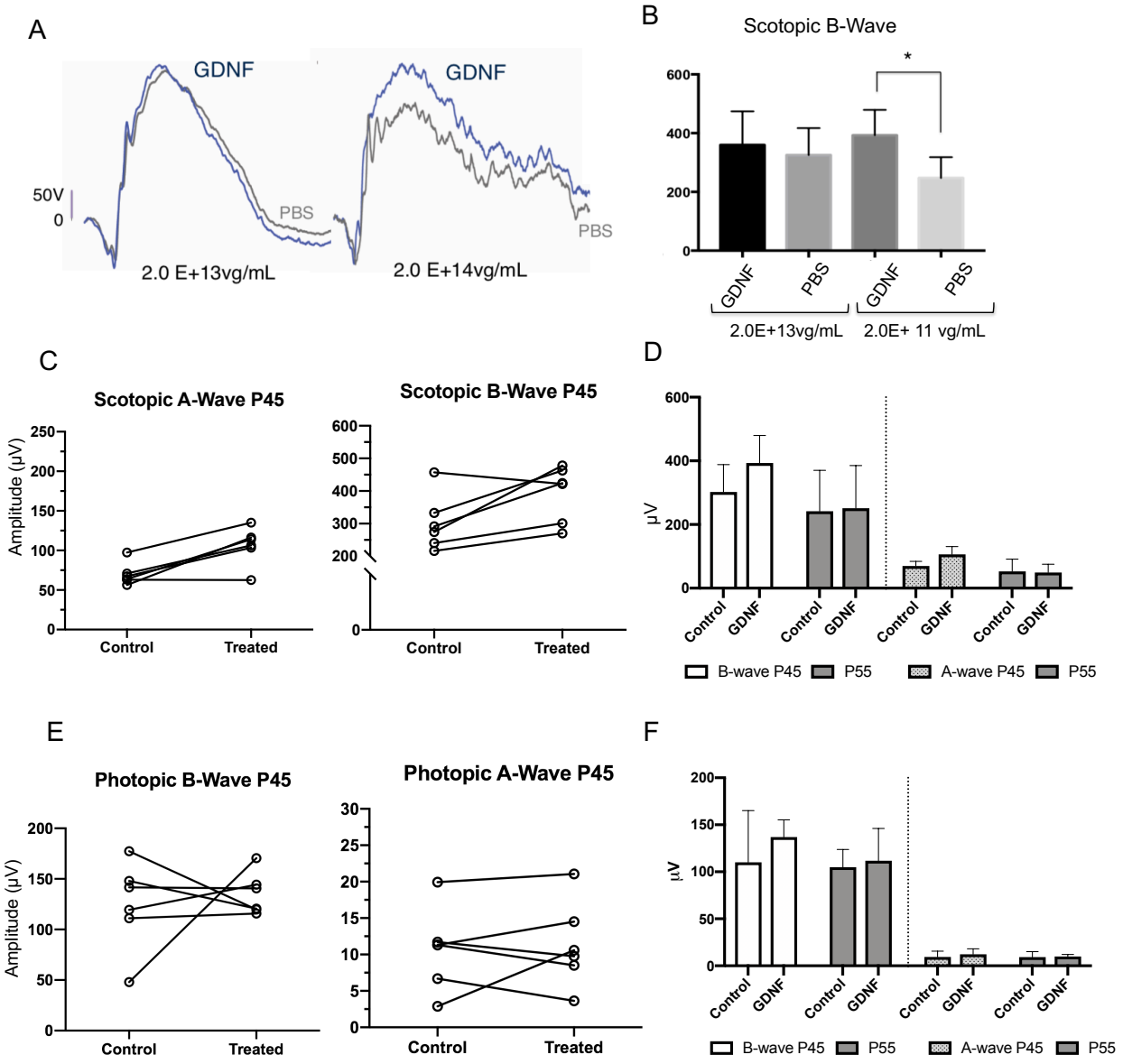

Figure 6: ERG A-wave and B-wave amplitudes in response to photopic and scotopic light levels in hGDNF treated and contralateral eyes 1 and 1.5 half months post-injection.

Representative B-waved amplitudes in response to 1 log cd x s/m^2 (**A)** measured in *rd10* mice (n=6) injected at P15 with ShH10Y455F.scCAG.GDNF (blue trace) and contralateral control (gray trace, PBS) eye. Results were plotted (**B)** with standard deviation error (SD). Significance difference was found in the group treated with 2.0E+14 vg/mL ShH10Y-GDNF.

Scatter plots of scotopic (**C**) and photopic (**E**) ERG traces show heterogeneity in among mice at P45. ERGs were compared to amplitude 10 days later, postnatal P55, and plotted (**DF**) to assess sustainable effect of the treatment. Statistical Mann-Whitney paired t-test was performed to compare ERG amplitudes in treated and contralateral control eyes. For all statistical test, ***=p<0.001, **=p < 0.01, *=p<0.05. Data represent mean ± SD.

Non-caspase dependent-apoptosis events occur in degenerative rd10 retina

Past consensus was that photoreceptor cell death mechanisms were relying the heaviest on apoptosis in rods affected by the genetic mutation, triggering necrosis in cones due to lack of nutrients and release of toxins molecules in the photoreceptor sub-space. XIAP was investigated as one of the leading therapeutic candidates to block apoptosis-mediated photoreceptor cell death. However, a strong indication for Ca^{2+} involvement has been shown in many RP models, which modulates calpain activity. Calpains, are Ca^{2+}-activated cysteine proteases, similarly to caspases, cleave substrates related to cell death signaling. It is linked to both non-caspase apoptotic as well as necrotic pathways.

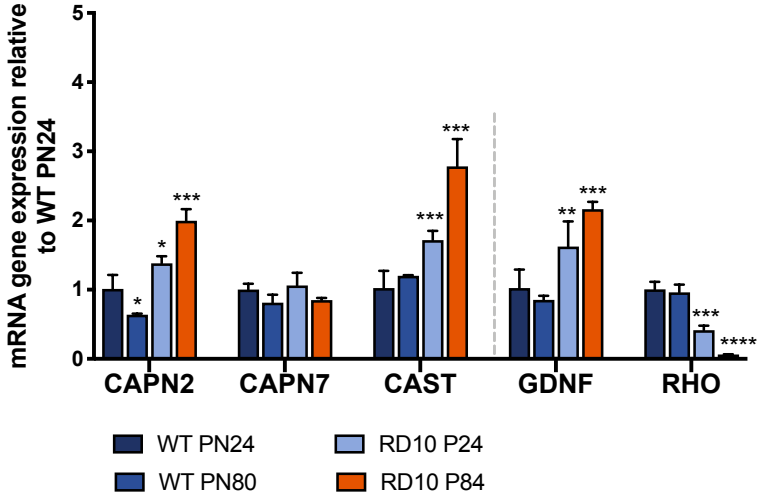

Figure 7: Calpains are overexpressed during retinal degeneration in *rd10*.
Gene expression levels of main retinal calpains (CAPN)-2 and -7, calpastatin (CAST), glial-derived neurotrophic factor (GDNF) and rhodopsin (RHO) in WT and *rd10* retinas (n=4) at postnatal day 24 and 80. Ct were normalized using the housekeeping gene GAPDH and plotted as fold expression change relative to WT P24. Two-way ANOVA, Tuckey's multiple comparisons test was performed (* $p<0.05$, *** $p<0.0005$, *** $p<0.0001$) to compare fold-changes between subgroups. Means ± SD was plotted.

We assessed calpains activity during degeneration in the *rd10* mouse model. We compared gene expression levels of the main calpains involved in neurodegeneration, such as calpain-2 and -7, as well as the ubiquitous calpain inhibitor, calpastatin, to genes that are known to be either up-regulated (GDNF) or down-regulated (RHO) during retinal degeneration[16] (**Fig7**). We extracted RNA from WT and *rd10* retinas at two different time points, 24 and 80-84 days postnatal (PN), and generated cDNA to assess transcriptional changes occurring in *rd10* during and after photoreceptor cell death. Both calpain-2 and CAST were significantly up-regulated in PN24 ($p=0.49$ and $p<0.001$ respectively) and PN84 *rd10 (*both $p<0.001$) retinas. Interestingly, levels of Calpain-2 in WT mice decreased at PN80 (0.637 ± 0.018, $p=0.0033$), showing activity only during retinal development. While Calpain-7 is one of the most expressed calpains in both human and mouse retina, no alteration was observed in degenerative or healthy retinas. As expected, progressive loss of photoreceptors in *rd10* correlated with down-regulation of *RHO*, with slight expression left at P84 (0.063 ± 0.005, $p<0.001$).

Non-caspase dependent-apoptosis events occur in degenerative rd10 retina

We further looked into whether blocking either the caspase-dependent or independent apoptotic pathways in dark-reared *rd10* mice will lead to photoreceptor rescue. Dark-reared *rd10* mice were injected at P15 in one eye with 7m8.scRHO.XIAP or RHO.CAST (1.0E+13vg/mL) and PBS in the contralateral eye.

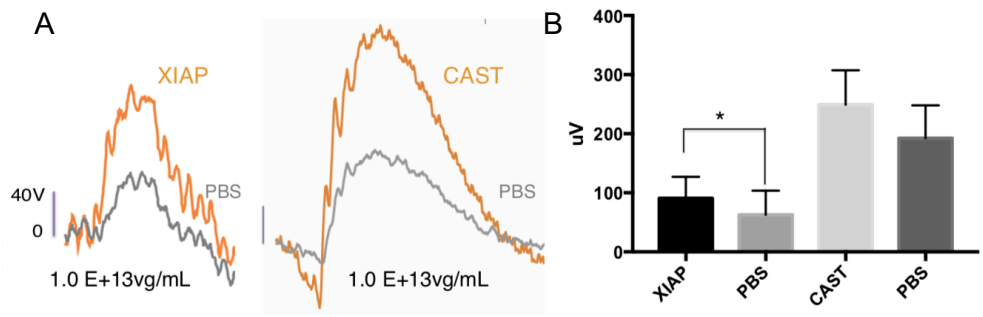

Figure 8: XIAP and hCAST gene expression in photoreceptors mildly delays degeneration Representative B-waved amplitudes in response to 1 log cd x s/m^2 **(A)** measured in dark-reared *rd10* mice (n=5-8) injected at P15 with either 7m8.Rho.hXIAP or hCAST (orange trace) and contralateral eye control (gray trace, PBS). Results were plotted **(B)** with standard deviation error (SD). A significant difference was found in the group treated with 1.0E+13 vg/mL 7m8-XIAP (Paired-t-test, * $p<0.05$) but not with CAST.

Interestingly, we saw a small rescue ($p=0.045$) toward scotopic B-wave amplitudes in eyes injected with AAV-XIAP. No therapeutic effect was observed under photopic light stimulus (data not shown). Mice injected with AAV-CAST had more mitigated and heterogenous improvement in the amplitudes. A few mice had over 2-fold improvement in the B-wave (**Fig8.A-B**); some showed no difference compared to the contralateral eyes. Optimizing the delivery and expression of CAST might help with the consistency of the rescue. Retinal thickness was measured by in vivo imaging of retinal layers using optical coherence tomography one month after injection. Surprisingly, even though the light response was slightly improved, eyes treated with XIAP showed structural preservation compared to some of the control eyes degenerating faster or subject to retinal detachment (data not shown) due to advanced degeneration.

Combination therapy slows retinal degeneration

We compared the combination of an equal amount of ShH10Y-GDNF and 7m8-XIAP to single delivery. As previously shown, lower ShH10Y titer did not improve the treated eye B-wave amplitude (302.4 ± 56.86µv) in comparison of the control (333.2 ± 41.96 µv). In contrast, delivering 1.0E+13 viral particles of 7m8-XIAP did again lead to a slight rescue. However, when 1:1 ratio mix injected, GDNF-XIAP treated eyes displayed higher B-wave amplitude than internal control (256.4 ± 4.53 vs. 186.2 ± 15.6µV, $p=0.012$), which was consistent in all treated eyes (**Fig 9.A-B).** The therapeutic effect was also conserved under photopic light stimulation, with B-wave higher in treated versus control eyes at P45 (96.6 ± 9.45 vs. 65 ± 15.6µv). The titer of AAV-GDNF and XIAP were 2-fold lower (5.0E+12vg/mL) in 1:1 mix than in single injection of GDNF or XIAP although it displayed similar if not higher scotopic and photopic ERG amplitudes at P45 and P55 (**Fig 9.C**) in response to light stimulus.

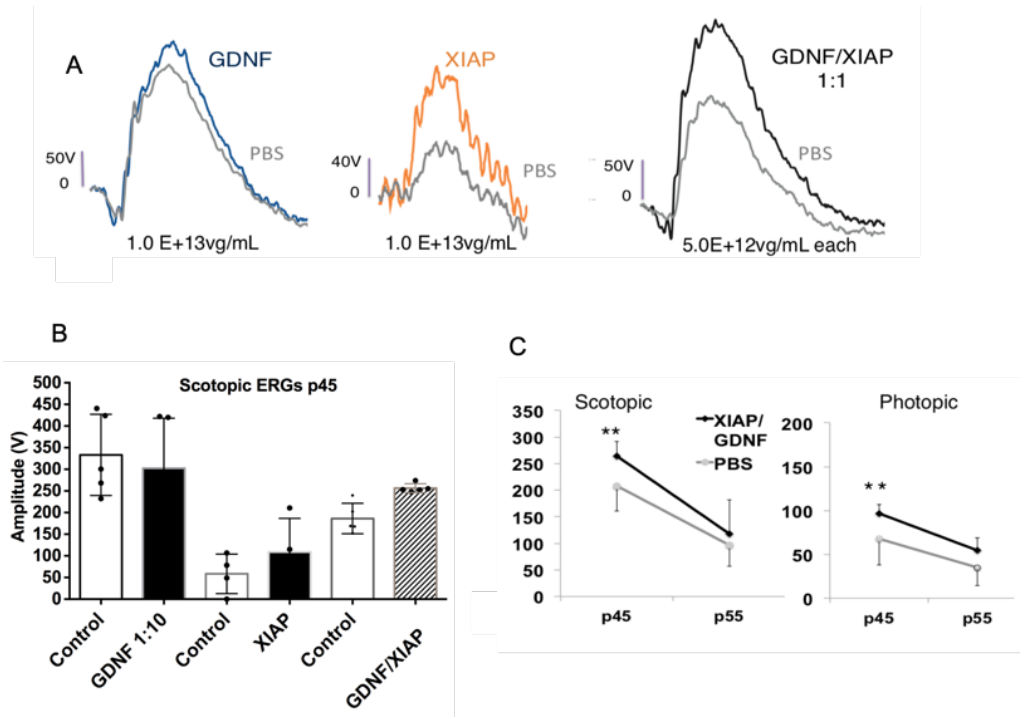

Figure 9: Combination therapy leads to significant rescue compared to single approach. Representative **(a)** and quantitative (**b**) scotopic B-wave ERGs at p45 from *rd10* mice raised in dim red light and injected in one eye with 2µL of equal titer of ShH10Y.scCAG.GDNF and 7m8.Rho.XIAP or AAV- GDNF/XIAP ratio 1:1. PBS was injected in the remaining untreated eye. **(c)** The therapeutic (XIAP/GDNF) mix shows significant rescue with higher B-Wave amplitude than the control at p45 (p-value = 0.01), which the effect is still persist 10 days later. Statistical Paired-t-test was performed on treated versus control eyes mean values. **=p<0.01, *=p<0.05.

Rescue experiments should be repeated with matching XIAP and GDNF viral titer in single injection versus combination mix to really assess more precisely synergetic rescue, however combination therapy approach showed promising results in efficiently delaying retinal degeneration.

Optimization of ShH10-mediated cell transduction and specificity in rd10 improved gene therapy.

AAV-mediated selective glia targeting from the vitreous has been a challenge in the retina until the development of the ShH10 variant. Natural occurring AAVs (e.g. AAV2) can transduce Müller glia cells, but large promoters (3000-2000 base pairs) are required to achieve selective expression, ruling out the use of AAV as delivery vector due to its limited carrying capacity. ShH10 has the advantage of bypassing the use of cell-specific promoters to restrict expression in MGCs. However, through our study, we found a higher off-target rate than the 5% reported in the original paper, with transduction in the amacrine and ganglion cell layers (**Fig 5.B, Fig 10.A**) as well as lower transduction efficiency in the *rd10* mouse model of degeneration.

A few recent studies have explored the combination of newly engineered small promoters such as GfaABC1D (680bp) to improve on glia selectivity. Here, we compared side by side eGFP expression driven by ShH10Y.scCAG and 7m8.scGfaABC1D. In wild-type retinas, 7m8 holds

high transduction levels in a broad, and therefore not cell-specific, retinal population compared to native AAVs. Under the control of the scGfaABC1D promoter, 7m8 achieves pan retinal and selective Müller Glia expression (**Fig 10.B**), with strong co-expression with MGC-specific glutamine synthetase (GS) marker. While ShH10.scCAG.GFP expression also co-localized with GS staining; fewer MGCs were targeted, with apparent off-target expression.
We then tested whether or not 7m8.scGFAP.GDNF improved visual rescue observed with ShH10.scCAG.GDNF in dark-reared *rd10*. ERG analysis pointed to steady improvement in both the B-wave and A-wave amplitudes of treated eyes generated following photopic and scotopic light stimulus compared to the contralateral eye. The therapeutic effect was consistent in individual experimental mice as well (**Fig 10.C-F**). Vector optimization for photoreceptor targeting will likely also improve on observed rescue.

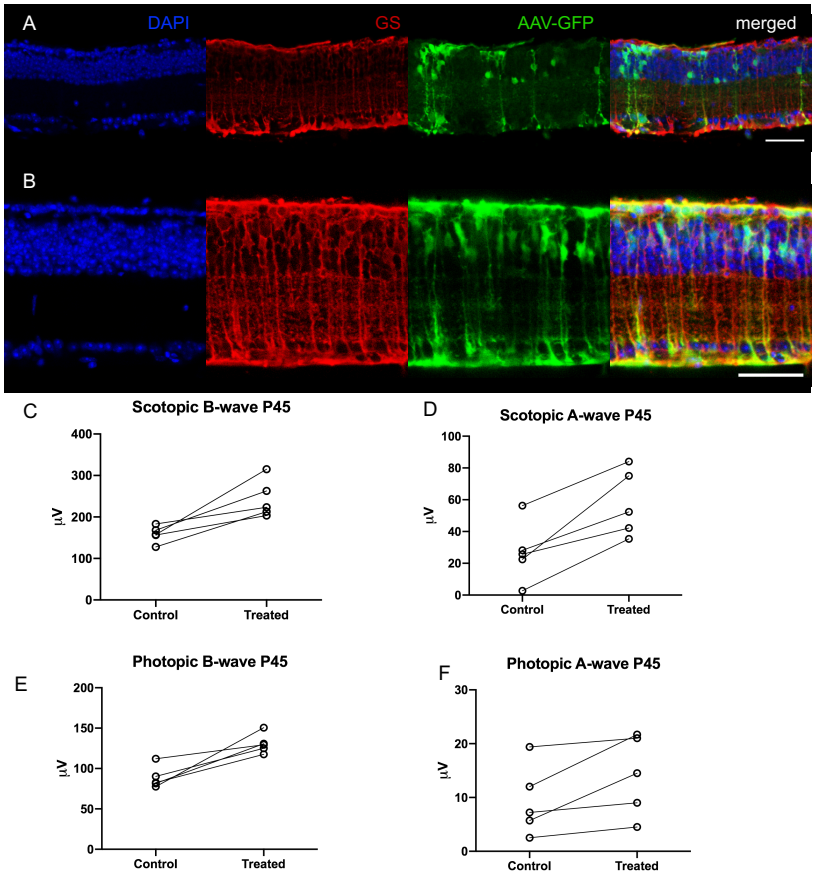

Figure 10: Müller Glia vector optimization leads to gene therapy improvement
Confocal imaging of agarose-embedded retinal sections from eyes injected with ShH10.scCAG.eGFP (**A**) and 7m8.gfaABC1D.eGFP (**B**). *Rd10* mice were sacrificed one-month post-injection, at PN60. Cell nuclei were labelled with DAPI (blue) and Müller glia were labelled with glutamine-synthetase (GS, red) staining. Colocalization between viral expression and Müller glia was observed in the yellow channel. The scale bars represent 50 µm. Scatter plots of scotopic (**C, D**) and photopic (**E, F**) ERG traces show rescue mediated by 7m8.gfaABC1D.eGFP in dark-reared treated eye at PN45.

Discussion

Mutation-independent therapies are a promising approach to treat a large group of inherited retinal degenerations arising from a diverse genetic background. To date, most studies show efficacy with subretinal injections. However, this route of administration has adverse side effects such as tissue atrophy and retinal detachment close to the site of injection. These mechanical injuries induce the secretion of neurotrophins in response to injury, which can veil the therapeutic outcome of the delivered treatment. This study recapitulates the benefits of intravitreal injections, achieving pan-retinal expression in the retina as well as noninvasive delivery of therapeutic vectors.

However, it required high viral titers (>2.0E+13vg/mL) to discern a significant therapeutic effect with the GDNF stand-alone gene therapy. High doses of viral particles are a concern for ocular toxicity. Viral vector optimization in the form of choice of the AAV capsid and cell-specific promoter reduces the dose needed to achieve stable and cell-selective transgene expression. Here, we showed that selective GDNF expression in Müller glia cells driven by a 680bp glial promoter (gfaABC1D) led to a more robust rescue in *rd10* than observed with the ShH10Y-GDNF. Higher transduction was also achieved by delivering with the high retinal penetrance AAV variant 7m8, over ShH10.Y445F. Furthermore, the current stage of retinal degeneration also dictates the gene therapy outcome. Deferring photoreceptor cell death to sustain visual function is dependent on the number of photoreceptors still left to treat. The *rd10* model is routinely used for early testing of therapies due to its relatively slow start of degeneration (PN18) compared to its rd1 parent (PN5), with no photoreceptor remaining by PN60 [17]. Dark-rearing *rd10* from birth extends the therapeutic window to the length required for viral vector expression (3-4 weeks) by preserving photoreceptors from light-evoked damage[18]. While AAV systemic delivery in neonatal pups can achieve the early and efficient expression[19] needed in a degenerative model, this is not a therapeutic approach applicable to human. Therefore, we preferred intravitreal injection in dark-reared *rd10* mice when eyes opened at PN15.

Calpain and related inhibitors (CAST) are a novel and promising target for neurological diseases. Their discovery paved the discovery of novel cell death mechanisms in the rd mouse model mimicking human retinitis pigmentosa disease phenotypes and genetics. However, overexpressing hCAST in photoreceptor did not lead to a significant rescue. We believe that this could also be due to the low transduction efficiency of the single-stranded AAV-RHO-hCAST, as we were able to see a slight improvement with eyes treated with XIAP, which was packaged in a self-complementary AAV vector. We questioned here whether the functionality of our AAV-RHO viral vectors impacted amplitude of visual rescue. Rod-specific genes are down-regulated in models of degeneration driven by the loss of rod photoreceptors. It likely affects transgenes expression driven by hRHO promoter. Alternatively, inclusive (targeting both cones and rods)[20] and short promoter sequences could improve photoreceptor transduction efficiency. Self-complementary AAV (~2.7kb) vectors have up to 100-fold higher transduction efficiency due to skipping second-strand DNA synthesis, conceding faster transgene expression than traditional single-stranded AAV [21,22].

Moreover, although inhibitors of programmed cell death are promising agents to delay neurodegenerative disease progression, it is unlikely that targeting only one pathway would stop cell death progression, as cells have several signaling cascades involved and complicated genetically programmed ways (caspase-dependent or independent apoptosis, necrosis, autophagy-

mediated) of death. Trichonas *et al.*[23] demonstrated that cells counterbalance pharmaceutical inhibition of apoptosis induced by retinal detachment through RIP-mediated necrosis mechanisms. Species-specific (human to mouse), as well as causative mutation differences in cell death initiation need to be more thoroughly investigated. It highlights mechanism heterogeneity, and complexity that stand-alone therapies are not able to address.

Combining XIAP-mediated blockage of rod photoreceptor apoptosis to Müller glia-induced hGDNF secretion showed a synergistic rescue effect compared to individual approaches. Perrelet *et al*[24]. found a 2-fold increase in endogenous levels of XIAP in motor neurons after GDNF treatment following axotomy. He further demonstrated unique cross-talk between XIAP and GDNF as inhibiting XIAP blocked GDNF-neuroprotective effects, but not other trophic factors.

Combination therapies may yield a general and widely applicable approach for retinitis pigmentosa treatment. As promising as these therapies are, anti-apoptotic and neurotrophin based-therapies cannot replace activity lost due to a loss-of-function mutation. Research must still focus on discovering the gene mutations involved in all forms of retinal degeneration. However, the fact that trophic factor treatments are beneficial supplements to any form of gene therapy, both to extend the timeline of gene-replacement therapy and to increase the long-term efficacy of the treatment, is a great benefit. This strategy can be used until the underlying mutations and treatments for the remain inherited retinal degenerations have been discovered and developed.

Materials and methods

AAV plasmid generation:

All plasmids used for AAV packaging (Fig1) contain inverted terminal repeats, as well as the bovine human growth factor polyadenylation signal and woodchuck post-transcriptional regulatory element WPRE.

pAAV.scRho.XIAP was constructed by amplifying cDNA encoding human XIAP (Addgene, Cambridge, USA) from scCAG.XIAP with the set of primers GCG GGC ATG ACT TTT AAC AGT TTT CA and CCA ATC AAC CTC TGG TTA AGA CAT AAA AAT TTT TT, using a Hi-Fidelity PCR kit (Roche, Indianapolis, USA). The PCR product was then purified (Qiagen PCR purification kit, Maryland, USA) and digested along backbone pAAV.RHO.(GFP) with SfiI and AfeI for 1 hour at 37°C. The 1604 bp fragment was cut out and gel purified (Qiagen Gel purification kit, Maryland, USA) and eluted in 30 µL of water. The insert and the backbone were ligated (Roche Quick Ligation kit, Indianapolis, USA) and transformed into competent cells.

Plasmids pAAV.scRHO.GFP and pAAV.scCAG.GDNF were already available from previous studies (Dalkara et al. 2011). Cloning of scCAG.mCherry was based on the same protocol. The mCherry gene (702bp) was amplified from pcDNA1/hChrR2(H134R) mCherry with the set of forward and reverse primers AgeI-mCherry 5'-ACCGGTCGCCACCATGCTTGTACAGCTCGTCCATGC-3' and mCherry-HindIII 5'-ACT ACC GGCGAAATCACTCGTTCC CGCTCCTCCTATTGT-3'. The PCR product and the backbone (pAAV.scCAG.GDNF) were digested with HindIII and AgeI, ligated and transformed. Human CAST (~2100bp) cDNA sequence were amplified from HEK293T cell using forward 5-ACTGTGTCTTGCATCTTCTTTAGCCT-3' and reverse 5'ACTGTGTCTTGCATCTTCTTTAGCCTTTGGC-3' primers. cDNA was inserted in a Topo vector to confirm sequencing and then cloned in the pAAV.RHO.GFP backbone.

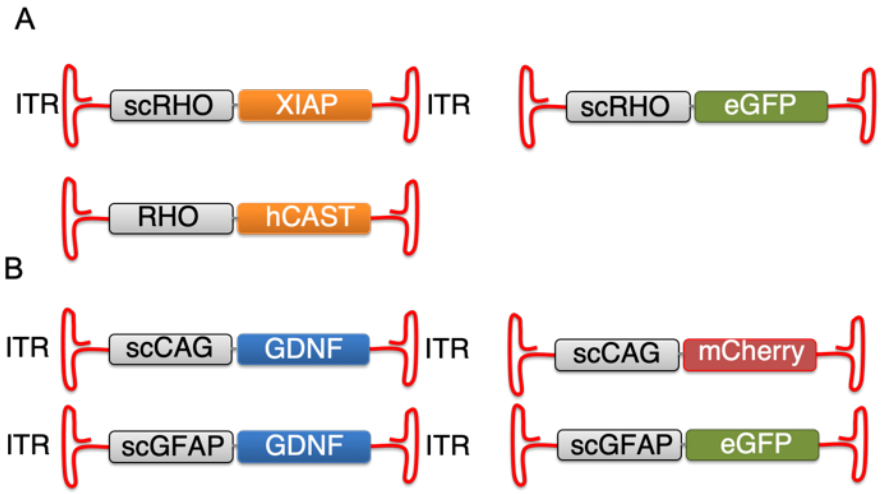

Figure: Schematic representation of all AAV plasmid vectors cloned and used in this study to achieve expression in photoreceptors (A) and Müller glia (B).

AAV viral vector production

AAV vectors were produced by the plasmid triple co-transfection method described in Visel et al [25]. AAV plasmids containing the AAV rep and capsid sequence of choice (7m8 or ShH10-Y445F) were co-transfected with pHelper plasmid in HEK293T cells.

Three days later, cells were harvested and spun down at 1000 rpm for 10 minutes. 1) Supernatant and 2) cell pellet were separated. 1) The supernatant was mixed with 40% PEG (8% final concentration) and incubated on ice for 2 hours to allow for protein precipitation before centrifugation at 4000 rpm for 20 minutes. 2) The cell pellet, containing majority of AAV particles, was resuspended in lysis buffer (0.15 NaCl, 50 mM Tris HCl, 0.05% Tween, pH 8.5) and exposed to three consecutive freeze/thaw cycles in a dry-ice/ethanol slurry and 37ºC water bath, respectively. The crude lysate was further treated with 250U/µl of Benzonase (Novagen #71205-3) for 30 minutes and spun at 4000 rpm for 20 min at 4ºC. The pellet resulting from the precipitation of the supernatant (1) was resuspended with the crude lysate supernatant (2) and incubated in 37ºC to allow proper homogenization. The lysate was layered onto an iodixanol density gradient (OptiPrep®) and ultracentrifuged for one hour at 69000 rpm at 18ºC to allow for protein separation based on molecular weight. The fraction between the 60% and 40% iodixanol was extracted, diluted with an equal volume of 1X PBS + 0.001% Pluronic F68 and then loaded into an Amicon Ultra-15 Centrifugal Filter Unit (Millipore, Tullgren, Ireland) and spun until 250 µl of concentrated vector remained. The concentration step was repeated three times with 5mL washes of fresh sterile PBS. A final viral concentrate of ~200 µl, devoid of iodixanol buffer, was ultimately obtained. The viral concentrate was subjected to DNase treatment to remove any residual plasmid DNA or unpackaged genomes, and the vector was then titered by quantitative PCR.

In vitro cell infection

HEK293T cells were seeded onto a poly-D-lysine coated glass coverslip or directly into 12-well plate at a density of ~100,000 cells. Next day, cells were infected with AAV at a MOI of 10^5. Three days later, fluorescence from reporter genes were quantitatively measured by extraction mRNA to assess eGFP or mCherry expression levels or qualitatively by fixing the cells on coverslip and imaging fluorescence using a confocal microscope.

Animals

C57BL6J (#000664), BALB/cJ (#000651) WT mice and *rd10* (*Pde6b*^{rd10}*/J,* #004297) mice were obtained from the Jackson Laboratories. WT mice were maintained in a normal 12/12 light/dark cycle. Experimental *rd10* mice were moved to a light-safe box in constant darkness and animal husbandry was conducted under dim red light. *rd10* were transported to the procedure room in covered cages to avoid light exposure. All animal procedures were conducted according to the ARVO Statement for the Use of Animals in Ophthalmic and Vision Research, and the guidelines of the Office of Laboratory Animal Care and Use at the University of California, Berkeley, CA.

Intravitreal injections

Mice were anesthetized with ketamine (58 mg/kg) and xylazine (6.5 mg/kg) by intraperitoneal injection. The topical anesthetic proparacaine (0.5%) was first applied to the eyes, and the pupils were dilated with phenylephrine (2.5%) and tropicamide (1%) drops. Eyes were immersed in Genteal gel to prevent from drying during procedure. A coverslip was positioned on the surface of the cornea to allow for direct visualization of the retina and vitreous space. An ultrafine 30 1/2-gauge disposable needle was passed through the sclera, posterior to the limbus, to create a small hole into the vitreous cavity. One to -two µl of virus with a titer $>1\times10^{13}$ vg/ml was then injected into the vitreous with direct observation of the needle above the optic nerve. Contralateral eyes of experimental *rd10* mice were injected with either viral vector expressing fluorescent reporter or PBS. Following injection, tobramycin drops were applied to prevent eye injection, followed by artificial tears ointment to keep the eye moisturized until the mouse recovered.

Fundus imaging

Transgene expression was assessed one to eight weeks after injections using a fundus camera (Retcam II; Clarity Medical Systems Inc., Pleasanton, CA) equipped with a wide angle 130° retinopathy of prematurity (ROP) lens to monitor eGFP expression. Pupils were dilated for fundus imaging with phenylephrine (2.5%) and Tropicamide (1%), and Genteal gel was applied to the cornea before imaging.

ELISA quantification of hGDNF levels

Treated and control eyes were enucleated after mouse euthanasia and stored in 1% PBS on ice. Retinas were dissected out the eye cup and placed in lysis buffer (50mM Tris-acetate, 65mM NaCl, 2mM $MgCl_2$, 2mM EDTA, 1% protease inhibitors cocktail) before sonicating the tissue. ELISA was performed using the DuoSet Kit for human GDNF (R&D Systems) according to manufacturer's instruction. A 96-well plate was coated overnight with the capture antibody diluted in PBS. After incubation, wells were washed 3 times in wash buffer (0.05% Tween-20 in PBS) then blocked for 3 hours at room temperature with 1% BSA in PBS. After 3 rinses, samples and standards were added in duplicate for 2 hours. Samples were washed and then incubated with the detection antibody. After the last series of washes, the substrate solution was added for 20 minutes. At the end of the incubation, stop solution was directly added to the wells. Absorbance was measured at both 450nm and 540nm wavelengths. The 540nm reads were subtracted from 450nm to correct for the optical imperfections of the plate. The amount of GDNF present in samples was calculated from a 2-fold serial dilution hGDNF (2000pg to 31.3pg/mL) standard curve. Results are the average of duplicates.

Electroretinogram (ERG) recording

Dark-reared *rd10* were transferred to a dark adaption room overnight before proceeding to a recording session. After anesthesia, eyes were dilated using both tropicamide and phenylephrine. Mice were placed on a 37°C heated pad during this preparation to maintain constant body temperature. Contact lenses were positioned on the cornea of both eyes. A reference electrode connected to a splitter was inserted into the forehead and a ground electrode was inserted in the tail. For scotopic conditions, electroretinograms were recorded (Espion E2 ERG system;

Diagnosys LLC, Littleton, USA) in response to one light flash intensity of 1 log cd × s/m² on a dark background. Each stimulus was presented in series of three. For photopic ERGs, the animal was exposed to a rod saturating background for 5 minutes. Stimuli of 1.4 log cd × s/m² was presented 20 times on a lighted background. Data were visualized in MATLAB (v7.7; MathWorks); Difference in A- and B-wave amplitudes between the treated and control contralateral eyes were calculated and compared using using a student t-test. The ERGs were conducted at P45, one-month post-injection and ten days after, at P55.

Agarose sections:

The animals were euthanized by CO_2 asphyxiation and cervical dislocation and the eyes were enucleated and immersion fixed in 10% formalin (in phosphate buffer, Ted Pella, Redding, USA). The cornea and lens were removed, and the retina was isolated and again conserved in 10% formalin. The retinas were embedded in an agarose block by pouring 5% melted agarose into a small weight boat. The tissues were then transferred from PBS to liquid agarose. After the agarose blocks had cooled, the retina was sectioned (Leica VT1000 S, Leica Microsystems, Nussloch, Germany) into 150-210 μm thick sections. The results were imaged by confocal microscopy LSM710. (Carl Zeiss Microimaging, Peabody, MA).

mRNA gene expression analysis

RNA was extracted from either from cultured cells or retinal tissue using the RNeasy Mini Qiagen kit and eluted in 30 μl of DEPC-treated water. During extraction, RNA was treated with DNAse. The resulting RNA was store at -80ºC until use. cDNA was synthetized from RNA primed with random primers, using the Superscript III first-strand synthesis system (ThermoFisher, #18080044). qRT-PCR samples were run in triplicate using a collection of primers and a housekeeping gene glyceraldehyde-3-phosphate dehydrogenase (GAPDH). The relative standard curve method was used to calculate fold differences in mRNA expression normalized to control conditions.

RT-PCR Primer sequences used for AAV co-infection study:
eGFP forward: 5' -CAACAGCCACAACGTCTATATCAT G- 3'
eGFP reverse 5' - ATGTTGTGGCGGATCTTGAAG- 3'
mCherry forward: 5' - CAACAGCCACAACGTCTATATCAT G - 3'
mCherry reverse 5' - ATGTTGTGGCGGATCTTGAAG - 3'

RP-PCR Primer sequences used in *rd10* and WT mice:
mGDNF forward 5'-AGTTATGGGATGTCGTGGCTGTCT-3'
mGDNF reverse 5'- TTCAGGCATATTGGAGTCACTGGT-3'
mCAPN2 forward 5'-AGCTAACAGGGCAGACCAAC-3'
mCAPN2 reverse 5'-AGCCTTCGGAATCCATCGTC-3'
mCAPN7 forward 5'-AGCCTTCGGAATCCATCGTC-3'
mCAPN7reverse 5'-GGCACGTTCTAGATCCAACTG-3'
mCAST forward 5'-GAGCAGTCAGCCTTCCAGAC-3'
mCAST reverse 5'-TCTGTGGTACTCATGCTGGG -3'
Immunohistochemical analysis, confocal microscopy, and cell counting

Mice were sacrificed using CO_2 inhalation followed by cervical dislocation. Enucleated eyes were placed in 10% formalin for 2-3 hours, and then dissected and rinsed in 1X PBS. Retinas were embedded in 5% agarose and sectioned at 120 μm. For IHC, the sections were blocked for at least 1 hour at room temperature in blocking buffer (10% normal goat serum, 1% FBS, 0.5% Triton-X 100) before antibody labelling overnight. The antibodies used were: rabbit anti-GS (Sigma G-2781, 1:1000), Alexa Fluor 594 goat anti-rabbit (Invitrogen, 1:2000). Images were taken on a Zeiss LSM 710 laser scanning confocal microscope (NIH Grant 1S10RR026866-01).

References

1. Schimmer, J. & Breazzano, S. Investor Outlook: Focus on Upcoming LCA2 Gene Therapy Phase III Results. *Hum. Gene Ther. Clin. Dev.* (2015). doi:10.1089/humc.2015.29001.sch
2. Ameri, H. Prospect of retinal gene therapy following commercialization of voretigene neparvovec-rzyl for retinal dystrophy mediated by RPE65 mutation. *Journal of Current Ophthalmology* (2018). doi:10.1016/j.joco.2018.01.006
3. Rodrigues, G. A. *et al.* Pharmaceutical Development of AAV-Based Gene Therapy Products for the Eye. *Pharm. Res.* **36**, 29 (2019).
4. Li, Z. Y., Possin, D. E. & Milam, A. H. Histopathology of Bone Spicule Pigmentation in Retinitis Pigmentosa. *Ophthalmology* (1995). doi:10.1016/S0161-6420(95)30953-0
5. Bravo-Gil, N. *et al.* Unravelling the genetic basis of simplex Retinitis Pigmentosa cases. *Sci. Rep.* **7**, 41937 (2017).
6. Chen, J. *et al.* bcl-2 overexpression reduces apoptotic photoreceptor cell death in three different retinal degenerations. *Proc. Natl. Acad. Sci.* (2002). doi:10.1073/pnas.93.14.7042
7. Bennett, J. *et al.* Adenovirus-mediated delivery of rhodopsin-promoted bcl-2 results in a delay in photoreceptor cell death in the rd/rd mouse. *Gene Ther.* (1998). doi:10.1038/sj.gt.3300733
8. Zadro-Lamoureux, L. A. *et al.* Effects on XIAP retinal detachment-induced photoreceptor apoptosis. *Investig. Ophthalmol. Vis. Sci.* (2009). doi:10.1167/iovs.08-2855
9. Kügler, S. *et al.* The X-linked inhibitor of apoptosis (XIAP) prevents cell death in axotomized CNS neurons in vivo. *Cell Death Differ.* (2000). doi:10.1038/sj.cdd.4400712
10. Wang, S. K., Xue, Y., Rana, P., Hong, C. M. & Cepko, C. L. Soluble CX3CL1 gene therapy improves cone survival and function in mouse models of retinitis pigmentosa. *Proc. Natl. Acad. Sci.* **116**, 201901787 (2019).
11. Kaur, J. *et al.* Calpain and PARP activation during photoreceptor cell death in P23H and S334ter rhodopsin mutant rats. *PLoS One* (2011). doi:10.1371/journal.pone.0022181
12. Paquet-Durand, F. *et al.* Calpain is activated in degenerating photoreceptors in the rd1 mouse. *J. Neurochem.* (2006). doi:10.1111/j.1471-4159.2005.03628.x
13. Dalkara, D. *et al.* AAV mediated GDNF secretion from retinal glia slows down retinal degeneration in a rat model of retinitis pigmentosa. *Mol. Ther.* (2011). doi:10.1038/mt.2011.62
14. Koerber, J. T. *et al.* Molecular evolution of adeno-associated virus for enhanced glial gene delivery. *Mol. Ther.* (2009). doi:10.1038/mt.2009.184
15. Klimczak, R. R., Koerber, J. T., Dalkara, D., Flannery, J. G. & Schaffer, D. V. A novel adeno-associated viral variant for efficient and selective intravitreal transduction of rat Müller cells. *PLoS One* (2009). doi:10.1371/journal.pone.0007467
16. Uren, P. J., Lee, J. T., Doroudchi, M. M., Smith, A. D. & Horsager, A. A profile of transcriptomic changes in the rd10 mouse model of retinitis pigmentosa. *Mol. Vis.* **20**, 1612–28 (2014).
17. Chang, B. *et al.* Retinal degeneration mutants in the mouse. *Vision Res.* (2002). doi:10.1016/S0042-6989(01)00146-8
18. Cronin, T., Lyubarsky, A., Bennett, J. & Kirby, F. M. Dark-Rearing the rd10 Mouse: Implications for Therapy. doi:10.1007/978-1-4614-0631-0_18
19. Dalkara, D. *et al.* Enhanced gene delivery to the neonatal retina through systemic

administration of tyrosine-mutated AAV9. *Gene Ther.* (2012). doi:10.1038/gt.2011.163
20. Boye, S. E. *et al.* The Human Rhodopsin Kinase Promoter in an AAV5 Vector Confers Rod- and Cone-Specific Expression in the Primate Retina. *Hum. Gene Ther.* (2012). doi:10.1089/hum.2012.125
21. McCarty, D. M. Self-complementary AAV vectors; advances and applications. *Molecular Therapy* (2008). doi:10.1038/mt.2008.171
22. McCarty, D. M., Monahan, P. E. & Samulski, R. J. Self-complementary recombinant adeno-associated virus (scAAV) vectors promote efficient transduction independently of DNA synthesis. *Gene Ther.* (2001). doi:10.1038/sj.gt.3301514
23. Trichonas, G. *et al.* Receptor interacting protein kinases mediate retinal detachment-induced photoreceptor necrosis and compensate for inhibition of apoptosis. doi:10.1073/pnas.1009179107
24. Perrelet, D. *et al.* IAPs are essential for GDNF-mediated neuroprotective effectsin injured motor neurons in vivo. *Nat. Cell Biol.* **4**, 175–179 (2002).
25. Flannery, J. G. & Visel, M. Adeno-Associated Viral Vectors for Gene Therapy of Inherited Retinal Degenerations. in 351–369 (Humana Press, Totowa, NJ, 2012). doi:10.1007/978-1-62703-080-9_25

Chapter 5: Optimization of AAV-mediated Mitochondrial Gene Targeting for the Outer Retina

Abstract

Mitochondria disorders are a diverse group of severe conditions from nuclear and mitochondrial DNA mutations. Growing evidence suggests that mitochondrial dysfunctions are involved in both age-related and inherited retinal neurodegenerative diseases. Gene therapy has the potential to treat such diseases, but efficient mitochondrial targeting remains a challenge in the field. In this study, we optimized adeno-associated virus (AAV) mediated gene-targeting of the mitochondria in the retina by evaluating the efficiency and selectivity of two different approaches used to rescue vision of pre-clinical models of Leber Hereditary Optic Neuropathy (LHON): an AAV-mediated import of a nuclear-encoded protein fused to a N'-terminal mitochondria target signal (MTS) to the mitochondria, and an engineered AAV with a MTS tagged on the surface of the viral capsid, to confer it preferential mitochondrial trafficking and delivery of a mitochondrial encoded transgene. We first screened *in vitro* for MTS sequences with different efficiency/selectivity levels of redirecting proteins of interest to the mitochondria and applied it to the building of the two different *in vivo* gene delivery approaches. We found that MTSs with selective mitochondria targeting negatively impacts the packaging of MTS-AAV capsids, re-directing the VP2 subunit to the mitochondria before proper capsid unit formation. MTSs with both nuclear and mitochondria tropism permit proper viral packaging but did not seem to lead to detectable mitochondria expression of transgene. AAV-mediated allotopic expression still seems the most promising approach for gene therapy. We identified a strong MTS that achieved selective mitochondrial-import of the fused protein. We further developed an AAV-toolbox with cell specific promoters to achieve efficient mitochondria targeting and expression *in vivo*, which are essential to treat animal models of mitochondrial disease and move forward research to clinical application.

Introduction

Mitochondria have a central role in maintaining cellular homeostasis. They are the primary source of energy metabolites (ATP, $NADH^+$, $FADH_2$) produced mainly by oxidative phosphorylation (OXPHOS). Referred to as the cell powerhouse, recent studies shed light on the organelle's intricate role in metabolism[1], development, immune responses[2] and cell death signaling pathways[3,4]. Thousands of proteins are involved with this machinery and the majority (99%) are encoded within the nucleus. However, mitochondria possess their own DNA (mtDNA), which encodes for 13 mitochondria proteins, mostly components of the OXPHOS (ND6, ND1, ATP6…) complexes, as well as replication genes[5] (2 ribosomal RNAs and 22 transfer RNAs). Unlike nuclear DNA, each mitochondrion possesses 100-1,000 copies of its genome.

Mutations in both nuclear DNA and mtDNA can trigger mitochondria disorders. The presence of a mutation in the mtDNA can vary from 0 to 100% of the copies, with a tissue-dependent

threshold to be pathogenic to the cell or phenotypically noticeable, showcasing not only the high genetic heterogeneity of these disorders but also the challenges underlying diagnosis such as mutations and disease linkage.

Mitochondria disorders (1:5000) have been reported to severely impair cell function, with more than 1/3 accounting for primary or secondary OXPHOS biogenesis impairments[6] through mtDNA replication, subunit formation, cellular trafficking or organelle structure. Mitochondrial dysfunctions have also been linked to tumor formation and the aging process[7]. Damage to the mtDNA can lead to a myriad of pathological conditions in tissues with high energy demands such as skeletal muscles, heart, brain, and retina. For that reason, many of the primary mitochondria diseases have ophthalmologic manifestations[8], such as Leber hereditary optic neuropathy (mutations in mtDNA ND1, ND4, and ND6 genes) or neurogenic muscle weakness, ataxia, and retinitis pigmentosa (NARP, mutations in ATP6 gene). In addition, mitochondrial dysfunction has begun to be investigated in ocular aging disorders, such as age-related macular degeneration (AMD)[9–12]. The highest oxygen consumer of the body, the eye and more specifically the retina, has been a tissue of choice for studying mitochondria disorders[13] and establishing proof-of-concept therapies. Easily accessible, immune-privileged compartment, the eye offers the ability to monitor easily and non-invasively disease progression and treatment outcomes. The retina has also been the tissue with the most successful gene therapy proofs-of-concepts with adeno-associated viral[14,15] vectors (AAV) to deliver the therapeutic payload for inherited retinal degenerations.

Current therapeutic and gene targeting approaches[16] take advantage of the existing cell mechanisms to redirect nuclear-encoded proteins to its proper mitochondrial location. Mitochondria proteins[17] translated outside of the organelle relay on an N-terminal pre-sequence, a mitochondrial target signal (MTS)[18,19], that is recognized[20] and cleaved by the inner or outer membrane translocase (TOM, TIM) in order to deliver its cleaved protein to the right subcellular compartment of the mitochondria. Commonly used MTSs are from genes involved in the OXPHOS pathways, such as the cytochrome c oxidase, subunit VIIIa COX8A, and have been used to redirect molecular tools (e.g., mTimer)[21], the nuclear-encoded transgene or adeno-associated viral (AAV) vector itself (MTS-AAV) to study and rescue degeneration in a model of blindness due to retinal degenerations.

Our study focused on optimizing two different AAV-mediated mitochondria targeting systems: allotopic expression of nuclear-encoded protein, and endogenous mitochondrial expression. Allotopic expression is achieved by AAV-delivery of the transgene fused to an MTS sequence, to traffic its translated protein from the cytoplasm to the mitochondria. Achieving endogenous mitochondrial expression of a therapeutic transgene, on the other hand, is a more complex approach since it requires first the delivery vector to be redirected from its natural nuclear route to the mitochondria and secondly, a transgene codon-optimized for mitochondrial expression under a mitochondria promoter. Proof-of concept therapies for LHON[22,23] have used each approach successfully in the retina, targeting ganglion cells to rescue LHON phenotype in different mouse models but has never been optimized for other retinal targets besides ganglion cells. Moreover, the endogenous expression approach has only been performed by only one research group and hasn't been replicated yet. Here, we screened and optimized mitochondrial vectors to improve on current gene delivery systems efficacy and better investigate the role of mitochondria dysfunction in inherited retinal degenerations.

Results

In Silico Prediction of Mitochondria Targeting Signal Sequences

We first used computational methods to identify and select MTS sequences. MitoFates tool[24] predicts cleavable N-terminal MTS pre-sequences of nuclear-encoded mitochondrial proteins. These pre-sequences reside within the first 10–90 residues, display a high composition of arginine and are characterized by a low amount of negative charged. We compared MTSs already used in literature (e.g., COX8A) to novel ones we generated from mitochondrial proteins that display a high MitoFates probability score. We selected MTSs that not only originate from diverse gene families (e.g., ATP synthase, apoptotic genes…) but also the native subcellular location (**Fig 1.A**).

A

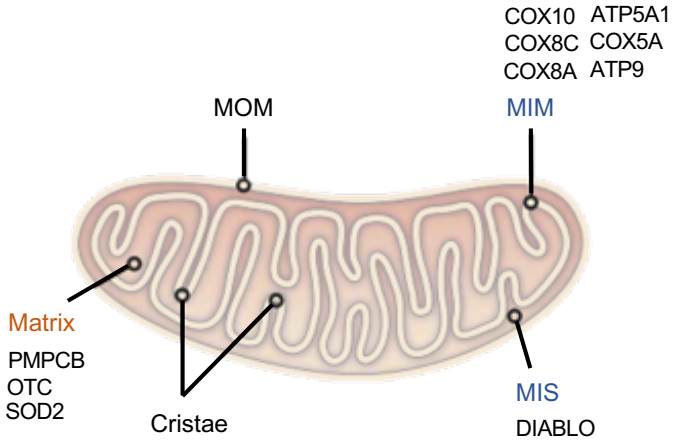

B

Family	Gene	Gene Nomenclature	MitoFate Score
ATP synthase	ATP5A1	mitochondrial ATP synthase F1 complex, alpha subunit	0.974
carbamoyltransferase	OTC	mitochondrial ornithine carbamoyltransferase	0.931
PAM complex	PMPCB	Mitochondrial-processing peptidase subunit beta	0.924
Complex I	NDUFB11	NADH dehydrogenase ubiquinone oxidoreductase beta subunit	0.924
superoxide dismutase	SOD2	Superoxide dismutase 2, mitochondrial	0.885
ATP synthase	ATP9	ATP synthase subunit 9, mitochondrial	0.87
complex IV	COX8A	cytochrome c oxidase, subunit VIIIa	0.854
complex IV	COX5A	cytochrome c oxidase, subunit Va	0.82
complex IV	COX8C	cytochrome c oxidase, subunit VIIIc	0.791
apoptotic genes	DIABLO	Diablo homolog, mitochondrial	0.274
complex IV	COX10(UTR)	cytochrome c oxidase assembly protein, heme A: farnesyltrans	0

Figure 1: Mitochondrial nuclear-encoded genes (MTS) used as mitochondrial targeting signal sequences. The vast majority of mitochondrial proteins are encoded in the nucleus and transported by the cell machinery to the suitable mitochondrial compartment. Schematic representation (**A**) of mitochondria structure, and list of nuclear-encoded genes studied and their mitochondrial protein sub-localization.
We selected MTS sequences of nuclear encoded genes with the highest MitoFates score (**B**), a predictive tool that can identify mitochondrial targeting signal sequences, to compare them to MTS currently used in the field of retinal gene delivery.
MOM: Mitochondrial (Mt) Outer Membrane; MIM: Mt Inner Membrane, MIS: Mt Intermembrane space.

MTSs of the mitochondrial inner membrane (MIM) are suitable for allotopic-based gene replacement strategies, supplying a healthy copy of the mutated mt gene (e.g., MTS-DN4). Gene editing approaches, on the other hand, would require an MTS able to relocate to the mitochondrial matrix, where mtDNA and transcription machinery are located.

MitoFates' algorithm scores high for conformations that form a local-helical secondary structure with high hydrophobicity and positively charged amino acid residues facing each other, as well as the presence of cleavage site motifs detectable by mitochondria processing enzymes (Oct1, MPP and Icp55) as well as TOM20, the outer membrane translocase (**Fig 1.B, supplemental S1**). The first 30 AA sequence of DIABLO/SmacI, a pro-apoptotic protein expressed in the inner membrane segment that interacts with the cytochrome c/Apaf-1/caspase-9 pathway, interestingly, did not possess a Tom20 recognition motif, therefore DIABLO had the lowest score (0.274).

In vitro screening of selective MTSs

We established an *in vitro* screening protocol to identify MTS sequences that achieved strong and selective mitochondrial expression. We fused MTS sequences to the N-terminal of the reporter tdTomato (tdT) gene to add negative pressure to our screen and allow selective trafficking of MTS-permissive folded protein to the mitochondria. The tdT protein has a higher molecular weight, leading tdT-fused proteins to be more susceptible to misfolding than eGFP. We transfected HEK293T cells with MTS-tdT constructs and 72 hours later characterized fused protein subcellular localization with immunohistology and western blot analysis.

As expected, naked tdTomato colocalized with the DAPI staining, and displayed classic cytoplasmic expression. COX8A-, COX8C-, COX5A-, and NDFUB11-tdT fused proteins showed some colocalization with the mitochondrial marker COXIV, but the majority exhibited more solid nuclear/cytoplasmic expression. MTSs with the highest MitoFates scores, ATP5A1, OTC, PMPCB strongly and selectively colocalized with COXIV staining (**Fig 2.A-B**). Interestingly, although the DIABLO N-terminal peptide sequence we designed had a low MitoFates prediction, DIABLO-tdT protein presented selective mitochondrial localization.

Because 2D imaging can be misleading when overlapping channel fluorescence to analyze protein colocalization within cells, it is not enough data on its own to fully support MTS-tdT efficient trafficking to the mitochondria. We further confirmed our finding by isolating total cell and mitochondrial isolated protein fractions from three independently transfected HEK293T wells and quantified the amount of mitochondrial tdT protein. The results concurred with the co-labeling staining. COX-MTSs showed similar tdT protein levels in the mitochondrial isolated fraction to our cytosolic expressed tdT control. We found about 20% of contamination of cytosolic tdT. While mitochondrial isolation fractions protocols/kits based on ultra-centrifugation are inexpensive and enable fast-extraction of high number of samples at once, it leads to some cytosolic contamination in the mt fraction. While useful to quickly screen a significant number of MTS-constructs, percoll/sucrose gradient separation protocols, although more time consuming, would result in more pure mitochondria fraction, with less to no cytosolic contamination. However, strong MTSs (PMPCB, OTC, DIABLO…) mediated high levels of tdT protein (60-80%) in the mitochondria fraction, significantly superior to weak MTSs (**Fig 2.C-D**).

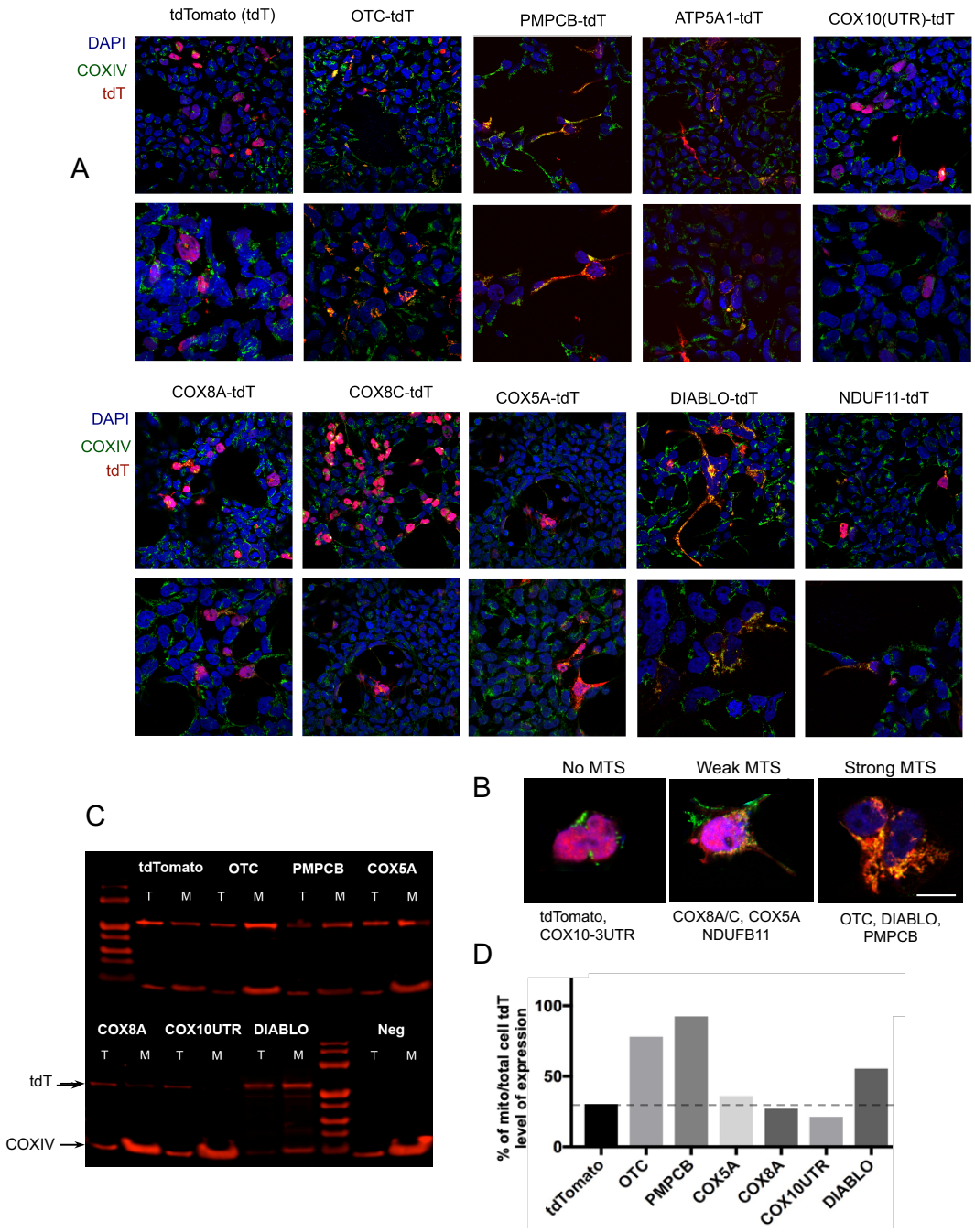

Figure 2: *In vitro* assessment of mitochondrial targeting sequences efficiency in redirecting a reporter protein in HEK cells. MTS sequences were fused to N-terminal of reporter gene tdT and expressed under the control of a ubiquitin promoter in HEK293T cells. 72 hours after transfection, cells were fixed, stained with a mitochondrial marker COXIV and mounted on slide for (**A**) confocal imaging. Cell nuclei were stained with DAPI (blue). Yellow channel shows colocalization between the tdT reporter (red) and mitochondria COXIV marker (green). 40x and 60x magnification for each MTS are represented in the top and bottom rows, respectively. We identified 3 different groups of MTSs (**B**). Cell lysate from 6 separate transfections were pulled together. Western blot on total cell (T) and mitochondrial (M) protein fraction samples, **(C)** stained with tdT and COXIV-antibody to quantify tdT protein levels **(D)** by normalizing signal in each lane (top band, ~55KDa) to its COXIV loading control (bottom band, 17KDa).

Transgene amino acid composition affects MTS-mediated mitochondria uptake

Folding, among other protein features, of fused proteins can negatively impact delivery to the mitochondria. We compared the Mitofates scores, which includes protein hydrophobicity and net charge in its predictive algorithm, of each MTS naked or fused to different transgenes: eGFP, tdTomato, and mtATP6, an endogenous mitochondria gene associated Leigh syndrome and NARP phenotype [25,26].

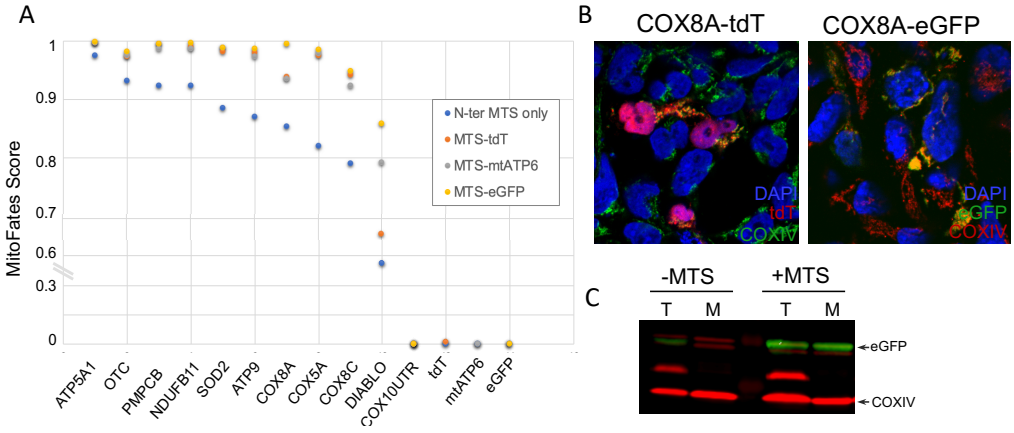

Figure 3: Fused transgene affects MTS-mediated trafficking to the mitochondria.
Plot of MitoFates prediction scores (**A**) based of MTS-tdT/eGFP or mATP6 fused protein. Representative confocal images (63x magnification) of HEK293T cells transfected with either Ubi.COX8A.tdT or Ubi.COX8A.eGFP and labelled with mitochondrial marker COXIV (green). DAPI stained nuclei in blue. COX8 MTS selectively traffics fused eGFP but not tdT protein to the mitochondria **(B).** Western blot of mitochondrial fraction (M) or total cell fraction (T) isolated from HEK cells transfected with Ubi.eGFP (without MTS) or Ubi.COX8A-eGFP (with MTS) quantifying eGFP (top green band, ~35kDa) and COXIV (~17kD) loading control.

As expected, MTS-eGFP proteins had the highest targeting prediction score (**Fig3.A**). Indeed, when COX8A-eGFP was transfected in HEK cells, eGFP colocalized selectively with COXIV marker (Fig3.B) while when fused to tdTomato, it led to strong cytoplasmic expression as well as previously found. Western blot confirmed the high level of GFP in the mt fraction of COX8A-GFP compared to N-terminal naked GFP.

Mitochondrially encoded ATP6 had the lowest prediction score (Fig3.A). The mitochondria protein is composed of five transmembrane domains. Studies have shown that MTS-mediated re-trafficking of nuclear-encoded ATP6 has low efficiency. Our results also highlight that a linearized fusion protein is critical for mitochondrial import and that selection and confirmation of MTS-transgene subcellular localization is one of the most critical components of experimental design. We are currently screening for/optimizing our most robust MTS sequences for efficient nuclear ATP6 mitochondrial import.

Tagged 3'UTR sequences from mitochondrial-encoded genes did not confer mitochondria targeting properties to transgene.

Specific nuclear-encoded proteins, based on their composition (too hydrophobic, secondary structure dramatically affecting folding and or recognition by cleavable mitochondria proteins), cannot be efficiently repurposed for mitochondria import.
As an alternative to the MTS, the 3' untranslated region (3'UTR) of mitochondria genes has been studied as a novel approach to redirect translatable mRNA to the mitochondria vicinity[27] and entrance. Previous studies [28–31] identified 3'UTRs with strong mitochondria localization properties, such as the human 3'UTR sequence of COX10 or SOD2.

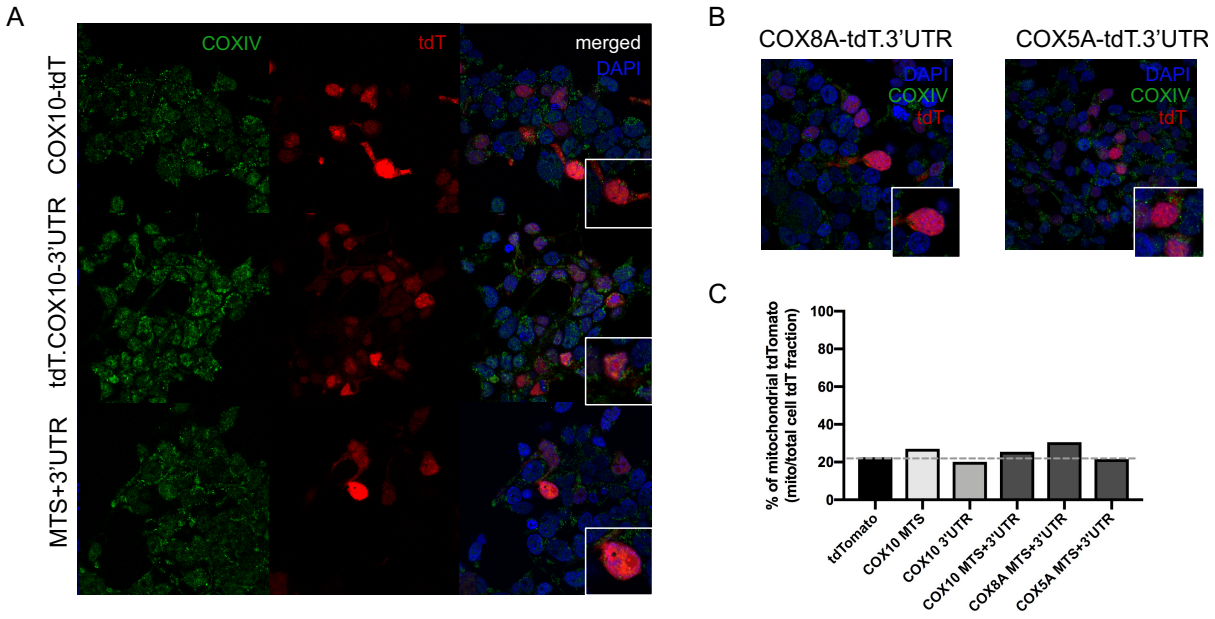

Figure 4: 3'UTR sequence does not improve mitochondria localization of protein
Representative confocal imaging (63x magnification) of HEK293T cells transfected with either tdT.3'UTR, MTS-tdT or MTS-tdT + 3'UTR of COX10 **(A)** or COX5A/8A **(B)**. Cells were stained with COXIV antibody as mitochondria marker (green channel), and DAPI to stain cell nuclei (blue channel). Western Blot was performed on mt and total cell fraction samples similar to Fig2.C, mitochondrial tdTomato protein levels **(C)** from MTS/3'UTR transfected constructs were plotted. Dotted line shows level of contamination in mitochondria fraction from cytoplasmic expressed tdT.

We selected 3'UTR sequences from genes that possess "weak" MTS sequences (COX family) to test whether they could increase the mitochondria import efficiency, alone or in combination with its matching MTS sequence. We replaced the polyA sequence with the COX10 UTR, COX8A UTR, or COX5A UTR in the Ubi.tdT and Ubi.MTS-tdT constructs. The 3'UTR of COX10 did not modify cytoplasmic expression of tdT found with COX10(MTS)-tdTomato. No benefit occurred from combining the COX10 MTS with a 3'UTR sequence (**Fig 4.A**). Constructs containing COX8A and COX5A 3'UTR alone (data not shown) or in combination with their respective MTS (**Fig 4.B**) also did not differ from a cytoplasmic sub-localization pattern. Western blots showed no significant increase in tdT protein levels in the mt fractions of 3'UTR or MTS+3'UTR samples compared to naked tdT (**Fig 4.C**).

Our next step will also be to confirm these results when using MTS/UTR-mediated trafficking to deliver nuclear-encoded ATP6 and determine whether the import of an endogenous

mitochondrial gene instead of a fluorescent reporter would unlock the 3'UTR ability to redirect nuclear-encoded mRNA to the mitochondria.

AAV-mediated allotopic and endogenous mitochondria expression systems

We selected the most potent MTS sequences from our *in vitro* screening and vector optimization findings to selectively re-traffic the fused protein of choice and implement it in two different AAV-mediated targeting systems previously published: MTS pre-sequence was fused to the transgene N-terminal for nuclear expression (redirecting Transgene, **Fig 5.A**) or tagged onto the AAV VP2 capsid sequence to redirect the viral particles (Redirecting AAV-Capsid, **Fig 5.B**) directly to the mitochondria. We aimed to evaluate which approach is better suited for mitochondrial gene therapy first *in vitro*, and then in the retina, to build better viral tools to investigate the role of mitochondria in inherited retinal degenerations.

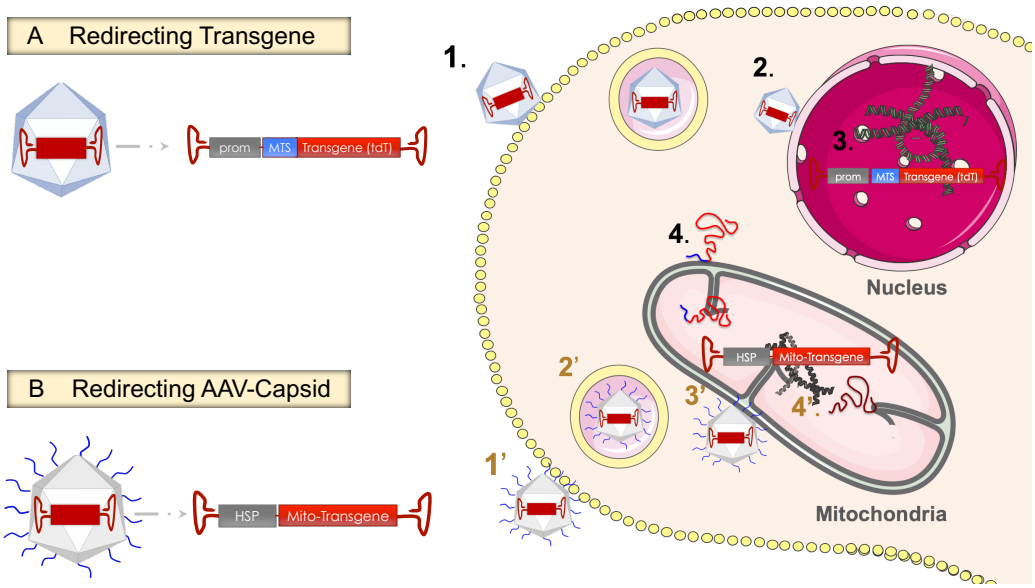

Figure 5: **AAV-mediated gene delivery approaches for targeting the mitochondria.**
Diagram representing two AAV-mediated gene targeting systems used in study. (**A**) Allotopic approach: rAAV vector bind to cell surface receptor (1.) is internalized in early-endosome (2.), and escapes to deliver its cargo to the nucleus (3.). The transgene, fused to an MTS sequence, is expressed under the control of promoter to allow cell-specific expression. Nuclear-encoded fusion protein is redirected from cytoplasm to mitochondria (4.) due to MTS recognition. (**B**) Endogenous approach: MTS peptides are tagged onto AAV capsid surface (MTS-AAV). MTS-AAV infects the cell through a similar mechanism as regular rAAV (1' and 2') but after endosomal escape, the MTS signal sequence allows MTS-AAV to preferentially bind to mitochondrial membrane (3') and release its payload. The mito-transgene (optimized for mitochondria translation) is expressed under the control of the mitochondria heavy strand promoter (HSP) in the matrix.

Building an MTS-AAV system

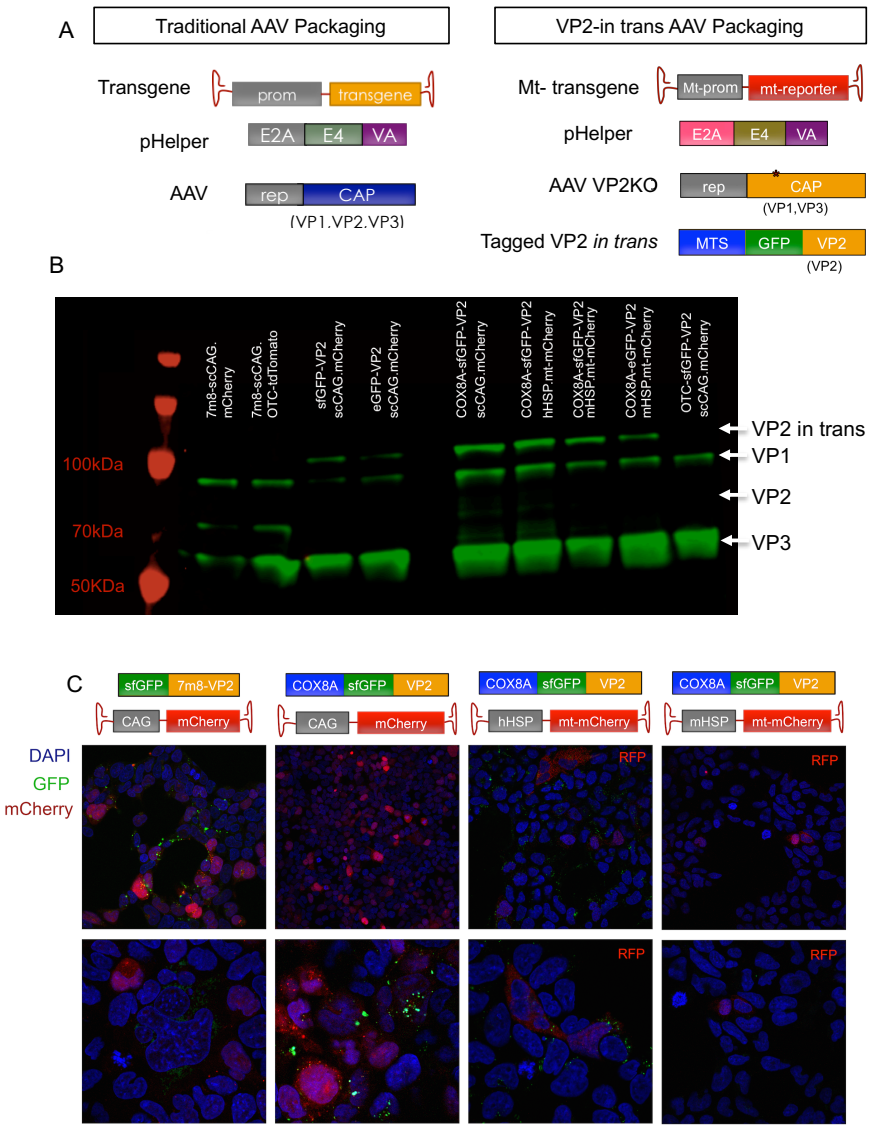

Figure 6: Mito-AAV does not efficiently redirect mt-encoded transgene to mitochondria
Diagram of AAV-mito packaging system **(A)**: additional VP2 subunit fused to an MTS is supplied in *trans* and the natural VP2 reading frame in AAV rep and cap plasmid abolished (*: mutation at VP2 start codon site). Western blot analysis of AAV VP1, VP2, VP3 subunits (87, 72 & 62 KDa, respectively) with the A40 antibody **(B)**. Equal amounts of viral particles of each of the 7m8 viruses were approximately analyzed (~5.10e10). Representative confocal images (40x & 60x) of HEK293T cells infected with different mito-AAVs (1.0e10vg/mL) and control VP2 in trans viruses. HEK293T cells were fixed after 48 hours and mounted on slides. COX8A-sfGFP-VP2 viruses carrying mt-transgenes were stained with an RFP antibody to amplify fluorescent signal.

A research group at the University of Florida developed an AAV system to achieve ectopic-trafficking of AAV to the mitochondria[32] by incorporating an MTS into the AAV capsid sequence. Previous studies have successfully inserted peptides onto the capsid VP subunits without abolishing AAV infectivity and packaging efficiency. The AAV cap gene encodes in the same open reading frame the VP1, VP2, and VP3 subunits, each comprising a unique codon initiation site leading to the translation of three, progressively shorter, proteins. VP2 is the only subunit that

is not essential[33] during packaging and can tolerate N-terminal peptide insertions. Conveniently, its N-terminal is exposed on the outside surface of the capsid while the C-terminal is internalized. GFP[34] and cell ligand[35]-tagged AAV virions have been successful in expressing the peptide-VP2 *in trans*, driven by a non-AAV promoter, during viral packaging. The initiation site of the VP2 reading frame in an AAV rep/cap plasmid was mutated to silence VP2, so the VP1 and VP3 subunits could be appropriately encoded (**Fig 6.A**) and resulting AAVs infectious.

Yu *et al*. tweaked this alternative packaging system by adding the human COX8A 23AA MTS pre-sequence to the GFP-VP2 protein supplied in trans, resulting in COX8A MTS motifs insertion into the capsid virion sequence. The transgene was also optimized for in-house mitochondrial transcription and translation: the human mitochondrial promoter HSP drove exogenous expression of a mitochondrial-encoded gene. We tested whether we could replicate and optimize their system.

Selective MTS sequences lead to incomplete packaging of AAV

We packaged nuclear transgene pTR.scCAG.mCherry with GFP-VP2.AAV or COX8A-eGFP-VP2.AAV-7m8. We used the human or mouse mitochondria HSP promoter to drive expression of mitochondrial codon optimized mCherry (mtmCherry) and packaged it with COX8A or OTC-eGFP-VP2. AAV vectors (~$1.0x10^{10}$ vg) were analyzed with western blot to show correct capsid VP subunit formation. We also infected HEK293T to confirm AAV were infectious and analyze the subcellular location of capsid-tagged AAV vectors.

AAV vectors produced by the standard triple transfection of pHelper, AAV transgene, and AAV rep/cap plasmids showed typical subunit formation and molecular weight (**Fig 6.B**) on the blot. AAV.scCAG.mCherry vectors packaged using AAV rep/cap (VP2KO) and in trans eGFP-VP2 plasmid did not present a band for wild-type VP2 at molecular weight size ~72kDa, but a higher one for tagged eGFP-VP2 protein (~100kDA: 72kDa in conjunction of the ~35kDa of GFP). Cells infected **(Fig 6.C)** with 7m8.scCAG.mCherry and 7m8(eGFP-VP2).scCAG.mCherry had strong nuclear/expression of mCherry, which overlapped with the DAPI staining. For eGFP-AAV virions, eGFP expression was visible around the nucleus of mCherry positive cells, likely from the AAV capsid protein releasing or trafficking its cargo to the nucleus. These results confirmed that 7m8 vectors packaged with the VP2 in trans system are infectious. We then compared 7m8 (COX8A or OTC-eGFP-VP2) vectors and found that while vectors packaged in trans with COX8A-AAV particles presented a ~100kDA band (for tagged COX8A-eGFP VP2 protein), OTC-AAV vectors were missing the tagged-VP2 subunit, with only VP1 and VP3 subunits.

We confirmed (data not shown) our results by repeating viral packaging and supplying in trans VP2 fused to other highly selective MTSs (PMPCB, DIABLO). We found again that only "weaker" MTSs (e.g., COX8A), allow complete packaging of viral particles, including MTS-tagged-VP2 subunits. Nuclear-encoded VP subunit proteins have to be in the same subcellular space to assemble and form complete AAV particles. Tagging in trans VP2 to selective MTS redirects fused VP subunit to the mitochondria before it can form in the nuclear space with VP1 and VP3 resulting in VP2-deficient viral particles.

We compared expression in HEK293T cells of scCAG.mCherry (nuclear-encoded) to scHSP.mtmCherry (mitochondrial-encoded) packaged in 7m8(COX8A-GFP-VP2). COX8A-AAV.scCAG.mCherry led to similar mCherry expression as AAV(GFP-VP2).scCAG.mCherry. mCherry expression was visually undetectable in cells infected with COX8A-AAV.HSP.mtmCherry. RFP-antibody stain showed both cytoplasmic and DAPI-overlapping

expression pattern, but only at an extremely low event rate. COX8A-AAV eGFP+ virions seemed to surround nucleus, similarly than AAV eGFP+ virions but also could also be observed in the mitochondria vicinity. Electron microscopy and immunogold staining against VP subunit would be needed to visualize precise subcellular localization. We repeated the experiment by delivering a codon optimized mtmCherry transgene **(Supplementals S2**), encoding for an early stop codon if nuclear encoded and only be fully translated if mitochondrial encoded, to remove any possible expression leakage, and could not observe any RFP signal in COX8-AAV.HSP.mtmCherry infected HEK cells.

We are currently switching from delivering a mitochondrially-encoded fluorescent reporter to a luminescent (luciferase) reporter to be able to quantify lower expression levels, so we can properly conclude whether the MTS-AAV system established does achieve ectopic expression. For now, we conclude that AAV-mediated allotopic expression is a more suitable approach for mitochondrial gene targeting in the retina.

AAV-MTS-tdTomato transgenes achieve allotopic expression in vivo as previously shown in vitro

We first looked at whether our *in vitro* characterization of MTS mitochondria trafficking potency led to similar results *in vivo* when delivered in an AAV vector.

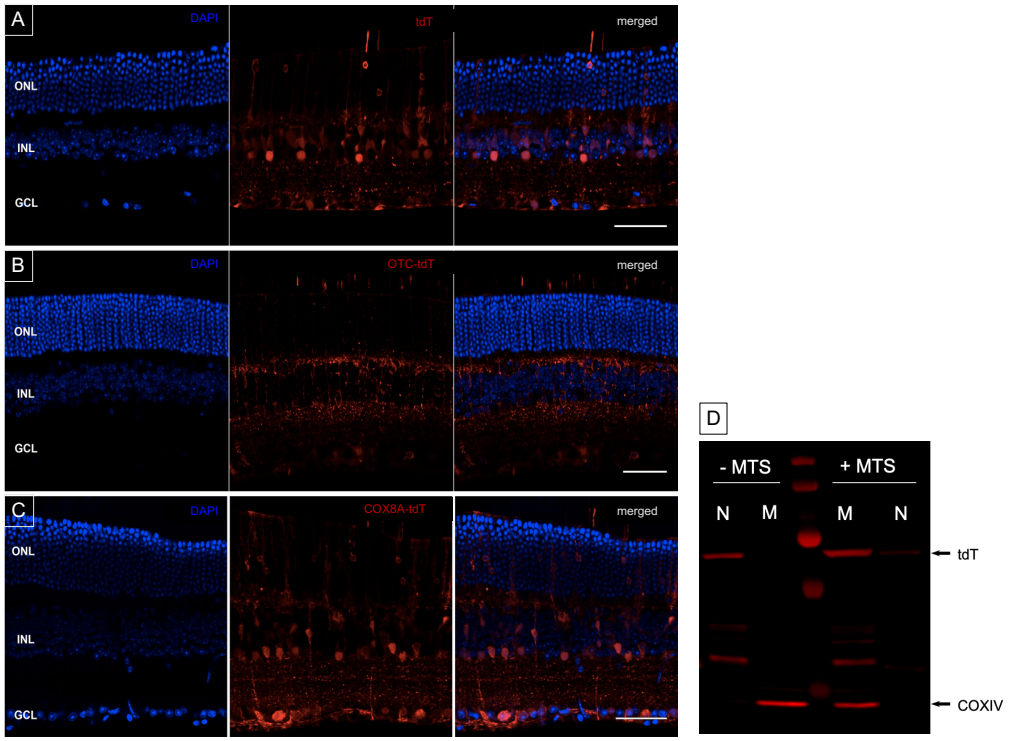

Figure 7: *In vivo* characterization of AAV-7m8-mediated expression of scCAG.tdTomato, scCAG.MTS-tDT in C57BL6/J retinas.

Representative confocal images of 120-150 µm agarose-embedded retinal sections from WT mouse eyes injected intravitreally with a 7m8 viral variant packaged with scCAG.tdT (**A**), scCAG-OTC-tdT (**B**) or COX8A-tdT (**C**). Eyes were enucleated 4 weeks post-injection. 7m8 achieves strong and panretinal expression of the transgene in the retina from vitreous route of administration, transducing a wide-range of retinal cells in the inner and outer retina. DAPI stains nuclei (blue channel). Scale bar, 50uM.

Western blot of nuclear (N) and mitochondrial (M) isolated protein fraction from retinas injected with 7m8.scCAG.tdT (without MTS) and OTC-tdT (with MTS) quantifying levels of tdT and COXIV proteins (~50 kDa and 17 kDa, respectively).

We cloned one MTS-tdT sequence from each group (no MTS, weak and strong MTS) from the Ubi promoter backbone into a self-complementary ITR backbone, under the control of an ubiquitous promoter (pTR.scCAG.MTS-tdtomato), and packaged it into 7m8[36], an AAV2 based variant with high retina transduction and panretinal penetration properties from the intravitreal route of administration. One-month post injection, eyes were enucleated and the subcellular pattern of tdTomato, OTC-tdTomato, and COX8A-tdTomato were analyzed. As expected, 7m8 vectors led to strong expression from the GCL to ONL layer. With the 7m8.scCAG.tdTomato vector, tdT was overlapping with DAPI staining (**Fig 7.A**). Consistent with our *in vitro* results, COX8A-tdT **(Fig 7.C**) had a similar expression pattern to scCAG.tdT, except for a few cells that seem to have mitochondrial expression. On the other hand, scCAG-OTC-tdT (**Fig 7.B**) displayed close to no cytoplasmic expression. We confirmed transgene trafficking to the mitochondria by isolating the nuclear and mitochondria protein fraction from injected retinas and running protein lysates on a western blot to quantify amount of tdT protein found in each fraction. pAAV.scCAG-tdT (-MTS) contained only tdT proteins in the nuclear fraction, with no COXIV labelling as expected. The mitochondria fraction, only COXIV positive, had no cytosolic tdT protein leakage. In the OTC (+MTS) sample, extremely faint tdT and no COXIV signals were detectable in the nuclear fraction. Instead, tdT was strongly enriched in the mitochondria fraction (**Fig 7.D**).

7m8-mediated toolbox to achieve mitochondria targeting in selective retinal cell type

AAV2 in combination with a ubiquitous promoter[23] has been used as the standard to allotopically deliver transgenes to ganglion cells, mostly to study optic neuropathy diseases, such as LHON. However, mitochondria dysfunction in the remaining layers of the retina has only started to be investigated as potential therapeutic targets for age-related disorders such as AMD. There is a growing interest in monitoring mitochondria health during retinal degenerations[37], using engineered sensor tools such as mKeima (mitophagy) or Timer (redox sensor), but also looking at Müller glia cells (MGCs)[38] or photoreceptors (PRs). It has been hypothesized that mitochondria function impairment in MGCs, a key retinal homeostasis actor, could explain secondary degeneration mechanisms seen in inner retinal neurons during AMD, due to diminished metabolic and structural support. Here, we developed an AAV-mediated gene targeting toolbox to cell-selectively express in the mitochondria of various retinal cells using viral variants and vectors engineered in our lab.

sc7m8 drives strong expression of eGFP under the control of a ubiquitous promoter CAG (**Fig 8.A**) and efficiently transduces all retinal cell types (ganglion cells, amacrine, bipolar, Müller glia, photoreceptors…). Using the strong MTS sequences (DIABLO, PMPCB) we identified and validated its selectivity. We were able to skew transgene cytoplasmic expression to relocate to the mitochondrial subcellular space (**Fig 8.B**), which colocalized with the COXIV mitochondria marker staining.

We then packaged transgenes under the control of the human 681bp Gfa_{ABC1D} promoter which has been shown to have high astrocytes specificity in the CNS similar to its 2.2kb parent, GFAP, but with 2-fold greater activity. In the retina, 7m8.scGfa$_{ABC1D}$.eGFP is highly selective for MGCs showing strong expression in the INL nuclear bodies and end feet processes located in the

nerve fiber layer (under the GCL, **Fig 8.C**). When redirecting MGC transgene's subcellular location to the mitochondria, we found expression through the retina, from the end feet through the soma, and the distal processes of the MGCs (**Fig 8.D**).

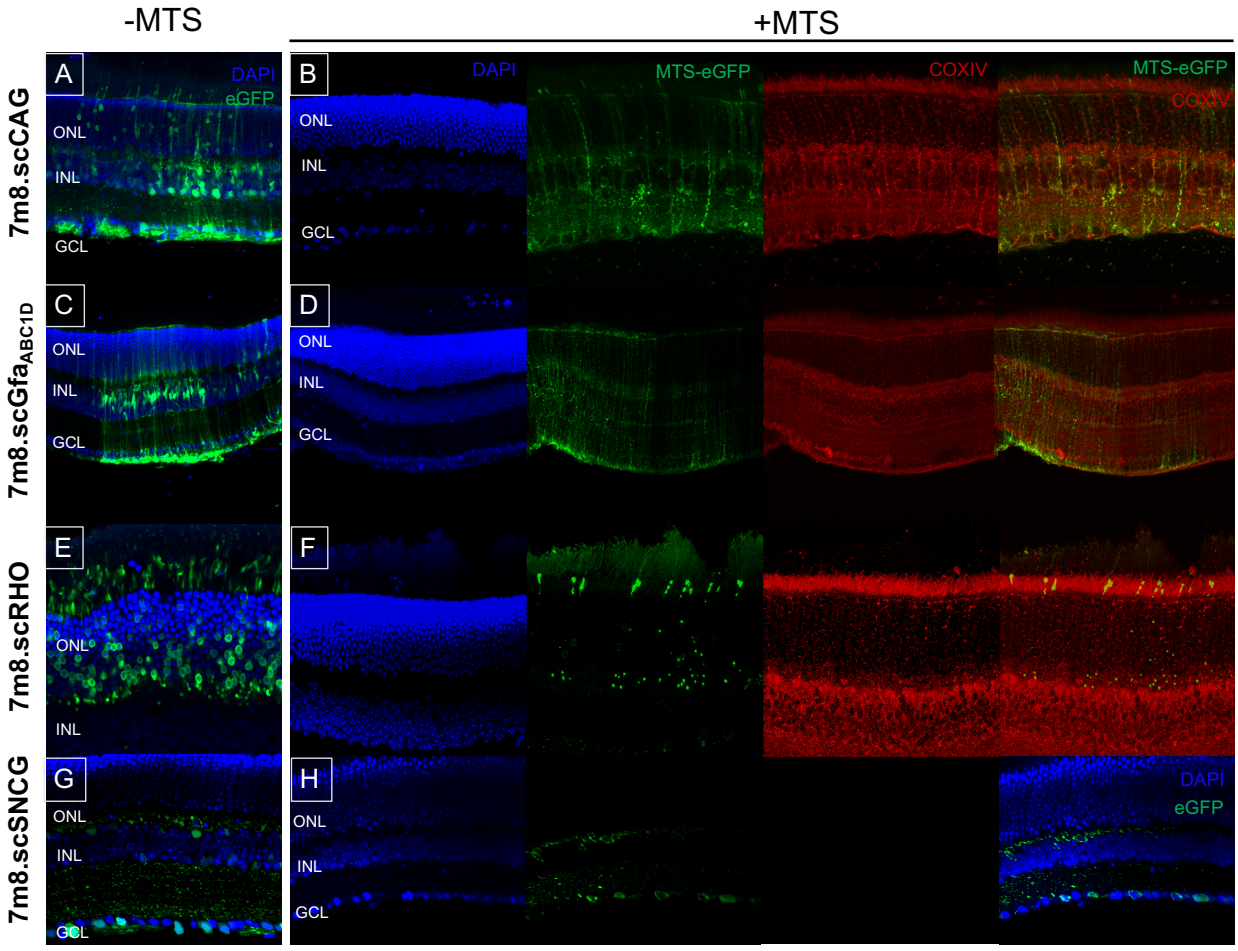

Figure 8: 7m8-mediated selective mitochondria targeting in all layers of the retina
Representative confocal images of 120-150 µm agarose-embedded retinal sections from WT mouse eyes injected intravitreally with 7m8 encoding for eGFP (A,C,E,G) or DIABLO MTS-eGFP (B,D,F,H) expression under the control of ubiquitous scCAG (A,B), glial specific Gfa_{ABC1D} (C,D), rod photoreceptor specific RHO (E,F) or ganglion cell specific SNGC (G,H) promoters. Cells were stained with nuclei marker DAPI (blue) and mitochondria marker COXIV (red). All images were acquired with 40x magnification except for images focused on photoreceptor layer in the E and F row which are at 63x.

7m8 achieves strong expression in rod photoreceptors under the control of the human RHO promoter (**Fig 8.E**). Mitochondrial expression was observed mostly at the limits between the outer nuclear and plexiform layers as well as the connecting cilium, between the outer and inner segment of the retina. Another study found similar results and showed by electron microscopy that mitochondria within the cell migrate towards the vasculature[39].

Lastly, recently the engineered human gamma-synuclein gene (SNCG) promoter [40] was shown to restrict expression to ganglion cells when delivered by AAV2. 7m8.SNCG led to strong expression in ganglion cells, but inner retinal cell off target expression with some eGFP positive

amacrine and bipolar cells (**Fig 8.G**). We observed mitochondria expression mostly in the surrounding cell soma (**Fig 8.H**).

Monitoring mitochondria health in age related and inherited retinal degeneration

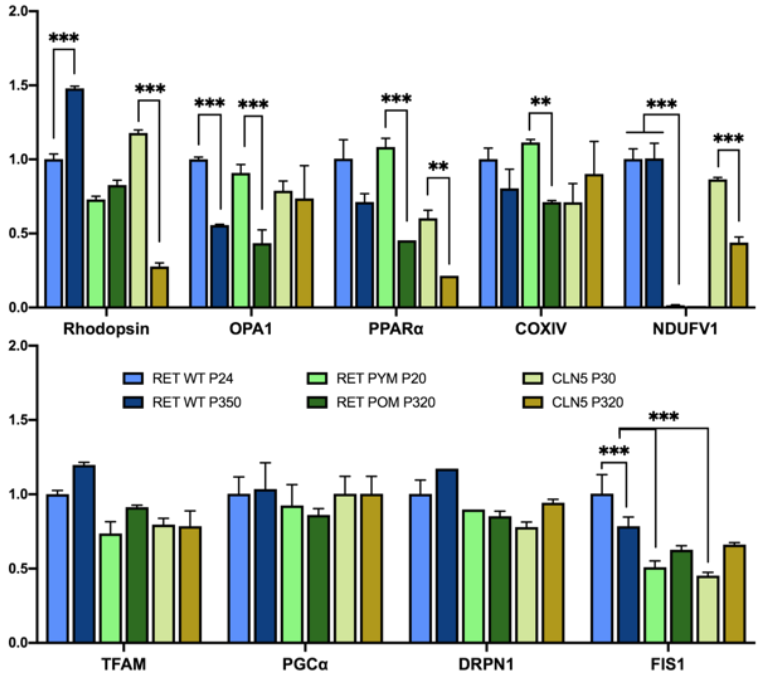

Figure 9: Mitochondrial transcriptional changes in young and old mice in the healthy and diseased retina. RT-qPCR analysis of relative mRNA levels of rhodopsin (RHO), and mitochondria markers of biogenesis (PGC1alpha, OPA1, Fis1 and DRP1, PPAR), OXPHOS (COXIV, NDUFV1) and mtDNA maintenance (TFAM) normalized to housekeeping gene GAPDH, from postnatal P20-30 and P320-P350 of WT C57BL6/J, CLN6 and PGRN mice. Fold changes in the expression of target genes were normalized to P20-WT values. The bars represent the average of 3-4 retinas per group, run in 3 qPCR triplicates. Statistical 2-way ANOVA, Tukey t test was performed. *=p <0.05, **p<0.001, ***=p <0.001. Means ± SD were plotted.

We analyzed the gene expression profile in both young or old and healthy or degenerated retinas. We first selected from the literature common markers of mitochondria function and health. We looked at a transcriptional activator, PGC1 alpha, that partially promotes mitochondrial biogenesis, increasing mitochondrial mass and copy number to boost production of ATP as a response to greater energy expenditure. Mitochondria fission, fusion and maintenance of normal crista structure is regulated from a diverse pool of mitochondria genes, such as dynamin-related GTPase OPA1 and fission factors Fis1 and Drp1. Mitochondrial dysfunction affects also both nuclear and mt expression of the transcription factor TFAM, involved in the maintenance of mtDNA. High expression of TFAM has been shown to confer protection in oxidative stress models. We also looked at the gene expression level of the complex I OXPHOS enzymes, COXIV and NDUFV1.

We extracted RNA from young and old retinas, from wild-type C57BL6 (WT) mice and mice with early (CLN5) and late onset (PGRN) of photoreceptor cell death. Both CLN5 and PGRN are mouse models of neuronal ceroid lipofuscinosis (NCL), a common childhood neurodegenerative disease that causes visual loss as well as impaired motor function. Accumulation of autofluorescent storage material, lipofuscin-like ceroids, into lysosomes is a common marker of NCL disorders. As expected, we found that RHO was downregulated in the CLN5 mouse model, at P320 compared to P30 (0.266 ± 0.024 vs. 1.17 ± 0.020, $p<0.001$). There was no significant difference found in PGRN retinas, correlating with reported late onset of photoreceptor cell death in mice over one-year old. WT, CLN5 and PGRN retinas from older animals showed significant down regulation ($p<0.001$) of genes involved in mitochondria fission and fusion (FIS1, OPA1) compared to younger retinas. Only the NCL mouse models showed transcriptional impairment in OXPHOS complex I genes, more specifically in the NDUFV1 gene expression, as well as the transcription factor PPAR alpha, linked to mitochondria biogenesis maintenance **(Fig 9**).

Here, we found significant differences in gene expression of mitochondrial markers of biogenesis and function, between young and aged retina, as well as in the healthy and inherited degenerative retinas. We are currently building vectors encoding biosensors such as pTimer and mKeima that can selectively target outer retina mitochondria to characterized difference stage of mitochondria dysfunctions through time and in specific cells.

Discussion

Mutations in mtDNA ultimately trigger mitochondria dysfunction and results in a range of neurodegenerative (seizures, deafness, optic atrophy) and metabolic (cardiomyopathy, abnormal developmental) disease phenotype in patients. To date, the major sites[7,41] of mt mutations have been identified, and development of mitochondrial gene therapies have emerged.

One promising approach is the delivery of a healthy copy of the mutated mitochondrial-encoded gene to restore proper protein function. However, the hydrophobic nature of those proteins, which has been suggested as the central evolutionary purpose of gene retention in the mammalian organelle, is a hurdle for gene therapy. The development of gene delivery systems that can pass through the mitochondrial double membranes is key to the success of this approach, along with the choice of delivery vector. Several successes have been reported in the eye in the past years, in both preclinical models and human clinical trials (Phase III[42]) studies for Leber Hereditary Optic Neuropathy, using an AAV vector to deliver a healthy copy of the mtND4 mutated gene to ganglion cells in the retina. AAV is currently one of the most promising vectors to achieve stable and long-term expression of genes in a variety of organs and tissues hard to infect. In addition, many preclinical AAV-mediated gene therapy proof-of-concept studies have been transformed into human clinical trial success and now drug commercialization.

Current AAV-mediated gene therapy and delivery approaches are based on the potency of the N-terminal pre-sequence of nuclear-encoded mitochondria genes to redirect its fusion protein selectively to the appropriate mitochondria compartment. Specific motifs in the early 10-90 amino acid residues are recognized by the translocase of the outer membrane (TOM) and then sorted through the intermembrane space to their dedicated location. Although we understand better the

different steps involved in the import of proteins synthetized on cytosolic ribosomes into the organelle, some of the mechanism remains elusive.

Our study looked at optimizing AAV-mediated mitochondrial gene targeting and improving tools to investigate mitochondrial dysfunction in the retina. We established an *in vitro* screening protocol, combining imaging techniques to western blot analysis of mitochondrial isolated protein fraction to characterization of the selectivity of MTSs used in the literature as well as novel sequences we designed. Predictive tools such as MitoFates, are very useful for determining the MTS sequence of thousands of candidate genes, although its algorithm, like others, discards any putative N-termini sequences that do not contain cleavable motifs by mitochondrial processing enzymes (Oct1, MPP). We isolated an MTS pre-sequence from one of the isoforms of DIABLO/SMAI, which didn't score well but led to selective import of fused protein to the mitochondria. As previously published, MTS sequences of IMS proteins differ from other organelle compartments. The MTS of PMPCB and OTC genes led to strong expression of fused protein in the mitochondria.

While most initial MTS screens rely on the import of easy-folding, truncation-permissive reporters, such as GFP, we showed that putting selective pressure on the mitochondrial import-screening process, delivering molecules that can easily misfold, or contain multiple transmembrane domains, and are highly hydrophobic, directly improves the identification of strong MTSs that perform well with a wide-range of fused protein. Our next step is to adapt our screen to the endogenous ATP6 protein and show functional rescue in an *in vitro* cell line.

Fascinatingly, organisms such Chlorophycean algae did not retain their mitochondrial genome through evolution[43–45]. While MTS sequences of their nuclear-encoded mitochondrial genes are usually short, big transmembrane proteins (>100 residues) such as ATP6 and ATP8, containing longer MTS sequences, hypothesized to allow for both mitochondria import in the matrix and insertion in the inner membrane. Furthermore, an alternative mechanism to MTS-mediated mitochondrial trafficking was found in yeast. Over a 100 mRNA were found to localize at the vicinity of mitochondria[46] in *Saccharomyces cerevisiae*. The 3'UTR sequence was shown to be an essential localization signal for the mRNA. Margeot *et al.*[29] provided additional evidence of 3'UTR localization role by showing that the substitution of the ATP2 3'UTR to a non-mitochondrial 3'UTR, led to respiratory deficiency in the yeast, as well as abnormal localization of the ATP2 mRNA.

We conducted a 3'UTR screen, using the 3'UTR of COX10 as a reference sequence, since it has been shown to display a high mitochondrial localization score and is already used in therapeutic transgene delivery in the eye. We tested the 3'UTR sequences of other COX genes for which the MTS was not efficient at redirecting protein of interest. Surprisingly, none of the 3'UTRs tested significantly increased the mitochondrial localization score of tdTomato-3'UTR or matching MTS + 3'UTR constructs. However, 3'UTR mitochondrial relocalization of mRNA might only be achievable with mitochondrial genes and not exogenous genes.

We then used MTS sequences to optimize and compare AAV-mediated allotopic mitochondria targeting to re-traffic the viral capsid to the mitochondria vicinity. While both approaches have been used to rescue visual loss induced in a ND4 mouse model of LHON, the efficiency was not compared. Delivering therapeutic DNA directly to the mitochondria has many benefits over the nuclear-mediated allotopic approach. It requires first mitochondria-selective transcriptional elements (HSP promoter, codon-optimized transgene), and therefore eliminates risk of nuclear/cytoplasmic off-target expression of the subsequent translated protein. It will also allow

faster protein translation by using the mitochondria replication machinery and skipping nuclear transcriptional and protein re-trafficking from the cytoplasm to the mitochondria.

The engineering of AAV with preferential trafficking to the mitochondria as well as functional proof-of-concept in different models has only been published by the same investigator[51]. It was achieved by tagging the MTS of COX8A to the N-terminal of the AAV VP2 subunit, expressed in trans during packaging. Chimeric MTS-AAV particles would then theoretically have 5 MTS sequences exposed on the capsid that could be recognized by the mitochondrial membrane proteins during cellular trafficking. While this novel approach is extremely promising, we encountered many hurdles while trying to replicate this system *in vitro*.

We first found that fusing selective MTS sequences (OTC, PMPBC) onto VP2, resulted in VP2-deficient AAV during viral packaging. The MTS-VP2 protein is redirected to the mitochondria before being able to assemble with the VP1 and VP3 subunits to form complete AAV particles. On the other hand, COX8A-AAV particles formed normally. We further confirmed that the COX8A-VP2 plasmid when transfected did not achieve mitochondrial re-trafficking. When COX8A-AAV was packaged with a nuclear-encoded reporter gene, it led to strong nuclear/cytoplasmic infection. When a mitochondrial-encoded transgene was used, we could not detect visible fluorescence. We hypothesized that the efficiency of this system is extremely low as other studies[48] have used a luminescent reporter to quantify endogenous mitochondria expression.

MTS-mediated AAV-preferential trafficking to the mitochondria is questionable. primarily due to the known MTS-import mechanisms which preferentially re-traffic linear proteins and therefore would be challenged with the icosahedral AAV virion structure. Also, linear amplification mediated PCR showed that naturally wild type AAV inserts in the mitochondria genome [47] bringing into doubt previous reports that did not directly control for this parameter. Furthermore, this study[47] looked at genomic insertion of rAAV in patients and mice injected intramuscularly with AAV1-LPL. Two and three AAV integration site hotspots identified had homology to the mitochondria genome in human and mouse muscle, respectively. This is evidence of an alternative AAV trafficking route than the current consensus on the late endosomal escape and travel to the nucleus. Finally, mitochondria import of naked mitochondrial-encoded DNA, without any import sequence was shown by a different group when hydrodynamically forced onto liver and skeletal muscle cells[48].

While we believe that endogenous expression of the therapeutic transgene is the most promising strategy for safe mitochondrial gene expression, we concluded that this approach requires more engineering and optimization. Natural AAV trafficking to the mitochondria is an incredible benefit over other inefficient methods like nanoparticles that currently require the use of cell penetrating peptides, which have been shown to be cytotoxic or require an extremely high dose for low expression efficiency[49].

On the other hand, we found that AAV-mediated allotopic expression led to a high level of selective protein expression *in vitro* and *in vivo*. By combining the use of a novel AAV variant with increased retinal transduction and penetration with strong MTS incorporation in the AAV transgene, we were able to achieve stable and visible expression in the retina, confirmed by colocalization with a mitochondria marker and western blot analysis of the mt fraction. Furthermore, we generated an AAV-toolbox with a cell-type specific promoter able to drive selective, efficient targeting of the glia and photoreceptors as well as selective transgene expression in mitochondria. These vectors are extremely valuable to closely investigate mitochondria dysfunction in age-related and inherited retinal degeneration. However, although allotopic expression has been successfully used in many studies, many questions and potential

caveats are still left unanswered regarding its efficacy and safety for gene therapies. Mitochondria are sensitive to its protein ratio and oxidative stress. It has been shown that allotopic-mediated delivery of protein led to increased mitochondria fragmentation[50]. More safety studies need to be conducted of the long-term effect of nuclear-encoded protein import to the mitochondria. Also, further experimental proof that the subsequent cleaved protein after mitochondrial import is localized to the correct compartment, is integral and functional is critical.

Materials and methods

Mitochondria Targeting Signal (MTS) Sequences and plasmids

We identified mitochondrial nuclear-encoded genes that possess a targeting signal (MTS) pre-sequence, which mediates trafficking of its fused protein to the mitochondria. MTS sequences were selected based on genes selected from the literature or that scored high with the MitoFates predication tool. MitoFates is a predictive tool for identifying putative mitochondria pre-sequences and cleavage sites [24]. It includes features such as charged amphiphilicity, pre-sequence motifs based on amino acid composition involved in mitochondria trafficking mechanisms.

Genes and protein sequences of all MTS used in study are listed below.

Gene	N-terminal MTS (Amino Acid)	Reference
COX5A	MLGAALRRCAVAATTRADPRGLLHSARTPGPAV	-
COX8A	MSVLTPLLLRGLTGSARRLPVPRAKI	[51]
COX8C	MPLLRGRCPARRHYRRLALLGLQPAPRFAHSGPP	-
COX10 (UTR)	SLQQIDEQCFFIMPTLYKKVGMAASPH	[23]
ATP5A1	MLSVRVAAAVVRALPRRAGLVSRNALGSSFI	-
PMPCB	MAAAAARVVLSSAARRRLWGFSESLLIRGAAGRSL	-
DIABLO	MAALKSWLSRSVTSFFRYRCGRVEGT	-
NDUFB11	MAAGLFGLSARRLLAAAATRGLPAARVRWES	-
OTC	MLFNLRILLNNAAFRNGHNFMVRNFRCGQPLQ	[52]

OTC, COX10UTR, DIABLO and PMPCB MTS sequences were synthetized using IDT DNA block synthesis services. COX8A, COX8C, COX5A, ATP5A1 and NDFUB11 were amplified from hARPE-19 cDNA and then cloned into TOPO vector (Thermofisher, K450001) for further manipulations. MTS sequences were cloned at the N-terminal of the tdTomato to create fusion fluorescent transgenes.

Plasmid containing ubiquitin-C promoter (pUbi.Cap2) was used to generate pUbi.tdtomato and pUbi.MTS-tdTomato constructs. Each MTS sequence were cloned in frame at the N-terminal of the tdTomato gene to create fusion florescent transgene. pUbi.tdTomato was cloned by first linearizing pUbi(Cap2) backbone with antisense gibUbiR 5'-GGTGGCTGCAGCCCAAGC -3' primer and forward 5'-TTTGTGCCTTCTAGTTGCCAGCC-'3 primers. 15bp-overlapping sequences to the 3' /5' end region of the linearized BB were added to forward and reverse PCR primers amplifying tdTomato (5'- aagcttgggctgcagccaccATGGTGAGCAAGGGCGAG-3' and 5'- tggcaactagaaggcacaaaTTACTTGTACAGCTCGTCCATG-3' respectively). MTS sequences were fused at N-terminal of tdTomato (ATG removed) of pUbi.tdTomato plasmid. The online NEB builder Assembly tool was used to generate primer sequences. pUbi-tdTomato BB was linearized using previous gibUbiR antisense primer and forward 5-'GTGAGCAAGGGCGAGGAGGTAT-3'. Primers with BB overlaps were designed for each MTS.

Backbone and insert were ligated using Gibson Master Mix (NEB E2611) and transformed in NEB5-alpha competent (NEB C2987H) cells. Ubiquitin-MTS-tdTomato (e.g. Ubiquitin-COX8A-tdtomato) plasmid was generated for each MTS sequence.

Cell culture and transfection

Human embryonic kidney cell line 293T were maintained as a monolayer culture at 37°C and 5% CO_2 in Dulbecco's modified Eagle's medium (DMEM), supplemented with 10% fetal calf serum, and 2 mM L-glutamine.
Ubiquitin-MTS-tdTomato constructs were transfected *in vitro* to analyze tdTomato expression localization. HEK293T cells were seeded on poly-D-lysine treated coverslips or directly in 12-wells a day prior to transfection. We transfected 500ng of DNA per construct with DNA/PEI (1mg/mL) of 1:3. Three days later, cells fluorescence was checked, and cells either harvested or fixed depending on experimental use.

Mitochondria isolation from cultured cells and mouse retinas

Total cell protein and mitochondria fraction were isolated from HEK293T cells transfected with MTS-tdTomato constructs. For the mitochondria isolation, harvested cells were lysed with Dounce homogenization and chemical method following Mitochondria Isolation Kit for Cultured Cells (ThermoFisher Scientific, # 89874) manufacturer's guidelines. The protocol was performed on ice and Halt™ Protease inhibitor cocktail EDATA-free (Thermofisher, 87785) was added to each reagent prior to use. Briefly, cells were detached and resuspended in Isolation Reagent A before either mechanical (Dounce) or chemical cell lysis. Post-nuclear supernatant obtained was spin at 5000g instead of 12,000 g to attain a more purified fraction. The mitochondria were then pelleted by centrifugation at 12,000g for 5 minutes at 4'C, washed once with Isolation Reagent C. Final pellet was resuspended in 1X RIPA buffer (50mM Tris, 150mM NaCl, 1mM EDTA, 1% Triton X-100, 1% Sodium Deoxycholate, 1mM NaF, 0.2mM Na3VO4). For total cell fractions, harvest cells were washed with PBS one time before being resuspended in 1X RIPA buffer with added proteinase inhibitor cocktail. Samples were briefly sonicated and spin to remove cell debris.
Mouse retinas were mechanically homogenized, and Qproteome Mitochondria Isolation kit (QIAGEN, #37612) used to isolate nuclear, cytosolic and mitochondria protein fractions following manufacturer's protocols. Subsequent protein pellets were also resuspended in 1X RIPA 1% proteinase inhibitor cocktail as well. Supernatant protein concentrations were measured using the Pierce™ BCA Protein Assay Kit (#23225). Samples were store at -80'C until processed.

Fluorescent Western Blotting

Samples were reduced in denatured in Laemmli buffer (Biorad, 161073) mixed with β-mercaptoethanol and boiled for 5 minutes at 95'C and chilled on ice. Mitochondria protein samples were run (150V, 60 min) on a Nuvex™ WedgeWell 6% Tris-Glycine (Thermofisher, XP00062BOX) gel in Running Buffer (25 mM Tris base, 190 mM glycine, 0.1% SDS) and viral samples on a 10-20% Tris-Glycine gel (Thermofisher, XP10202BOX). Protein samples were transferred (20V, 3 hours) to a PVDF membrane in blotting buffer (10 mM NaHCO3, 3mM

Na2CO3, pH 9.9, 20% methanol). Membrane was blocked in 5% dry non-fat milk in 1x PBS-T (1x PBS, 0.1% Tween-20, 0.1% BSA) for 1 hour. The membrane was then washed 3x 5 minutes in PBS-T, and incubated in primary antibodies (in 1% BSA, PBST-T) overnight in 4'C. Following day, the blot was washed in 1xPBS for 15 minutes followed by 4x 5 5 minute and incubated for 1 hour at RP with secondary antibodies (licor, IRDye® 680RD and 800CW) in 1% BSA, PBST-T. Blot was washed thoroughly before fluorescence was imaged with the Odyssey CLx Near-Infrared Fluorescence Imaging System.
For mitochondria samples, rabbit polyclonal primary antibodies against RFP (1:2500, Rockland 600-401-379), rabbit polyclonal primary antibodies against COXIV (1:1000, Abcam ab16056) and IRDye® 680RD donkey anti-Rabbit IgG Secondary antibody secondaries were used.
For viral samples, mouse monoclonal primary antibody against AAV VP1, VP2, VP3 subunits (1:50, Progen #65168) and IRDye® 800 CW goat anti-mouse IgG secondary antibody.

Generation of mito-AAV plasmids

AAV-VP2KO plasmid
7m8 and AAV2 rep and cap plasmid (encoding for VP1, VP2, VP3) were modified through QuickChange Lightning (stratagene) according to the manufacturer's protocol. Residue T138 was mutated (ACG -> ACT) to knock down VP2 without altering VP1 and VP3 reading frame (AAV2-VP2K0 and 7m8-VP2KO) with forward primer 5'-ttttttcccggagcggtcttaacaggttcctcaac-3' and reverse primer 5'-gttgaggaacctgttaagacCgctccgggaaaaaa-3'. Resulting plasmids were called 7m8VP2KO and AAV2VP2KO.

Generation of VP2 in trans plasmid:
Ubi.(7m8)VP2 was cloned downstream of an ubiquitin C promoter. Original plasmid used already contained AAV2 VP2 (pUbi.Cap2). Superfolder GFP (Addgene, #54579), eGFP sequences were fused to N-terminal of VP2 with GSSS linker sequence in between generate ubiquitinC.sfEGFP-VP2. Two other linkers, $(GSSS)^3$ and EAAAK were tested (see supplementals).
COX8A-eGFP-VP2 was generated as previously described[51]. COX8A MTS was fused to N-terminal of GFP sequences. Primers were designed with the online Gibson Assembly tool for Gibson cloning. Primers sequences are listed in the **supplementals**.

Generation of mt-encoded transgenes
We used human mitochondria promoter HSP previously published (X). It was synthetized using complementary oligonucleotides (IDTDNA) flanked with Age I and KnpI restriction sites: forward 5'-cTAACCCCATACCCCGAACCAACCAAACCCCAAAGACACa-3' and reverse 5'-ccggtGTGTCTTTGGGGTTTGGTTGGTTCGGGGTATGGGGTTAggtac-3'primers. Mouse HSP promoter (~200bp) published sequence[48] was synthesized with IDT block fragment synthesis service. 5'and amplify to insert flanking AgeI and KpnI restriction sites on its 5' and 3' end: forward 5'-GTA AAG GTA CCT CGC CAC TAA TCT CAT CAA TAC-3' and reverse 5'- GTA AAC CGG TGA GCT GTG TCT TTG GGG TTT GG -3' primers.

pTR.scCAG.eGFP backbone, PCR products were digested with KpnI and AgeI. Human HSP oligos were annealed to reconstitute double-stranded sequence. Inserts were ligated into the pTR.scCAG. BB to give plasmid pTR.schHSP.eGFP and pTR.scmHSP.eGFP.

Mitochondria encoded mCherry (mtmCherry) was engineered by Quikchange Lightning site directed mutagenesis. Nuclear encoded arginine residue AGG leads to a stop coding in mitochondrial-encoded genome. Nucleotide A at position 505 was mutated to C(AGG->CGG), which results in both nuclear and mitochondria-read arginine residue. Primers 5'-ccttcagcttcagccgctgcttgatctcgcc-3' and 5'-ggcgagatcaagcagcggctgaagctgaagg-3' were used on topo plasmid containing mCherry.

To generate pTR.sc(human/mouse)HSP.mtmCherry, pTR.HSP.eGFP plasmids were digested with AgeI and HindIII to cut out eGFP sequence. MtmCherry was then amplified with primers flanking AgeI (5'-GAT AAC CGG TGC CAC CAT GGT GAG CAA GGG C-3') and HindIII (5- GAT AAG CTT TTA CTT GTA CAG CTC GTC CAT GCC G-3') restriction sites and ligated into each pTR.HSP backbone.

rAAV production

rAAV vectors with all cap VP subunit were provided *in cis*, were produced by the plasmid triple co-transfection method described in Visel et al[53]. AAV rep /cap, as well as transgene plasmid were co-transfected with pHelper plasmid in HEK293T cells in equal molar ratio 1:1:1.
Three days later, cells were harvested and spun down at 1000rpm for 10 minutes and subsequent pellet and supernatant separated. 40% PEG was added to supernatant for a 8% final PEG concentration and incubated on ice for 2. The cell pellet was resuspended in lysis buffer (0.15 NaCl, 50 mM Tris HCl, 0.05% Tween, pH 8.5) and freezed/thawed in dry-ice/ethanol and 37'C water bath respectively for 3 cycles. The crude lysate was treated with 250U/uL of Benzonase (Novagen #71205-3) for 30 minutes and spun at 4000 rpm for 20 min at 4'C. PEG-supernatant solution was spun at 4000 for 25 minutes. Resulting pellet was resuspended with the crude lysate supernatant and, incubated in 37'C for at least 1 hour to allow proper homogenization. AAV lysate was layered onto an iodixanol density gradient (OptiPrep®) and ultracentrifuged for one hour at 69000 rpm at 18'C to allow for protein separation. The interface between the 60% and 40% iodixanol fraction was extracted, diluted with an equal volume of 1X PBS + 0.001% Pluronic and then loaded onto an Amicon® Ultra-15 Centrifugal Filter Unit (Millipore, Tullgren, Ireland) and spun until 250 µl of concentrated vector remained. Filter was washed 3 times with 5mL loads of fresh sterile PBS and concentrated down to 200uL of the final viral concentrate. Purified virus was subjected to DNase treatment to remove any residual plasmid DNA or unpackaged genomes, and the vector was then tittered by quantitative PCR using diluted plasmid DNA as a standard.

Generation of rAAV vectors with VP2 provided *in trans*, were generated with similar protocol described than above except for the HEK293T transfection step. AAV-VP2KO (7m8 or AAV2) were co-transfected with pHelper, transgene plasmid and UbiquitinC.sfGFP.VP2-*in trans* plasmid (with or without MTS) cells in equal molar ratio 1:1:1:1.

Agarose sectioning:

The animals were euthanized by CO2 asphyxiation and cervical dislocation and the eyes were enucleated and immersion fixed in 10% formalin (in phosphate buffer,Ted Pella, Redding, USA). The cornea and lens were removed, and the retina was isolated and again conserved in 10% formalin. The retinas were embedded in an agarose block by pouring 5% melted agarose into a

small weight boat. The tissues were then transferred from PBS to liquid agarose. After the agarose blocks had cooled, the retina was sectioned (Leica VT1000 S, Leica Microsystems, Nussloch, Germany) into 120-150 μm thick sections.

Immunohistochemical analysis, confocal microscopy, and cell counting

For IHC, the sections were blocked for at least 1 hour at room temperature in blocking buffer (10% normal goat serum, 1% FBS, 0.5% Triton-X 100) before antibody labelling overnight. The antibodies used were: rabbit anti-GS (Sigma G-2781, 1:1000), Alexa Fluor 594 goat anti-rabbit (Invitrogen, 1:2000). Images were taken on a Zeiss LSM 710 laser scanning confocal microscope (NIH Grant 1S10RR026866-01).

mRNA gene expression analysis

RNA was extracted from either from cultured cells or retinal tissue using the RNeasy Mini Qiagen kit and eluted in 30uL -f DEPC-treated water. During extraction, RNA was treated with DNAse. The resulting RNA was store at -80'C until use. cDNA was synthetized from RNA primed with random primers, using the superscript III first-strand synthesis system (thermofisher). qRT-PCR samples were run in triplicate using a collection of primers and a housekeeping gene glyceraldehyde-3-phosphate dehydrogenase (GAPDH). The relative standard curve method was used to calculate fold difference in mRNA expression normalized to control conditions.
RT-PCR Primer sequences used are listed in the **supplementals S3**.

Supplementals Figures

Presequence
- Possessing mitochondrial presequence (Precision:0.83, Recall:0.73)
- Possessing mitochondrial presequence (Precision:0.79, Recall:0.80)
- No mitochondrial presequence

Cleavage site
- MPP cleavage site
- Oct1 cleavage site
- Icp55 cleavage site

Motif
- TOM20 recognition motif (ΦχβΦΦ)
- Max positively charged amphiphilicity (PA) score region (high)
- Max positively charged amphiphilicity (PA) score region (low)
- Φ β σ γ Reduced letters composing statistically significant 6mer in presequence Φ(hydrophobic), β(basic), σ(polar), γ(secondary structure breaker)

Sequence ID	Probability of presequence	Cleavage site (processing enzyme)	Net charge	Sequence (100 amino acids from N terminal)
ATP5A1	0.974	24 MPP	0.208	MLSVRVAAAVVRALPRRAGLVSRNALGSSFI
OTC	0.931	24 MPP	0.125	MLFNLRILLNNAAFRNGHNFMVRNFRCGQPLQ
PMPCB	0.924	29 MPP	0.138	MAAAAARVVLSSAARRRLWGFSESLLIRGAAGRSL
NDUFB11	0.906	13 MPP, 14 Icp55*	0.154	MAAGLFGLSARRLLAAAATRGLPAARVRWES
SOD2	0.885	24 MPP	0.125	MLSRAVCGTSRQLAPVLGYLGSRQKHSLPD
ATP9	0.870	24 MPP	0.125	MQTAGALFISPALIRCCTRGLIRPVSASFLNSP
COX8A	0.854	11 MPP, 12 Icp55*	0.091	MSVLTPLLLRGLTGSARRLPVPRAKI
COX5A	0.820	9 MPP	0.222	MLGAALRRCAVAATTRADPRGLLHSARTPGPAV
COX8C	0.791	28 MPP	0.250	MPLLRGRCPARRHYRRLALLGLQPAPRFAHSGPP
DIABLO	0.274	11 MPP	0.182	MAALKSWLSRSVTSFFRYRCGRVEGT
COX10 (UTR)	0.000	11 MPP	-0.182	SLQQIDEQCFFIMPTLYKKVGMAASPH

S1: Mitofates Prediction Score of MTS sequences.
Its algorithm scores high position that form a local-helical secondary structure with high hydrophobicity and positively charged residues facing each other on each side of the protein. It also correlates presence of cleavage site motif detectable by mitochondria processing enzymes (Oct1, MPP and Icp55) as well as recognition of the TOM20 motif. Sequences without a Tom20 recognition motifs had the lowest score. High scores were given to MTS/motif that could form a local-helical secondary

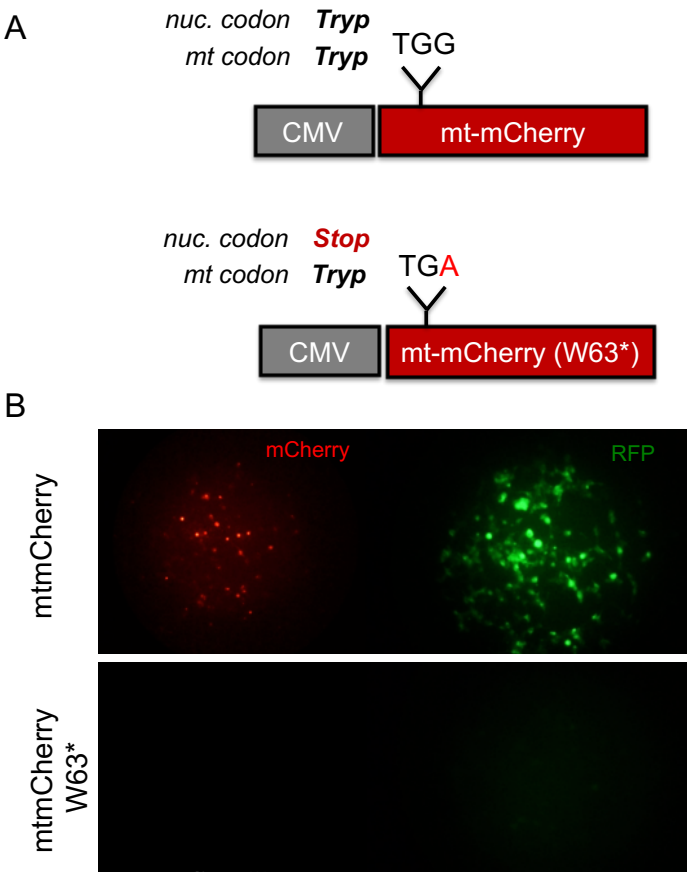

S2: Codon optimization of mtmCherry transgene abolishes nuclear off target expression

Diagram (**A**) of mitochondrial encoded mtmCherry (mtmCherry) codon optimization. Quikchange lightning site directed mutagenesis was performed on mtmCherry plasmid to mutate the nucleotide G at position to an A, translating to an early stop codon for nuclear encoded protein (W63*), without modifying mitochondrial Tryptophan (W) codon read. Primers used: Forward 5'- GGG ACA GGA TGT CTC AGG CGA AGG GCA- 3'; reverse 5'- TGC CCT TCG CCT GAG ACA TCC TGT CCC-3'. Representative images **(B)** of HEK293T cells transfected with pCMV.mtmCherry and pCMV.mtmCherry(63*). pCMV.mtmCherry led to strong nuclear expression (red channel). Signal was amplified using primary RFP antibody (1:1000, Rockland) and 488-alexa fluor secondary antibody (1:2000, green channel). No nuclear off-target was detected in HEK293T cells transfected with pCMV.mtmCherry W63*.

mDrp1 RT-PCR F	5’-TCACCCGGAGACCTCTCATT-3’
mDrp1 RT-PCR R	5’-TGCTTCAACTCCATTTTCTTCTCC-3’
mPPARα RT-PCR F	5’-ATTTGCTGTGGAGATCGGC-3’
mPPARα RT-PCR R	5’-GCTTTGGGAAGAGGAAGGTGT-3’
mOpa1 RT-PCR F	5’-TCTGAGGCCCTTCTCTTGTT-3’
mOpa1 RT-PCR R	5’-TCTGACACCTTCCTGTAATGCT-3’
mFis1 RT-PCR F	5’-ACGAAGCTGCAAGGAATTTTGA-3’
mFis1 RT-PCR R	5’-AACCAGGCACCAGGCATATT-3’
mCOXIV RT-PCR F	5’-TAC TTC GGT GTG CCT TCG A-3’
mCOXIV RT-PCR R	5’-TGA CAT GGG CCA CAT CAG-3’
mPGC-1α RT-PCR F	5’-TGA TGT GAA TGA CTT GGA TAC AGA CA-3’
mPGC-1α RT-PCR R	5’-GCT CAT TGT TGT ACT GGT TGG ATA TG-3’
mNdufv1 RT-PCR F	5’-CTT CCC CAC TGG CCT CAA G-3’
mNdufv1 RT-PCR R	5’-CCA AAA CCC AGT GAT CCA GC-3’
mTfam RT-PCR F	5’-CTTCGATTTTCCACAGAACAG-3’
mTfam RT-PCR R	5’-TGGTAGCTCCCTCCACAG-3’
mGAPDH RT-PCR F	5’-AACTTTGGCATTGTGGAAGG-3’
mGAPDH RT-PCR R	5’-GGATGCAGGGATGATGTTCT-3’

S3: Table of mouse RT-PCR primers used to quantify marker of mitochondria biogenesis and health

References

1. McBride, H. M., Neuspiel, M. & Wasiak, S. Mitochondria: More Than Just a Powerhouse. *Current Biology* (2006). doi:10.1016/j.cub.2006.06.054
2. Weinberg, S. E., Sena, L. A. & Chandel, N. S. Mitochondria in the regulation of innate and adaptive immunity. *Immunity* (2015). doi:10.1016/j.immuni.2015.02.002
3. Ott, M., Gogvadze, V., Orrenius, S. & Zhivotovsky, B. Mitochondria, oxidative stress and cell death. *Apoptosis* (2007). doi:10.1007/s10495-007-0756-2
4. Tait, S. W. G. & Green, D. R. Mitochondria and cell death: Outer membrane permeabilization and beyond. *Nature Reviews Molecular Cell Biology* (2010). doi:10.1038/nrm2952
5. D'Souza, A. R. & Minczuk, M. Mitochondrial transcription and translation: overview. *Essays Biochem.* **62**, 309–320 (2018).
6. Smits, P., Smeitink, J. & van den Heuvel, L. Mitochondrial translation and beyond: processes implicated in combined oxidative phosphorylation deficiencies. *J. Biomed. Biotechnol.* **2010**, 737385 (2010).
7. Schrier, S. A. & Falk, M. J. Mitochondrial disorders and the eye. *Curr. Opin. Ophthalmol.* **22**, 325–331 (2011).
8. Carelli, V., Ross-Cisneros, F. N. & Sadun, A. A. Mitochondrial dysfunction as a cause of optic neuropathies. *Progress in Retinal and Eye Research* (2004). doi:10.1016/j.preteyeres.2003.10.003
9. Jarrett, S. G., Lin, H., Godley, B. F. & Boulton, M. E. Mitochondrial DNA damage and its potential role in retinal degeneration. *Progress in Retinal and Eye Research* (2008). doi:10.1016/j.preteyeres.2008.09.001
10. Terluk, M. R. *et al.* Investigating Mitochondria as a Target for Treating Age-Related Macular Degeneration. *J. Neurosci.* **35**, 7304–7311 (2015).
11. Kaarniranta, K., Kajdanek, J., Morawiec, J., Pawlowska, E. & Blasiak, J. PGC-1α protects RPE cells of the aging retina against oxidative stress-induced degeneration through the regulation of senescence and mitochondrial quality control. The significance for AMD pathogenesis. *International Journal of Molecular Sciences* (2018). doi:10.3390/ijms19082317
12. Hyttinen, J. M. T., Viiri, J., Kaarniranta, K. & Błasiak, J. Mitochondrial quality control in AMD: does mitophagy play a pivotal role? *Cellular and Molecular Life Sciences* (2018). doi:10.1007/s00018-018-2843-7
13. Caprara, C. & Grimm, C. From oxygen to erythropoietin: Relevance of hypoxia for retinal development, health and disease. *Progress in Retinal and Eye Research* (2012). doi:10.1016/j.preteyeres.2011.11.003
14. Trapani, I. & Auricchio, A. Seeing the Light after 25 Years of Retinal Gene Therapy. *Trends Mol. Med.* **24**, 669–681 (2018).
15. Rodrigues, G. A. *et al.* Pharmaceutical Development of AAV-Based Gene Therapy Products for the Eye. *Pharm. Res.* **36**, (2019).
16. Oca-Cossio, J., Kenyon, L., Hao, H. & Moraes, C. T. Limitations of allotopic expression of mitochondrial genes in mammalian cells. *Genetics* **165**, 707–20 (2003).
17. Schmidt, O., Pfanner, N. & Meisinger, C. Mitochondrial protein import: From proteomics to functional mechanisms. *Nat. Rev. Mol. Cell Biol.* **11**, 655–667 (2010).

18. Omura, T. Mitochondria-targeting sequence, a multi-role sorting sequence recognized at all steps of protein import into mitochondria. *Journal of Biochemistry* (1998). doi:10.1093/oxfordjournals.jbchem.a022036
19. Regev-Rudzki, N., Yogev, O. & Pines, O. The mitochondrial targeting sequence tilts the balance between mitochondrial and cytosolic dual localization. *J. Cell Sci.* (2008). doi:10.1242/jcs.029207
20. Herrmann, J. M. & Hell, K. Chopped, trapped or tacked - Protein translocation into the IMS of mitochondria. *Trends in Biochemical Sciences* (2005). doi:10.1016/j.tibs.2005.02.005
21. Hernandez, G. *et al.* MitoTimer: A novel tool for monitoring mitochondrial turnover. *Autophagy* (2013). doi:10.4161/auto.26501
22. Yu, H. *et al.* Next-generation sequencing of mitochondrial targeted AAV transfer of human ND4 in mice. *Mol. Vis.* **19**, 1482–1491 (2013).
23. Ellouze, S. *et al.* Optimized Allotopic Expression of the Human Mitochondrial ND4 Prevents Blindness in a Rat Model of Mitochondrial Dysfunction. doi:10.1016/j.ajhg.2008.08.013
24. Fukasawa, Y. *et al.* MitoFates: Improved Prediction of Mitochondrial Targeting Sequences and Their Cleavage Sites* □ S. *Mol. Cell. Proteomics* **14**, 1113–1126 (2015).
25. Thorburn, D. R., Rahman, J. & Rahman, S. *Mitochondrial DNA-Associated Leigh Syndrome and NARP*. *GeneReviews®* (1993).
26. López-Gallardo, E. *et al.* NARP syndrome in a patient harbouring an insertion in the MT-ATP6 gene that results in a truncated protein. *J. Med. Genet.* (2009). doi:10.1136/jmg.2008.060616
27. Kaltimbacher, V. *et al.* mRNA localization to the mitochondrial surface allows the efficient translocation inside the organelle of a nuclear recoded ATP6 protein. *RNA* (2006). doi:10.1261/rna.18206
28. Bonnet, C. *et al.* [mRNA localization to the mitochondrial surface: a tool to treat retinal pathologies due to mitochondrial DNA mutations]. *J. Soc. Biol.* **201**, 69–74 (2007).
29. Margeot, A. *et al.* In Saccharomyces cerevisiae, ATP2 mRNA sorting to the vicinity of mitochondria is essential for respiratory function. *EMBO J.* **21**, 6893–6904 (2002).
30. Marc, P. *et al.* Genome-wide analysis of mRNAs targeted to yeast mitochondria. *EMBO Rep.* **3**, 159–164 (2002).
31. Chin, R. M., Panavas, T., Brown, J. M. & Johnson, K. K. Optimized Mitochondrial Targeting of Proteins Encoded by Modified mRNAs Rescues Cells Harboring Mutations in mtATP6. *Cell Rep.* **22**, 2818–2826 (2018).
32. Yu, H. *Next-generation sequencing of mitochondrial targeted AAV transfer of human ND4 in mice*. (2013).
33. Pillay, S. *et al.* An essential receptor for adeno-associated virus infection. *Nature* (2016). doi:10.1038/nature16465
34. Lux, K. *et al.* Green fluorescent protein-tagged adeno-associated virus particles allow the study of cytosolic and nuclear trafficking. *J. Virol.* **79**, 11776–87 (2005).
35. Münch, R. C. *et al.* Displaying high-affinity ligands on adeno-associated viral vectors enables tumor cell-specific and safe gene transfer. *Mol. Ther.* (2013). doi:10.1038/mt.2012.186
36. Dalkara, D. *et al.* In vivo-directed evolution of a new adeno-associated virus for therapeutic outer retinal gene delivery from the vitreous. *Sci. Transl. Med.* (2013).

doi:10.1126/scitranslmed.3005708
37. Lefevere, E. *et al.* Mitochondrial dysfunction underlying outer retinal diseases. *Mitochondrion* (2017). doi:10.1016/j.mito.2017.03.006
38. Toft-Kehler, A. K. *et al.* Mitochondrial function in Müller cells - Does it matter? *Mitochondrion* **36**, 43–51 (2017).
39. Stone, J., van Driel, D., Valter, K., Rees, S. & Provis, J. The locations of mitochondria in mammalian photoreceptors: Relation to retinal vasculature. *Brain Res.* **1189**, 58–69 (2008).
40. Chaffiol, A. *et al.* A New Promoter Allows Optogenetic Vision Restoration with Enhanced Sensitivity in Macaque Retina. *Mol. Ther.* **25**, 2546–2560 (2017).
41. Tuppen, H. A. L., Blakely, E. L., Turnbull, D. M. & Taylor, R. W. Mitochondrial DNA mutations and human disease. *Biochim. Biophys. Acta - Bioenerg.* **1797**, 113–128 (2010).
42. Moster, M. L. *et al.* rAAV2/2-ND4 for the Treatment of LHON: 72-week Data from the REVERSE Phase III Clinical Trial (Plen02.002). *Neurology* (2019).
43. Vahrenholz, C., Riemen, G., Pratje, E., Dujon, B. & Michaelis, G. Mitochondrial DNA of Chlamydomonas reinhardtii: the structure of the ends of the linear 15.8-kb genome suggests mechanisms for DNA replication. *Curr. Genet.* **24**, 241–7 (1993).
44. Denovan-Wright, E. M. & Lee, R. W. Comparative structure and genomic organization of the discontinuous mitochondrial ribosomal RNA genes of Chlamydomonas eugametos and Chlamydomonas reinhardtii. *J. Mol. Biol.* (1994). doi:10.1006/jmbi.1994.1505
45. Fan, J. & Lee, R. W. Mitochondrial Genome of the Colorless Green Alga Polytomella parva: Two Linear DNA Molecules with Homologous Inverted Repeat Termini. *Mol. Biol. Evol.* **19**, 999–1007 (2002).
46. Marc, P. *et al. Genome-wide analysis of mRNAs targeted to yeast mitochondria*. *EMBO reports* **3**, (2002).
47. Kaeppel, C. *et al.* A largely random AAV integration profile after LPLD gene therapy. *Nat. Med.* **19**, 889–891 (2013).
48. Yamada, Y., Ishikawa, T. & Harashima, H. Validation of the use of an artificial mitochondrial reporter DNA vector containing a Cytomegalovirus promoter for mitochondrial transgene expression. *Biomaterials* **136**, 56–66 (2017).
49. Lehmann, D. & McFarland, R. Overview of Approaches to Mitochondrial Disease Therapy. *J. Inborn Errors Metab. Screen.* **6**, 232640981775296 (2018).
50. Chin, R. M., Panavas, T., Brown, J. M. & Johnson, K. K. Optimized Mitochondrial Targeting of Proteins Encoded by Modified mRNAs Rescues Cells Harboring Mutations in mtATP6. *Cell Rep.* **22**, 2818–2826 (2018).
51. Yu, H. *et al. Mutant NADH dehydrogenase subunit 4 gene delivery to mitochondria by targeting sequence-modified adeno-associated virus induces visual loss and optic atrophy in mice*. (2012).
52. Yano, M., Terada, K. & Mori, M. AIP is a mitochondrial import mediator that binds to both import receptor Tom20 and preproteins. *J. Cell Biol.* **163**, 45–56 (2003).
53. Flannery, J. G. & Visel, M. Adeno-Associated Viral Vectors for Gene Therapy of Inherited Retinal Degenerations. in 351–369 (Humana Press, Totowa, NJ, 2012). doi:10.1007/978-1-62703-080-9_25

Chapter 6: Non-coding mutations: Elucidating the ocular structural changes and molecular mechanisms underlying 5'UTR mutations in a LCA9 mouse model of retinal degeneration

Abstract:

Recent advances in whole genome sequencing have highlighted the role of non-coding regions in genetic human diseases, thought until recently to be non-functional. However, we have yet to understand and characterize the complex pathways and mechanisms affected in patients possessing mutations in non-coding regions. In this study, we engineered and are characterizing the retinal phenotype of two novel mouse model of noncoding mutation, presenting mutation in the 5'untranslated region (UTR) of the NNMNAT1 gene. Using this model, we aimed at elucidating similar molecular mechanisms behind recently discovered noncoding missense mutations found in LCA9 patients suffering from severe and early onset retinal degeneration.

Introduction

Decades of genetics research have focused primarily upon a small fraction of DNA: the coding regions that are transcribed and later translated into functional proteins. However, recent advances in whole genome sequencing highlighted the role of non-coding regions, thought until recently to be non-functional. The human genome project[1,2] gave a novel dimension to human genetics. Genome wide association studies[3] critically linked disease phenotypes to non-coding variations, referred to as single-nucleotide polymorphisms in patients missing an inheritable causative mutation. Since then growing evidence[4,5] showed non-coding regions are involved in gene function and expression regulation and shed new light on how deciphering the underlying mechanisms is crucial for understanding inherited human diseases.

Inherited retinal diseases are a heterogeneous group of early-onset blindness, characterized in 95% of cases by the progressive dysfunction and death of retinal photoreceptor[6,7] and RPE cells. Mutations in more than 240 genes have been implicated in causing disease, with the overwhelming majority in coding regions. Despite great effort, the genetic cause of ~30% of cases of inherited retinal disease remains unknown. There is accumulating evidence for genetic defects in understudied non-coding regions, such as deep intronic regions[8] or untranslated regions (UTRs), which could explain the genetic basis of these idiopathic degenerations.

However, we have yet to understand and characterize the complex pathways and cell mechanisms affected in patients possessing mutations in non-coding regions. To address this gap, this study focuses on elucidating the molecular mechanisms underlying non-coding mutations recently found in a severe early onset case of Leber's Congenital Amaurosis (LCA) and understanding more broadly how UTRs affect gene regulation in diseases.

LCA[9] (MIM 204000) is the most severe childhood form of early onset retinal degeneration, resulting in profound and severe visual loss, with reduced or unrecordable electroretinogram (ERG) in the first year of life. LCA is genetically and clinically heterogeneous, with 19 genes

explaining 70% of the cases. A recently discovered LCA gene, NMNAT1[10], encodes a rate-limiting enzyme involved in nicotinamide adenine dinucleotide (NAD+) biosynthesis but also was shown to have essential roles in cell signaling, DNA repair, gene regulation, and apoptosis among others[11–13]. Until recently, only biallelic missense mutations[14,15] were reported, with the vast majority occurring in exon 5 (58%), until a screening in unrelated families presenting typical NMNAT1 associated phenotypes revealed a novel and "hidden" genetic defect in the NMNAT1 non-coding region. De Baere *et al.* described two novel 5'UTR mutations[16] at positions c.-70A>T and c.-69C>T. The research group hypothesized that these point mutations result in an alteration of retinal-specific transcription factor binding sites, as the disease phenotype has only been limited to the retina. The molecular mechanisms behind these novel mutations remain to be elucidated and would greatly benefit from animal models that can closely mimic the human disease. However, the lack of genetic homology across cis-regulatory sequences of different mammalian species challenges the development of mouse or other models to study human diseases.

In this study, we identified and investigated the effect of mutating human conserved nucleotides in the mouse *NMNAT1* 5'UTR. We further evaluated genome editing tools to engineer mouse models of NMNAT1 non-coding mutations to elucidate the underlying molecular mechanisms and role of specific 5'UTR regions in regulating gene expression.

Results

Human and mouse 5'UTRs share region homology

We first found that although different, the human and mouse *NMNAT1* 5'UTR sequences share some sequence homology with a total of 121 nucleotide matches (**Fig 1**).
Nucleotides c.-70A and c.-69C found in the human 5'UTR sequence, and mutated in NMNAT1 patients, are predicted to be conserved in the wild-type mouse sequence.

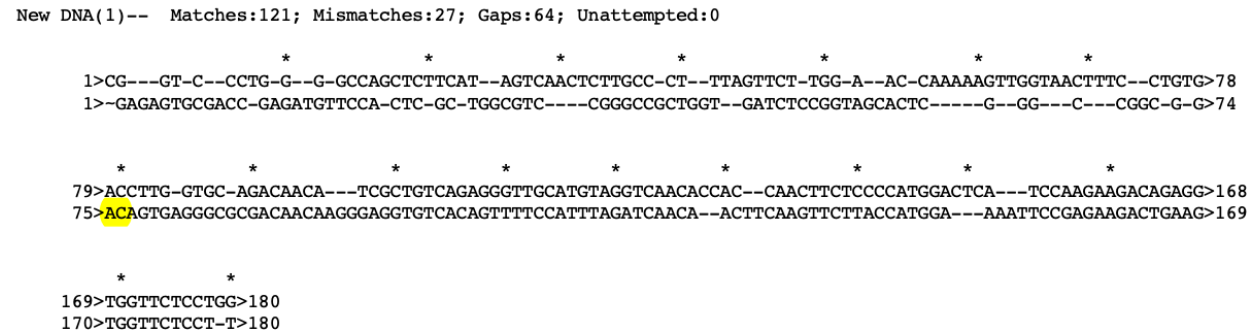

Figure 1: Portion of NMNAT1 5'UTR sequence is conserved from human to mouse
Sequence alignment between mouse (top) and human (bottom) sequence. 5'UTR nucleotides c.-70A and c.-69, mutated in LCA9 patients are highlighted in yellow.

Targeted mutation of human and mouse 5'UTRs decrease gene expression of transgene

We next investigated whether mutating these conserved nucleotides could impact gene expression in a similar fashion as observed in the 5'UTR of LCA9 patients. The non-coding 5'UTR region has previously been shown to regulate gene expression using different functional elements, such as alternative initiation start (uAUG) or binding sites for RNA, as well as folding properties.

We first observed the effect of these mutations on transcription, performing a dual luciferase assay. We cloned both the human and mouse full 5'UTR DNA sequence downstream of the CMV and SV40 promoters driving expression of the firefly luciferase (fLuc). HEK293T and C2C12 cells were transfected with either the wild-type or mutated 5'UTR-fLuc construct (**Fig 2.A,B**). Similar to results found for the c.-69C>T and c.70A>T mutations in the human 5'UTR (**Fig 2.C),** mutating mouse parental c.-65A>T led to strong luminescence decrease. Interestingly, we did not observe a significant expression decrease when expression construct containing the 5'UTR c.>-64C>T mouse mutation, although in patient, the -69C>T[16] mutation led to the most severe retinal degeneration.

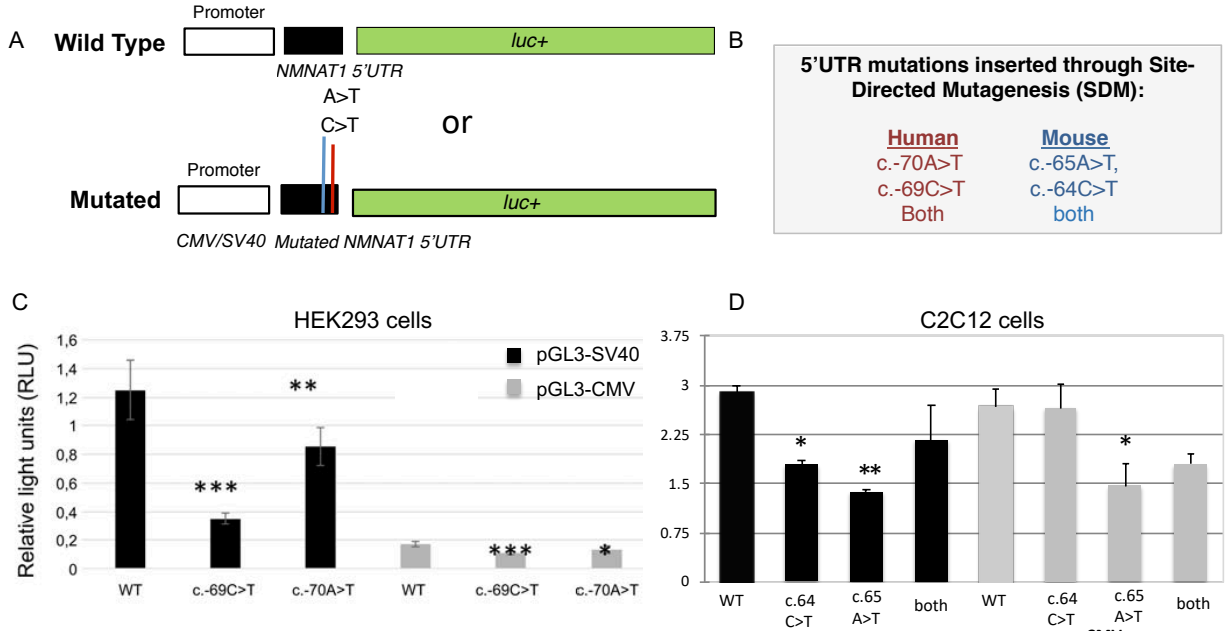

Figure 2: Point mutations in human and mouse 5'UTRs decrease gene expression in dual luciferase reporter assay. Plasmids were constructed to contain an SV40 or CMV promoter, followed by either the mouse or human *NMNAT1* 5'UTR to express Firefly luciferase. Control plasmid encoding for Renilla luciferase under the control of SV40 promoter was used (**A**). List of mutations introduced through site-directed mutagenesis (**B**). Relative light units were quantified by the ratio of Firefly over Renilla luciferase luminescence measurements. Assays were performed in human HEK293T (**C**) and mouse C2C12 (**D**) cell lines (when testing effect of *NMNAT1* human and mouse 5'UTR mutations, respectively). Student T-test was performed to assess statistical significance. Error bars are mean ±SD. *** = P<0.001, **= P<0.01, * = P<0.05.

Transcription factor binding site motif analysis reveals different transcriptional factor profiles between the mouse and human 5'UTRs.

Mutations of adjacent nucleotides (c.-70, c.-69 and unpublished data) in the human NMNAT1 5'UTR were detected in unrelated LCA9 families. Therefore, a strong possible explanation for reduced expression has been the disruption of a retinal specific transcription factor. We therefore compared the transcription factor binding site (TFBS) motifs found in the human and mouse 5'UTR NMNAT1 regions (**Supplemental S2**) and changes underlying point mutations of interest.

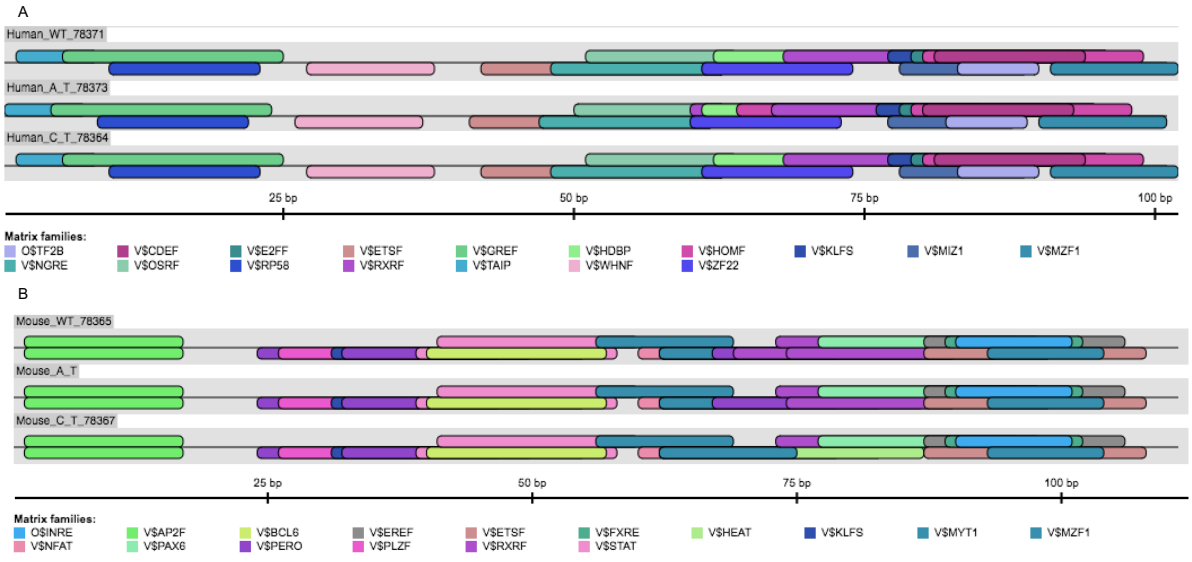

C

Matrix Fam.	Description	p	WT	c.-70A>T	c.-69C>T
O$TF2B	RNA polymerase II transcription factor II B	0.002	1	1	1
V$CDEF	Cell cycle regulators: Cell cycle dependent element	0.006	1	1	1
V$E2FF	E2F-myc activator/cell cycle regulator	0.091	1	1	1
V$ETSF	Human and murine ETS1 factors	0.007	1	1	1
V$GREF	Glucocorticoid responsive and related elements	0.089	1	1	1
V$HDBP	Huntington's disease gene regulatory region binding pr	0.006	1	1	1
V$HOMF	**Homeodomain transcription factors**	0.023	1	1	2
V$KLFS	Krueppel like transcription factors	0.028	1	1	1
V$MIZ1	Myc-interacting Zn finger protein 1	0.028	1	1	1
V$MZF1	Myeloid zinc finger 1 factors	0.105	1	1	1
V$NGRE	Negative" glucocoticoid response elements	0.065	1	1	1
V$OSRF	Odd-skipped related factors	0.017	1	1	1
V$RP58	RP58 (ZFP238) zinc finger protein	0.026	1	1	1
V$RXRF	**RXR heterodimer binding sites**	0.012	1	1	2
V$TAIP	TGF-beta induced apoptosis proteins	0.071	1	1	1
V$WHNF	Winged helix binding sites	0.021	1	1	1
V$ZF22	C2H2 zinc finger transcription factors 22	0.003	1	1	1

D

Matrix Fam.	Description	p	WT	c.-65A>T	c.-64C>T
O$INRE	Core promoter initiator elements	0.084	1	1	1
V$AP2F	Activator protein 2	0.087	2	2	2
V$BCL6	POZ domain zinc finger expressed in B-Cells	0.105	1	1	1
V$EREF	Estrogen response element	0.050	1	1	1
V$ETSF	Human and murine ETS1 factors	0.007	2	2	2
V$FXRE	Farnesoid X - activated receptor response elements	0.019	1	1	1
V$HEAT	Heat shock factors	0.052	1	1	1
V$KLFS	Krueppel like transcription factors	0.028	1	1	1
V$MYT1	MYT1 C2HC zinc finger protein	0.081	2	2	2
V$MZF1	Myeloid zinc finger 1 factors	0.105	1	1	1
V$NFAT	Nuclear factor of activated T-cells	0.083	1	1	1
V$PAX6	PAX-4/PAX-6 paired domain binding sites	0.063	1	1	1
V$PERO	**Peroxisome proliferator-activated receptor**	0.103	3	3	2
V$PLZF	C2H2 zinc finger protein PLZF	0.097	1	1	1
V$RXRF	**RXR heterodimer binding sites**	0.012	3	2	1
V$STAT	Signal transducer and activator of transcription	0.050	2	2	2

Figure 3: Transcriptional analysis of the effect of human and mouse 5'UTR non-coding mutations on predicted transcription factor binding site motifs.
Graphic representation and table comparing transcription factor matrix families found in WT or mutated human (**A,C**) and mouse **(B,D)** exon 1 of the *NMNAT1* 5'UTR.

Interestingly, c.-70A>T and c.-69A>C point mutations in the human 5'UTR completely removed the probability of binding site motif presence for the Histone H4 nuclear transcription factor. On the other hand, the c.-69C>T mutation increased the presence of retinoid acid X receptor (RXR) and homeodomain transcription factor binding sites (**Fig 3.A,C**).

Oppositely, mouse homologous mutations c.-65A>T and c.65C>T were deleterious for the presence of the RXR heterodimer binding sites (**Fig 3.B,D**). Retinoid acid (RA) has been suggested to play an important role in vertebrate embryonic development and cell differentiation. RXR TFBS motif alteration could potentially explain LCA9-associated unproper retinal cell differentiation during development.

5'UTR point mutations alter RNA folding conformation

Non-coding RNA secondary structure regulates gene expression[17]. More is known of the coding/messenger mRNA importance in localization and stabilization of the RNA molecule. More evidence points toward the functional role (e.g., inhibiting translation) of RNA folding as well. In silico calculated thermodynamic stability refers to the stability of the RNA.

Human 5'UTR RNA is more stable than the mouse (-50 kcal/mol vs ~-30 kcal/mol, respectively). Human c.-70A> T drastically alters RNA folding conformation (**Fig.4 B,C)** without modifying native stability (-50.61 kcal/mol compared to WT -50.61 kcal/mol value). Interestingly, a similar finding was found with the homologous c.-65A>T mutation (**Fig.4 A,C).**

While in silico models are helpful with predicting 5'UTR-mediated inhibition of translation, within the cell, RNA secondary structure can entirely differ from predicted through interaction with RNA-binding proteins.

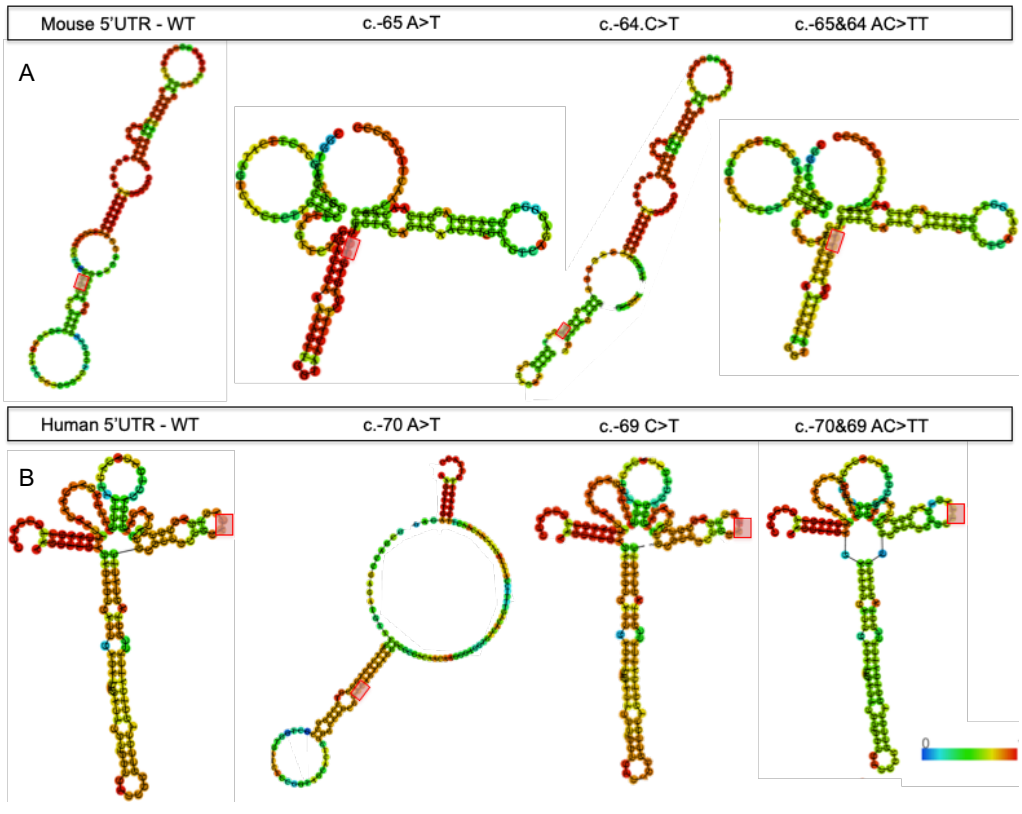

C

	Human				Mouse			
Variants	**WT UTR**	**AC>TC**	**AC>AT**	**AC>TT**	**WT UTR**	**AC>TC**	**AC>AT**	**AC>TT**
MFE structure frequency (%)	0.33%	0.38%	0.33%	0.26%	0.40%	0.49%	0.72%	0.37%
Thermodynamic free energy (kcal/mol)	-50.63	-52.13	-50.61	-50.78	-36.61	-37.68	-34.74	-34.95
Ensemble diversity	32.54	29.72	31.06	44.51	29.72	35.05	31.9	40.4

Figure 4: Effect of 5'UTR point mutations on RNA stability and folding
Graphic representation of RNA conformation of WT and mutated 5'UTRs of mouse (A) and human (B) *NMNAT1* gene. Heat scale represents the base pair probability of the structural ensemble, with red indicating likely and blue unlikely. Table (**C**) recapitulates the minimum free energy (MFE) structure frequency, the thermodynamic equilibrium of RNA (free energy in kcal/mol) as well as ensemble diversity.

A

Pos. #	Strand	Sequence	PAM	Specificity Score (%)	Efficiency Score (%)
26	+	GACCGAGATGTTCCACTCGC	TGG	94.3	51.05
33	+	ATGTTCCACTCGCTGGCGTC	CGG	88.4	40.31
46	-	GTGCTACCGGAGATCACCAG	CGG	71.6	81.20
62	+	GGTGATCTCCGGTAGCACTC	CGG	59.4	91.10
100	+	GGCGCGGTAAGCTCCCCGCA	AGG	82.4	60.95
102	-	TTTCTCAGGGGCTCCTTGCG	GGG	68.4	53.07
114	-	AAAAGCGACCAGTTTCTCAG	GGG	62.8	73.36

B

Pos. #	Strand	Sequence	PAM	Specificity Score (%)	Efficiency Score (%)
199	-	ACTATGAAGAGCTGGCCCCA	GGG	55.5	69.54
207	-	AAGAGTTGACTATGAAGAGC	TGG	56.1	52.93
248	+	AGTTCTTGGAACCAAAAAGT	TGG	50.1	56.80
274	-	GGGGGAACTGACCTGCACCA	AGG	72.8	73.30
292	+	GCAGGTCAGTTCCCCCACTT	GGG	56.4	74.5
293	+	CAGGTCAGTTCCCCCACTTG	GGG	74.5	56.36
296	+	GTCAGTTCCCCCACTTGGGG	TGG	76.0	50.65

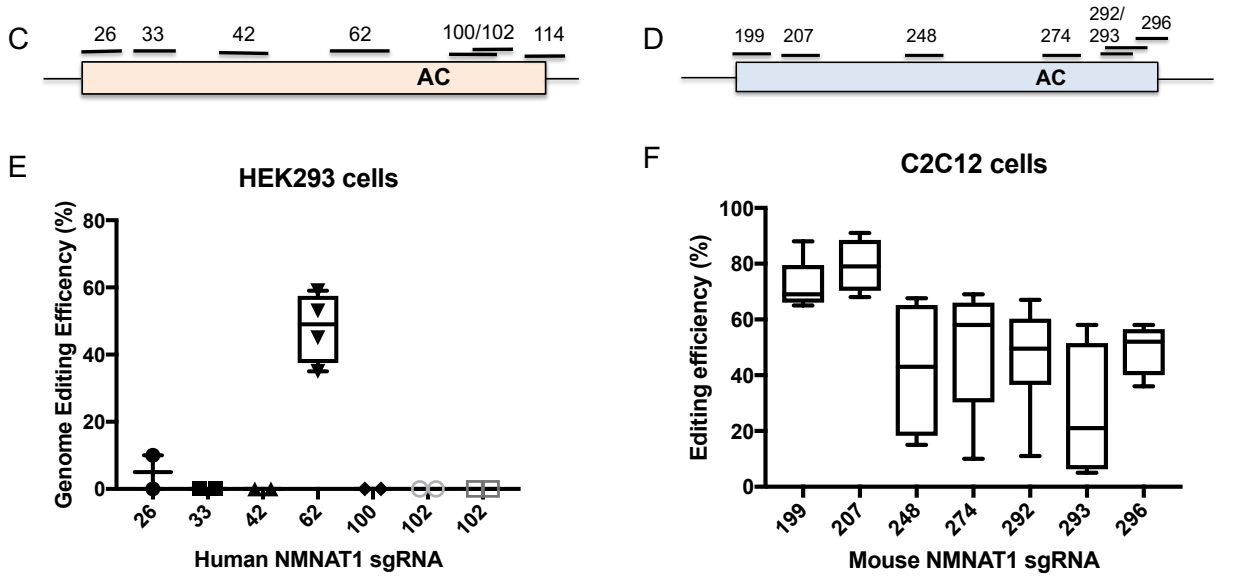

Figure 5: Cas9 sgRNA guide selection *in vitro*
Table with guide number, targeting sequence against human (**A**) or mouse (**B**) 5'UTRs and proto-adjacent motif (PAM). sgRNA nucleotide target for human **(C)** and mouse (**D**) 5'UTRs. Specificity and efficiency score, with high % accounting for low off-target and high editing levels, respectively. Editing efficiency of sgRNA against human 5'UTR (**E**) was lower than against the mouse 5'UTR (**F**) in HEK293T and C2C12 cells, respectively, harvested 72 hours after transfection with sgRNA-X + Cas9.

We moved to building genome editing tools to edit *in vivo* the human and mouse 5'UTRs, for further characterization of the retinal phenotype resulting from NMNAT1 5'UTR mutations. We tested 7 sgRNA against diverse locations of the exon 1 of the 5'UTR and compared efficiency in the human and mouse regulatory sequence. We found that only one guide, #62, led to consistent editing efficiency >40% in the human sequence, close to the c.-69 and c.-70 nucleotides **(Fig 5.A,C,E).** Although all the other sgRNA sequences were predicted to lead to 60-100% editing efficiency, no editing was detectable with the T7 endo assay.

On the other hand, all mouse 5'UTR sgRNAs led to editing, with different efficiency. sgRNA targeting 5' of exon 1 triggered the highest level of editing (~70-90%) while sgRNA targeting sequences closer to the 3' and conserved AC site (**Fig 5.B,D,F**), showed more variability.

Engineering LCA9 mouse model of a 5'UTR non-coding mutation

We designed two different strategies to study the role of the 5'UTR exon 1 on regulating *NMNAT1* gene expression. First, we used 2 sgRNAs at the 5' and 3' end of exon 1 to delete the majority of the exon (**Fig 6.A).** For the second strategy, we intended to more precisely edit the exon by inserting the human homologous c.-65A>T and 64C>T mouse mutations, inducing one double stranded break with sgRNA 274-Cas9, and supplying a donor DNA with mutations of interested flanked by homology arms to trigger recombination (**Fig. 6B**).

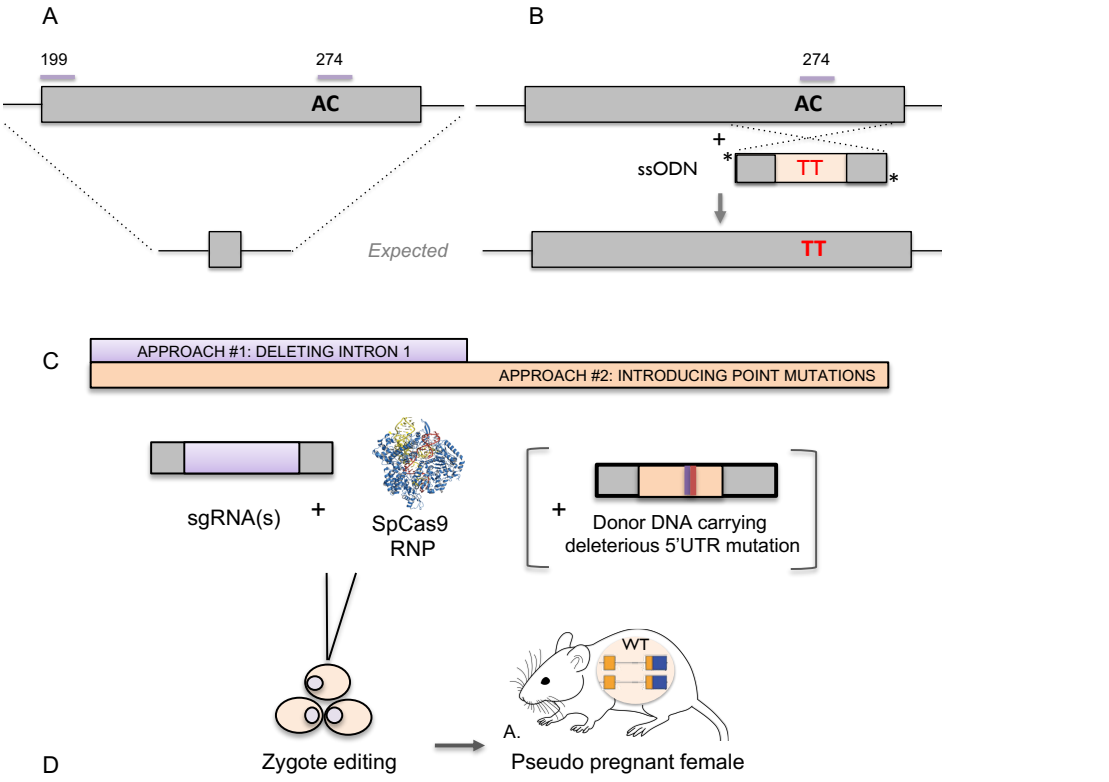

Figure 6: Editing strategies to study effect of non-coding mutations and truncation in mouse 5'UTR. Schematic representation of two different editing approaches to study the effect of mutations in mouse 5'UTR: SgRNA #199 and 274 (**A**) injected along Cas9RNP used to excise exon 1. sgRNA #274 -Cas9 (**B**) supplied with a donor DNA with the nucleotides of interest mutated (ssODN) and injected into zygotes (**D**), culture and inserted back into pseudopregnant mice (**D**).

While we measured high levels of editing *in vitro, in vivo* editing happened at lower efficiency with 15% and ~20% of mice edited for the first (2sgRNAs) and second (1sgRNA + ssODN) approaches, respectively. Interestingly, no mice presented the full exon 1, while many mice showed evidence of editing on the 5' and 3' end of the exon were found (**Fig 6.D**). One mouse was bi-allelic heterozygous for editing in the 5' and 3' end, respectively. For the precise editing, donor DNA insertion was observed a few nucleotides away from the c.-65A and c.-64C site. Although ssODN arms contained homology on each side of the nucleotides of interest, the recombination happened downstream of the intended location.

As we were interested in creating a mouse model that would mimic the human phenotype and underlying molecular mechanism behind the non-coding mutations the closest, we selected mouse #77 and #64 to study effect of 3' truncation.

Exon 1 mutation decreased NMNAT1 gene expression in the retina and triggers degeneration

RNA was extracted from heterozygous and homozygous #64 and #77 LCA9 retinas (n=4) at P60, as well as C57BL/6J retina. We generated cDNA to assess the level of expression of NMNAT1 versus rhodopsin, as a marker of degeneration. Overall a significant difference in NMNAT1 gene expression was not yet observed, although both homozygous #64 and #77 mice showed a slight decrease compared to heterozygous and WT controls **(Fig 7.A)**. Only homozygous #64 retinas displayed decreased expression in rhodopsin, which could signal early rod degeneration. We confirmed these results with retinal histology.

We sectioned fixed retinas from P60 #64hom, #77hom and WT mice and stained against rhodopsin (RHO) and cone arrestin (CAR). Preliminary results showed no difference in the CAR staining, however, a decrease in the RHO staining was observed, more noticeable in the #64 homozygous mice, although thickness of the outer nuclear layer didn't seem compromised.

Interestingly, decrease in the ONL and INL nuclei density was observed consistently in the #64 homozygous retinas, but not in the other retinal sections **(Fig 6.B).** Electroretinogram recording confirmed progressive degeneration in both models. Scotopic B-wave amplitudes started decreasing significantly after 3 (583 ± 110µV, p=0.0339) months in $NMNAT1^{64/64}$ mice, while cone-mediated amplitudes were recorded at similar levels in WT mice. Photopic B-wave amplitudes only decreased significantly in 5-month old $NMNAT1^{64/64}$ mice (125 ± 131µV, $p<0.001$) compare to wild type mice (200.68 ± 16.5µV, **Fig 6.C**)**.** Decrease in light sensitivity was observed at later stage in the $NMNAT1^{77/77}$ mouse model. Significant difference in scotopic B-wave amplitude compared to WT mice, was recorded at 4-month old (520.760 ± 62.9µV vs. 730.6 ± 53.5µV, $p<0.0015$). No significant decrease in photopic light response was detected.

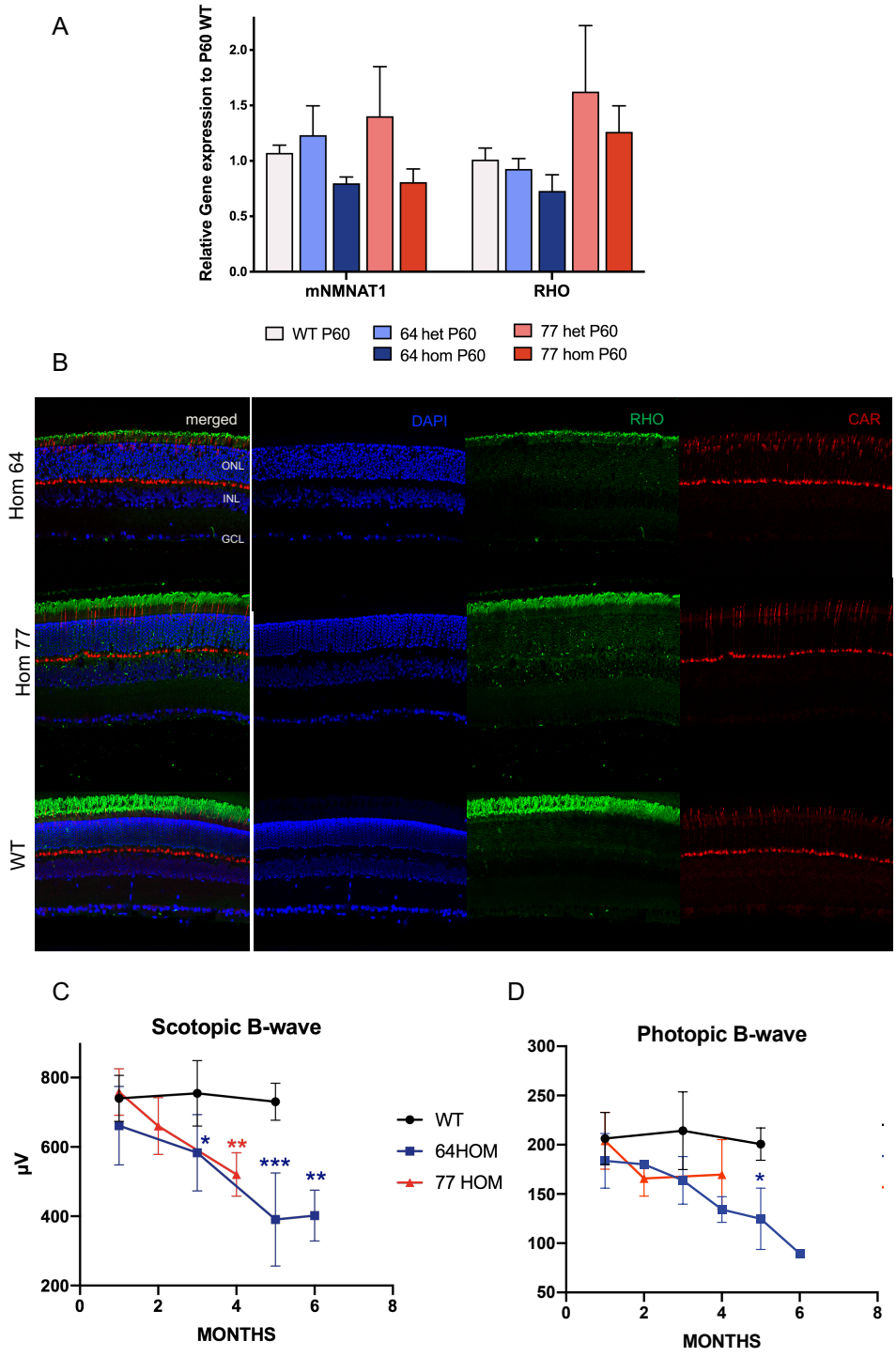

Figure 6: Non-coding LCA9 mouse models display progressive retinal degeneration
RT-qPCR analysis (**A**) from RNA extracted from wildtype and LCA9 homozygous and heterozygous retinas at P60 (normalized to GAPDH). (**B**) Retinas collected from P60 mice and labeled with anti-rhodopsin (1:1000) and cone arrestin (1:5000) antibodies showed reduce labeling of rhodopsin in outer segments with no apparent structural difference in cone photoreceptors compared to control C57BL/6J eyes. ERGs recorded from 1- to 6-month postnatal in LCA9 (n=5 mice per group) showed progressive decreases in scotopic B-wave amplitudes compared to WT (**C**) while maintaining normal photopic response (**D**). Error bars are mean ± SD. *** = P<0.001, * = P<0.05.

Discussion

Identifying the genetic cause of inherited diseases is essential to provide gene therapies to patients, as shown by the RPE65 gene therapy success with the recent commercialization of Luxterna for patients diagnosed with LCA2. However, challenges still remain as 30% of these diseases still remain idiopathic, leaving patients carrying the unidentified mutation with no treatment options. Until now, clinical genomics have focused on protein-coding gene mutations. However, advances in next-generation sequencing combined with rise of novel genome-editing technologies[18–20] enabling precise editing of the genome are unlocking novel horizons for the non-coding gene therapy landscape. Editas is leading the way, currently developing a CRISPR/Cas9-mediated gene editing therapy for CEP290 (LCA9)[21]. It is one of the rare diseases for which a non-coding mutation occurs the most in patients (15% of congenital blindness in Europe). A point mutation within intron 26 of the CEP290 gene creates a novel splice donor site and premature stop codon in the mRNA sequence, abolishing its protein translation. However, unlike the intronic CEP290 mutation, very little is still known about molecular mechanisms underlying novel non-coding mutations like the 5'UTR NMNAT1 point mutations. Moreover, while we are now able to link SNPs to disease phenotypes with GWAS studies, we are still missing the molecular tools, such as relevant animal models, to investigate cell mechanisms *in vivo*.

Here, we report the first mouse models of retinal degeneration carrying a non-coding mutation. In the first part of the study, we identified homologous nucleotides to the one mutated in LCA9 patients in the mouse 5'UTR sequences. Mutation of these nucleotides similarly disrupt the RNA secondary structure of the 5'UTR in both species, while transcription factor analysis revealed different TFBS profile. Interestingly, both mutations seemed to affect retinoid acid X receptor TFBS family, which could explain the retinal specific phenotype of the NMNAT1 mutation. We engineered two different mouse models, #77 mice with a small 3bp deletion at the 3'end of the exon 1 of the 5'UTR and #64 mice which present a longer truncation of the 3' exon 1 spreading to the first initial base-pairs of the neighboring intron. Both models showed a decrease in NMNAT1 gene expression at P60, although protein levels and enzyme activity will need to be evaluated. Tho]ese results are in line with the phenotype observed with coding and non-coding mutations.

Phenotype variability has been observed in the severity of the degeneration with NMNAT1 mouse model of coding mutations. NMNAT1$^{V9M/V9M}$ mice have the most severe rod-cone dystrophy phenotype while mice carrying homozygous D243G mutation had a more delayed retinal degeneration[22]. NMNAT1$^{E257K/E257}$ mice have low phenotype penetrance and display slow retinal degeneration when bred with NMNAT1$^{+/-}$ mice[14]. NMNAT1$^{64/64}$ and NMNATdel$^{77/77}$ showed signs of degeneration at P60 days, and preliminary results show progressive loss of scotopic B-wave ERG. These results suggest that the severity of the degeneration is linked to the decrease level of NMNAT1, as earlier mutations in the gene seemed to lead to the most severe phenotype. NMNAT1$^{-/-}$ mice showed that *NMNAT1* protein is essential during development as abolishing gene expression is embryonic lethal[23].

Further studies to identify and characterize the molecular mechanism behind the loss of NMNAT1 gene expression are needed, but these two non-coding LCA9 mouse models are promising tools to pioneer a novel class of gene therapies. Moreover, our *in silico* comparison of 5'UTR function in different mammalian species (human versus mouse) could be applied to larger animal models (i.e. pig, primate), who would be more physiologically more relevant as LCA9 is characterized by macular degeneration, and mice do not possess a macula. However, these small

animal models enable pre-clinical studies to test both NMNAT1 gene expression and gene editing approaches to correct non-coding mutations and will help uncover the complex molecular pathogenesis of NMNAT1-associated LCA by being, to our knowledge, the first animal model of retinal dystrophy caused by a non-coding region mutation. This study brings to light the importance of exploring non-coding regions in genetic disease.

Materials and Methods

Dual luciferase gene expression assay

Different luciferase constructs containing either the human or mouse 5'UTRs of the NMNAT1 gene upstream of the dual luciferase coding region. Expression was driven by NMNAT1 promoter vector (pGL3-NMN), a truncated CMV (pGL3-CMV) and SV40 (pGL3-SV40) promoter promoters.
pGL3-hNMNAT1/ pGL3-SV40 (SV40) plasmid containing the human 5'UTR were provided by the group(ref).
Mouse 5'UTR was amplified from mouse retina DNA, poly a-tailed and ligated into a TOPO vector for sequence verification, before being cloned in pGL3-SV40/CMV-luciferase plasmids.

SMD m5UTR a329t_c330t_antisense	cgatgttgtctgcaccaagaacacaggaaagttaccaact
SDM m5UTR a329t_c330t_	agttggtaactttcctgtgttcttggtgcagacaacatcg
SMD m5UTR a329t_antisense	tgttgtctgcaccaaggacacaggaaagttaccaa
SMD m5UTR a329t_	ttggtaactttcctgtgtccttggtgcagacaaca
SMD m5UTR c330t_antisense	gatgttgtctgcaccaagatcacaggaaagttaccaa
SMD m5UTR c330t_	ttggtaactttcctgtgatcttggtgcagacaacatc

HEK293T and C2C12 cells were grown in DMEM-F12 medium supplemented with 10% FBS and 2mM of glutamine. ~10,000 cells per well were seeded in a 96-well plate 24 hours prior t o transfection. Each well was transfected with 100ng of 5'UTR-Firefly luciferase and transfection control (SV40-Renilla luciferase) plasmids. Forty-eight hours after transfection, cells were rinsed with PBS and incubated for 15 minutes at room temperature after adding 20uL of Lysis buffer (Promega kit). We measured Firefly and Renilla luciferase activities using the Dual-Luciferase Reporter Assay System (Promega). Ratio of Firefly and Renilla luciferase activity are reported as relative light units. Each value is the mean of five independent transfection.

SgRNA guide and ssODN construction

Seven gRNA sequences targeting 5'UTR regions of the human and mouse NMNAT1 (Fig 1.A-B) gene, respectively, were designed using Benchling CRISPR analysis software (https://benchling.com). Complementary oligonucleotide primers to each of the 20 nucleotide sgRNAs sequences were synthetized (IDT) with flanking BsmBI restriction sites. Matching primers were then annealed and digested with BsmBI enzyme (NEB), and ligated with T7 ligase into pX330 Addgene plasmid (#42230), containing spCas9 nuclease sequence.

Single stranded oligonucleotide donor DNA was ordered on IDT as ultramer: C*T*T*TAG TTC TTG GAA CCA AAA AGT TGG TAA CTT TCC TGT G**TT AA**T GGT GCA GGT CAG TTC CCC CAC TTG GGG TGG CCT GGA*T*T*C
Phosphorothiate (*) bonds to improve ssODN resistance to nuclease degradation, was added on the 5' and 3' ends. 3'end was phosphorylated.

T7 endo assay for cleavage efficiency

Genomic DNA (gDNA) was extracted with the DNeasy extraction kit (Qiagen) according to manufacturer's instructions. The mouse and human 5'UTR target sequences (~900-1000bp) were PCR-amplified from 100 ng of gDNA per sample with the Q5 NEB (x) DNA Polymerase. For human 5'UTR, forward 5'-TTGAGGAAAATCCCCGCATCCGGA-3' and reverse 5'-CATGAGTGTCAAACCACCTCCAGC-3' primers were used. Forward 5'-ACAGACGAACTCCAAGCTCC-3' and reverse 5'-AAAGGGCAGAACCAGAGAATAGG-3' primers were used to amplify target sequence from mouse samples.

Resulting PCR products were run on a 2% gel and DNA bands were gel extracted and purified. Two sets of 200 ng per sample of clean DNA were denatured at 95 °C for 10 min and re-annealed at −2 °C per second temperature ramp to 85 °C, followed by a −1 °C per second ramp to 25 °C to allow for random double stranded annealing. The heterocomplexed PCR products were then incubated with 5 U T7E1 enzyme (New England Bio Labs) at 37 °C for 20 min. Products from mismatch assays were both run on a 2% gel to visualize cleavage or DNA cleaned up and submitted to a Fragment Analysis Service. Editing efficiency was calculated as the following:

$$\% \text{ cleavage} = \frac{\text{molecular conc. of cuts products}}{\text{molecular conc. of cut products + uncut band}}$$

Editing efficiency percentages were averaged from 4-5 separate transfections for each sgRNA.

Mouse Tail Snip Genotyping

Mouse tails snips were collected at postnatal 21 days and placed in a mix of 180uL of ATL buffer and 20uL of Proteinase K (DNeasy extraction kit, Qiagen). Samples were then incubated at 56ºC overnight or for 3-4 hours. Genomic DNA was extracted according to manufacturer's protocol. Mouse NMNAT1 5'UTR target region was amplified from 100 ng of gDNA sample using following T7 Q5 Forward 5'-ACAGACGAACTCCAAGCTCC-3' and T7 Q5 R- 5'-AAAGGGCAGAACCAGAGAATAGG-3' primers with GXL Prime Star Polymerase (Takara). Purified DNA band from 2% gel was then submitted to Sanger sequencing with m5UTR Sv+ 5'-GGTAAGCAACCACCGAGGT-3' primer. Absorbance read was analyzed to detect biallelic or heterozygous mutations.

Delivery of Cas9 mRNA and sgRNA to Mouse Zygotes by Microinjection

The Gene Targeting Core Facility (University of California at Berkeley) performed the microinjection experiments. Pronucleus embryos were pre-selected from collected superovulated embryos. Microinjection was performed in M2 media (Sigma, # M7176) under inverted microscope using micromanipulators. 100 ng/µl Cas9 mRNA (Life Technologies,#A25640) and 50 ng/µl *in vitro* transcribed sgRNAs were injected into pronucleus embryos by microinjection.

The embryos were then cultured at 5.0% CO_2, 37 °C overnight, and then transferred into post-coitum CD1 pseudopregnant mothers via oviduct transfer.

Animals

C57BL/6J (#000664) mice were obtained from the Jackson Laboratories. Transgenic mice #77 and #64 were engineered at UC Berkeley Gene Targeting core. Mice were maintained in a normal 12/12 light/dark cycle. All animal procedures were conducted according to the ARVO Statement for the Use of Animals in Ophthalmic and Vision Research, and the guidelines of the Office of Laboratory Animal Care and Use at the University of California, Berkeley, CA.

Electroretinogram (ERG) recording

Mice were transferred to a dark adaption room overnight before proceeding to a recording session. After anesthesia, eyes were dilated using both tropicamide and phenylephrine. Mice were placed on a 37°C heated pad during this preparation to maintain constant body temperature. Contact lenses were positioned on the cornea of both eyes. A reference electrode connected to a splitter was inserted into the forehead and a ground electrode was inserted in the tail. For scotopic conditions, electroretinograms were recorded (Espion E2 ERG system; Diagnosys LLC, Littleton, USA) in response to one light flash intensity of 1 log cd × s/m² on a dark background. Each stimulus was presented in series of three. For photopic ERGs, the animal was exposed to a rod saturating background for 5 minutes. Stimuli of 1.4 log cd × s/m² was presented 20 times on a lighted background. Data were visualized in MATLAB (v7.7; MathWorks). B-waves values were calculated and compared using a student t-test.

Agarose sections:

The animals were euthanized by CO_2 asphyxiation and cervical dislocation and the eyes were enucleated and immersion fixed in 10% formalin (in phosphate buffer, Ted Pella, Redding, USA). The cornea and lens were removed, and the retina was isolated and again conserved in 10% formalin. The retinas were embedded in an agarose block by pouring 5% melted agarose into a small weight boat. The tissues were then transferred from PBS to liquid agarose. After the agarose blocks had cooled, the retina was sectioned (Leica VT1000 S, Leica Microsystems, Nussloch, Germany) into 150-210 μm thick sections. The results were imaged by confocal microscopy LSM710. (Carl Zeiss Microimaging, Peabody, MA).

mRNA gene expression analysis

RNA was extracted from either cultured cells or retinal tissue using the RNeasy Mini Qiagen kit and eluted in 30 μl of DEPC-treated water. During extraction, RNA was treated with DNAse. The resulting RNA was store at -80ºC until used. cDNA was synthetized from RNA primed with random primers, using the Superscript III first-strand synthesis system (ThermoFisher, #18080044). qRT-PCR samples were run in triplicate using a collection of primers

and a housekeeping gene glyceraldehyde-3-phosphate dehydrogenase (GAPDH). The relative standard curve method was used to calculate fold differences in mRNA expression normalized to control conditions.

RT-PCR Primer sequences:

Rhodopsin F	5'-CAA GAA TCC ACT GGG AGA TGA-3'
Rhodopsin R	5'-GTG TGT GGG GAC AGG AGA CT-3'
mNMNAT1 F	5'-TACGAGTCCGATGTGCTGTG-3'
mNMNAT1 R	5'-CCTTCGCTCTCCGTGTTGTA-3'

Immunohistochemical analysis, confocal microscopy, and cell counting

Retinal agarose sections were blocked for at least 1 hour at room temperature in blocking buffer (10% normal goat serum, 1% FBS, 0.5% Triton-X 100) before antibody labelling overnight. The antibodies used were: mouse anti-RHO (Abcam 4D2, 1:1000), rabbit anti-CAR (Millipore, 1:5000) and rabbit anti-NMNAT1 (Bethyl, 1:1000), Alexa Fluor 594, 488 goat anti-rabbit (Invitrogen, 1:2000) as well as 488 goat anti-mouse (1:2000). Images were taken on a Zeiss LSM 710 laser scanning confocal microscope (NIH Grant 1S10RR026866-01).

Transcription factor binding site analysis

Wild-type and mutated 5'UTR sequences were analyzed for putative transcription factor binding sites using Mat Inspector software version 8.1, Matrix Library 9.1 from the Genomatix suite v3.4. Parameters for binding sites were set at matrix similarity and core similarity of 0.9.

Supplemental Materials

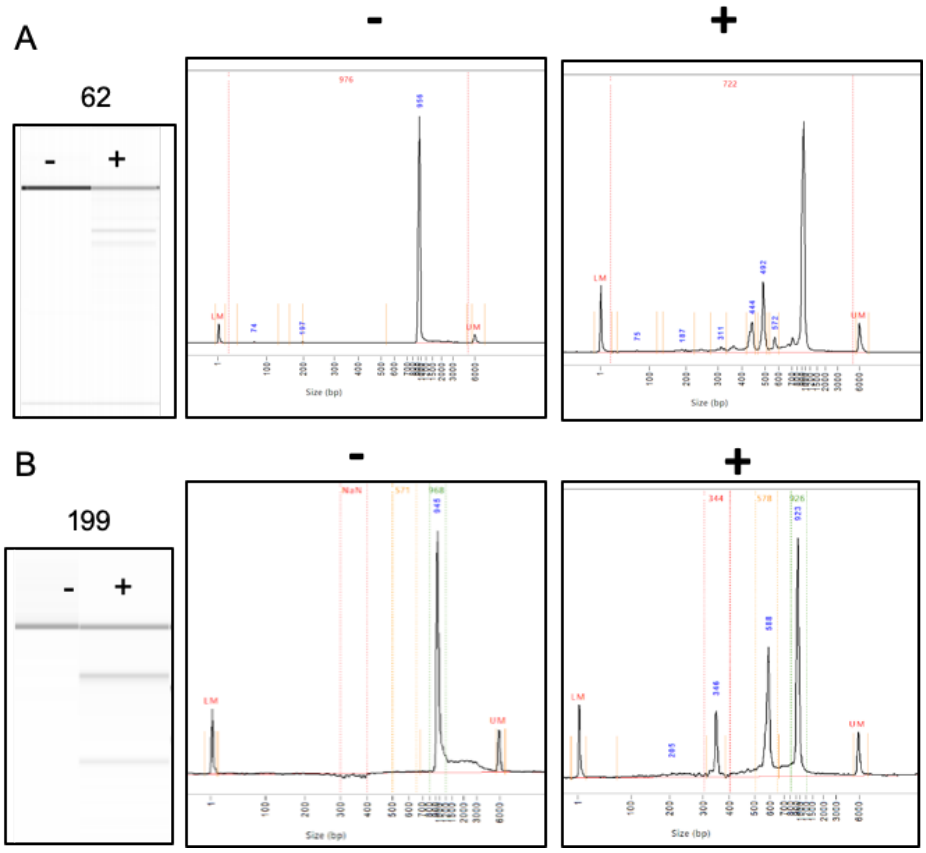

Figure S1: Representative results of from a fragment analyzer system.
gDNA from HEK293T or C2C12 cells transfected with sgRNA#62-Cas9 (**A**) or sgRNA#199 (**B**)-Cas9 targeting the human and mouse NMNAT1 5'UTR, respectively.

	Matrix Family	Detailed Family Information	Detailed Matrix Information	Anchor pos.	Matrix sim.	Sequence
Human	V$WHNF	Winged helix binding sites	Winged helix protein, involved in hair keratinization and thymus epithelium differentiation	17	0.956	cggACGCcagc
	V$NRSF	Neuron-restrictive silencer factor	Neural-restrictive-silencer-element	25	0.72	cggagatcaccagcggccCGGAcgc
	V$PAX5	PAX-2/5/8 binding sites	B-cell-specific activator protein	29	0.737	taccggagatcaccAGCGgcccggac
	V$ETSF	Human and murine ETS1 factors	Ets variant 4	37	0.896	gtgctacCGGAgatcaccagc
	V$NGRE	"Negative" glucocoticoid response elements	Repressive binding sites for glucocorticoid receptor (IR1)	40	0.858	gtgctaccGGAGatc
	V$OSRF	Odd-skipped related factors	Odd-skipped related 2	42	0.898	ctccgGTAGcact
	V$HDBP	Huntington's disease gene regulatory region binding proteins	Huntington's disease gene regulatory region-binding protein 1 and 2 (SLC2A4 regulator and papillomavirus binding factor)	56	0.846	ctcgggCCGGcggacagtg
	V$HNFP	Histone nuclear factor P	Histone H4 transcription factor, MIZF, dimeric binding	64	0.775	ggCGGAcagtgagggcgcg
	V$RXRF	RXR heterodimer binding sites	VDR/RXR Vitamin D receptor RXR heterodimer, DR3	65	0.873	ccggcggacagtGAGGgcgcggtaa
	V$MIZ1	Myc-interacting Zn finger protein 1	Myc-interacting Zn finger protein 1, zinc finger and BTB domain containing 17 (ZBTB17)	68	0.965	cgcgcCCTCac
	O$TF2B	RNA polymerase II transcription factor II B	Transcription factor II B (TFIIB) recognition element	71	1	ccgCGCC
	V$KLFS	Krueppel like transcription factors	Kruppel-like factor 7 (ubiquitous, UKLF)	71	0.934	agtgagGGCGcggtaagct
	V$CDEF	Cell cycle regulators: Cell cycle dependent element	Cell cycle-dependent element, CDF-1 binding site (CDE/CHR tandem elements regulate cell cycle dependent repression)	72	0.872	agggCGCGgtaag
	V$E2FF	E2F-myc activator/cell cycle regulator	E2F, involved in cell cycle regulation, interacts with Rb p107 protein	72	0.92	tgaggGCGCggtaagct
	V$WHNF	Winged helix binding sites	Winged helix protein, involved in hair keratinization and thymus epithelium differentiation	17	0.956	cggACGCcagc
	V$NRSF	Neuron-restrictive silencer factor	Neural-restrictive-silencer-element	25	0.72	cggagatcaccagcggccCGGAcgc
	V$PAX5	PAX-2/5/8 binding sites	B-cell-specific activator protein	29	0.737	taccggagatcaccAGCGgcccggac
	V$ETSF	Human and murine ETS1 factors	Ets variant 4	37	0.896	gtgctacCGGAgatcaccagc
	V$NGRE	"Negative" glucocoticoid response elements	Repressive binding sites for glucocorticoid receptor (IR1)	40	0.858	gtgctaccGGAGatc
	V$OSRF	Odd-skipped related factors	Odd-skipped related 2	42	0.898	ctccgGTAGcact
	V$HDBP	Huntington's disease gene regulatory region binding proteins	Huntington's disease gene regulatory region-binding protein 1 and 2 (SLC2A4 regulator and papillomavirus binding factor)	56	0.842	ctcgggCCGGcggtcagtg
	V$RXRF	RXR heterodimer binding sites	Retinoid X receptor alpha homodimer, DR1 sites	58	0.852	actcgggccggcGGTCagtgagggc
	V$HOMF	Homeodomain transcription factors	T-cell leukemia homeobox 1	59	0.859	gggccggCGGTcagtgagg
	V$RXRF	RXR heterodimer binding sites	VDR/RXR Vitamin D receptor RXR heterodimer, DR3	65	0.904	ccggcggtcagtGAGGgcgcggtaa
	V$MIZ1	Myc-interacting Zn finger protein 1	Myc-interacting Zn finger protein 1, zinc finger and BTB domain containing 17 (ZBTB17)	68	0.965	cgcgcCCTCac
	O$TF2B	RNA polymerase II transcription factor II B	Transcription factor II B (TFIIB) recognition element	71	1	ccgCGCC
	V$KLFS	Krueppel like transcription factors	Kruppel-like factor 7 (ubiquitous, UKLF)	71	0.934	agtgagGGCGcggtaagct
	V$CDEF	Cell cycle regulators: Cell cycle dependent element	Cell cycle-dependent element, CDF-1 binding site (CDE/CHR tandem elements regulate cell cycle dependent repression)	72	0.872	agggCGCGgtaag
	V$E2FF	E2F-myc activator/cell cycle regulator	E2F, involved in cell cycle regulation, interacts with Rb p107 protein	72	0.92	tgaggGCGCggtaagct
	V$WHNF	Winged helix binding sites	Winged helix protein, involved in hair keratinization and thymus epithelium differentiation	17	0.956	cggACGCcagc
	V$NRSF	Neuron-restrictive silencer factor	Neural-restrictive-silencer-element	25	0.72	cggagatcaccagcggccCGGAcgc
	V$PAX5	PAX-2/5/8 binding sites	B-cell-specific activator protein	29	0.737	taccggagatcaccAGCGgcccggac
	V$ETSF	Human and murine ETS1 factors	Ets variant 4	37	0.896	gtgctacCGGAgatcaccagc
	V$NGRE	"Negative" glucocoticoid response elements	Repressive binding sites for glucocorticoid receptor (IR1)	40	0.858	gtgctaccGGAGatc
	V$OSRF	Odd-skipped related factors	Odd-skipped related 2	42	0.898	ctccgGTAGcact
	V$HDBP	Huntington's disease gene regulatory region binding proteins	Huntington's disease gene regulatory region-binding protein 1 and 2 (SLC2A4 regulator and papillomavirus binding factor)	56	0.846	ctcgggCCGGcggatagtg
	V$RXRF	RXR heterodimer binding sites	VDR/RXR Vitamin D receptor RXR heterodimer, DR3 sites	65	0.859	ccggcggatagtGAGGgcgcggtaa
	V$HINFP	Histone nuclear factor P	Histone H4 transcription factor, MIZF, dimeric binding	69	0.775	ggCGGAcagtgagggcgcg
	V$MIZ1	Myc-interacting Zn finger protein 1	Myc-interacting Zn finger protein 1, zinc finger and BTB domain containing 17 (ZBTB17)	68	0.965	cgcgcCCTCac
	O$TF2B	RNA polymerase II transcription factor II B	Transcription factor II B (TFIIB) recognition element	71	1	ccgCGCC
	V$KLFS	Krueppel like transcription factors	Kruppel-like factor 7 (ubiquitous, UKLF)	71	0.934	agtgagGGCGcggtaagct
	V$CDEF	Cell cycle regulators: Cell cycle dependent element	Cell cycle-dependent element, CDF-1 binding site (CDE/CHR tandem elements regulate cell cycle dependent repression)	72	0.872	agggCGCGgtaag
	V$E2FF	E2F-myc activator/cell cycle regulator	E2F, involved in cell cycle regulation, interacts with Rb p107 protein	72	0.92	tgaggGCGCggtaagct
	V$WHNF	Winged helix binding sites	Winged helix protein, involved in hair keratinization and thymus epithelium differentiation	17	0.956	cggACGCcagc
	V$NRSF	Neuron-restrictive silencer factor	Neural-restrictive-silencer-element	25	0.72	cggagatcaccagcggccCGGAcgc
	V$PAX5	PAX-2/5/8 binding sites	B-cell-specific activator protein	29	0.737	taccggagatcaccAGCGgcccggac
	V$ETSF	Human and murine ETS1 factors	Ets variant 4	37	0.896	gtgctacCGGAgatcaccagc
	V$NGRE	"Negative" glucocoticoid response elements	Repressive binding sites for glucocorticoid receptor (IR1)	40	0.858	gtgctaccGGAGatc
	V$OSRF	Odd-skipped related factors	Odd-skipped related 2	42	0.898	ctccgGTAGcact
	V$HDBP	Huntington's disease gene regulatory region binding proteins	Huntington's disease gene regulatory region-binding protein 1 and 2 (SLC2A4 regulator and papillomavirus binding factor)	56	0.842	ctcgggCCGGcggttagtg
	V$HOMF	Homeodomain transcription factors	T-cell leukemia homeobox 1	59	0.872	gggccggCGGTtagtgagg
	V$MYBL	Cellular and viral myb-like transcriptional regulators	c-Myb, important in hematopoesis, cellular equivalent to avian myoblastosis virus oncogene v-myb	61	0.994	cgccctcacTAACcgccggcc
	V$RXRF	RXR heterodimer binding sites	VDR/RXR Vitamin D receptor RXR heterodimer, DR3	65	0.89	ccggcggttagtGAGGgcgcggtaa
	V$MIZ1	Myc-interacting Zn finger protein 1	Myc-interacting Zn finger protein 1, zinc finger and BTB domain containing 17 (ZBTB17)	68	0.965	cgcgcCCTCac
	O$TF2B	RNA polymerase II transcription factor II B	Transcription factor II B (TFIIB) recognition element	71	1	ccgCGCC
	V$KLFS	Krueppel like transcription factors	Kruppel-like factor 7 (ubiquitous, UKLF)	71	0.934	agtgagGGCGcggtaagct
	V$CDEF	Cell cycle regulators: Cell cycle dependent element	Cell cycle-dependent element, CDF-1 binding site (CDE/CHR tandem elements regulate cell cycle dependent repression)	72	0.872	agggCGCGgtaag
	V$E2FF	E2F-myc activator/cell cycle regulator	E2F, involved in cell cycle regulation, interacts with Rb p107 protein	72	0.92	tgaggGCGCggtaagct

	V$HNF1	Hepatic Nuclear Factor 1	Hepatocyte nuclear factor 1 beta (HNF1B)	17	0.816	tcttcataGTCAactct
	V$MYT1	MYT1 C2HC zinc finger protein	MyT1 zinc finger transcription factor involved in primary neurogenesis	21	0.756	caaGAGTtgacta
	V$PERO	Peroxisome proliferator-activated receptor	PPAR/RXR heterodimers, DR1 sites	26	0.799	aactaaagggcaagAGTTgacta
	V$PLZF	C2H2 zinc finger protein PLZF	Promyelocytic leukemia zink finger (TF with nine Krueppel-like zink fingers)	30	0.882	aacTAAAgggcaaga
	V$KLFS	Krueppel like transcription factors	Gut-enriched Krueppel-like factor	31	0.901	aagaactaaAGGGcaagag
	V$PERO	Peroxisome proliferator-activated receptor	Peroxisome proliferator-activated receptor gamma, DR1 sites	34	0.837	gttccaagaactAAAGggcaaga
	V$BCL6	POZ domain zinc finger expressed in B-Cells	B-cell CLL/lymphoma 6, member B (BCL6B)	39	0.902	tggTTCCaagaactaaa
	V$STAT	Signal transducer and activator of transcription	Signal transducer and activator of transcription 5A	39	0.979	ttggTTCCaagaactaaag
	V$STAT	Signal transducer and activator of transcription	STAT5: signal transducer and activator of transcription 5	41	0.948	ttagTTCTtggaaccaaaa
	V$MYT1	MYT1 C2HC zinc finger protein	MyT1 zinc finger transcription factor involved in primary neurogenesis	53	0.889	aaaAAGTtggtaa
	V$MYT1	MYT1 C2HC zinc finger protein	Myelin transcription factor 1-like, neuronal C2HC zinc finger factor 1	59	0.967	ggaaAGTTaccaa
Mouse	V$NFAT	Nuclear factor of activated T-cells	Nuclear factor of activated T-cells 5	60	0.919	cacaGGAAagttaccaact
	V$ETSF	Human and murine ETS1 factors	v-ets erythroblastosis virus E26 oncogene homolog	63	0.935	aggtcacaGGAAagttaccaa
	V$ESRR	Estrogen-related receptors	Estrogen-related receptor alpha, homodimer DR5 binding site	64	0.829	caaggtcacaggAAAGttaccaa
	V$HEAT	Heat shock factors	Heat shock factor 1	65	0.889	accaaggtcacaGGAAagttaccaa
	V$RXRF	RXR heterodimer binding sites	Highly conserved DR1 element selected by LXRbeta/RXR heterodimers	65	0.743	accaaGGTCacaggaaagttaccaa
	V$NR2F	Nuclear receptor subfamily 2 factors	TR4 homodimer, DR1 site	67	0.844	gcaccaAGGTcacaggaaagttacc
	V$PERO	Peroxisome proliferator-activated receptor	Peroxisome proliferator-activated receptor gamma	69	0.898	tgcaccaaggtcACAGgaaagtt
	V$RORA	v-ERB and RAR-related orphan receptor alpha	RAR-related orphan receptor alpha1	69	0.939	ctgcaccaaGGTCacaggaaagtta
	V$NBRE	NGFI-B response elements, nur subfamily of nuclear receptors	Monomers of the nur subfamily of nuclear receptors (nur77, nurr1, nor-1)	71	0.947	caccAAGGtcacagg
	V$RXRF	RXR heterodimer binding sites	Retinoid X receptor alpha homodimer, DR1 sites	72	0.85	gacctgcaccaaGGTCacaggaaag
	V$SF1F	Vertebrate steroidogenic factor	SF1 steroidogenic factor 1	72	0.993	gcacCAAGgtcacag
	V$NR2F	Nuclear receptor subfamily 2 factors	Chicken ovalbumin upstream promoter transcription factor 2, NR2F2 homodimer, DR1 sites	74	0.866	ctgacctgcaccaaGGTCacaggaa
	V$ESRR	Estrogen-related receptors	Estrogen-related receptor alpha	75	0.993	ctgacctgcaccAAGGtcacagg
	V$RXRF	RXR heterodimer binding sites	Thyroid hormone receptor, beta (ER6 - everted repeat, spacer 6)	76	0.903	cctgtgaccttggtgcAGGTcagtt
	V$RXRF	RXR heterodimer binding sites	Thyroid hormone receptor, beta (ER6 - everted repeat, spacer 6)	77	0.902	gaactgacctgcaccaAGGTcacag
	V$PAX6	PAX-4/PAX-6 paired domain binding sites	PAX6 paired domain and homeodomain are required for binding to this site	78	0.89	gaccttggtGCAGgtcagt

Figure S2: Table of transcription factor binding sites found in human and mouse 5'UTRs.

References

1. Goodwin, S., McPherson, J. D. & McCombie, W. R. Coming of age: Ten years of next-generation sequencing technologies. *Nature Reviews Genetics* (2016). doi:10.1038/nrg.2016.49
2. Broadgate, S., Yu, J., Downes, S. M. & Halford, S. Unravelling the genetics of inherited retinal dystrophies: Past, present and future. *Progress in Retinal and Eye Research* (2017). doi:10.1016/j.preteyeres.2017.03.003
3. Gallagher, M. D. & Chen-Plotkin, A. S. The Post-GWAS Era: From Association to Function. *Am. J. Hum. Genet.* **102**, 717–730 (2018).
4. Madelaine, R. *et al.* A screen for deeply conserved non-coding GWAS SNPs uncovers a MIR-9-2 functional mutation associated to retinal vasculature defects in human. *Nucleic Acids Res.* **46**, 3517–3531 (2018).
5. Giral, H., Landmesser, U. & Kratzer, A. Into the Wild: GWAS Exploration of Non-coding RNAs. *Front. Cardiovasc. Med.* **5**, 181 (2018).
6. Wright, A. F., Chakarova, C. F., Abd El-Aziz, M. M. & Bhattacharya, S. S. Photoreceptor degeneration: Genetic and mechanistic dissection of a complex trait. *Nature Reviews Genetics* (2010). doi:10.1038/nrg2717
7. Gregori, N. Z. *et al.* Current Concepts and Emerging Gene Therapies for Inherited Retinal Diseases. *Int. Ophthalmol. Clin.* **59**, 83–110 (2019).
8. Coppieters, F., Lefever, S., Leroy, B. P. & De Baere, E. CEP290, a gene with many faces: Mutation overview and presentation of CEP290base. *Hum. Mutat.* (2010). doi:10.1002/humu.21337
9. den Hollander, A. I., Roepman, R., Koenekoop, R. K. & Cremers, F. P. M. Leber congenital amaurosis: Genes, proteins and disease mechanisms. *Progress in Retinal and Eye Research* (2008). doi:10.1016/j.preteyeres.2008.05.003
10. Chiang, P. W. *et al.* Exome sequencing identifies NMNAT1 mutations as a cause of Leber congenital amaurosis. *Nat. Genet.* (2012). doi:10.1038/ng.2370
11. Belenky, P., Bogan, K. L. & Brenner, C. NAD+ metabolism in health and disease. *Trends in Biochemical Sciences* (2007). doi:10.1016/j.tibs.2006.11.006
12. Sobol, R. W. NAD metabolism and signaling: Critical pathways in bacteria, yeast and mammals influencing genome stability, cell survival and disease. *DNA Repair* (2014). doi:10.1016/j.dnarep.2014.10.007
13. Verdin, E. NAD+ in aging, metabolism, and neurodegeneration. *Science* (2015). doi:10.1126/science.aac4854
14. Eblimit, A. *et al.* NMNAT1 E257K variant, associated with Leber Congenital Amaurosis (LCA9), causes a mild retinal degeneration phenotype. *Exp. Eye Res.* **173**, 32–43 (2018).
15. Kuribayashi, H. *et al.* Roles of Nmnat1 in the survival of retinal progenitors through the regulation of pro-apoptotic gene expression via histone acetylation. doi:10.1038/s41419-018-0907-0
16. Coppieters, F. *et al.* Hidden Genetic Variation in LCA9-Associated Congenital Blindness Explained by 5′UTR Mutations and Copy-Number Variations of NMNAT1. *Hum. Mutat.* (2015). doi:10.1002/humu.22899
17. Araujo, P. R. *et al.* Before It Gets Started: Regulating Translation at the 5′ UTR. *Comp. Funct. Genomics* **2012**, 1–8 (2012).
18. Yanik, M. *et al.* In vivo genome editing as a potential treatment strategy for inherited

retinal dystrophies. *Progress in Retinal and Eye Research* (2017). doi:10.1016/j.preteyeres.2016.09.001
19. Hung, S. S. C. *et al.* AAV-Mediated CRISPR/Cas Gene Editing of Retinal Cells in Vivo. *Investig. Ophthalmol. Vis. Sci.* (2016). doi:10.1167/iovs.16-19316
20. Fu, X. *et al.* Clinical applications of retinal gene therapies. *Precis. Clin. Med.* **1**, 5–20 (2018).
21. Maeder, M. L. *et al.* Development of a gene-editing approach to restore vision loss in Leber congenital amaurosis type 10. *Nat. Med.* **25**, 229–233 (2019).
22. Greenwald, S. H. *et al.* Mouse Models of NMNAT1-Leber Congenital Amaurosis (LCA9) Recapitulate Key Features of the Human Disease. *Am. J. Pathol.* **186**, 1925–1938 (2016).
23. Conforti, L. *et al.* Reducing expression of NAD+ synthesizing enzyme NMNAT1 does not affect the rate of Wallerian degeneration. *FEBS J.* (2011). doi:10.1111/j.1742-4658.2011.08193.x

Appendix A: Retinoschisin gene therapy in photoreceptors, Müller glia, or all retinal cells in the *Rs1h*−/− mouse

Leah C. Byrne, [1,2], Bilge E. Öztürk[1], Trevor Lee[1], Cécile Fortuny[1], Meike Visel[1], Deniz Dalkara [1,2], David V. Schaffer[2], and John G. Flannery[1]

[1]Department of Molecular and Cellular Biology and The Helen Wills Neuroscience Institute, The University of California, Berkeley, CA 94720

[2]Department of Chemical and Biomolecular Engineering, Department of Bioengineering, and The Helen Wills Neuroscience Institute, The University of California, Berkeley, CA 94720

Peer review article published in Molecular & Gene Therapy (2014).

Abstract

X-linked retinoschisis, a disease characterized by splitting of the retina, is caused by mutations in the retinoschisin gene, which encodes a secreted cell adhesion protein. Currently, there is no effective treatment for retinoschisis, though viral vector-mediated gene replacement therapies offer promise. We used intravitreal delivery of three different AAV vectors to target delivery of the RS1 gene to Müller glia, photoreceptors, or multiple cell types throughout the retina. Müller glia radially span the entire retina, are accessible from the vitreous, and remain intact throughout progression of the disease. However, photoreceptors, not glia, normally secrete retinoschisin. We compared the efficacy of rescue mediated by retinoschisin secretion from these specific subtypes of retinal cells in the *Rs1h*−/− mouse model of retinoschisis. Our results indicate that all three vectors deliver the RS1 gene, and that several cell types can secrete retinoschisin, leading to transport of the protein across the retina. The greatest long-term rescue was observed when photoreceptors produce retinoschisin. Similar rescue was observed with photoreceptor-specific or generalized expression, though photoreceptor secretion may contribute to rescue in the latter case. These results collectively point to the importance of cell targeting and appropriate vector choice in the success of retinal gene therapies.

Introduction

X-linked retinoschisis (XLRS), which results from mutations in the gene encoding the secreted protein retinoschisin (RS1)[1], is a retinal degenerative disease affecting between 1/5,000 and 1/25,000 people worldwide[2–4]. The defining characteristics of XLRS include the formation of cystic cavities in the inner and outer retina and deterioration in vision caused by retinal disorganization. The binding partners and molecular mechanism of retinoschisin have not yet been definitively characterized[5,6], though it is generally thought to be a cell adhesion protein. The mouse model of XLRS, which lacks the mouse homolog of retinoschisin, has a highly disorganized retina, mimicking the human condition, with formation of cavities and progressive loss of photoreceptors as a result of apoptosis that peaks 18 days after birth[7,8]. As the underlying cause of this recessive monogenic disease is well understood, it is an excellent candidate for gene augmentation therapy. Previous studies have shown that delivery of a normal copy of the RS1 gene using a variety of AAV vectors and routes of vector administration targeting a variety of cell types can ameliorate degeneration[9–16]. However, a direct comparison of the efficacy of rescue obtained via expression of RS1 from specific subsets of cells has not been conducted. Recently, our group has created two novel variants of AAV that target specific populations of cells in the retina upon intravitreal injection. ShH10 is a variant of AAV6 that infects Müller glia specifically and efficiently[17,18], and 7m8 is a variant of AAV2 that efficiently infects inner and outer retina[9]. While 7m8 infects cells throughout the retina, its transgene expression can be limited to rod photoreceptors using a rhodopsin promoter. Finally, both ShH10 and 7m8 mediate pan-retinal gene delivery following intravitreal administration, without a need for subretinal injection and accompanying retinal detachment.

Here, we evaluate structural and functional rescue following intravitreal injections of three different viral vectors targeting different subsets of retinal cells (**Fig. 1**). Müller glia have been implicated in RS1 transport and normally provide structural support to retinal neurons. Müller cells have end feet that are easily accessible from the vitreous as well as processes reaching to the outer retina, and they remain intact in late stages of the disease. They may therefore be strong candidates to provide therapeutic protein, especially in later stages of the disease. In contrast, 7m8 with a rhodopsin promoter mediates protein expression specifically in photoreceptors. Since RS1 is strongly expressed by photoreceptors in normal retina, photoreceptors may be the best-suited cell type for delivering the protein. Lastly, 7m8 with a ubiquitous promoter transduces mixed populations of cells throughout the retina including ganglion cells, amacrine cells, Müller glia and photoreceptors. We found expression of RS1 from photoreceptors to provide more effective long-lasting rescue than expression from Müller glia, with a similar rescue effect using a rhodopsin promoter or a ubiquitous promoter. These results suggest that the normal source of RS1 in the retina -- photoreceptors -- is optimal for processing and delivery of retinoschisin, as well as demonstrate the importance of vector selection and cell type targeting in the development of gene replacement therapies.

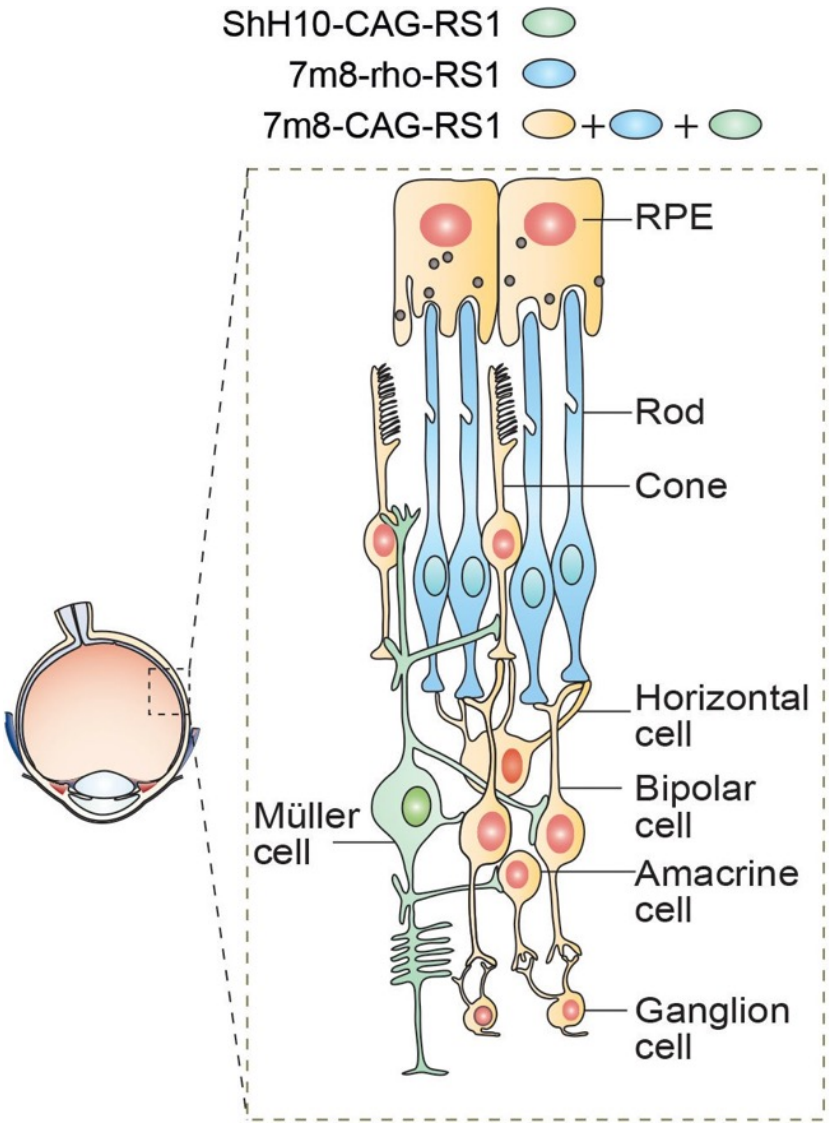

Figure 1. Illustration of experimental plan

Three vectors were used to deliver RS1 to specific populations of retinal cells following intravitreal injection. ShH10 targets Müller glia (in green), which contact all retinal neurons and span the retina from the inner limiting membrane to the outer limiting membrane. 7m8 with a rhodopsin promoter specifically expresses in photoreceptors (in blue). 7m8 with a ubiquitous CAG promoter penetrates to the outer retina from the vitreous and infects all retinal cell types (orange), including ganglion cells, photoreceptors and Müller glia.

Results

Characterization of vector expression

The expression profiles of 7m8-rho, 7m8-CAG and ShH10-CAG following injection at P14– into both WT and Rs1h−/− mice – were characterized using a GFP reporter and by immunolabeling of RS1 (**Fig. 2a–c**). The expression profiles of the vectors were confirmed in WT and Rs1h−/− mice (**Fig. 2a**). 7m8 with a photoreceptor-specific rhodopsin promoter driving GFP led to photoreceptor-limited expression in the outer nuclear layer (ONL) in both WT and Rs1h−/− eyes. Additionally, 7m8-CAG-GFP targeted cells in all retinal layers, including ganglion, Müller, amacrine, photoreceptor and RPE cells. Finally, ShH10-CAG-GFP led to expression primarily in Müller cells in WT and Rs1h−/− retinas.

The distribution of secreted protein following injection of the vectors carrying cDNA for the human RS1 gene was evaluated by immunolabeling in WT and Rs1h−/− retinas (**Fig. 2b**). Labeling in eyes injected with 7m8-rho-RS1 showed high levels of RS1 protein in the retina, and a RS1 pattern localization comparable to WT indicated that the protein was transported to its natural target locations. Specifically, staining of RS1 was observed in photoreceptor inner segments, ONL, outer plexiform layer, inner plexiform layer and inner nuclear layer (INL). Injection of 7m8-CAG-RS1 resulted in strong RS1 labeling in photoreceptor inner segments, as well as inner retina, including in ganglion cells (white bordered inset). Finally, ShH10 led to significant production of the protein that was apparently transported from Müller cells in the inner retina to photoreceptors in the outer retina. In particular, photoreceptor inner segments were labeled with anti-RS1 antibody after ShH10 delivery, though the labeling at the inner segments was less intense than the staining observed in 7m8- rho-RS1 or 7m8-CAG-RS1 injected eyes. Co-labeling with an anti-glutamine synthetase (GS) antibody also showed RS1 protein on the surface of processes running parallel to Müller cells, which by their morphology and localization are likely bipolar cells. Intravitreal injection with each of three vectors thus produced strong panretinal retinoschisin expression with a distribution similar to wild-type.

To confirm secretion of RS1 from Müller cells, a western blot was performed on primary cultured Müller cells infected with ShH10-RS1 (**Fig. 2c**). RS1 was present in both Müller cell lysate and in the culture media, showing that Müller cells secrete RS1. In addition, a Western blot of retinas injected with the three vectors (3 retinas pooled for each condition) indicate similarly high levels of protein using all three vectors, comparable to the levels in a WT retina (**Fig. 2d**). In contrast, no retinoschisin protein was detectable in uninjected Rs1h−/ control eyes.

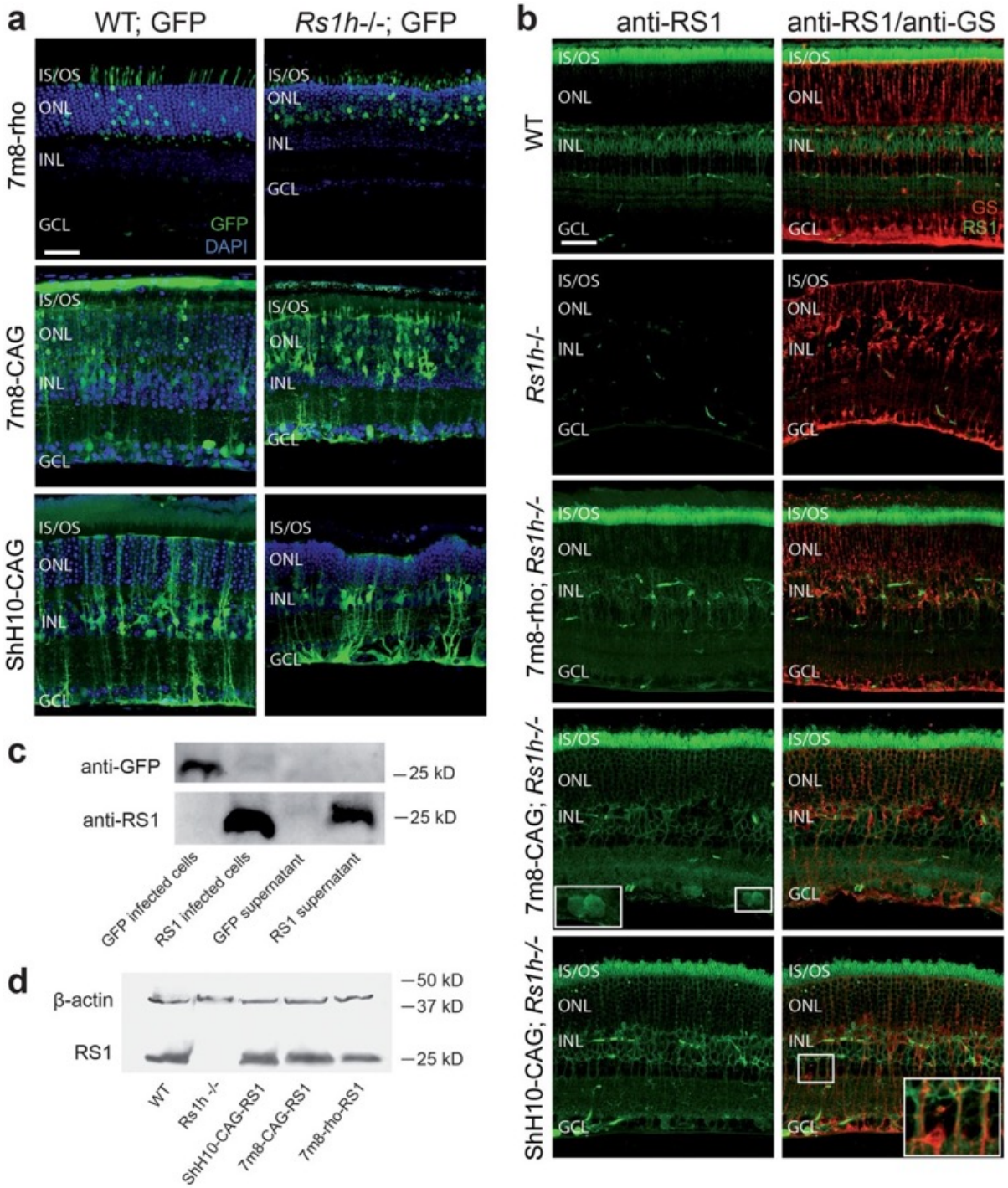

Figure 2. Characterization of viral vectors

(**a**) GFP expression in WT and *Rs1h*−/− retinas four months after intravitreal injection of viral vectors shows the cell types targeted. 7m8-rho-GFP leads to expression specifically in photoreceptors. 7m8-CAG-GFP leads to expression in all retinal layers. ShH10-CAG-GFP specifically expresses in Müller glia. Blue is DAPI labeled nuclei. Green is native GFP expression. (**b**) Expression of RS1 4 months after intravitreal injection of the three vectors. First row: Labeling of retinoschisin in the WT retina shows localization in inner segments of photoreceptors, bipolar cells and the photoreceptor-bipolar cell synapse, while *Rs1h*−/− retinas (second row) are devoid of the protein. Third row: 7m8-rho-RS1 injection in Rs1h−/ mice leads to

strong expression of the protein with localization of the protein like in the segments and the inner plexiform layer, although the protein is also expressed from Müller cells and ganglion cells. Inset shows magnification of RS1 expression in ganglion cell bodies. Fifth row: ShH10-CAG-RS1 injection in *Rs1h−/−* mice leads to RS1 protein localization in all retinal layers, including inner segments of photoreceptors, although the staining in photoreceptors was less strong than with the 7m8 vectors. Inset shows detail of RS1 staining on bipolar cell processes running parallel to Müller glia. Red is labeling of the Müller cell marker glutamine synthetase (GS). Green is labeling of RS1. (**c**) Mouse Müller cells infected with ShH10-RS1 secrete RS1. Primary Müller cell cultures were infected with ShH10-GFP or ShH10-RS1. GFP was present only in cell lysate from cells infected with ShH10-GFP, but not in culture media or in cells infected with ShH10-RS1 (top row). RS1, in contrast, was secreted and was found in both cell lysate and culture media (bottom row). (d) A western blot from retinas injected with ShH10, 7m8-CAG or 7m8-rho shows that levels of expression are similar to WT following treatment with all three vectors. IS/OS = inner and outer segments; ONL=outer nuclear layer; INL = inner nuclear layer; GCL = ganglion cell layer.

Time course of functional rescue

One important functional assessment of the XLRS retina is the electroretinogram (ERG), which records the change in the electrical potential of the retina in response to a flash of light. A decrease in the amplitude of the ERG b-wave with relative preservation of the a- wave is a hallmark of disorganization of the photoreceptor-bipolar cell synapse and reflects a defect in synaptic transmission. To track functional rescue, the amplitude of the full-field scotopic electroretinogram b-wave was measured on a monthly basis after injection with all three vectors (**Fig. 3a**). Administration of all three vectors led to an improvement in b-wave amplitude 1 month after injection relative to control GFP-injected or untreated eyes (7m8- CAG-RS1: 276±51 μV, 7m8-rho-RS1: 299±78 μV, ShH10-CAG-RS1: 274±51 μV, 7m8-GFP: 236±39 μV, untreated: 192±55μV)

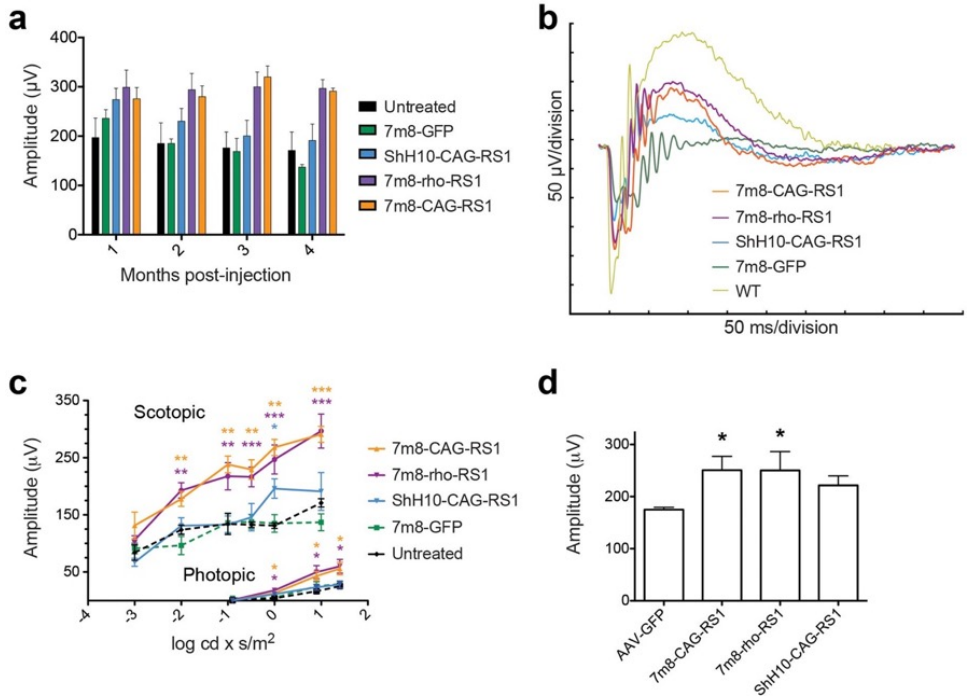

Figure 3. Time-course of functional rescue

(**a**) The amplitude of the b-wave resulting from a high intensity (1 log cd x s/m^2) stimulus was recorded on a monthly basis beginning one month after P14injection for each condition (ShH10-CAG-RS1 n=5, 7m8-rho-RS1 n=8, 7m8-CAG-RS1 n=5. 7m8-rho-GFP n=8, untreated n=8). In eyes injected with ShH10-CAG-RS1, b-wave amplitudes were slightly higher than control eyes for all time points measured, although the amplitude decreased over time. 7m8-CAG-RS1 and 7m8-rho-RS1 injected eyes were similar to each other and had markedly increased amplitudes compared to contralateral control GFP-injected eyes. (**b**) Representative ERG traces from all injected conditions, four months post-injection, illustrate a larger amplitude in 7m8-CAG or 7m8-rho-RS1 injected eyes compared to 7m8-GFP- injected eyes. ShH10-CAG-RS1 injected eyes had a slightly increased amplitude. (**c**) The amplitude of the ERG b-wave recorded four months after injection under a range of light intensities and under scotopic (upper traces) and photopic (lower traces) conditions. 7m8- CAG and 7m8-rho injected eyes had increased amplitudes at all light intensities, while ShH10-RS1-injected eyes were only slightly increased, mostly at higher light intensities greater than 0 log cd x s/m^2. Asterisks above the plot indicate the statistical significance of the difference between treated and GFP-injected eyes for ShH10-CAG-RS1 (blue asterisks) 7m8-CAG-RS1 (orange asterisks) or 7m8-rho-RS1 (purple asterisks). (d) Average b-wave amplitudes of mice injected at P30 and tested four months after injection. Rescue with 7m8- CAG and 7m8-rho is similar, while the amplitudes of mice injected with ShH10 are increased compared to control eyes but lower than but lower than 7m8 (n=5 for all groups). Error bars are mean±SD. * = P<0.05; ** = P<0.01; ** = P<0.001.

Over the course of four months, 7m8-CAG-RS1 and 7m8-rho-RS1 mediated significant and stable improvement in the b-wave amplitude compared to control eyes (7m8-rho-RS1 P<0.0001, 7m8-CAG-RS1, P<0.001, one-way ANOVA with post-hoc Tukey's multiple comparison test), while ShH10-mediated expression of RS1 from Müller glia led to a transient rescue effect at one month (P<0.01) that decreased over time. Four months after injection, amplitudes were 7m8-CAG-RS1: 291±14 μV, 7m8-rho-RS1: 297±47 μV, ShH10-CAG-RS1: 191±75 μV, 7m8-GFP: 137±15 μV, untreated: 171±75 μV. ShH10-CAG-RS1 n=5, 7m8-rho-RS1 n=8, 7m8-CAG-RS1 n=5.7m8-rho-GFP n=8, untreated n=8. Representative ERG traces illustrate the amplitude of ERG recordings 4 months after injection (**Fig. 3b**)

ERGs were recorded from the same mice 4 months post-injection over a range of stimulus intensities under photopic (rod-saturating) and scotopic (dark-adapted) conditions (**Fig. 3c**). These recordings revealed that both 7m8-CAG-RS1 and 7m8-rho-RS1 led to rescue across the spectrum of light intensities tested, while ShH10-CAG-RS1 led to increases only at higher light intensities Because Müller glia often survive to later stages of retinal degeneration, we then tested the rescue potential of the three vectors using injections at a later time point. Injections made 30 days after birth also led to improvement of the amplitude of the scotopic b-wave when measured 4 months post-injection (**Fig. 3d**), though injection with 7m8-CAG-RS1 (n=5, 251±27 μV, P<0.05) and 7m8-rho-RS1 (n=5, 250± 36 μV P<0.05) led to greater rescue than ShH10 (n=5, 221±18 μV, not significantly different from GFP-treated eyes: 175±5 μV).

Statistical significance was determined using a using a one-way ANOVA with posthoc Tukey's multiple comparison. Rescue with all three vectors was reduced with injection at this later time point relative to the P14 administration.

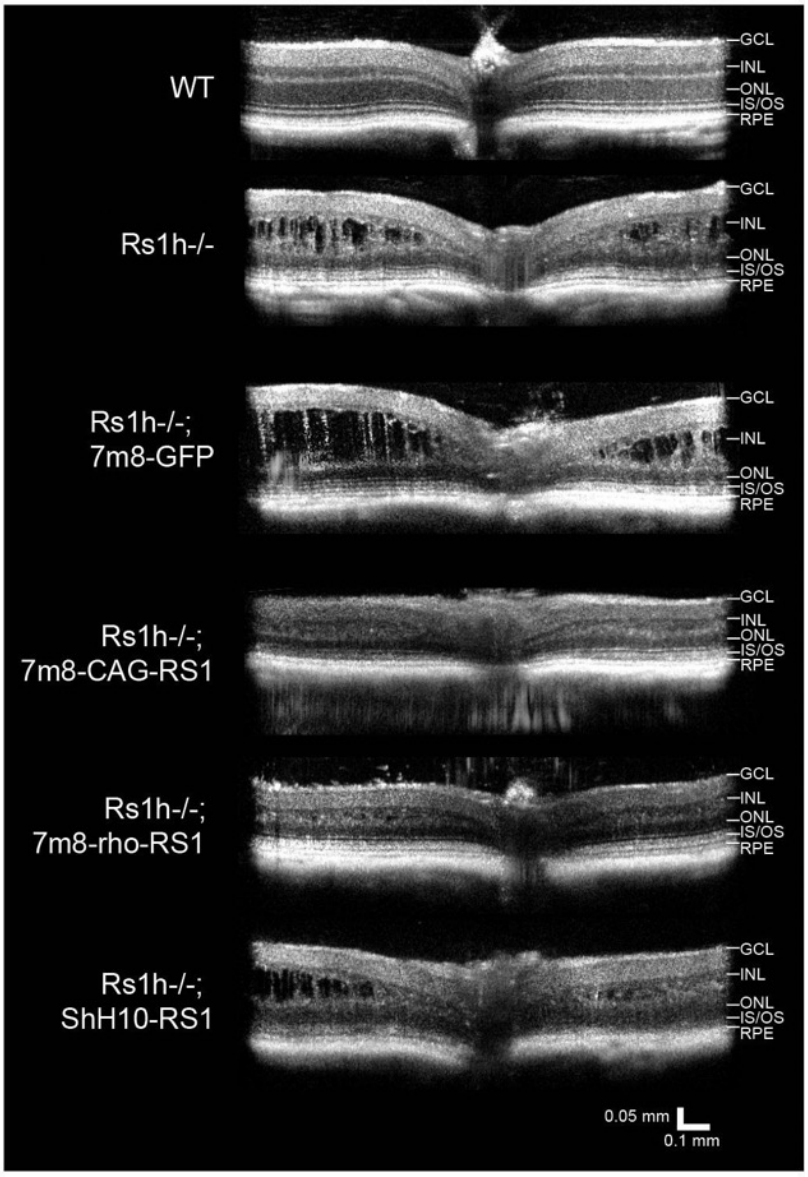

Figure 4. In vivo imaging of treated eyes 4 months after injection
Imaging of treated retinas showed that compared to WT mice, *Rs1h*−/− retinas were marked by the presence of large cavities in the superior and inferior retina. Similarly, 7m8-GFP treated eyes were highly disorganized, with large cavities. In comparison, 7m8-CAG-RS1 and 7m8-rho-RS1 retinas had fewer and smaller holes. ShH10-RS1-injected eyes were also marked by the presence of cavities. For each treatment group n=5 animals were imaged.

Structural improvement

High-resolution spectral domain optical coherence tomography (SD-OCT) images of retinas were gathered four months post-injection to evaluate the structure of the retina. Untreated

eyes or control eyes treated with 7m8-GFP were marked by large cavities across the retina, (**Fig. 4**), whereas retinas treated with 7m8-rho-RS1, and 7m8-CAG-RS1 had fewer cavities and improved retinal organization. Treated retinas were thinner than WT retinas of the same age, with decreased ONL thickness, indicative of loss of photoreceptors. ShH10-CAG-RS1 retinas appeared similar to untreated eyes, though some improvement was noted in individual cases.
Long-term structural rescued thickness of the retina in RS1 injected eyes and improved retinal organization in inferior and superior quadrants of the retina (**Fig. 5a**). Quantification of thickness of retinal layers showed improved thickness of the retina, primarily in the ONL and photoreceptor inner and outer segments (**Fig. 5b**).

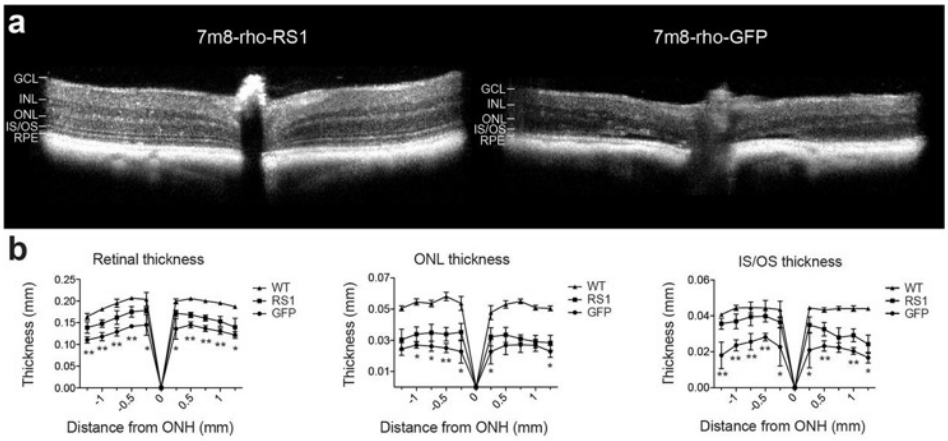

Figure 5. In vivo imaging of long-term structural rescue
(**a**) SD-OCT images of 7m8-rho-RS1 or 7m8-rho-GFP treated retinas 10 months post- injection showed improved retinal structure in 7m8-treated eyes. (**b**) Measurements of retinal thickness, ONL thickness and inner and outer segment thickness showed increased thickness in 7m8-rho-RS1 treated retinas in superior and inferior portions of the retina. Asterisks indicate statistical significance of the difference between treated and untreated eyes at the eccentricity measured as determined by a paired 2-tailed Student's t-test. * = P<0.05, **=p<0.01.

Histology in aged mice

Immunolabeling was used to determine the benefits of gene replacement on the integrity of the photoreceptor-bipolar cell synapse in aged animals (**Fig. 6a**). Specifically, retinas from animals injected at P14 were collected 15 months post-injection and labeled with anti- synaptophysin antibodies (a presynaptic marker labeling synaptic vesicles). The presence of synaptophysin labeling in the outer plexiform layer indicates synaptic transmission at the photoreceptor-bipolar cell synapse. In WT mice, dense labeling of synaptophysin at the photoreceptor-bipolar cell synapse was observed (arrowhead). In contrast, *Rs1h*−/− retinas were largely deficient of synaptophysin 15 months after birth, and control, 7m8-rho-GFP injected eyes were unchanged compared to untreated eyes. In contrast, 7m8-rho-RS1 injected eyes had dense labeling of synaptophysin. These retinas were also thicker, with a clear improvement of synaptic structure and retinal organization. Finally, ShH10-CAG-RS1 retinas were not significantly improved.

Over time, *Rs1h*−/− mice lose photoreceptors. PNA labeling of flatmounted retinas from 15-month-old animals showed increased densities of cones in 7m8-rho-RS1-treated eyes compared to untreated, GFP-injected or ShH10-injected eyes (**Fig. 6b**). Imaris software was used to count individual cones in PNA-labeled flatmounts.10X images were collected from the periphery of the retina and centered on the optic nerve head. Quantification of cones showed higher numbers of cones in animals treated with 7m8-rho-RS1, but not with ShH10.

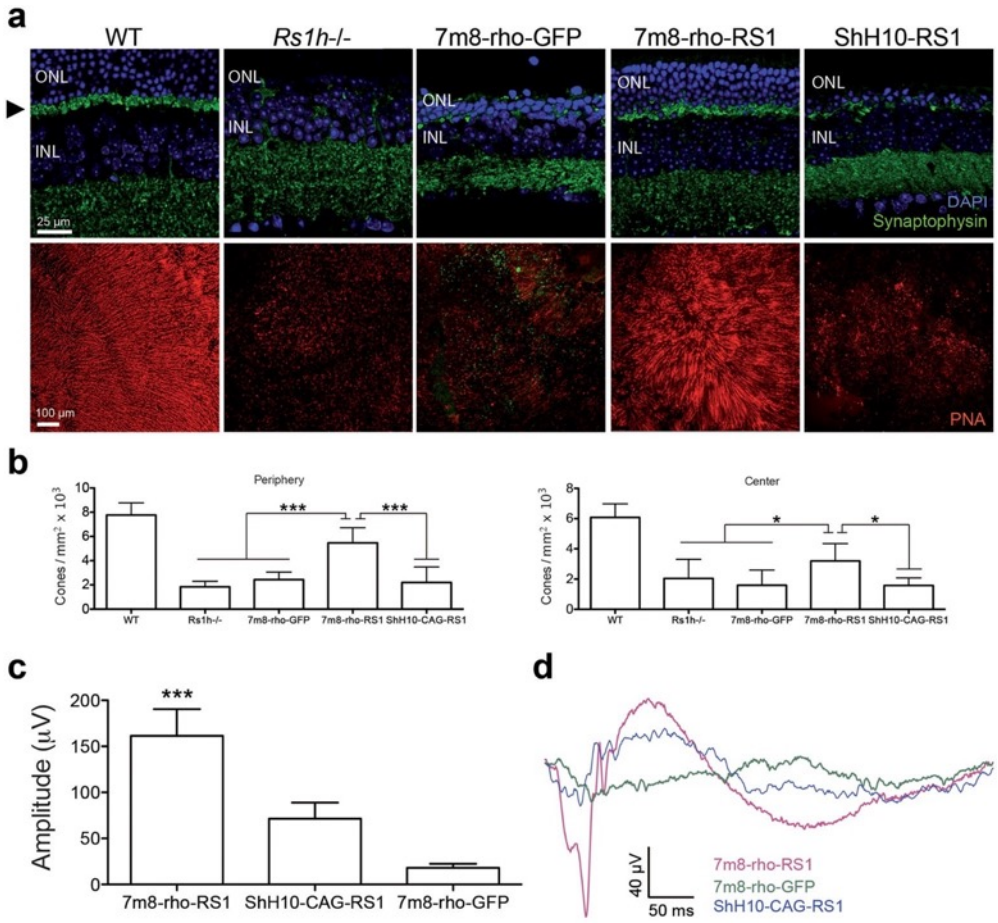

Figure 6. Long-term structural and functional rescue

(**a**) Retinas collected from mice 15 months post-injection and labeled with anti- synaptophysin antibodies showed that the structure of the photoreceptor-bipolar cell synapse was maintained in mice injected with 7m8-rho-RS1, and looked more like WT compared to untreated *Rs1h*−/− eyes or control 7m8-GFP-injected eyes. ShH10-RS1 injected eyes also showed synaptic deterioration. PNA labeling, which labels cones, showed that the population of structurally intact cones in *Rs1h*−/− mouse retinas is nearly eliminated by 15 months after birth. Mouse eyes treated with 7m8-rho-RS1 showed a much-improved cone histology, with widespread labeling of surviving cones. However, at this time point ShH10- injected eyes showed no cone preservation compared to control eyes. (**b**) Quantification of cone labeling in peripheral and central retina showed that 7m8-rho-RS1 treated eyes had significantly greater numbers of cones compared to untreated or control eyes (n=5 for each group). ShH10-treated eyes (n=5) had similar numbers of cones compared to untreated eyes. (**c**) ERGs recorded 15 months after injection showed preservation of the b-wave in 7m8-rho- RS1-treated eyes compared to 7m8-rho-GFP-treated eyes or ShH10-CAG-RS1-treated eyes (n=5 per

group). (**d**) Representative ERG traces show that 7m8-rho-RS1 treated eyes had a more normal wave form and a higher amplitude of the a- and b-wave compared to ShH10 or contralateral control eyes. Error bars are mean±SD. *** = P<0.001, * = P<0.05.

Long-term functional rescue

The long-term functional benefit of 7m8-rho-RS1 was determined by ERG recordings collected 15 months after injection. At this late time point, 7m8-rho-RS1 injected eyes were significantly improved over control contralateral eyes expressing GFP or ShH10-CAG-RS1- injected eyes (7m8-rho-RS1: 161.4±29 μV; ShH10-CAG-RS1: 71.33 ±30.57 μV; 7m8-rho- GFP: 10.0±6 μV; P=0.0008) (**Fig. 6c**). Representative ERG waveforms illustrate higher amplitude of the a- and b-waves as well as a well-maintained wave form in treated eyes (**Fig 6d**).

Discussion

XLRS is a well-characterized monogenic inherited retinal degenerative disease and represents a promising candidate for gene replacement immediately amenable to the clinic. Recent clinical trials for LCA2 have proven the safety of AAV vector administration in the eye, though the invasive subretinal injections used in LCA2 may not be suitable for structurally compromised retinas. For example, XLRS is characterized by the formation of cystic cavities in the inner and outer layers of the retina and an increased risk for retinal detachment, and subretinal injections may therefore represent surgical risks in these fragile retinas. Additionally, subretinal injections transduce only a fraction of the retina. Retinoschisin is a secreted protein that may diffuse to a certain degree laterally across the retina, though in a larger human eye the extent of this diffusion is uncertain, and RS1 gene therapy would likely require several injections to fully treat the condition. The ideal vector, therefore, should transduce the optimal cell type pan-retinally via an intravitreal injection. Previous studies in the mouse model of XLRS demonstrated that the disease is amenable to gene therapy[9,10,13,15], though significant hurdles exist in translating these studies to clinical use.

Here we tested a Müller glia-targeted approach to deliver RS1 to the *Rs1h*−/− retina as previous studies have suggested that Müller glia are involved in the transport of the protein to the inner retina[19,20]. In addition, we hypothesized Müller cells could provide advantages for a gene therapy approach due to their morphology, location and relative preservation in late stage retinal degeneration. In areas with large cavities, Müller glia may bridge schisis in the retina to deliver protein to the inner retina after photoreceptors have lost contact with the inner retina. However, our results showed that Müller cell-mediated expression was suboptimal for achieving rescue in the retinoschisin mouse model, demonstrably less effective than expression from photoreceptors. This suggests that if Müller cells are normally involved in RS1 trafficking, this mechanism alone is insufficient for normal retinal function. Our results show that Müller cells are able to express and secrete RS1, resulting in distribution of the protein throughout the retina, but must lack the ability for some other necessary aspect of processing or delivery of the protein to its molecular targets. It would therefore be necessary to understand and overcome these shortcomings in order for Müller cell-targeted RS1 delivery to be an adjunctive to photoreceptor-based therapy for RS1 gene replacement.

It is thus surprising that the rescue effect with ShH10 was less than that of 7m8-rho-RS1, although the onset of expression, pattern of localization and expression levels of RS1 protein are similar to WT in the ShH10-RS1 treated mice. This may indicate that Müller cells are unable to efficiently traffic RS1 to its binding partners, which recent studies show include the Na/K-ATPase subunits ATP1A3 and ATP1B2[21]. While photoreceptors express both of these subunits strongly, Müller glia do not express ATP1A3[22]. A lack of the normal binding partners of RS1 in Müller cells could thus affect the stability or processing of the protein. Future work should evaluate possible differences in the stability, trafficking, post- translational modifications and isoforms of RS1 secreted from Müller glia and photoreceptors

In contrast, we have shown previously[9] and here that 7m8-rho-RS1, which mediates expression specifically in rods, rescues the morphology of the *Rs1h*−/− retina and thereby leads to long-lasting

structural and functional preservation. This agrees with previous studies demonstrating that subretinal injections of AAV-mouse opsin promoter-RS1 mediated strong rescue through targeting photoreceptors[15]. All retinal neurons express RS1 during development, with a wave of expression moving outward starting at P1 in ganglion cells, proceeding to bipolar cells, followed by photoreceptor expression by P7[23]. In addition, ganglion cells have been reported to express RS1 into adulthood[23]. We therefore tested whether simultaneous expression from all cell types in the retina would increase the rescue effect of gene replacement. We found that expression from multiple cell types afforded no measurable improvement over expression exclusively in rods (using the rhodopsin promoter), indicating that photoreceptor expression is sufficient for effective rescue when injections are made at P14. Additional benefit from ubiquitous expression may only be observed in the *Rs1h*−/− mouse model if injections are made early enough for RS1 protein to be expressed during retinal development, when retinoschisin is expressed strongly in a wave of expression in other cell types. However, anterograde transport of some AAV serotypes has been observed[24], and therefore a photoreceptor-specific promoter may represent a safer approach to gene augmentation therapy.

None of the vectors tested prevented the photoreceptor loss that peaks at P18, which occurs soon after the injections made at P14, likely due to the fact that gene expression takes several days to initiate and is thus not sufficiently rapid to avert this early wave of apoptosis. However, in humans the rate of degeneration in XLRS is much slower than in the murine model[3], and the therapeutic window for gene replacement treatments is longer. In summary, this work indicates the importance of a rational approach to the design of gene replacement therapies and evaluation of the strategies used for viral vector-mediated delivery, including the cell type targeted and the delivery method. These results emphasize the potential for gene therapy in XLRS, highlighting the importance of careful design and optimization for specific, minimally invasive and long-lasting gene therapy.

Materials & Methods

Production of viral vectors

AAV vectors carrying human RS1 cDNA or GFP were produced by the plasmid co- transfection method [25]. Recombinant AAV was purified by iodixanol gradient ultra centrifugation followed by a buffer exchange and concentration with Amicon Ultra-15 Centrifugal Filter Units in PBS + 0.001% Pluronic F-68. Titers were determined by quantitative PCR relative to a standard curve[26].

Immunohistochemistry

Retinas were freshly dissected and immediately placed in 10% formalin overnight. Relief cuts were made and the retinas were embedded in 5% agarose. Using a vibratome, 150 μm transverse sections were cut and the sections were floated in PBS. After blocking in 1% bovine serum albumin, 0.5% Triton X-100, and 2% normal donkey serum for 2–3 hours, sections were incubated in primary antibody overnight at 4° C. After washing in PBS, secondary antibodies were applied at room temperature for 1 hour. Sections were again washed and then mounted for confocal microscopy (LSM710, Carl Zeiss). Antibodies were as follows: 3R10 mouse anti-RS1[7] (gift of Professor Robert Molday, 1:5); rabbit anti-GS (Sigma, 1:1000); rabbit anti-synaptophysin (abcam, 1:1000).

Intravitreal injections

C57BL/6J or *Rs1h−/−* mice on a C57BL/6 background[7] were used for all experiments, which were conducted according to the ARVO Statement for the Use of Animals and the guidelines of the Office of Laboratory Animal Care at the University of California Berkeley, CA. P14 or P30 mice were anesthetized with ketamine (72 mg/kg) and xylazine (64 mg/kg) by intraperitoneal injection. An ultrafine 30 1/2-gauge disposable needle was then passed through the sclera, at the equator and posterior to the limbus, into the vitreous cavity. One μL of AAV with a titer of 5E+13 vg/mL was injected into the vitreous cavity with direct observation of the needle directly above the optic nerve head. Contralateral control eyes received vectors carrying the gene encoding GFP.

Western blot

Three retinas for each condition were pooled. Retinas were removed from the eye cup in cold PBS, sonicated in buffer with proteinase inhibitor cocktail and pooled. Protein concentration was measured using a BCA kit and normalized. Protein was run on a 4–20% Tris-HCL gradient gel. Protein was transferred to a PVDF membrane, and blocked in 5% milk for 2 hours. The membrane was then washed 2X 5 minutes in PBST, and incubated in primary antibodies overnight at RT: 3R10 mouse anti-RS1 (1:50); anti-B-actin (Abcam, 1:2000) PNA (Molecular probes, 1:50). Secondary antibodies conjugated to alkaline phosphatase were applied for 2 hours at RT before washing and visualization using NBT/ BCIP (Roche).

Electroretinograms

Mice were dark-adapted for 2 hours and then anesthetized, followed by pupil dilation. Mice were placed on a 37°C heated pad and contact lenses were positioned on the cornea of both eyes. A reference electrode connected to a splitter was inserted into the forehead and a ground electrode was inserted in the tail. For scotopic conditions electroretinograms were recorded (Espion E2 ERG system; Diagnosys LLC, Littleton, MA) in response to six light flash intensities ranging from −3 to 1 log cd × s/m^2 on a dark background. Each stimulus was presented in series of three. For photopic ERGs the animal was exposed to a rod saturating background for 5 minutes. Stimuli ranging from −0.9 to 1.4 log cd × s/m^2 were presented 20 times on a lighted background. Stimulus intensity and timing were computer controlled. Data were analyzed with MatLab (v7.7; Mathworks, Natick, MA). ERG amplitudes were compared using a one-way ANOVA with posthoc Tukey's multiple comparison on Graphpad Prism Software.

High-resolution spectral domain optical coherence tomography

Histological imaging was performed using an 840nm SDOIS OCT system (Bioptigen, Durham, North Carolina) including an 840nm SDOIS Engine with 93nm bandwidth internal source providing < 3.0um resolution in tissue. Retinal thickness, ONL and inner and outer segment thickness measurements were gathered and analysis done using InVivoVue software. Mice were anesthetized and the pupils dilated with atropine before imaging. Images of retinal cross sections were averaged from 8 contiguous slices.

Primary Müller culture

Mouse retinas were dissociated with 0.25% trypsin followed by trituration, and then cultured in DMEM containing 20% FBS, 2mM L-glutamine with antibiotics (100 U penicillin/mL and 100 ug/mL streptomycin). After 5 days in culture, retinal neurons no longer survive, leaving only Müller cells. Müller glia were then passaged and grown to 80% confluency before infecting in culture with ShH10-CAG-RS1 (MOI of 20,000). Conditioned media and cultured cells were then collected for western blotting.

Acknowledgments

The authors thank Robert Molday for providing the 3R10 anti-RS1 antibody. We thank Bernhardt Weber and Bill Hauswirth for supplying the mouse model of XLRS. We thank Günter Niemeyer, Greg Nielsen, and Matt LaVail for valuable advice on ERG recordings. Tim Day assisted with plasmid cloning. Jonathan Jui helped with immunohistochemistry. This work was supported by funding from the NIH and FFB.

References

1. Sauer CG, Gehrig A, Warneke-Wittstock R, Marquardt A, Ewing CC, Gibson A, et al. Positional cloning of the gene associated with X-linked juvenile retinoschisis. Nat Genet. 1997; 17:164–70. [PubMed: 9326935]
2. George ND, Yates JR, Moore AT. X linked retinoschisis. The British journal of …. 1995
3. Sikkink SK, Biswas S, Parry NRA, Stanga PE, Trump D. X-linked retinoschisis: an update. J Med Genet. 2007; 44:225–32. [PubMed: 17172462]
4. Forsius HH, Krause UU, Helve JJ, Vuopala VV, Mustonen EE, Vainio-Mattila BB, et al. Visual acuity in 183 cases of X-chromosomal retinoschisis. Can J Ophthalmol. 1973; 8:385–93. [PubMed: 4742888]
5. Vijayasarathy C, Takada Y, Zeng Y, Bush RA, Sieving PA. Retinoschisin is a peripheral membrane protein with affinity for anionic phospholipids and affected by divalent cations. Investigative Ophthalmology & Visual Science. 2007; 48:991–1000. [PubMed: 17325137]
6. Molday LL, Wu WWH, Molday RS. Retinoschisin (RS1), the protein encoded by the X-linked retinoschisis gene, is anchored to the surface of retinal photoreceptor and bipolar cells through its interactions with a Na/K ATPase-SARM1 complex. J Biol Chem. 2007; 282:32792–801. [PubMed: 17804407]
7. Weber BHF, Schrewe H, Molday LL, Gehrig A, White KL, Seeliger MW, et al. Inactivation of the murine X-linked juvenile retinoschisis gene, Rs1h, suggests a role of retinoschisin in retinal cell layer organization and synaptic structure. Proc Natl Acad Sci U S A. 2002; 99:6222–7. [PubMed: 11983912]
8. Gehrig A, Janssen A, Horling F, Grimm C, Weber BHF. The role of caspases in photoreceptor cell death of the retinoschisin-deficient mouse. Cytogenet Genome Res. 2006; 115:35–44. [PubMed: 16974082]
9. Dalkara D, Byrne LC, Klimczak RR, Visel M, Yin L, Merigan WH, et al. In vivo-directed evolution of a new adeno-associated virus for therapeutic outer retinal gene delivery from the vitreous. Science Translational Medicine. 2013; 5:189ra76.
10. Park TK, Wu Z, Kjellstrom S, Zeng Y, Bush RA, Sieving PA, et al. Intravitreal delivery of AAV8 retinoschisin results in cell type-specific gene expression and retinal rescue in the Rs1-KO mouse. Gene Ther. 2009; 16:916–26. [PubMed: 19458650]
11. Takada Y, Vijayasarathy C, Zeng Y, Kjellstrom S, Bush RA, Sieving PA. Synaptic pathology in retinoschisis knockout (Rs1-/y) mouse retina and modification by rAAV-Rs1 gene delivery. Investigative Ophthalmology & Visual Science. 2008; 49:3677–86. [PubMed: 18660429]
12. Janssen A, Min SH, Molday LL, Tanimoto N, Seeliger MW, Hauswirth WW, et al. Effect of late- stage therapy on disease progression in AAV-mediated rescue of photoreceptor cells in the retinoschisin-deficient mouse. Mol Ther. 2008; 16:1010–7. [PubMed: 18388913]
13. Kjellstrom S, Bush RA, Zeng Y, Takada Y, Sieving PA. Retinoschisin gene therapy and natural history in the Rs1h-KO mouse: long-term rescue from retinal degeneration. Investigative Ophthalmology & Visual Science. 2007; 48:3837–45. [PubMed: 17652759]

14. Molday LL, Min S-H, Seeliger MW, Wu WWH, Dinculescu A, Timmers AM, et al. Disease mechanisms and gene therapy in a mouse model for X-linked retinoschisis. Adv Exp Med Biol. 2006; 572:283–9. [PubMed: 17249585]
15. Min SH, Molday LL, Seeliger MW, Dinculescu A, Timmers AM, Janssen A, et al. Prolonged recovery of retinal structure/function after gene therapy in an Rs1h-deficient mouse model of x- linked juvenile retinoschisis. Molecular Therapy. 2005; 12:644–51. [PubMed: 16027044]
16. Zeng Y, Takada Y, Kjellstrom S, Hiriyanna K, Tanikawa A, Wawrousek E, et al. RS-1 Gene Delivery to an Adult Rs1h Knockout Mouse Model Restores ERG b-Wave with Reversal of the Electronegative Waveform of X-Linked Retinoschisis. Investigative Ophthalmology & Visual Science. 2004; 45:3279–85. [PubMed: 15326152]
17. Klimczak RR, Koerber JT, Dalkara D, Flannery JG, Schaffer DV. A novel adeno-associated viral variant for efficient and selective intravitreal transduction of rat Müller cells. PLoS ONE. 2009; 4:e7467. [PubMed: 19826483]
18. Koerber JT, Klimczak R, Jang J-H, Dalkara D, Flannery JG, Schaffer DV. Molecular evolution of adeno-associated virus for enhanced glial gene delivery. Mol Ther. 2009; 17:2088–95. [PubMed: 19672246]
19. Reid SNM, Yamashita C, Farber DB. Retinoschisin, a photoreceptor-secreted protein, and its INTERACTION with bipolar and muller cells. Journal of Neuroscience. 2003; 23:6030–40. [PubMed: 12853421]
20. Reid SNM, Farber DB. Glial transcytosis of a photoreceptor-secreted signaling protein, retinoschisin. Glia. 2005; 49:397–406. [PubMed: 15538749]
21. Friedrich U, Stöhr H, Hilfinger D, Loenhardt T, Schachner M, Langmann T, et al. The Na/K-ATPase is obligatory for membrane anchorage of retinoschisin, the protein involved in the pathogenesis of X-linked juvenile retinoschisis. Human Molecular Genetics. 2011; 20:1132–42. [PubMed: 21196491]
22. Wetzel RK, Arystarkhova E, Sweadner KJ. Cellular and subcellular specification of Na, K-ATPase alpha and beta isoforms in the postnatal development of mouse retina. Journal of Neuroscience. 1999; 19:9878–89. [PubMed: 10559397]
23. Takada Y, Fariss RN, Tanikawa A, Zeng Y, Carper D, Bush R, et al. A retinal neuronal developmental wave of retinoschisin expression begins in ganglion cells during layer formation. Investigative Ophthalmology & Visual Science. 2004; 45:3302–12. [PubMed: 15326155]
24. Stieger K, Colle M-A, Dubreil L, Mendes-Madeira A, Weber M, Le Meur G, et al. Subretinal delivery of recombinant AAV serotype 8 vector in dogs results in gene transfer to neurons in the brain. Mol Ther. 2008; 16:916–23. [PubMed: 18388922]
25. Grieger JC, Choi VW, Samulski RJ. Production and characterization of adeno-associated viral vectors. Nat Protoc. 2006; 1:1412–28. [PubMed: 17406430]
26. Aurnhammer C, Haase M, Muether N, Hausl M, Rauschhuber C, Huber I, et al. Universal real-time PCR for the detection and quantification of adeno-associated virus serotype 2-derived inverted terminal repeat sequences. Hum Gene Ther Methods. 2012; 23:18–28. [PubMed: 22428977]